



Pilkington Library

Author/Filing Title . TILLEMA

Vol No Class Mark T

**Please note that fines are charged on ALL
overdue items.**

2011 10/13/2013 10/13/2013 /

0402508181



AN INVESTIGATION INTO UNDERGROUND
NAVIGATION USING ELECTROMAGNETIC WAVES

N.J.P. TILLEMA

2000

Loughborough University


An Investigation into Underground Navigation Using
Electromagnetic Waves

By

Nico J.P. Tillema
ing, M.Sc

Being a thesis submitted to the
Department of Electronic & Electrical Engineering
At
Loughborough University

In fulfilment of the requirements for the degree of
Doctor of Philosophy
June 2000

| |
|--|
|  Loughborough University Physical Education Library |
| Date Mar 02 |
| Class |
| Acc No. 040250818 |

Acknowledgements

This project was sponsored by the Engineering and Physical Sciences Research Council (EPSRC) in a DTI/Link project GR/H 89104

I would like to thank all the members of the Wireless Communication Group at Loughborough University who have offered advice throughout the duration of my research. In particular, I would like to thank Prof. J.C. Vardaxoglou.

Also I would like to thank Prof. Chris Rogers and Dr. Dave Chapman, now both at the University of Birmingham, for their advice regarding the Civil Engineering aspects of the project. The help of Gary Briggs with the field trials was invaluable. Thanks to Dr. Dave Parish for the useful discussions.

I would also like to acknowledge my parents and friends for their support and encouragement. I would like to thank Ann for her support and understanding while conducting this work.

Abstract

This thesis explores the possibility of measuring the movement of an underground transmitter using electromagnetic waves. The displacement of the transmitter was estimated based on the magnitude and phase of the received electromagnetic wave, using receiver antennas at fixed locations. Electromagnetic wave propagation underground was dependent on the frequency used, soil type, soil moisture content and environmental conditions. An extensive investigation has been conducted in measuring the soil dielectric constant and conductivity. When the sample moisture was increased, its dielectric constant increased, being disperse for clays, but fairly linear for sands. Clays show a higher conductivity. The optimum antennas to use underground were dielectric loaded electric monopole and dipole antennas. A method was developed to predict the admittance of insulated monopole antennas in soil using measured data of the ambient medium. The field trials have shown that propagation of an electromagnetic wave from a transmitter underground to a receiver underground was possible over a distance of up to 30 m and to a depth of 1.5 m. A simulation model was developed to predict the electromagnetic wave propagation from the source underground using the measured ϵ_r and σ . Its predictions compared well with the measured results. The model predicted that the lateral wave was the strongest mode of propagation in the majority of the field trials. The field trials confirmed these findings. The lateral wave starts at the source underground, travels to the boundary, follows the air-ground boundary and then propagates back into the ground to the receiver antenna. As the wave travels a significant part of its path in air, it was less susceptible to irregularities underground. Measurement of the phase has shown it to be sensitive to errors caused by reflections. This was the reason why reliable information of the phase was not always available during the measurements. The field trials have shown the possibility of using electromagnetic waves to track a moving transmitter underground. Any system that estimates the underground displacement of the transmitter should have two or more receiver antennas. The experiments have shown a possible accuracy of such a system of approximately 2 m or less.

Nico J P Tillema

June 2000

Contents

ACKNOWLEDGEMENTS..... II

ABSTRACT III

MATHEMATICAL SYMBOLS AND CONSTANTS..... VII

1. INTRODUCTION..... 1

1 1. Background 1

1.2. Aim of the Thesis..... 3

1.3. Work Done..... 3

References 5

2. DIELECTRIC CONSTANT OF SOILS AND ROCKS..... 6

2.1. Introduction..... 6

2.2. Dielectric Constant theory 6

2 3 Background 9

2.4. Measurement techniques..... 11

2 4 1.Coaxial probe 12

2 4.2.Sample preparation 14

2.5. Measurement results..... 14

2.5.1.Relaxation model 16

2.5.2.Site Survey 17

2.6. Conclusion 19

References 33

3. INSULATED WIRE ANTENNAS IN A LOSSY DIELECTRIC MEDIUM. 35

3.1. Theoretical Formulation..... 36

| | | |
|-------------|--|-----------|
| 3.1 | 1.Theory Constraints | 38 |
| 3 | 1.2 Antenna Effective Length | 38 |
| 3.2. | Experiments | 39 |
| 3.2 | 1.Antennas used in Experiments..... | 39 |
| 3.2.2. | Experimental Results | 40 |
| 3.2.3. | Antennas Underwater..... | 40 |
| 3.2.4. | Soil as Ambient medium..... | 41 |
| 3.2.5. | Antenna Admittance in Various Soil Types..... | 41 |
| 3.2.6. | Antenna Effective Height..... | 42 |
| 3 | 2.7.Radiated Field | 42 |
| 3.3. | Conclusion | 43 |
| References | | 51 |
| 4. | UNDERGROUND PROPAGATION | 52 |
| 4.1. | Introduction..... | 52 |
| 4.2. | Background | 53 |
| 4 | 3. Theory | 55 |
| 4.3.1. | Modes of Propagation | 55 |
| 4.3.2 | Approximate Equations for the Lateral Wave..... | 57 |
| 4.4. | Equipment for Field Trials..... | 63 |
| 4.4.1. | Frequencies used | 63 |
| 4 | 4 2 Antennas Used | 63 |
| 4.5. | Underwater Propagation Experiments | 64 |
| 4.6. | Underground Propagation Experiments | 65 |
| 4.6.1. | Field Trial 1, Receiver Antenna Underground..... | 66 |
| 4.6.2. | Field Trial 2, Receiver Antenna Underground..... | 69 |
| 4.6.3. | Field Trial 3, Receiver Antenna Underground..... | 70 |

| | | |
|------------|---|------------|
| 4.6.4. | Field Trial 4, Receiver Antenna Underground..... | 70 |
| 4.6.5 | Field Trial 5, Phase Measurement... .. | 71 |
| 4.6.6 | Scattering..... | 72 |
| 4.6.7. | Field Trial 6, Receiver Antenna in Air .. | 73 |
| 4.6.8. | Field Trial 7, Two Receiver Antennas | 74 |
| 4.7. | Optimum Frequency .. | 75 |
| 4.8. | Underground Navigation..... | 76 |
| 4.9. | Conclusion .. | 81 |
| References | | 100 |
| 5. | CONCLUSIONS AND FURTHER WORK..... | 102 |
| 5.1. | Summary | 102 |
| 5.2. | Sponsor Problems | 104 |
| 5.3. | Recommendations for Further Work | 104 |
| A. | SURVEY RESULTS..... | 106 |
| B. | CO-ORDINATE SYSTEMS..... | 119 |
| C. | FIELD TRIALS | 121 |
| D. | UNDERWATER MEASUREMENTS | 124 |
| E. | UNDERGROUND ANTENNA MEASUREMENTS | 125 |
| F. | COMPLEX DIELECTRIC CONSTANT MEASUREMENTS | 126 |

Mathematical Symbols and Constants

| | |
|----------|--|
| a | radius of wire antenna |
| b | outer radius of single insulating layer |
| c | outer radius of second insulating layer |
| d | vertical distance from horizontal antenna to air-earth boundary |
| E_ρ | radial electric field |
| E_ϕ | transverse electric field |
| f_{re} | reflection coefficient, electric polarisation |
| f_{rm} | reflection coefficient, magnetic polarisation |
| h | half length of dipole antenna |
| h | full length of monopole antenna |
| h_e | effective length antenna |
| i | $-j$ |
| j | $\sqrt{-1}$ |
| $I(z)$ | current distribution on linear antenna |
| k | complex wave number |
| k_L | complex wave number of line |
| l | series inductance per unit length |
| r | radius of ground screen of a monopole antenna |
| S | Pointing vector |
| V | terminal voltage |
| X | input reactance |
| x' | internal reactance per unit length |
| Y | driving point admittance |
| y_L | shunt admittance |
| Z | input impedance |
| z | vertical distance from underground/water antenna to air boundary |
| Z_L | load impedance |
| z^e | series external impedance per unit length |
| z^i | series internal impedance per unit length |

| | |
|-----------------------------|--|
| z_{12} | mutual impedance |
| β | phase constant |
| β_L | phase constant in line |
| ϵ_r | complex relative permittivity |
| $\epsilon'_r, \epsilon''_r$ | real and imaginary parts of ϵ_r |
| ϕ | azimuth angle |
| λ | wavelength |
| λ_0 | wavelength in free space |
| μ_r | relative complex permeability |
| μ_0 | relative complex permeability in free space |
| σ | complex conductivity (in S/m: 1 S/m = 1 mho) |
| σ', σ'' | real and imaginary parts of σ |
| ω | angular frequency |

1.Introduction

This thesis was initially inspired by the need for a system that can locate and trace the movements of an underground micro-tunnel drilling machine. This machine is used for laying pipes and cables. Its direction can be steered by an operator. Use of a micro-tunnelling machine makes it unnecessary to dig a trench in the road. As the financial cost and also the social cost of this type of roadwork is high, there is a growing demand for 'trenchless' pipelaying. Furthermore, laying an underground pipe or cable that crosses a railway line or a river can be very difficult with conventional techniques. The best system available to locate the drill is based on magnetic induction, in which a coil on the drill generates a magnetic field underground that is received by a coil on the ground surface, above the drill. The requirement of the receiver to be positioned above the drill is its limitation. The work described in this thesis is an examination of the possibility of using electromagnetic waves to trace the underground drill. In addition the thesis describes the analyses the problem of underground navigation using electromagnetic waves through experiments and simulations. The simulation model and the measurement procedures developed in the research are tools that can be used in the development of a commercial system.

1.1. Background

The project described in this thesis aims to research into a method of remote positional control for steerable drills and surface directional drilling technique, by radical development of existing location technology and research into new techniques. At present, location of the drillhead is effected by a transmitter fitted into the drilling head transmitting a signal to a hand-held receiver placed directly above the line of the drilling operation. The maximum distance between drillhead and receiver is 6 m, which is the limitation of the system.

There are different systems for the position control of a micro-tunnelling machine. Many of them are based on the use of different sensors to detect the drill's position. Some position control systems are based on measuring the displacement of the drilling machine mechanically [1]. The use of magnetic induction is most common. [2-3] In such a system, two coils, with their axis perpendicular to each other, are attached to the drill. The magnetic field generated by these coils is detected by an operator above the ground. The position of the different coils makes it possible to also detect the rotation and the elevation. The strength of the magnetic field is a measure of the depth of the drill. The maximum range is approximately 6 m, up to a depth of approximately 2 m. Adding a gyroscope to the magnetic induction system will improve its accuracy [4].

Another proposed method of positioning control is based on measuring the earth's gravity and magnetic field vectors [5,6]. But the vibration noise during the drilling and the circular movement of the drill makes it difficult to signal process the output of actuators. One method of solving that problem is the use of fuzzy reasoning in combination with the above mentioned sensors [7]. However, this system has been shown to work only in very limited situations. Hence, in 90% of the drillings, the drill is located using the magnetic induction system. Long range boring rigs working on a 2 or 3 km long bore under a railway or river can give an electromagnetic transmitter information system in addition to the traditional, accelerometers, magnetometers and inclinometers [8]. The transmitter is switched on when the bore is nearly completed so that the tool can be guided to a set end position. The literature survey confirms the need for an accurate system that can position the drill remotely

An application related to underground positioning is radar. Georadar is based on electromagnetic wave propagation in soil [20-23]. The frequency used is in the range of 500 MHz to 2 GHz. In some cases more frequencies are used when surveying a particular site. The depth of penetration in the ground ranges from 3 m to 6 m, depending on the moisture content of the soil, when using power levels up to 2 W. The radar has to be positioned on the ground surface, above its target. Penetration depths of 1 km or more have been achieved in the desert for water detection. The transmitter antenna is positioned very close to the receiver antenna to achieve an angle of incidence with the boundary between air and ground of $\approx \frac{1}{4} \pi$ for both the incident and the reflected waves.

1.2. Aim of the Thesis

The main objective of this thesis is to analyse and explore the possibilities for measuring the displacement of an underground transmitter using electromagnetic waves. In this system it is assumed that the starting position is known. The thesis reports on the results of a significant number of field trials. The areas examined are: optimum antennas for use underground, dielectric constant and conductivity of soils, propagation modes of electromagnetic waves underground and their attenuation and the optimum frequency to use.

The objective of developing tools that can be used to predict underground propagation is for the development of a commercial system and also to aid future examinations of this fascinating field and other similar areas.

1.3. Work Done

One objective of the study was the reception of an electromagnetic wave from a source underground at up to 30 m distance and up to 1.5 m deep. To achieve this, careful study of the soil dielectric constant and conductivity, the characteristics of an antenna underground and the modes of propagation underground, was done.

For understanding the modes of propagation of the electromagnetic wave underground, it was necessary to know the environmental conditions of the medium the wave travels in. One of the major problems in the study of underground propagation was the uncertainty of what is underground. Chapter 2 discusses a method that has been developed in which the dielectric constant and conductivity was determined on-site. The research shows that when the sample was wet, the water bonds with the soil particles and changes its dielectric behaviour. The magnitude of the complex dielectric constant increases and becomes frequency dependent. An extensive site survey was done in which samples are taken to a depth of 2 m. The results were used in simulations of the performance of dielectric loaded wire antennas and in the predictions of underground electromagnetic wave propagation.

The antennas used in this project were thin wire antennas such as the monopole and the dipole. Using a wire antenna in a lossy dielectric, like soil, resulted in current leaking out into the medium, changing the current distribution, and hence the antenna gain, antenna pattern and impedance which became a function of the surrounding medium. This effect was reduced by placing a dielectric shield around the antenna filament. Dielectric loaded wire antennas are analysed in chapter 3. Various different antennas were constructed and tested. The measured results showed good agreement with the simulations.

Calculations showed that the attenuation of a plane wave underground was approximately 10 to 15 dB per m, except at VLF when the attenuation is less. Chapter 4 is an examination of the modes of propagation of the electromagnetic wave underground. Although the attenuation was high, an electromagnetic wave was received from an underground transmitter located at 30 m distance. This chapter further analyses the modes of propagation and finds an optimum frequency range. A simulation tool was developed and used to understand the results from the field trials. Based on the field trials and predictions a feasibility study was done on underground navigation and location using electromagnetic waves.

Concluding remarks and ideas for future work are outlined in chapter 5. Appendix A describes the site survey in which the dielectric constant and conductivity of samples were measured. Appendix B further explains the co-ordinate systems used in the thesis. The conditions and environment in which the field trial took place are explained in appendix C for underground propagation, appendix D for underwater propagation and appendix E for measurements of wire antennas underground.

References

- [1] Flowmole Corporation, "Method and apparatus for instalment of Underground utilities," Patent ,Espace 86/037, EP 0195559 A1 860924
- [2] Berringer, I. "Rohrvortriebssystem mittels elektromagnetischen Messeinrichtung". Vortrag im HdT Essen, Germany, November 1984
- [3] Gas Research Institute, "Control system for guiding boring tools and a sensing system for locating the same," Patent, Espace 91/0038 first 91/003, EP 0428180 A1 910522
- [4] Tomohiro, K , Kazuyoshi, K. and Yoshihiko, N. "A New Position Detection System for Microtunneling using a Mounted Optical Fibre Gyroscope," in *No Trenches in Town*, edited by J P. Henry and M.Mermet. *Proceedings International Conference NO-DIG '92* Paris 12-14 October 1992
- [5] McDonald, W.J. , Pittard, G. T. and Steele, C.G. "Accurate Remote Guidance Instrumentation for Directional Boring," *International NO-DIG '92 Washington D C* April 5-8 1992. section L1, pp.1-13
- [6] Harrison, W.H. and Rubin, L.A. "New Low Cost Cableless Steeringtools for Directional Drilling," *International NO-DIG '92 Washington D C*. April 5-8 1992. Section L2. pp 1-4.
- [7] Kawakami, K. et al. "Microtunneling System Employing Fuzzy Logic Reasoning for Directional Control," Nippon Telephone and Telegraph.
- [8] Garnett, A.F., "Electromagnetic Location and Monitoring Technology," *NO-DIG '90 Osaka, 6th International Conference on Trenchless Construction for Utilities* 16-17 October 1990.

2. Dielectric Constant of Soils and Rocks

2.1. Introduction

To investigate the propagation of electromagnetic waves in the ground, it was necessary to have a method available to measure the electrical properties of soils in the frequency domain, especially the loss, in the search for an optimum frequency for transmitting a VHF radio wave through different layers of soil using low power. As soil materials, whether moist or not, were usually in-homogeneous mixtures, often containing more than one substance, it was difficult to understand their electrical behaviour. It was not the aim to understand this process completely, but the soil electrical properties were investigated, as these were input parameters for the simulation model for antennas in the ground and underground electromagnetic wave propagation. The dielectric constant and conductivity of the soil determines the strength of the strongest signal received, the velocity at which it propagates and the path it travels. The propagation loss and the frequency dispersion are calculated in chapter four, based on the results presented in this chapter.

Three methods were developed whereby the dielectric constant was estimated by using a coaxial probe, coaxial sample holder and wave-guide. Results were presented for a number of known soil materials. The coaxial probe measurement method was used in the field for a comprehensive survey at the site where underground propagation studies were done.

2.2. Dielectric Constant theory

All matter consists of molecules that contain charges. When the matter is exposed to an electric field there is force acting on these charges. An ideal dielectric contains only bound charges that influence the field in which they are placed. To derive the dielectric constant from Maxwell's field equation, the first step is the separation of the vectors \mathbf{E}

and \mathbf{H} in the equations. Then differentiate the equations with respect to time and substitute the one equation into the other gives the wave equation for a homogeneous plane wave:

$$\frac{d^2 \mathbf{E}}{dx^2} = \epsilon^* \mu^* \frac{d^2 \mathbf{E}}{dt^2} \quad \frac{d^2 \mathbf{H}}{dx^2} = \epsilon^* \mu^* \frac{d^2 \mathbf{H}}{dt^2} \quad (2.1)$$

The wave propagates in the x-direction. The equation is simplified by assuming that \mathbf{E} and \mathbf{H} are a function of x and t only. Solutions of the wave equations are in the form:

$$\mathbf{E} = \mathbf{E}_0 e^{j\omega t - \gamma x} \quad \mathbf{H} = \mathbf{H}_0 e^{j\omega t - \gamma x} \quad (2.2)$$

The wave propagates in the x-direction with a complex propagation constant:

$$\gamma = j\omega \sqrt{\epsilon^* \mu^*} = \alpha + j\beta \quad (2.3)$$

The real part of the propagation constant α is the attenuation factor and the imaginary part β is the phase factor of the wave. The complex dielectric constant ϵ^* and magnetic permeability μ^* determine the storage and dissipation of electric and magnetic energy in a medium. The ratio of the coupled electric and magnetic field vectors, independent of x distance, for a plane wave is.

$$\frac{\mathbf{E}}{\mathbf{H}} = \frac{\gamma}{j\omega \epsilon^*} = \sqrt{\frac{\mu^*}{\epsilon^*}} = Z \quad (2.4)$$

This ratio Z is the intrinsic impedance of the dielectric. The propagation factor γ is proportional to $(\epsilon^* \mu^*)^{1/2}$, while Z is equal to $(\mu^* / \epsilon^*)^{1/2}$. These parameters are measured to find ϵ^* and μ^* individually. For this, both magnitude and phase of Z and γ have to be evaluated. The definition of the intrinsic impedance makes it clear that this value may depend not only on the physical properties of the medium, but also on the nature of the field, which propagates in the dielectric. In this study, the samples were assumed to be non-magnetic.

The complex dielectric constant ϵ_r^* is normalised to the dielectric constant of vacuum $\epsilon_0 = 8.85 \times 10^{-12}$ F/m, hence: $\epsilon^* = \epsilon_r^* \epsilon_0 = (\epsilon_r' - j \epsilon_r'') \epsilon_0$. In this equation ϵ_r'' is the loss factor. The conductivity is defined as $\sigma = \omega \epsilon''$ [1]. The conductivity quantifies ions of opposite polarity in pairs moving in the electric field according to Ohm's law. In the Maxwell equations and the associated boundary conditions ϵ and σ always appear in the following combination [2]:

$$\sigma + j\omega\epsilon = \sigma' + \omega\epsilon'' + j\omega\left(\epsilon' - \frac{\sigma''}{\omega}\right) \equiv \sigma_e + j\omega\epsilon_e \quad (2.5)$$

From (2.5) the real effective conductivity $\sigma_e \equiv \sigma' + \omega\epsilon''$ and the real effective dielectric constant $\epsilon_e \equiv \epsilon' - \sigma''/\omega$ are defined and will be used here. The conductivity is a measure of all the losses in the dielectric caused by the migration of charge carriers or the friction of aligning polar molecules. A damped microscopic oscillator emits a spectrum of frequencies because the oscillation dies out in a finite time. To consider the relations between \mathbf{E} and \mathbf{H} in time, the wave can be expressed in the space domain at time t_0 as:

$$\mathbf{E} = E_1 e^{-\gamma x} = E_1 e^{-\alpha x} e^{-j2\pi \frac{x}{\lambda}} \quad (2.6)$$

Expression (2.6) is graphically analysed in figure 2.1. The wave amplitude attenuates exponentially with α being the attenuation factor in figure 2.1.a. The polar diagram in 2.1.b shows the wave as a vector rotating in the clockwise direction and the displacement is expressed in radians. The attenuation per radian is called index of absorption and is defined as:

$$k = \frac{\alpha \lambda}{2\pi} = \frac{\alpha}{\beta} \quad (2.7)$$

The phase relation between the \mathbf{E} and \mathbf{H} field vectors can be derived from the impedance:

$$\text{if } \mathbf{E} = E_0 e^{j\phi_1} \text{ and } \mathbf{H} = H_0 e^{j\phi_2}, \text{ then } \frac{\mathbf{E}}{\mathbf{H}} = Z e^{j(\phi_1 - \phi_2)} = Z e^{j\xi} \quad (2.8)$$

When the dielectric is non-magnetic, ξ is the advance of the \mathbf{E} field vector. When $\mu''=0$, the index of absorption is equal to the phase advance and $\tan \xi = k$ [1]. Hence the phase of the intrinsic impedance is the arctan of the index of absorption. When a conductor is placed in an external electric field the free charges move to the surface and make the interior charge density and electric field vanish. The dielectric constant of a conductor can be modelled as $(1 - j\infty)$.

An ideal dielectric does not contain free charges but the bound charges have an effect on the electric field. All molecules consist of atoms that comprise positive nucleus surrounded by negative charged electrons. Electric forces on these charge carriers results in small displacement of the positive and negative charges in opposite directions. Although on a macroscopic level the dielectric is neutral, the displacement causes polarisation of the dielectric. These charge carriers can be electrons around the nuclei

(electronic polarisation) or the displacement of atoms in molecules with an uneven charge distribution (atomic polarisation). Some molecules, like water, have permanent dipole moments, due to asymmetric charge distribution around the molecules. These particles align to the incident E field polarisation. This is called orientation polarisation. Another form of polarisation occurs when the material exists of particles that have charges built up at their interfaces. This is the space-charge polarisation.

Debye [3] gave the theoretical analysis of the behaviour of a dielectric material containing molecules with a permanent dipole moment. This theory predicts that when such a material is placed in a DC electric field, the polarisation moment caused by the dipoles aligning to the field does increase exponential with a time constant τ . In the transition region of anomalous dispersion there is an absorption conductivity and the situation may be described in terms of a complex dielectric constant $\epsilon^* = \epsilon' - j\epsilon''$. The relaxation process is described by Debye by the equation [3]:

$$\epsilon^* - \epsilon_0 = \frac{\epsilon_0 - \epsilon_\infty}{1 + j\omega\tau_0} \quad (2.9)$$

where ϵ^* is the complex dielectric constant with a value of ϵ_0 at low frequencies and ϵ_∞ at high frequencies and τ_0 is a characteristic constant which is called the relaxation time. This suggests that the relaxation is independent of the frequency. However, experimental data of soils [4,5] has shown the dispersion frequency range to be narrower than predicted by (2.9) and the dispersion maximum to be higher. Their behaviour can be described with two relaxation processes:

$$\epsilon^* = \epsilon_{10} + \frac{\epsilon_{10} - \epsilon_{1\infty}}{(1 + j\omega\tau_1)^{1-\alpha_1}} + \epsilon_{20} + \frac{\epsilon_{20} - \epsilon_{2\infty}}{(1 + j\omega\tau_2)^{1-\alpha_2}} \quad (2.10)$$

where subscripts 1 and 2 refer to the two separate relaxation processes. The effect of α is to broaden the relaxation. Dispersion and absorption can also occur in non-homogeneous materials. Many dielectric materials do not show the behaviour as described by Debye. However, the relaxation process of water is very close to the one predicted by Debye and the contribution of water to the dielectric constant of moist soil is significant.

2.3. Background

Research into dielectric properties of rocks and minerals is focussed on various applications and the measured data published is valid for a limited frequency range. In

many calculations the electric properties of a soil are estimated. Knowledge of the electrical properties of a soil is of great importance for underground radar or communications, remote sensing and geophysical prospecting. Remote sensing is used to estimate the moisture content of the soil in order to predict quantities like crop yields. The skin depth of the electromagnetic radiation in the ground can be calculated from knowledge of the dielectric properties. In contrast to visible and infrared, microwave sensors are not affected by clouds, especially in the lower microwave frequencies and can function independently of weather or sunlight level. In geophysical prospecting the conductivity of the earth is important to measure the detailed structure of the ground. The corrosion of buried structures is due to an interchange of current between the corroding conductors and the environment. The current interchange is a result of potential differences causing stray currents in the earth. Also, the probability of a lightning strike hitting a particular point depends, among other factors, on the conductivity of the earth. Hence, publications in civil engineering journals focus on soil conductivity at low frequency.

In 1934 Smith and Rose [6] measured the dielectric constant of moist soil at $f=50$ Hz and concluded that $\epsilon_r = 100\,000$ at this frequency. Electrodes were used in the measurement. For a long time dielectric constant measurements of moist soil samples were difficult to make and the high values of the moist samples have been attributed to measurement errors caused by electrochemical processes at the electrodes. Measurements [7] conducted with an electrode in a specially designed sample holder were in the frequency range of 100 Hz - 1 MHz. The resistance of earth varies within extremely wide limits between 1 and 10000 Ω/m . The dielectric constant of dry soil samples varies from 2 to 15 at 100 Hz [7]. For samples with higher water content, the dielectric constant and the conductivity increase over the measured frequencies [7]. The dielectric constant of moist sand ($w=2.34\%$), is reported to be significantly higher at 0.1 Hz ($\epsilon_r=1.65 \cdot 10^6$) while low at 5 MHz ($\epsilon_r=3.94$) [8]. Measurement of the sand after heating and vacuum drying alters the electrical properties of the sample significantly. In the frequency range of 0.3 - 1.3 GHz, the real part of the dielectric constant is frequency independent, while ϵ'' decreases with frequency between 0.3 and 0.5 GHz and is constant above 0.5 GHz. The dependence of ϵ' and ϵ'' on soil texture composition (sand, silt and clay fractions) is a consequence of the role played by bonded water.

Much of the published work on dielectric constant measurements of soils and civil engineering has been related to road construction. In particular the measurement of dielectric constant of base course aggregates in roads can be related to moisture content [9,10]. Also the dielectric constant is related to the strength and deformation properties of base coarse aggregates [9]. There appears to be a very good correlation between the dielectric properties and strength and deformation properties of all types of soils and aggregates. These results were based on DCP (Dynamic Cone Penetration) test and resilient modulus measurements on various materials ranging from iron ore graves to granites. As the strength of a soil depends in part on inter-particle attractions [11]: it would be expected, therefore, that the strength would also be influenced by the dielectric constant. The dielectric constant will change with moisture content for various reasons including the physiochemical properties of the soil, the proportion of solid, liquid and air phases and also the structure and void ratio of the solid phase [11]. Thus the relationship of dielectric constant of a soil sample to moisture content will be non-linear and dependent on soil type. It is investigated [12,13] to what extent the electrical properties of soils could be used to characterise the mineralogy, state of packing and area of contact for predicting engineering properties, explaining soil behaviour, and developing a classification of soils based on both composition and environmental parameters. Experiments carried out show that there is a strong relationship between dielectric constant and clay mineralogy [12,13]. It is known that the cation-exchange capacity of clays increases in the sequence: kaolinite < illite < montmorillonite. This sequence is also clearly shown when dielectric constant is plotted against frequency. It is also investigated how the dielectric constant is affected by different sand-clay mixtures, changes in water content, and the effect of adding sodium chloride to the water within the soil. The sand-clay mixtures showed a decrease in dielectric constant with increase in sand content. The dielectric constant decreases with decreased water content. The addition of sodium chloride to the water decreases the dielectric constant.

2.4. Measurement techniques

Various methods for measuring the dielectric constant of materials have been proposed, in which the sample is put into a sample holder [14-16]. The disadvantage of using a sample holder is that the preparation of the sample has to be done very carefully in order not to disturb the sample density and to avoid any air gaps between the sample and the holder. In

[17] a coaxial probe is used to measure the dielectric constant of soil in the frequency range of 0.3 - 1.3 GHz. In this method a semi-empirical model is used to predict the complex dielectric constant of a sample. The model is shown to be valid for three types of clay samples with various moisture contents. The method proposed by Athey [18] also makes use of a coaxial probe to measure the complex dielectric constant of high loss and low loss materials. The complex dielectric constant is derived from the measured probe impedance which makes this method more straightforward compared to [17].

2.4.1. Coaxial probe

For this study, the method proposed by Athey [18] was used. The probe used was made of a semi-rigid cable with a specific length. The open-ended probe capacitance was modelled as a two parallel capacitance's circuit to ground. These represent the transmission line capacitance and the fringing field capacitance. This fringing field capacitance, C_f , models the reactive near-field, which was the electromagnetic field at the interface with air at the probe end. When the probe was terminated with the sample, the relative dielectric constant can be calculated from the reflection coefficient using the equation [18]:

$$\epsilon_r^* = \frac{1 - \hat{\Gamma}}{j\omega Z_0 C_0 (1 + \hat{\Gamma})} - \frac{C_f}{C_0}, \quad (2.11)$$

where ϵ_r^* is the complex relative dielectric constant,

$\hat{\Gamma}$ is the complex reflection coefficient,

Z_0 is the transmission line impedance,

C_f is the fringing field capacitance and

C_0 is the transmission line capacitance at the open end.

At frequencies below 2.0 GHz, C_f can be assumed to be negligible small and ϵ_r can be found from the reflection coefficient, when Z_0 and C_0 are known. The coaxial probe used in the measurement was a 3.6 mm diameter open-ended semi-rigid cable with a length of 0.049 m. The semi-rigid cable was a standard cable used in microwave measurements. The probe was made by connecting a standard SMA (Semi Miniature-A) connector to one end of the cable and then trim the cable's length. The magnitude of $\hat{\Gamma}$ at the point of measurement also depends on the probe's length. Three probes were made with lengths of 0.049 m, 0.055 m and 0.106 m. The one with 0.049 m length gave the best results, based on the measurement of distilled water and methanol, which were compared with

published results. A probe with these dimensions was suitable for measuring high-loss materials at frequencies up to 2.0 GHz. The dimensions of the probe have to be small compared to the wavelength, so the open end does not radiate out other than the fringing field. The end of the probe was polished to get a slight tapered end to ensure good contact with the sample, but also to increase the fringing field. The conductivity was calculated from the dielectric loss factor.

Calibration

Two vector analysers, the HP8410 and HP4195 were used to measure the reflection coefficient. Before the measurement started, a 'three standard' error correction model was used to improve the accuracy of two vector analysers. These standards were a conventional matched load, an open/short circuit and the probe in contact with a known dielectric. These standards were used as the outcome of these measurements could be calculated and, therefore, the accuracy of the measurements could be determined. The matched load was used to determine the directivity error. Then, the probe was connected and the 'probe-open' and 'probe-short' were measured to find the source mismatch and the frequency tracking errors. Initially, an open circuit capacitance was assumed. In the calibration procedure this value was adjusted in order to find the smallest difference between the measured and theoretical values of the dielectric constant of distilled water. The theoretical values were calculated using the Debye equation for distilled water. For our probe two values of the transmission line open-end capacity C_0 , 0.0185 pF and 0.0215 pF, gave the smallest error, when using the HP8410 and HP4195 respectively. The comparison between the measured and predicted value is shown in Figure 2.3. The dielectric constant of methanol was measured and compared with published data [9] as an additional test in the calibration. The maximum error was under 4%. A reason for this might have been the mismatch between the connector and the probe, as the magnitude of the reflection shows a rippled pattern. The imaginary part of the dielectric constant of distilled water shows an error at frequencies above 300 MHz. Therefore, the HP4195 ANA was used in the frequency range of 1.0 MHz to 300 MHz, taking a total of 200 measurement points. The frequency range of 60 MHz to 2.0 GHz was covered by the HP8410 ANA, taking 250 points. The dielectric constant of distilled water was measured as a part of the calibration procedure, before every measurement. As movement of cables

resulted in different measurement results, the probe was fixed in a clamp. The measurement set-up was used on-site for field measurements.

2.4.2. Sample preparation

The samples used in the measurement are taken from various sites or prepared in the laboratory. The samples were kept in airtight containers to maintain their moisture content constant. After the measurement the moisture content was established by measuring the mass of the moist sample: placing it in an oven for 16 hours, and finally measuring the mass of the dry sample. The gravimetric water content was calculated as:

$$w = \text{mass H}_2\text{O} / \text{mass dry sample} \quad (2.12)$$

Clay samples were prepared in the laboratory by mixing dry clay with distilled water to create samples with various moisture content. The granular nature of dry samples makes it difficult to achieve a homogeneous density. Variations in dry density and, therefore, in volumetric water content were unavoidable. At least three probe measurements were taken from every sample and the average was taken as the final result.

2.5. Measurement results

The soil samples used were prepared from known materials with different gravimetric moisture content. The samples were: Wyoming bentonite clay, keuper marl clay, English China clay, Leighton Buzzard sand and river sand. The main difference between the samples was that the particle size of clay was smaller than that of sand, which has an effect on the binding forces between particles. This interparticle attraction was the result of two types of forces on soil particles that are related to its size: surface forces, like Coulomb forces, are proportional to the surface area, whereas gravitational forces are proportional to its particle volume. As particle size decreases, as with the clays, the surface forces become more dominant. As with clays, electric charges dominate the bonding of the particles, they were expected to be electromechanically more active than sands. Samples were prepared with a different moisture content. Due to the granular nature of soils, the dielectric constant is also a function of the equilibrium void ratio at different pressures in the sample. The pressure in the sample was very difficult to control, resulting in a limited repeatability of the measurements. Therefore, from the substantial number of data some typical results have been selected to illustrate the dependence of the complex dielectric constant on the frequency, soil type and moisture content.

In figure 2.5, the plots for keuper marl and English China clay with moisture content of approximately 20% are compared with plots of clay-loam [20]. The lines for the dielectric constant in figure 2.5 presents the Weighted Least Square of the measurement data. The dielectric constant of the samples with a very similar moisture content differs in magnitude, but show a similar curve. The dielectric behaviour of soils below 100 MHz was attributed to the orientation polarisation of the soil particles. Above 100 MHz, the speed of the particle alignment was falling behind the electromagnetic wave polarisation resulting in a decrease in the effective dielectric constant. At frequencies above 100 MHz, the response of the sample to an incident electromagnetic wave was mainly ionic polarisation. This explains the increase in conductivity at the higher frequencies, shown in figure 2.5.

In these measurements, keuper marl shows the highest dielectric constant, which suggest that the particle size of keuper marl was smaller than that of China clay and therefore the particle alignment was slower as the Coulomb forces were stronger. But the dielectric constant of soil also depends on soil density [20]. During the measurements the density of the samples was kept constant. Nevertheless, a smaller particle size may result in less air gaps between them, resulting in a higher density, which will be measured as a higher effective dielectric constant. Figures 2.5 shows that there is good agreement between the measurements and the published data. Especially the trend of an increased dielectric constant with decreasing frequency from 200 MHz down to 60 MHz was seen in all the clay measurements. The samples in figure 2.5 have similar moisture content. The line for the conductivity is the average value of the measurement points. The conductivity represents all loss in the dielectric. This may be caused by migrating charge carriers as well as energy loss associated with the friction accompanying the orientation of dipoles. Charge carriers in soils can be magnesium, calcium or sodium. Figures 2.6 shows the measurement results for keuper marl samples with different moisture contents. When the sample is wet, the water bonds with the soil particles and changes its dielectric behaviour. The magnitude increases. The curve is steeper between 1.0 MHz and 400 MHz, when the moisture content increases. More water molecules bond to the soil particles. The plots show that the bonding of water makes the soil electrical properties frequency dependent as only relatively dry soil show a fairly constant dielectric constant and conductivity. For all the samples examined in the experiment, the dielectric constant increased with moisture content. The dielectric constant of wet clay reached about 40 at 1.0 MHz, while its value

is about 36 at higher frequencies. At 2.0 GHz the highest conductivity measured was 0.7 S/m. The measurement results of English China clay confirmed these observations. The dielectric constant of Bentonite was very high at low frequencies, being near 100 at 1 MHz, when the sample is wet. The conductivity increased with frequency.

The real part of the dielectric constant of River sand was not frequency dependent. Increasing the water content increases the dielectric constant also. When the sand was wet the imaginary part was frequency dependent, being near 50 at frequencies below 100 MHz. The conductivity increased with frequency, being near 0.02 S/m when the sample was moist ($w=20\%$). The plots of Leighton Buzzard sand show a very similar result. The dielectric constant of dry samples, both clays and sands, varies between 4 - 8, while the conductivity was close to zero.

2.5.1. Relaxation model

Analysis of the graphs for moist soil show a trend towards a relaxation curve as described by one or two Debye relaxation models. The relaxation process of water is very close to the one predicted by Debye and the contribution of water to the dielectric constant of moist soil is significant. This suggests a major contribution of the relaxation process to the dielectric constant. Therefore, it was investigated what relaxation curve fits the data by estimating ϵ_0 and τ_0 and taking ϵ_∞ from the measured data at 2 GHz.

As shown in figure 2.8 there was a good agreement between the measured data for the keuper marl sample with a moisture of 21.3% and the relaxation curve. In this graph, the relaxation process was modelled as one relaxation, as given by equation (2.9), with $\tau_0 = 6 \cdot 10^{-10}$, $\epsilon_0 = 100$ and $\epsilon_\infty = 26$. At $f = 2\text{GHz}$, the relaxation model predicted ϵ'' to reduce to nil. At this frequency the nature of the relaxation process changes, as ionic polarisation becomes dominant. The relaxation time of water is $\tau_{\text{water}} = 0.25 \cdot 10^{-10}\text{s}$ [1]. A relaxation time longer than that of water suggest that the rotating unit involved in the relaxation process was bigger than the water molecule. Figure 2.9 shows the measured data for keuper marl with a moisture content of 11.3%. The curve fits the measured data only when the dielectric constant was predicted using two relaxation processes. For this sample $\tau_{10} = 5 \cdot 10^{-10}\text{s}$, $\epsilon_{10} = 220$, $\epsilon_{1\infty} = 5$ and $\tau_{20} = 1 \cdot 10^{-10}\text{s}$, $\epsilon_{20} = 28$, $\epsilon_{2\infty} = 13$. Samples with intermediate moisture content tend to be inhomogeneous for particle size. Clay particles clumped together where the moisture was, while other parts remain dry. A distribution in

the sizes and shapes of the granules will tend to extend the losses over a large frequency band. Therefore the relaxation was modelled with two relaxation processes. Finding a relaxation curve to fit data of a relatively dry sample, as in figures 2.10 and 2.11 where the moisture content of keuper marl is $w=1.5\%$ and $w = 6.5\%$ respectively, was difficult. Between 1 MHz and 300 MHz the curve fits the measurement points in the graph. The discontinuity in the measured data above 300 MHz was caused by a measurement error. Due to the granular nature of in particular these samples, the repeatability of the measurement is reduced. The dielectric constant bentonite clay was predicted with two relaxation processes as is shown in figure 2.12. For this prediction $\tau_{10} = 4 \cdot 10^{-11} \text{ s}$, $\epsilon_{10} = 35$, $\epsilon_{1\infty} = 4$ and $\tau_{20} = 8 \cdot 10^{-11} \text{ s}$, $\epsilon_{20} = 12$, $\epsilon_{2\infty} = 6$. The moisture of the sample is 9.6%. Figure 2.13 shows the dielectric constant for China clay sample with a moisture content of 22.8%. This prediction was done with two relaxation processes with the parameters: $\tau_{10} = 2 \cdot 10^{-9} \text{ s}$, $\epsilon_{10} = 150$, $\epsilon_{1\infty} = 3$ and $\tau_{20} = 9 \cdot 10^{-11} \text{ s}$, $\epsilon_{20} = 17$, $\epsilon_{2\infty} = 10$.

2.5.2. Site Survey

Environmental factors are uncertainties in the research of underground propagation. Seldom it is known what is underground, what is the structure and type of the soil at a given location. A thorough site survey was therefore undertaken at the location where the underground propagation experiments were conducted. The distribution of the soil dielectric constant and conductivity were determined so as to be able to estimate general underground conditions.

Previous studies [21] show that the 24 hour average volumetric water content can be accurately found by sampling one hour before solar noon. Diurnal variation depends strongly on depth, irrigation times and other factors. The spatial soil moisture variability decreases with depth [22]. Published results [21, 22] suggest that the number of samples required to get accurate information on moisture decreases with depth, being 25 – 35 samples at $d=1\text{-}2\text{ cm}$ depth to 7-10 samples at $d=30 \text{ cm}$ in a field of 40 acres. In conducting the site survey at Loughborough University campus a hollow pipe was drilled into the ground at 12 locations as shown in figure 2.15, to a depth of 2 m. Then the pipe was pulled out of the ground and samples were taken from inside it through a side-slot. The samples were virtually undisturbed. The samples were taken at locations that correspond to depths of: 0.10, 0.25, 0.50, 0.75, 1.00, 1.25, 1.50, 1.75 and 2.00 m. Two samples were taken at every depth and the average dielectric constant was taken as the

final value for that depth and location. The area of the site is 600 m² or 0.15 acre. The samples were taken between 11 a.m. and 3 p.m. on two consecutive days in March 1996. The results for the site survey are illustrated in the form of contour graphs in figures 2.16 to 2.20, as listed in table 2.1.

| Figure | Parameter | Range | Frequency |
|--------|--------------|--|-----------|
| 2.16 | σ | $0.34 \text{ S/m} < \sigma < 0.41 \text{ S/m}$ | 1 MHz |
| 2.17 | ϵ_r | $31 < \epsilon_r < 65$ | 1 MHz |
| 2.18 | σ | $0.34 \text{ S/m} < \sigma < 0.41 \text{ S/m}$ | 146 MHz |
| 2.19 | ϵ_r | $9 < \epsilon_r < 24$ | 146 MHz |
| 2.20 | σ | $0.34 \text{ S/m} < \sigma < 0.41 \text{ S/m}$ | 300 MHz |
| 2.21 | ϵ_r | $3 < \epsilon_r < 20$ | 300 MHz |

Table 2.1 Range of the dielectric constant and conductivity as derived from the results of the site survey

The graphs show the soil electric properties in the vertical plane using results from locations A1 to A4, as shown on the map in figure 2.15. The results for the vertical plane at locations B and C and the horizontal graphs for different depth are included in Appendix A. At the start of the research it was anticipated that the soil consisted of stratified layers of dielectric mediums. However, figures 2.16 to 2.21 show that this was not correct for the site under investigation. The soil structure here had a more circular character, with the highest conductivity in its centre, as shown in figure 2.16. For all graphs the conductivity varies between 0.34 S/m and 0.41 S/m. The relative dielectric constant changes per frequencies, the range being the smallest at 300 MHz. This suggests that the wave impedance for an electromagnetic wave travelling through the medium changed less at 300 MHz, compared to the discontinuities at lower frequencies. Hence less reflection and refraction was expected at this frequency. Many intrinsic and extrinsic factors were responsible for this variation because bulk density, soil texture and water content have the same level of variation [23]. These results (for a field considered to be generally uniform) indicate the intrinsic level of variability of soil water properties. The distribution of the dielectric constant and conductivity are shown in figures 2.22 and 2.23. At 1 MHz, 80% of the samples have a dielectric constant in the range of $\epsilon_r = 26 - 65$ (a variation of 39). At 146 MHz this is $\epsilon_r = 5 - 26$ (21) and at $f=300$ MHz 80% of the

samples are in the range of $\epsilon_r = 3 - 22$ (19). The distribution of the relative dielectric constant was narrower at the higher frequencies. This means that the propagation constant varies less at higher frequencies, reducing the probability of reflections underground. The survey results were obtained at temperatures between 5°C and 20°C. Publications have shown the temperature dependence of the electrical properties of water, as are shown in figures 2.22 and 2.23. The conductivity shows a significant decrease at temperatures above 30°C at microwave frequencies. It is therefore expected that the conductivity of soils decrease with temperature because water plays an important role in its electrical properties. Measurements of moist soil samples at 10 GHz [4] indicated a temperature dependence of the dielectric constant and conductivity. The measurements were done in the temperature range of -20°C and 25°C. Between -20°C and just below 0°C, both the ϵ_r and σ were fairly constant. For wet samples, ϵ_r and σ increased sharply at 0°C, to level out in the temperature range from just above 0°C to 25°C. The change at 0°C was more apparent for wet samples. At subzero temperatures and also above 30°C, σ measured was lower than at 5°C - 20°C at which the samples in this study were measured. It is well possible that in the 150 - 300 MHz frequency range the same process takes place, resulting in a lower attenuation of the electromagnetic wave at these temperatures.

2.6. Conclusion

The coaxial probe used in the experiments was suitable for measuring the dielectric constant of high loss and low loss soil samples in the frequency range of 1 MHz to 2 GHz. The measurement system was portable, making it possible to conduct a survey on-site. No sample preparation was necessary. The dielectric constant of dry soil was not frequency dependent and was rated in between 4 - 8. Its conductivity was very low. This applies both to clays and sands. When the sample moisture was increased, its dielectric constant increases, being dispersed for clays, but fairly linear for sands. Wet samples exhibit a higher dielectric conductivity, being dispersed for both sands and clays. Clays showed a higher dielectric conductivity. The dielectric constant of soil may be as high as 50 at 1.0 MHz. Soil moisture content was an important factor of its dielectric behaviour, as was its grain size. A site survey had been conducted at the location where the underground propagation measurements were undertaken. The dielectric constant and conductivity was measured at 12 different locations and to a depth of 2 m. The iso-dielectric bars in the

graphs for the vertical plane show that the soil structure here had a circular character, with the highest conductivity and highest dielectric constant in its centre. The distribution of the relative dielectric constant was narrower at the higher frequencies. This suggests that the wave impedance for an electromagnetic wave travelling through the medium changes less at 300 MHz, compared to the changes at lower frequencies. Hence, less reflection and refraction was expected at this frequency. The dielectric constant and conductivity of soil was temperature dependent.

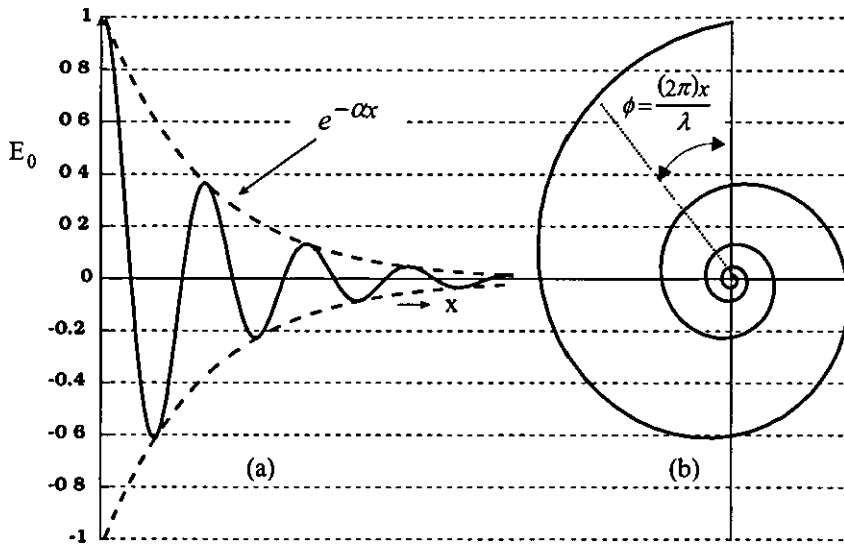


Figure 2.1 Electric wave propagating in the x-direction

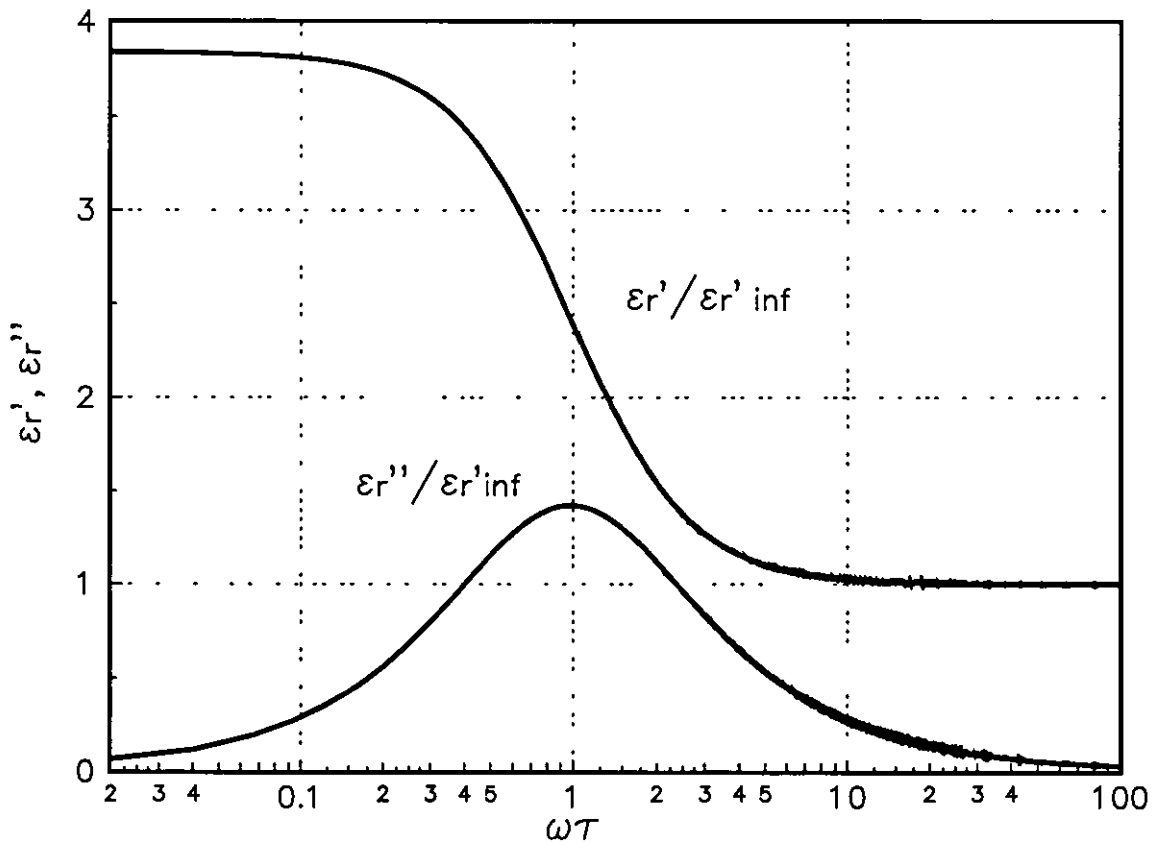


Figure 2.2 Relaxation curve for bk20 sample One Debye equation.

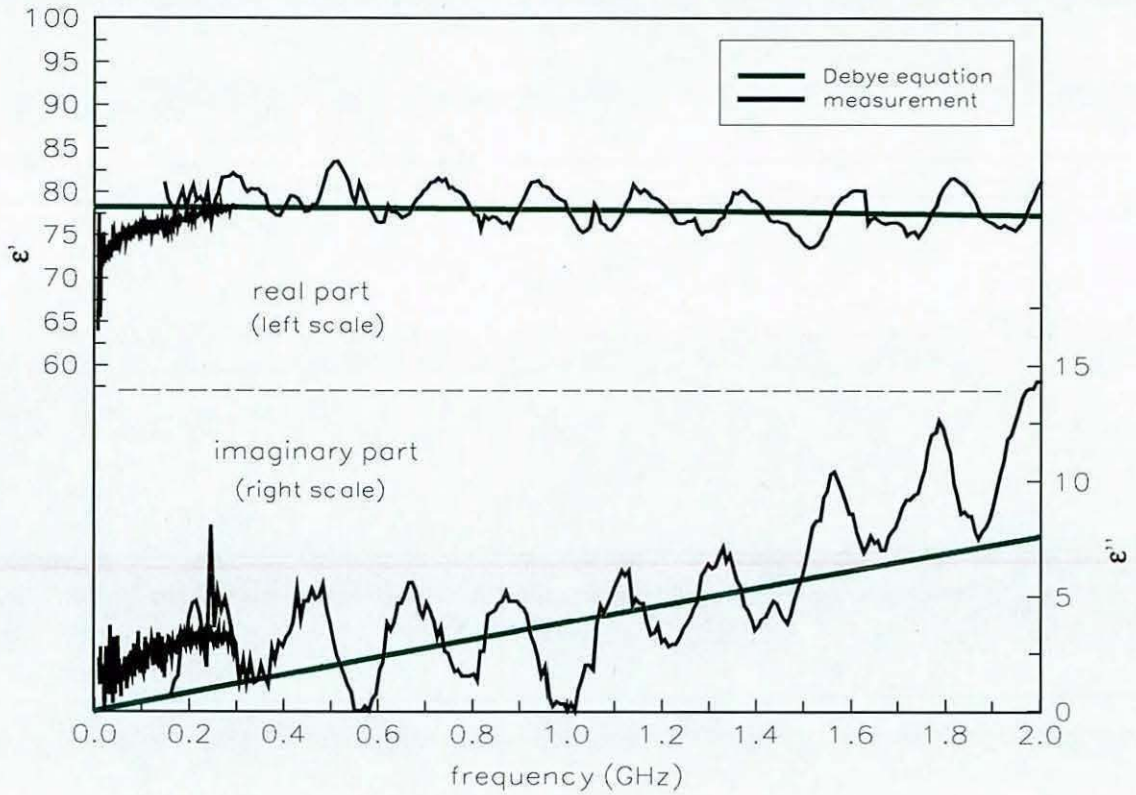


Figure 2.3 Distilled water compared with Debye equation

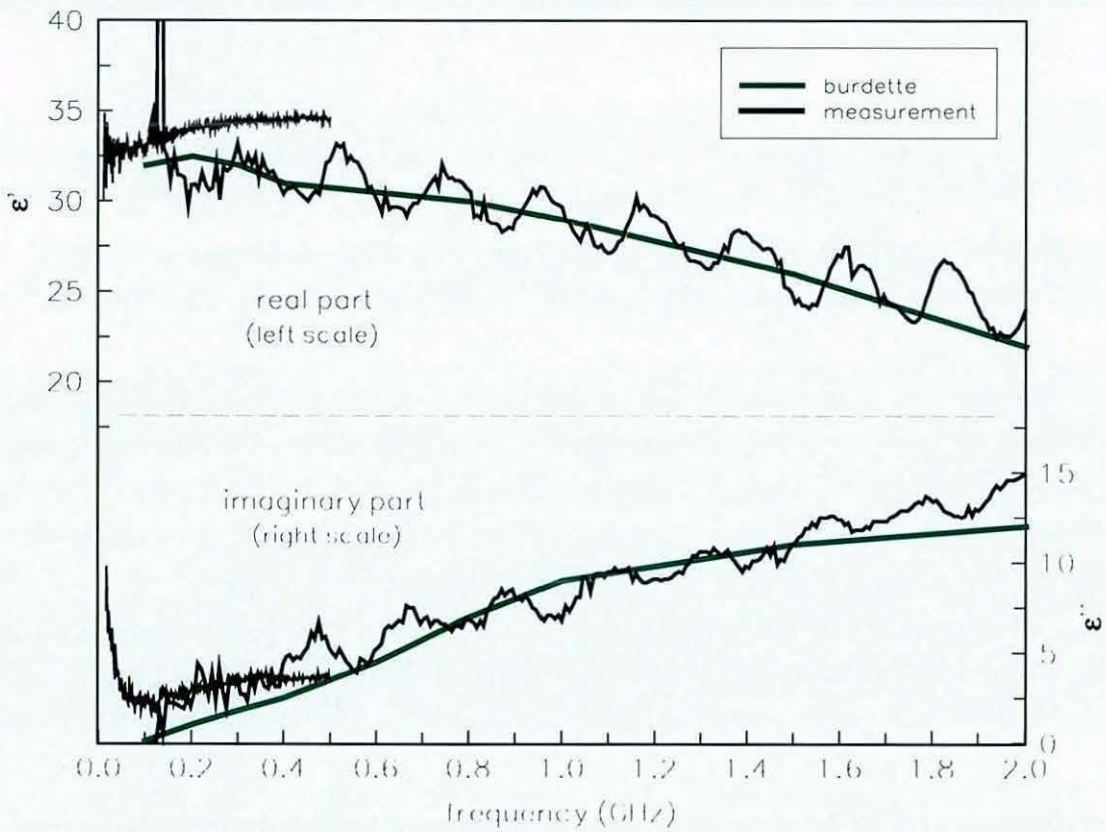


Figure 2.4 Methanol compared with results published by Burdette et.al. [9]

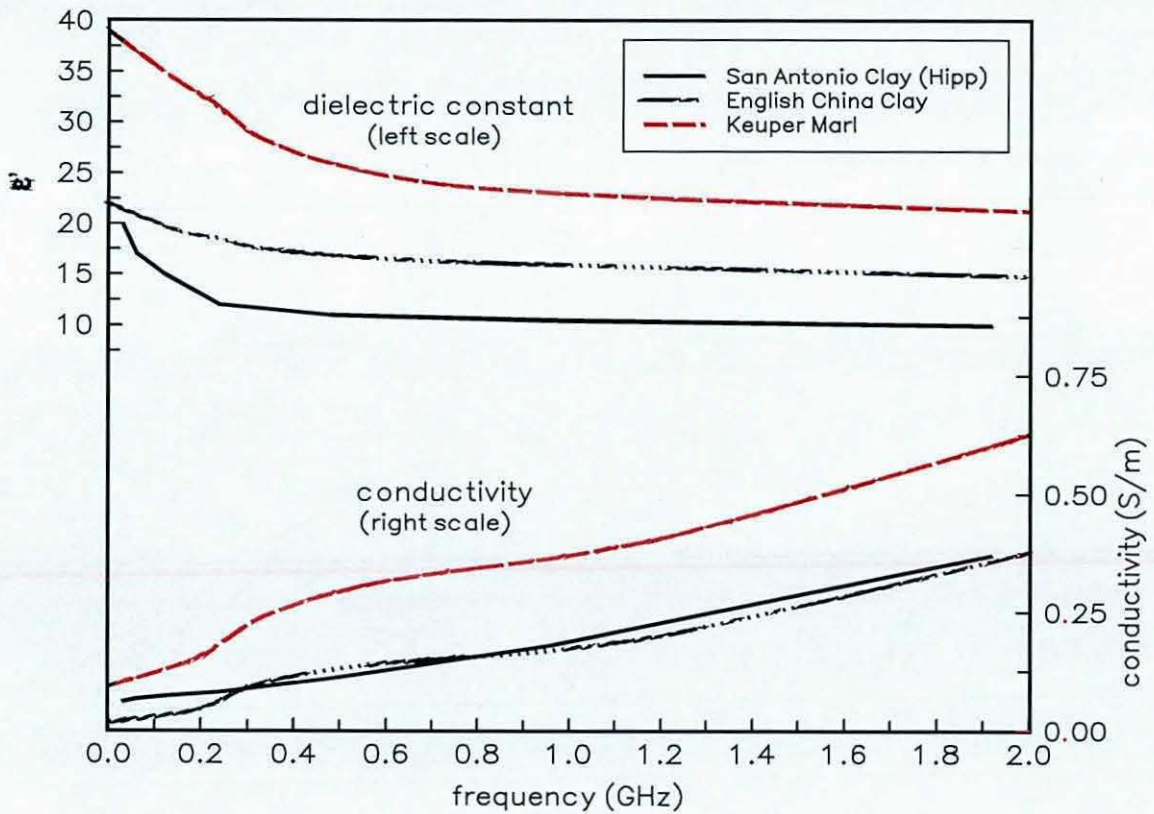


Figure 2.5 Weighted Square Root of experimental data of English China clay and Keuper marl, compared with data of San Antonio clay [19].

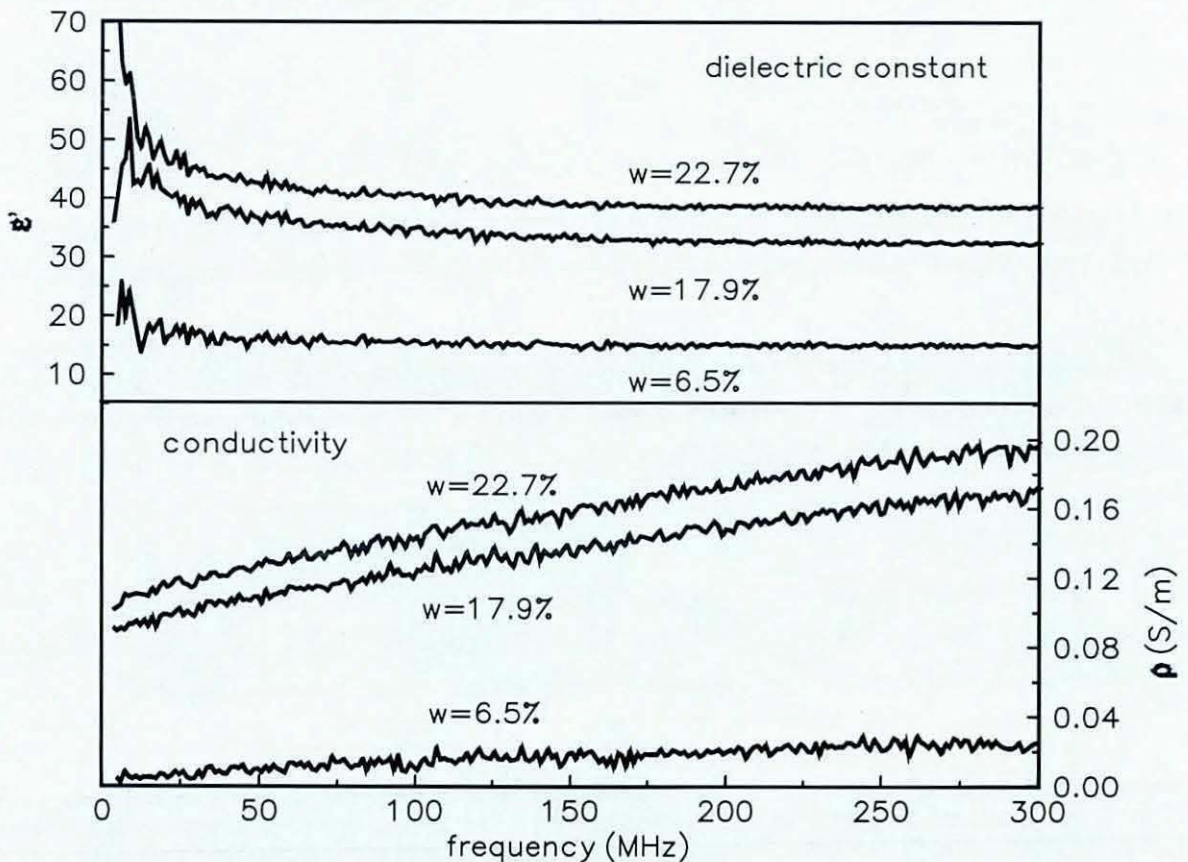


Figure 2.6 Dielectric constant and conductivity of Keuper marl samples with a different gravimetric moisture content

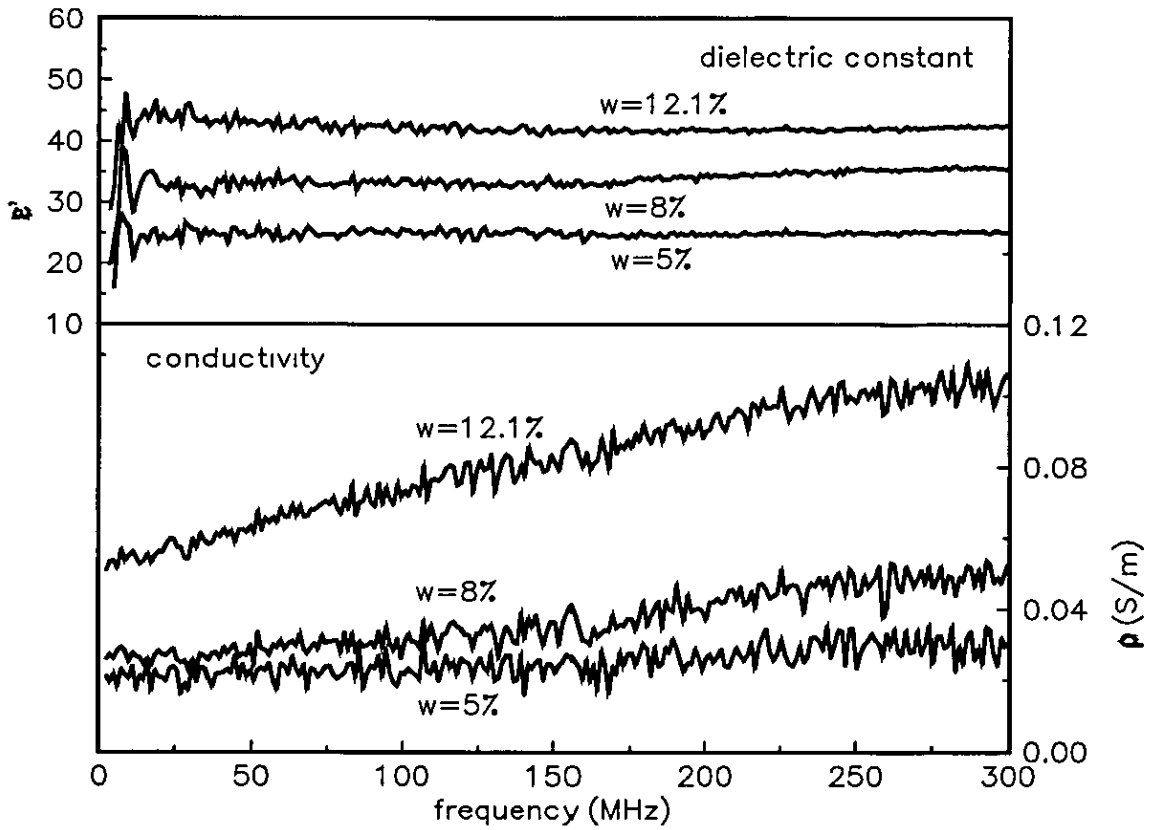


Figure 2.7 Dielectric constant and conductivity of Leighton Buzzard sand with a different gravimetric moisture content

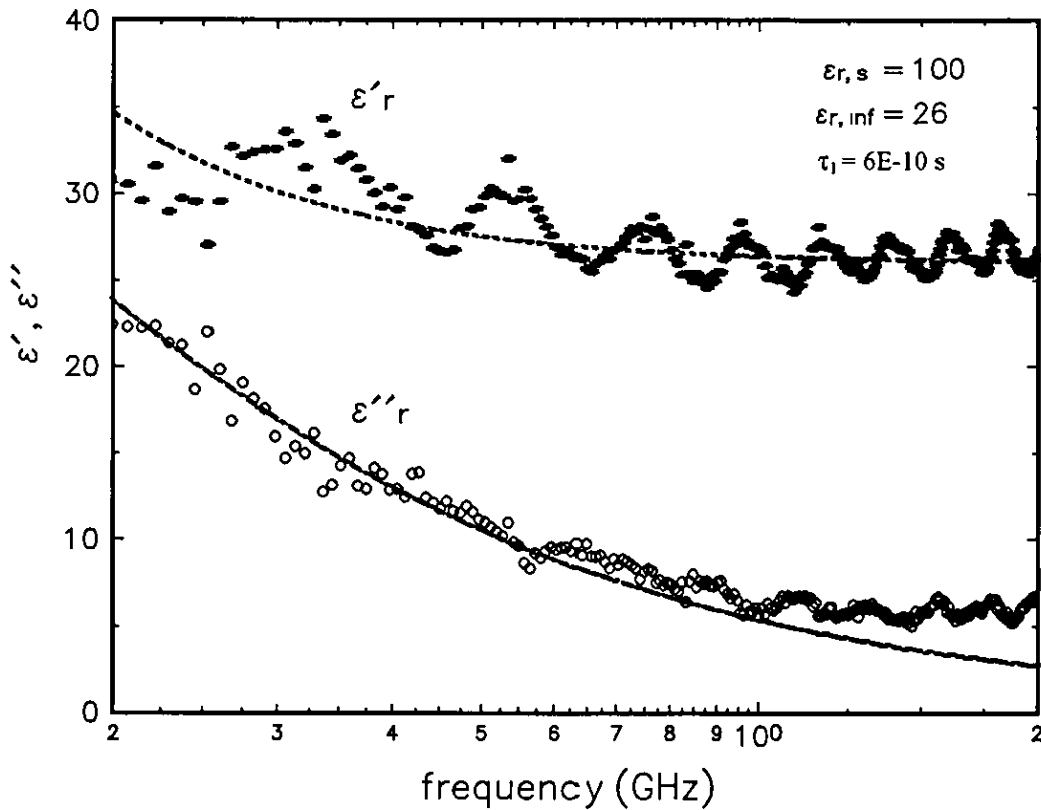


Figure 2.8 Relative complex dielectric constant of Keuper marl, $w = 21.3\%$ compared with relaxation curve using one Debye relaxation model

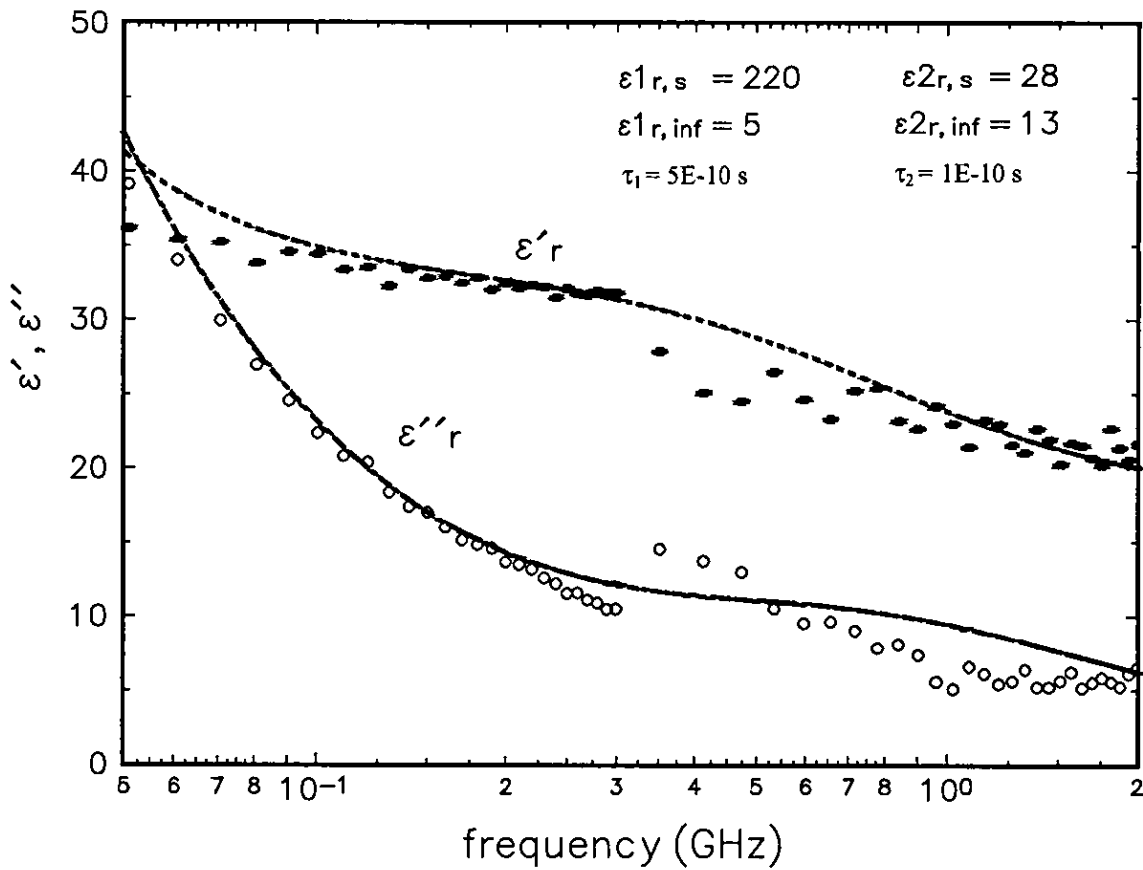


Figure 2.9 Relative complex dielectric constant of keuper marl, $w = 11.3\%$ compared with relaxation curve using one Debye relaxation model

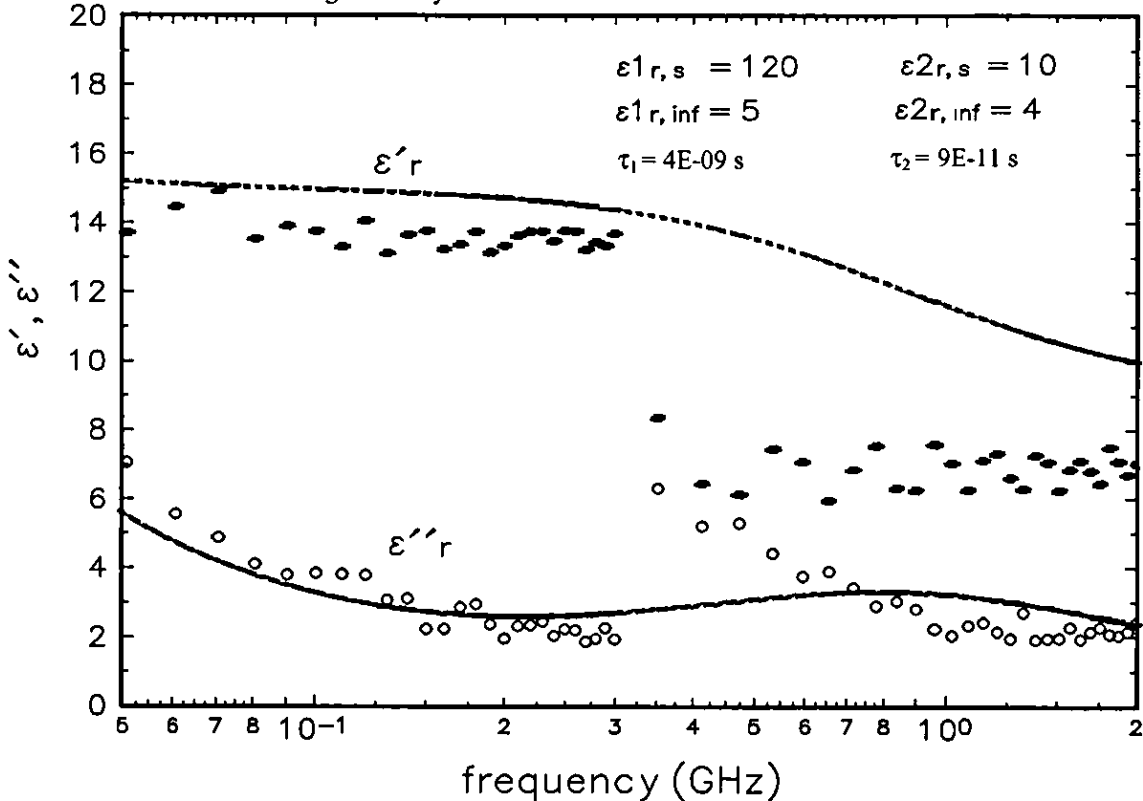


Figure 2.10 Relative complex dielectric constant of Keuper marl, $w = 1.5\%$ compared with relaxation curve using one Debye relaxation model

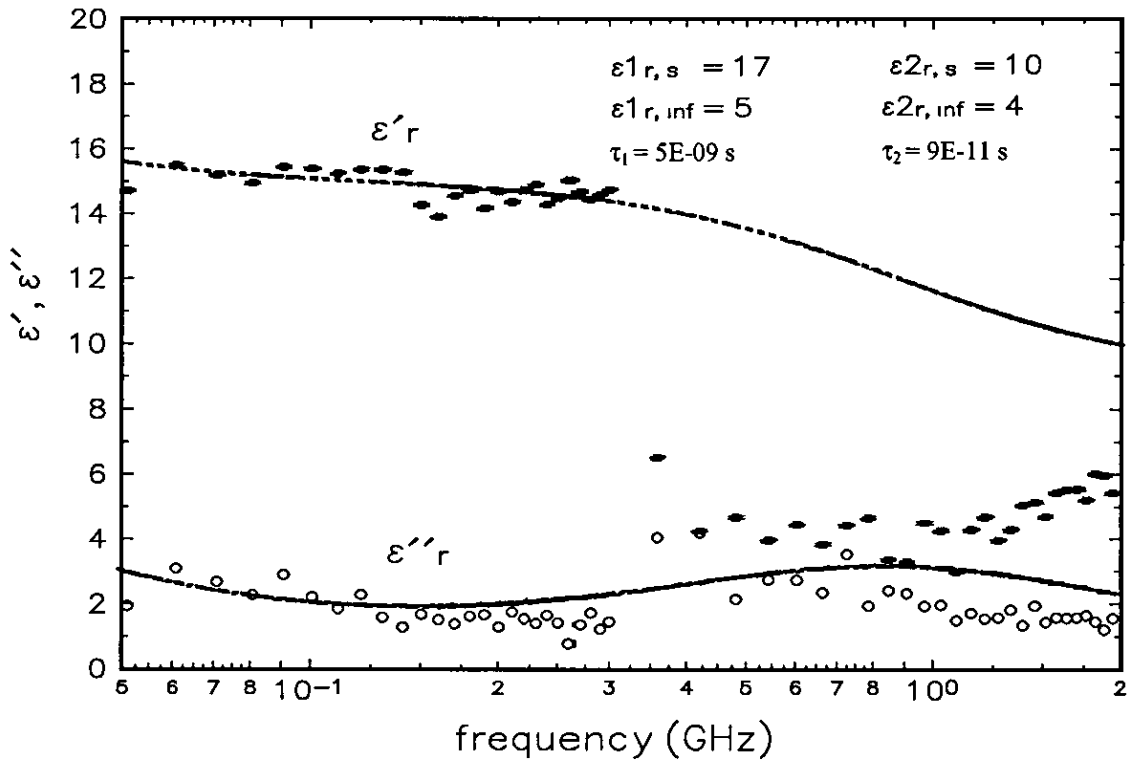


Figure 2.11 Relative complex dielectric constant of Keuper marl, w= 6.5% compared with relaxation curve using one Debye relaxation model

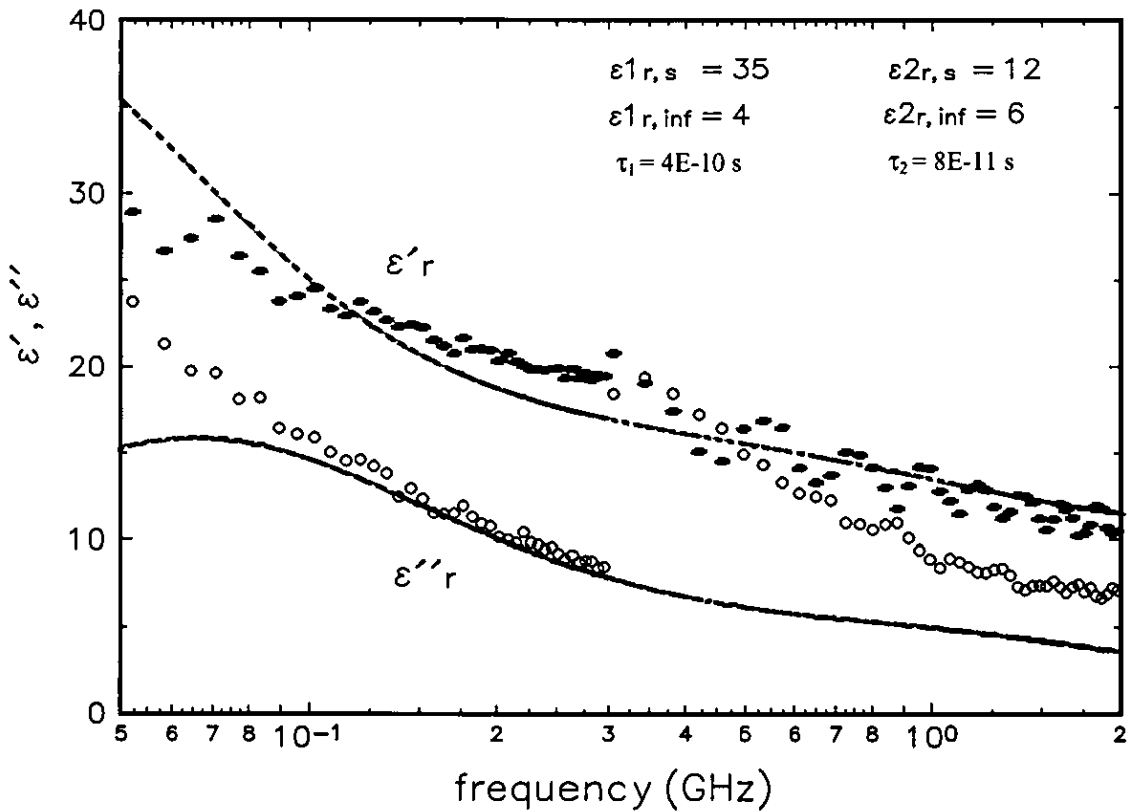


Figure 2.12 Relative complex dielectric constant of Bentonite, w= 9.6% compared with relaxation curve using one Debye relaxation model

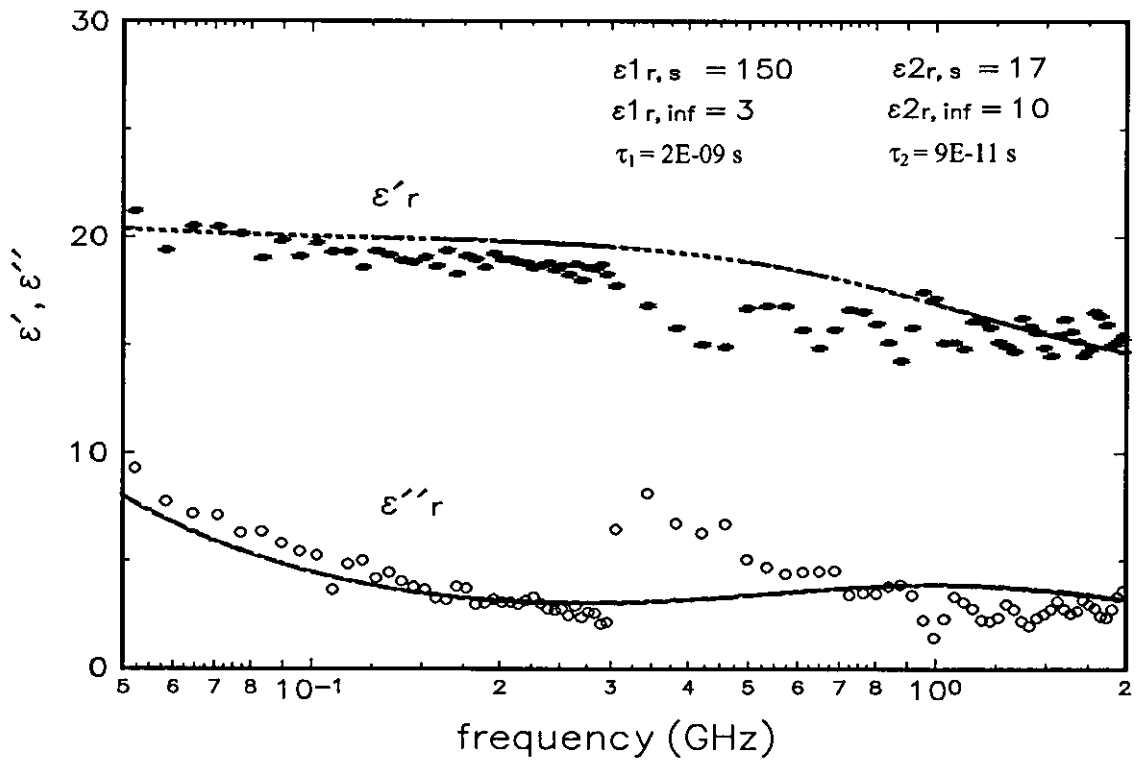


Figure 2.13 Relative complex dielectric constant of China clay, w= 22.8% compared with relaxation curve using one Debye relaxation model

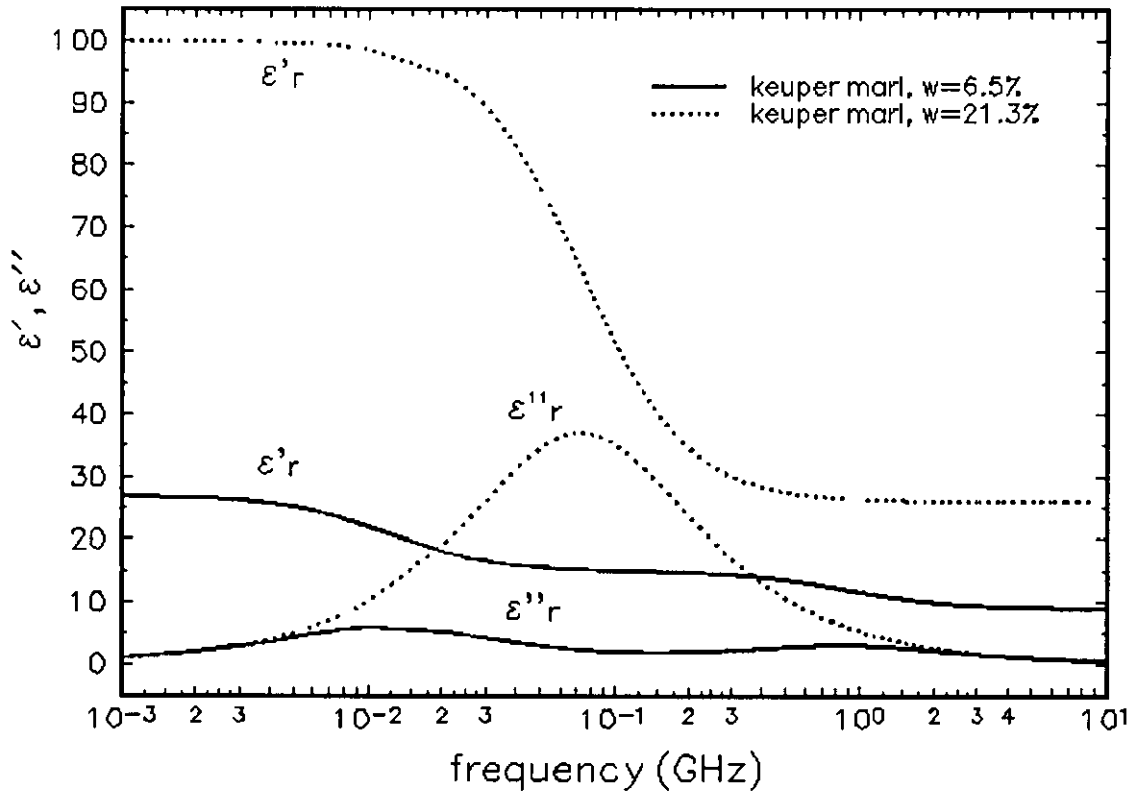


Figure 2.14 Relaxation curve keuper marl, w= 6.5% and 21.3%

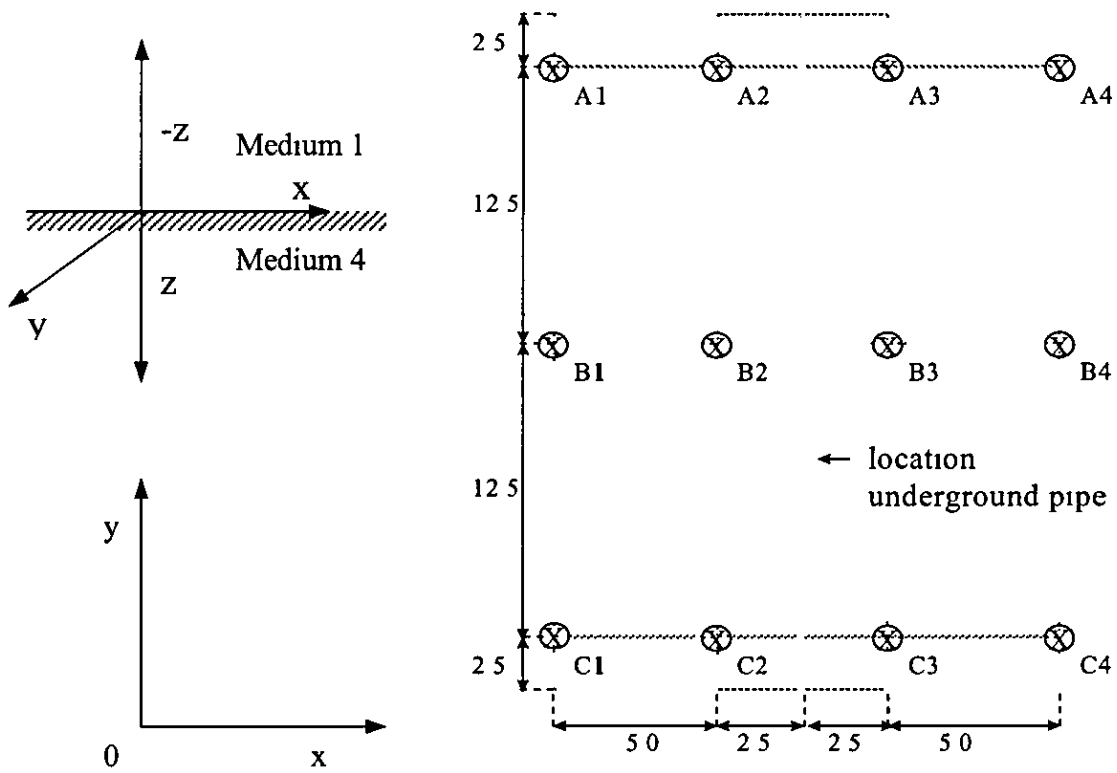


Figure 2.15 Drill locations on the XY plane where the samples were taken

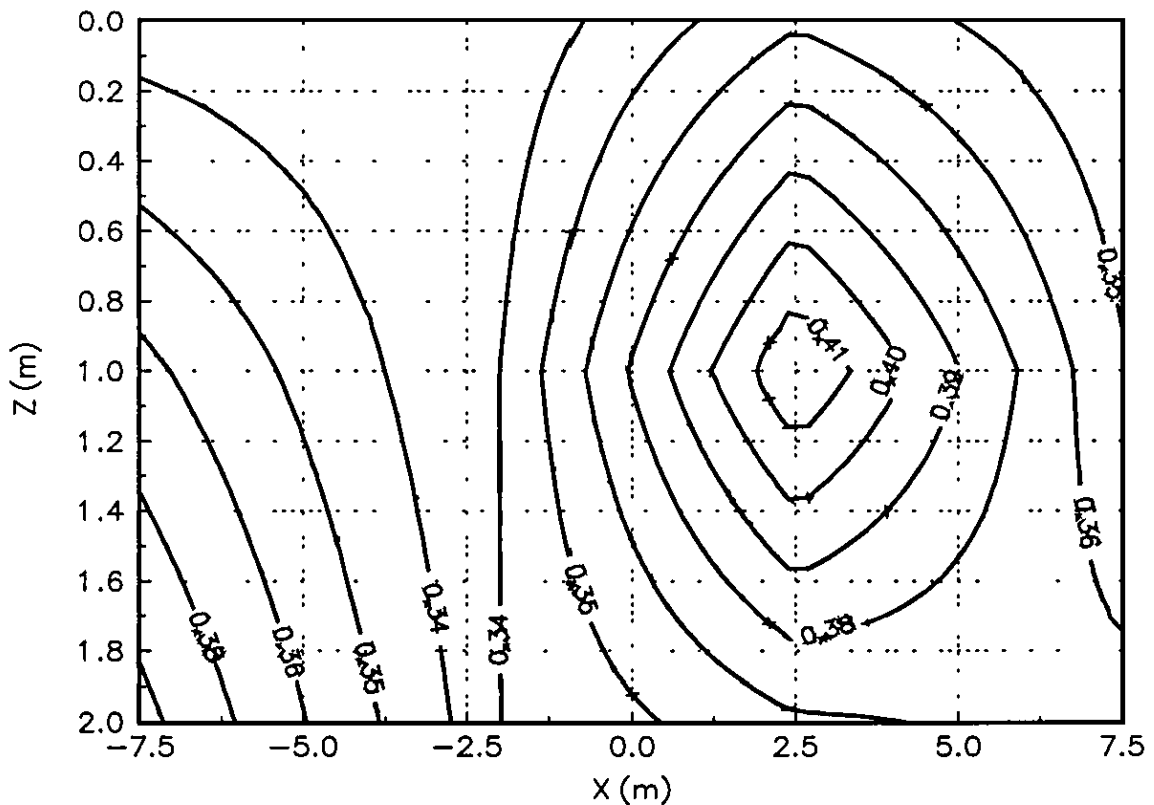


Figure 2.16 Iso-conductivity bars as a function of Z (depth) and X at point A. The frequency is 1 MHz

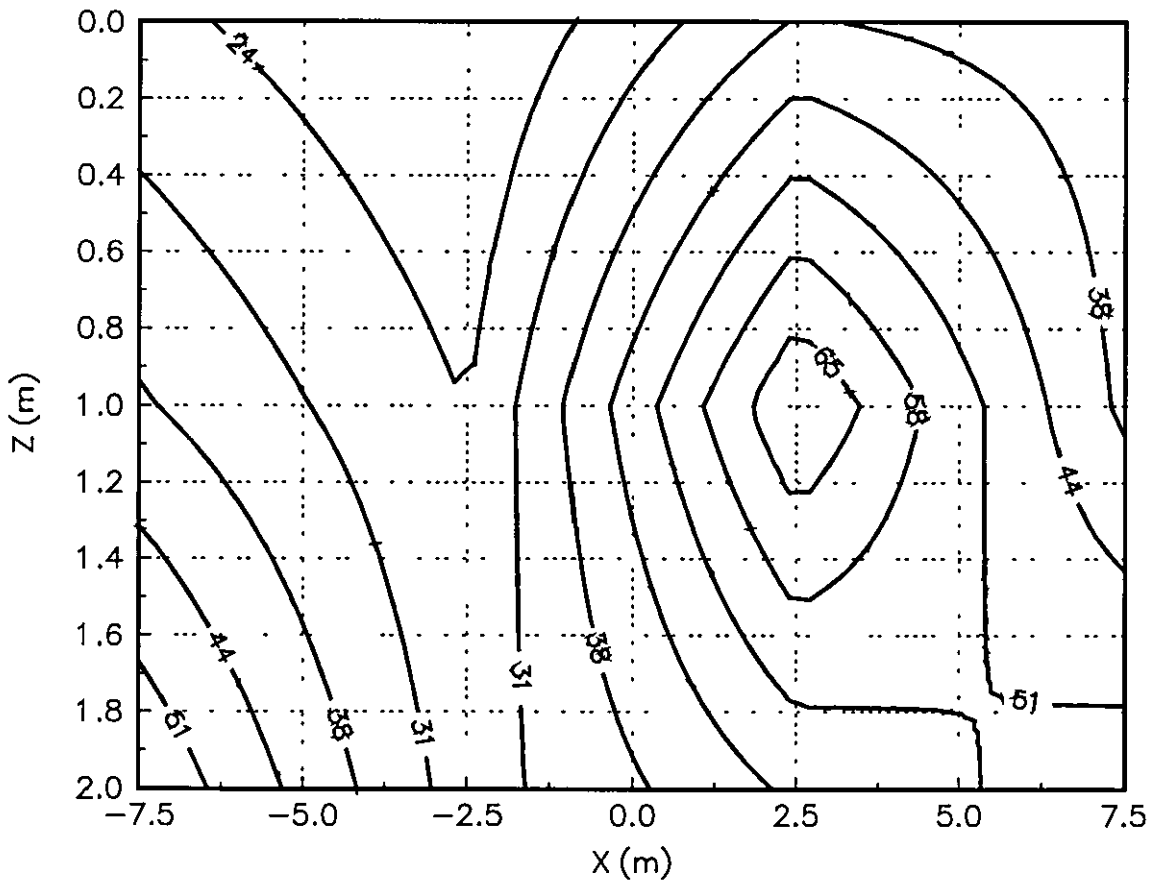


Figure 2.17 Iso-bars for the relative dielectric constant as a function of Z (depth) and X at point A
The frequency is 1 MHz

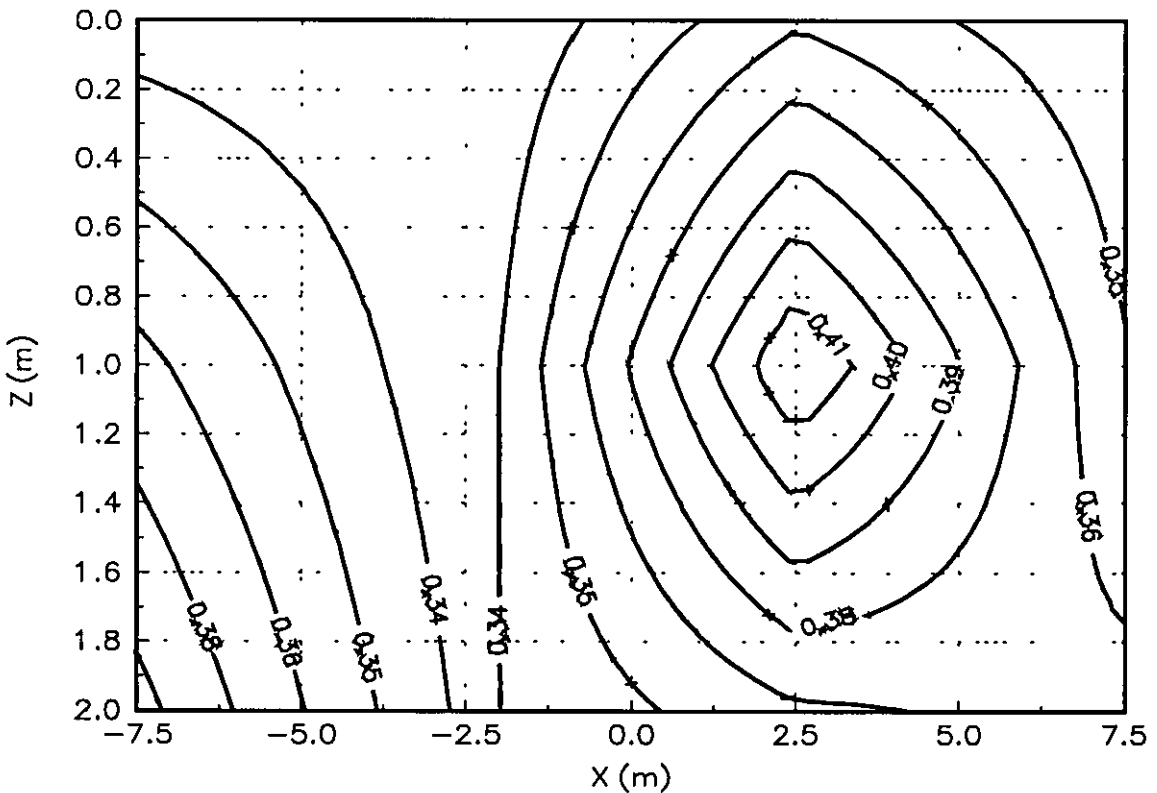


Figure 2.18 Iso-conductivity bars as a function of Z (depth) and X at point A. The frequency is 146 MHz

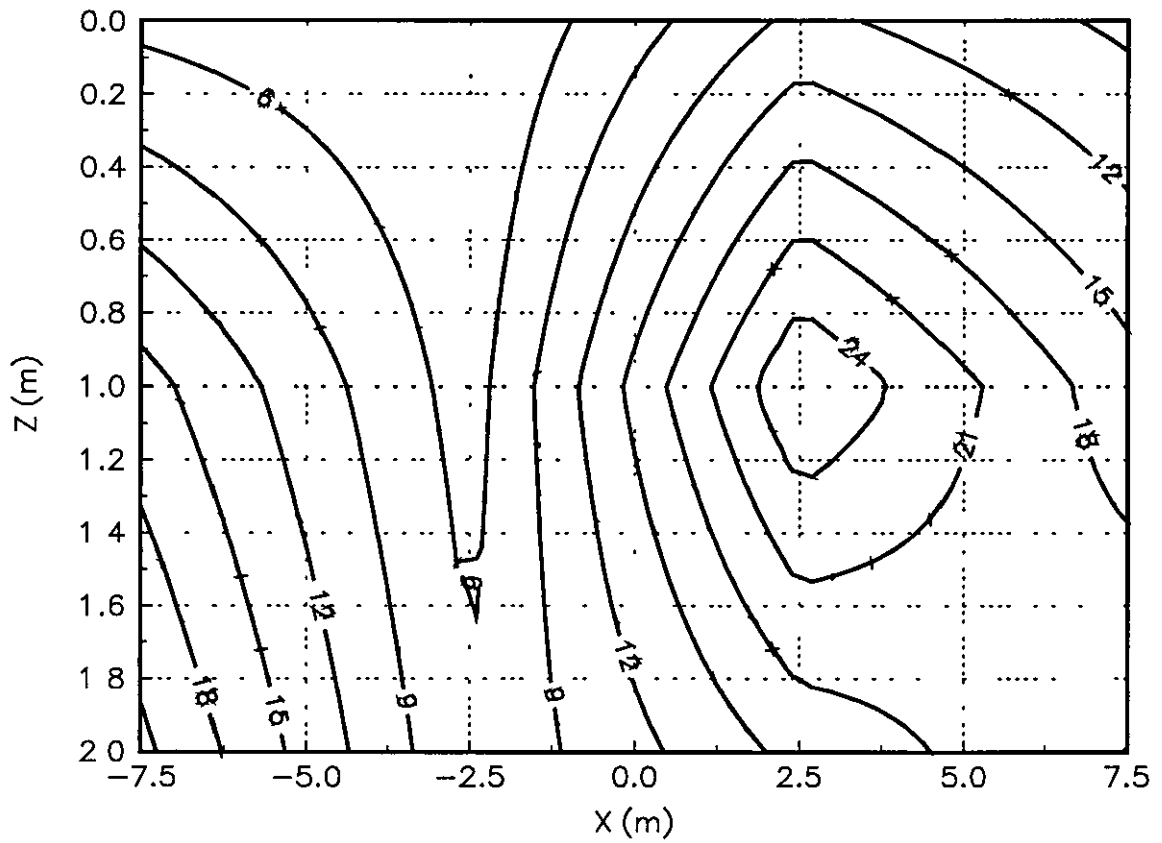


Figure 2.19 Iso-bars for the relative dielectric constant as a function of Z (depth) and X at point A. The frequency is 146 MHz

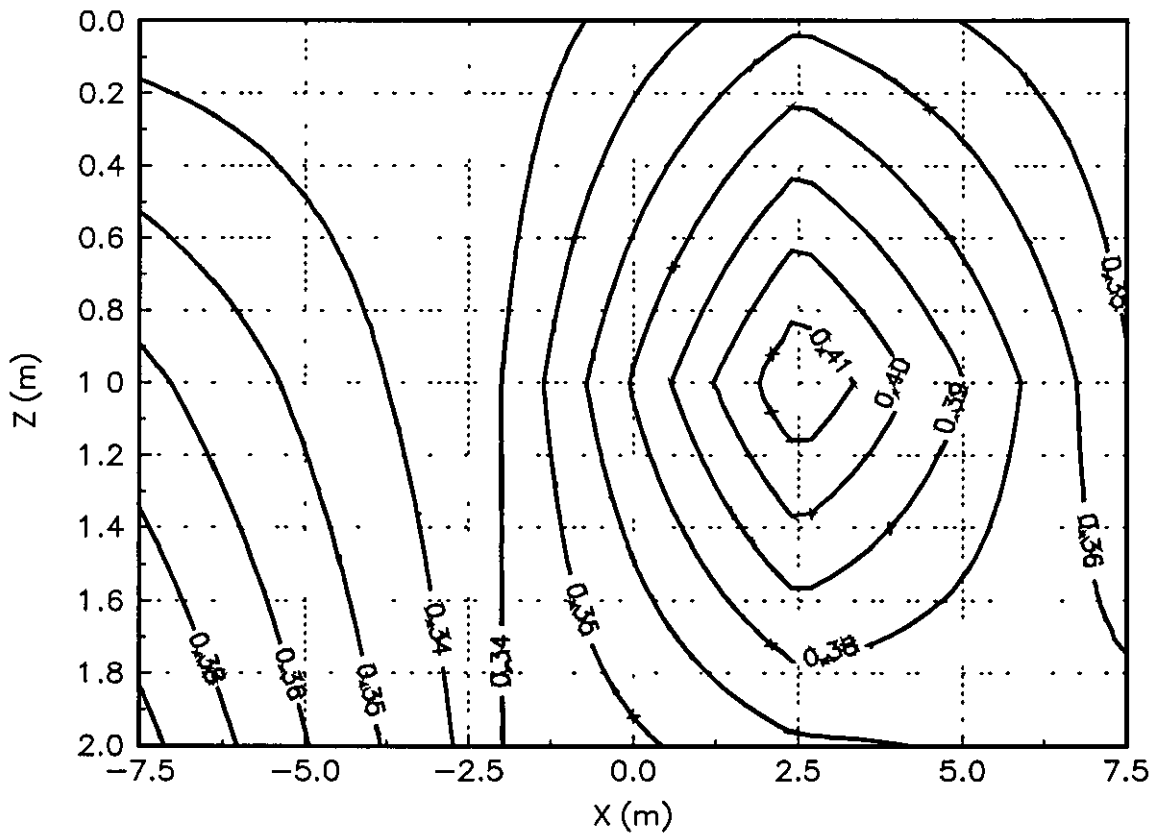


Figure 2.20 Iso-conductivity bars as a function of Z (depth) and X at point A. The frequency is 300 MHz

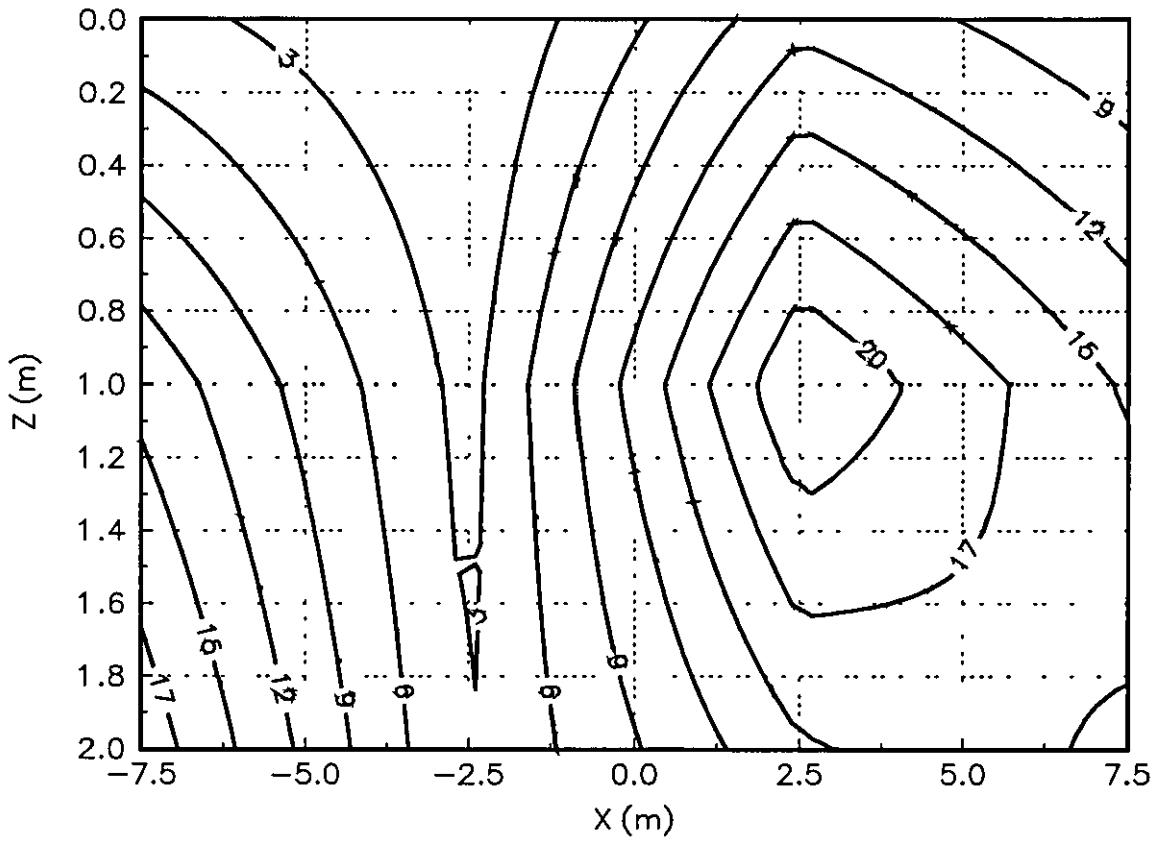


Figure 2.21 Iso-bars for the relative dielectric constant as a function of Z (depth) and X at point A. The frequency is 300 MHz

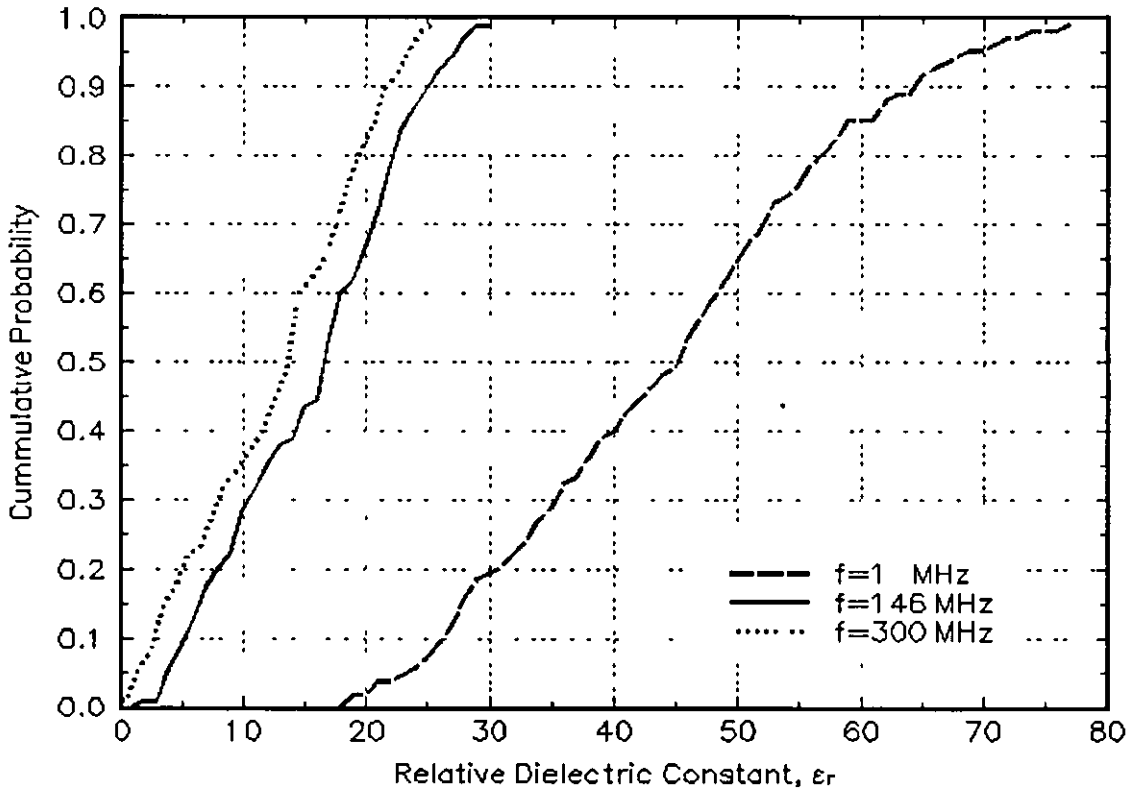


Figure 2.22 Cumulative Distribution Function of the relative dielectric constant from samples in the site survey

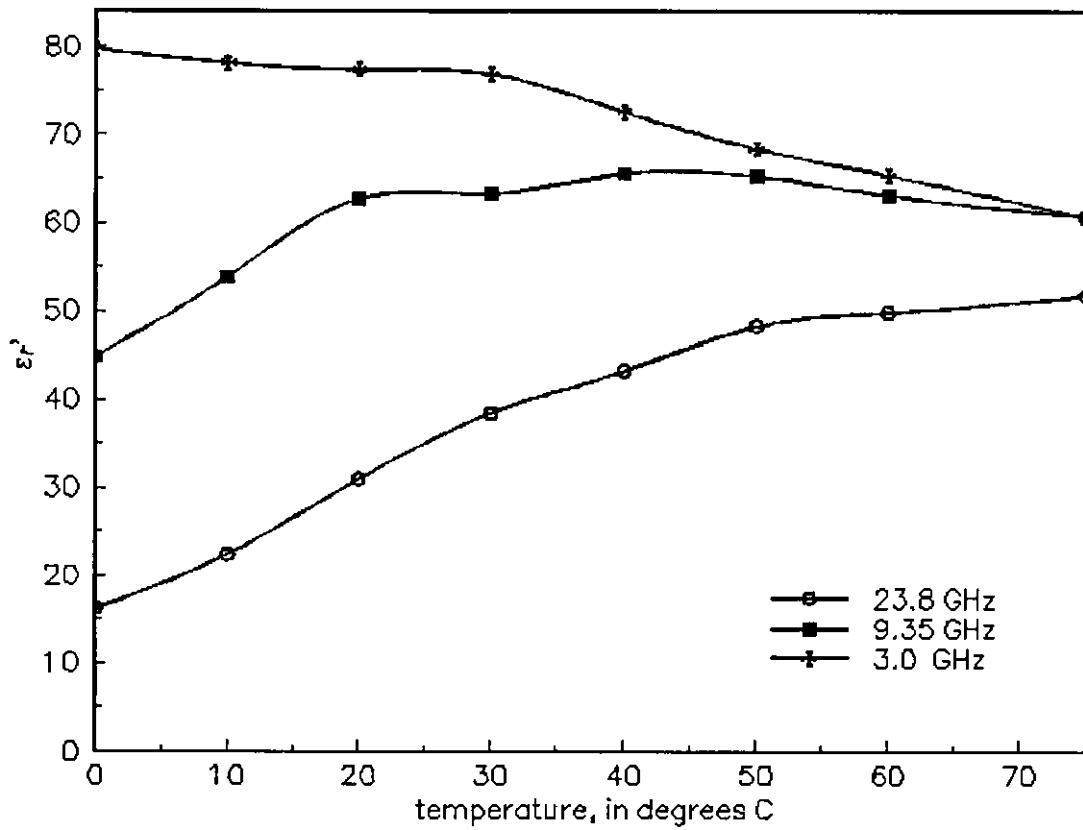


Figure 2.23 Relative dielectric constant of water at various temperatures [24]

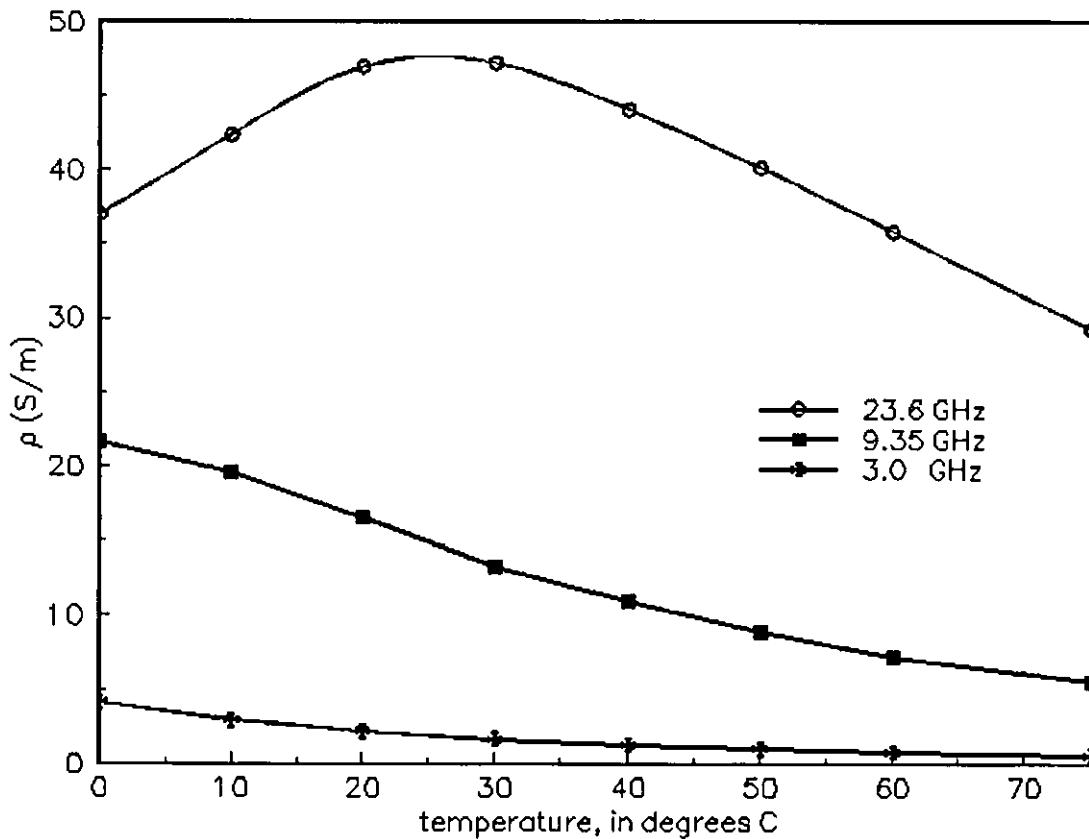


Figure 2.24 Conductivity of water at various temperatures, calculated from the imaginary part of the dielectric constant [24]

References

- [1] Hippel, A.R.Von, '*Dielectric Materials and Applications*,' The MIT Press, MIT, Cambridge, MA, Fourth Printing, August 1966.
- [2] King, R.W.P., '*Antennas in Matter*,' MIT Press, MIT, Cambridge, MA, 1984
- [3] Debye, '*Polar Molecules*,' Chemical Catalogue Company, New York, 1929.
- [4] Hoekstra, P., Delaney, A , 'Dielectric Properties of Soils at UHF and Microwave Frequencies,' *Journal of Geophysical research*, Vol .79, No. 11, April 10 , 1974.
- [5] Bhagat, P.K., 'Relaxation Models for Moist Soils Suitable at Microwave Frequencies,' *Materials Science and Engineering*, No. 28, 1977, pp. 47-51.
- [6] Smith-Rose, R.L , 'Electrical measurements on soil with altering currents', *J Inst Elec Engrs.*, No 75, 1934, pp. 221-237.
- [7] Scott, J.H. et.al. , 'Dielectric Constant and Electrical Conductivity Measurements of Moist Rock: A New Laboratory Method', *J Geophysics Res.* Vol 72, Nr 20, pp. 5101-5115, 15 Oct. 1967.
- [8] Shahidi, M. Hasted, J.B , Jonkscher, A.K., 'Electrical Properties of Dry and Humid Sand', *Nature*, Vol. 258, Dec 18, 1975, pp. 595 -597.
- [9] Saarenketo, T. and Scullion, T , 'Laboratory and GPR test to Evaluate Electrical and Mechanical Properties of Texas and Finnish base course Aggregates', *Proceeding of the Sixth International Conference on Ground Probing Radar*, 1996, pp. 477-482.
- [10] Selig, E.T and Mansukhani, A.M., 'Relationship of soil moisture to the dielectric property', *Journal of the Geotechnical Engineering Division*, Proceedings of the American Society of Civil Engineers, Vol. 101, No. GT8, August, 1975, pp. 755-770
- [11] Michell, J.K , '*Fundamentals of Soil Behaviour*,' Second Edition, John Wiley and Sons, 1992, p. 437.
- [12] Arulanadam, K and Smith, S.S., 'Electrical Dispersion in Relation to Soil Structure,' *Journal of the Soil Mechanics and Foundations Division*, proceedings of the American Society of Civil Engineers, Vol 99, No. SM12, December 1973, pp. 1113-1133.
- [13] Sachs, S B. and Spiegler, K.S , 'Radiofrequency Measurements of Porous Conductive Plugs' Ion-Exchange Resin-Solution Systems, *Journal of Physical*

- Chemistry*, Vol 68, 1964, pp. 1214-1223.
- [14] Weir, W B. "Antenna Measurements of Complex Dielectric Constant and Permeability at microwave Frequencies," *Proc IEEE*, Vol 62, No 1, January 1974, pp. 33 – 36.
 - [15] Nicolson, A.M., Ross, G.F. "Measurement of the intrinsic Properties of Materials by Time Domain Techniques," *IEEE Trans Instrumentation and Measurement*, Vol IM-19, No. 4. November 1970, pp 337-382.
 - [16] Tillema, N.J.P., Vardaxoglou, J.C. "Dielectric Constant Measurement of Soil Samples with the Transmission/Reflection Method," *Joint URSI UK 12th National Radio Science Colloquium & QMW 1995 Antenna Symposium*, Queen Mary and Westfield College, London, 11 - 13 July 1995.
 - [17] Peplinski, N.R., Ulaby, F T., Dobson, M.C. , "Dielectric Properties of Soils in the 0.3 - 1.3 GHz Range", *IEEE Trans Geoscience and Remote Sensing*, Vol 33, Nr.3, May 1985
 - [18] Athey, T.W., Stuchly, M.A., Stuchly, S.S. "Measurement of Radio Frequency Permittivity of Biological Tissues with an Open-Ended Coaxial Line: Part I," *IEEE Trans. Microwave and Technology*, Vol. MTT-30, No. 1. January 1982.
 - [19] Burdette, E.C., Cain, F L , Seals, J., "In Vivo Probe Measurement Technique for Determining Dielectric Properties at VHF Through Microwave Frequencies," *IEEE Trans Microwave Theory and Techniques*, Vol. MTT-28, No.4, April 1980
 - [20] Hipp, J.E. , "Soil Electromagnetic Parameters as Functions of Frequency, Soil Density, and Soil Moisture," *Proc IEEE*, Vol. 62, No 1, January 1974.
 - [21] Jackson, R D., Reginato, R.J., Idso, S.B., 'Timing of Ground Truth Acquisition During Remote Assessment of Soil-Water Content,' *Re. Sens. Environ.*, No. 4, 1974, pp. 249-255.
 - [22] Rao, R.G.S., Ulaby, F.T , 'Optimal Spatial Sampling Techniques of Ground Truth Data in Microwave Remote Sensing of Soil Moisture,' *Remote Sensing of Environment*, No. 6, 1977, pp 289-301, Elsevier North Holland.
 - [23] Bell, R.K., Blanchard, B.J. Schmugger, T.J., Witeczak, M.W. 'Analyses of Surface Moisture Variations Within Large Field Sites,' *Water Resources Research*, Vol16, No. 4, pp. 796-810, August 1980
 - [24] Collie, et al , *Proc. Phys. Soc. London*, v. 60, p. 145, 1948.

3. Insulated Wire Antennas in a Lossy Dielectric Medium

In applications where transmitter power is limited, the antenna efficiency may be a critical parameter in determining the feasibility of a system. In this chapter, the characteristics of subsurface insulated linear antennas are investigated. Insulated antennas are used in a wide area of applications such as submarine communications, microwave hyper-thermal treatment, telemetry and geophysical exploration. These experiments were part of a study of an underground navigation system, using electromagnetic waves. The application is to develop a system that is able to locate a micro-tunnel drilling machine, used for laying cables, underground. In principle, an antenna was mounted on the drill, transmitting an electromagnetic wave through the ground. Both transmitter and receiver antennas were positioned underground. The transmitter was powered by battery and therefore transmission through sand, clay or rock has to be achieved using low power. As the signal attenuation was high, the antenna electrical length may be a critical parameter in determining the feasibility of the overall system. The aim of this work was to study the effects of soil type and soil moisture content on antenna design.

Many numerical computational codes exist for calculating the characteristics of wire antennas. Some of the numerical models for insulated antennas are valid for antennas in a high loss dielectric only [1,2]. Transmission line theory can be applied to insulated antennas in matter [3,4] by expansion of the wall thickness of the tubular metal shield of the conventional coaxial line. This theory has shown to be valid for insulated antennas in seawater (high loss) [3] and sand (low loss dielectric) [4]. In the measurements of antenna characteristics published [3,4], the soil constitutive parameters are fairly constant functions of frequency. In the predictions the soil electrical parameters are assumed to be constant. However, previous investigations show that this assumption is not correct for soil samples [5]. The constitutive parameters of soils vary significantly with soil condition

and frequency. In this study, the prediction of antenna impedance was based on the measured soil constitutive parameters, which were used as input data into the computer simulation program. The aim of this work was to study and predict the influence of soil type and soil moisture content on subsurface antenna admittance and, in particular, on its effective length.

3.1. Theoretical Formulation

The charge and current distribution of a bare wire antenna in the ground was changed by the ground constitutive parameters, making the antenna performance a function of the ambient medium. The current in the antenna element leaks into the lossy dielectric and that result in a high loss as well as a significant change in the current distribution. When using a matching network, a part of the impedance change can be compensated for, but the loss in the matching network is a function of the antenna terminal impedance. By placing a dielectric sheath around the antenna element, the effect of the ambient medium on the antenna characteristics can be reduced substantially. The current distribution in dielectric insulated antennas in highly conducting dielectric materials can be calculated using transmission line like equations [3,4]. The antennas are modelled as infinitely long, perfectly conducting tubes in an insulating cylinder. When the cross section of the insulation tube is sufficiently small, the wave will propagate in a TEM mode. The antenna consists of a conducting wire of radius a , surrounded by two layers of dielectric insulation with outer radii b and c . The dielectrics of the insulation regions 2 and 3 have wavenumbers $k_2 = \omega(\mu_0 \epsilon_2)^{1/2}$ and $k_3 = \omega(\mu_0 \epsilon_3)^{1/2}$ respectively. The lossy ambient medium, region 4, has a wavenumber $k_4 = \omega[\mu_4(\epsilon_4 + i\sigma_4/\omega)]^{1/2}$ in which $\epsilon = (\epsilon_r' - i\epsilon_r'')\epsilon_0$ is the dielectric constant, $\mu = \mu_0$ is the magnetic permeability and $\sigma = \omega\epsilon_r''\epsilon_0$ is the conductivity of the medium. The ambient medium and the insulation are assumed to be non-magnetic. The wave number in the antenna element k_L and the characteristic impedance per m Z_c can be calculated using the equations [4]:

$$k_L = (-z_L y_L)^{1/2} \quad Z_c = \left(z_L / y_L \right)^{1/2} \quad (3.1.1)$$

with

$$z_L = z^i - i\omega l + z^e + z_{12}; \quad y_L = g_L - i\omega c_L \quad (3.1.2)$$

Here, z^i is the internal impedance per unit length, defined by:

$$z^i = r_i - ix_i = r_0 \frac{k_1 a}{2} \frac{J_0[k_1 a]}{J_1[k_1 a]} \quad (3.1.3)$$

in which $r_0 = (\pi a^2 \sigma_1)^{-1}$ is the characteristic resistance of the conductor. The series inductance per unit length is given by:

$$l = \frac{\mu_0}{2\pi} \ln\left[\frac{b}{a}\right], \quad (3.1.4)$$

and the series external impedance per unit length z^e is:

$$z^e = r^e - ix^e = \frac{i\omega\mu_0}{2\pi} \left(\frac{H_0[k_4 b]}{k_4 b H_1[k_4 b]} \right) \quad (3.1.5)$$

The position of the antenna in a half space at a distance d from the boundary causes a reflection of the radiated wave. This wave creates a co-directional current in the antenna element. This reflects the characteristic impedance and is included in the model as the mutual impedance Z_{12}

$$z_{12} = r_{12} - ix_{12} = -\frac{i\omega\mu_0}{2\pi} \left(\frac{H_0[2k_4 d]}{k_4 b H_1[k_4 b]} \right) \quad (3.1.6)$$

The shunt admittance is defined as follows.

$$y_L = g_L - i\omega_L = -\frac{i2\pi k_2^2}{\omega\mu_0 \ln[b/a]} \quad (3.1.7)$$

The current distribution of the open-ended linear insulated cylindrical dipole antenna of length $2h$ or monopole antenna of length h is well approximated by

$$I(z) = I(0) \frac{\sin[k_L(h-|z|)]}{\sin[k_L h]} \quad \text{where} \quad I(0) = \frac{V_0^e}{Z_c} \quad (3.1.8)$$

The charge per unit length along the antenna element is calculated from the continuity equation [3]. The current and charge distribution of insulated monopole antennas in lake water and in salt water, have been measured and shown to be in very good agreement with the theory [7]. As the published measurements [7] and the calculated distributions of charge are in good agreement and as the slope of these distributions also agrees, the entire near field and far field can be calculated from the theoretical distribution of current. A Fortran computer programme based on [8] was used to calculate the field in the dissipative medium.

3.1.1. Theory Constraints

For the theory to be valid, the antenna ambient medium should satisfy the equations.

$$|k_4^2| \geq 2|k_4^2| \quad |k_4^2| \geq 2|k_3^2| \quad (3.1.1.1)$$

When the antenna is of finite length, this constraint can be written as:

$$|k_4^2|/|k_2^2| \gg 1 \quad (3.1.1.2)$$

This constraint means that the ambient medium is required to have a higher dielectric constant and conductivity than the insulating dielectric. The wavenumber k_4 is at a minimum for a given medium when its dielectric constant and conductivity are relatively small, or at low frequencies.

3.1.2. Antenna Effective Length

The effective height h_e of an antenna is one of the parameters in measuring its performance. When an antenna has the same polarisation as the incident wave $E(\rho, \phi, z)$, the output voltage is, $V = h_e * E(\rho, \phi, z)$. The effective length of antenna can be found by multiplying its physical length with the normalised average current. The effective length of the receiver antenna is a function of angle of incident of the incoming wave and can be calculated from the current distribution:

$$h_e = \int_0^h \frac{\sin[k_L(h-z')]}{\sin[k_L h]} e^{-ik_4 z' \cos[\phi_0]} dz' \quad (3.1.2.1)$$

$$\begin{aligned} &= \frac{2k_L e^{-1hk_4 \cos[\phi_0]}}{(2k_L^2 - k_4(1 - \cos[2\phi_0])\sin[hk_L])} \\ &- \frac{2k_L \cos[hk_L] - ik_4 \sin[hk_L - \phi_0] - ik_4 \sin[hk_L + \phi_0]}{(2k_L^2 - k_4(1 - \cos[2\phi_0])\sin[hk_L])} \end{aligned} \quad (3.1.2.2)$$

In the direction of maximum field $\phi_0=0$ the equation reduces to:

$$= \frac{e^{-ikh_4} k_L - k_L \cos[k_L h] - ik_4 \sin[k_L h]}{(k_L^2 - k_4^2) \sin[k_L h]} \quad (3.1.2.3)$$

3.2. Experiments

3.2.1. Antennas used in Experiments

The antennas used in the experiment were monopole and dipole wire antennas. The antennas wires were made of aluminium and had a diameter of 5 mm. The conductivity of aluminium was found in literature to be 3.0×10^7 S/m. The antenna feed point was an aluminium ring with an outside diameter of 37 mm, with in its centre a 29 mm diameter PVC ring that holds the antenna element in its place. The relative dielectric constant of the PVC was measured in the frequency range of 8 - 12 GHz using waveguide reflection/transmission technique and was found to be constant at 2.7. As publications show [ref. 1, chapter 2] that the dielectric constant of PVC is fairly frequency independent, it was assumed that the dielectric constant of the PVC used was 2.7 in the frequency band of 100-300 MHz. A foam sheath with a radius of 17 mm was used as insulation around the antenna element. This foam was measured to have a relative dielectric constant of 1.0, using the same measurement technique. The PVC tube with a radius of 19 mm holds the foam in place. The monopole antenna element was a aluminium wire of length h and 2.5 mm radius, on a ground screen consisting of 6 equal spaced radial wires of 0.69 m length and of 2.5 mm radius as shown in figure 3.1. These dimensions were used in the simulations. When modelling the feed point as an infinite transmission line, its characteristic impedance was calculated to be 50 Ohm, based on these radii and dielectric constant. The ground screen was defined in the model as 6 finite wires of 0.719 m, instead of using the infinite ground screen option in Mininec. The 0.719 m length accounts for the wire length plus the radius of the aluminium ring, holding it. Four monopole antennas were made with in-air resonant frequencies of 125, 150, 175 and 200 MHz. Figure 3.2 shows that the agreement between measurement and simulation in Mininec is very good up to 200 MHz. The anti-resonance was measured at a higher frequency than expected. This is due to the antenna feeding that was not included in the simulation. For antennas in a lossy dielectric, if R is the radius of the ground plane and λ_0 is the wavelength in air, then if $R/\lambda_0 > 0.2$ the effect of the ground plane on the monopole admittance is negligible

[8]. At 300 MHz, $R/\lambda_0 = 0.69$ as $R = 0.69\text{m}$ and therefore in these experiments the effect of the ground screen on the admittance is negligible.

3.2.2. Experimental Results

The problem of measuring and predicting the characteristics of antennas underground was made difficult by the fact that in most cases the soil was not homogeneous. Also the granular properties of most soils makes it more complicated to position the antenna in the ground without disturbing the soil density. Therefore to evaluate the experimental method, the admittance of antennas submerged in an in-door water basin was predicted and measured. The dielectric constant and conductivity of the water was measured in the frequency range of 100 - 300 MHz using a coaxial probe and was used in the simulation.

3.2.3. Antennas Underwater

Figure 3.3 shows the comparison between measurement and prediction. The difference in the magnitude of the admittance suggests a mismatch between the antenna and the feeder or water leaking into the insulation. However when the antenna was deeper in the water, the resonant frequency was measured to be slightly lower than predicted. The effect of the distance between the antenna and the water-air boundary on antenna characteristics is illustrated in figure 3.4 which compares the complex admittance, defined as $Y = G + jB$, at 0.5 m deep with the same measurement at 0.1 m deep. For both depths there was a good agreement between theory and measurement. The radiated field reflects against the ground-air boundary and generates an additional component of the antenna admittance. The measurements indicate that the radiation admittance changes with depth. The high input conductivity of the antenna at resonance makes the antenna at this particular frequency a relative efficient radiator. In anti-resonance the reactance and susceptance were zero, as in resonance, but the conductivity was near a minimum. To achieve a high efficiency the antenna was to be used at its resonance frequency. Therefore, a further study examined the effect of a changing environment on the resonant frequency.

3.2.4. Soil as Ambient medium

In this investigation, the soil constitutive parameters measured at the frequency range of 1 MHz to 300 MHz were used for predicting the antenna characteristics. The coaxial probe used in the experiments was suitable for measuring the dielectric constant of high loss and low loss soil samples. The measurement system was portable, making it possible to conduct a survey on-site. No sample preparation was necessary. Figures 3.5 and 3.6 are results from Keuper marl clay and Leighton Buzzard sand. The dielectric constant of dry soil was not frequency dependent and was in between 4 - 8. Its conductivity was very low. This applies both to clays and sands. When the sample moisture was increased, its dielectric constant increased, being disperse for clays, but fairly linear for sands. Wet samples exhibited a higher dielectric conductivity, being dispersed for both sands and clays. Clays showed a higher dielectric conductivity. The dielectric constant of soil may be as high as 50 at 1.0 MHz.

3.2.5. Antenna Admittance in Various Soil Types

Figure 3.7 shows the difference between the prediction using a constant ϵ_r and σ taken at 150 MHz and ϵ_r and σ measured. Around the resonant frequency, the prediction based on the ϵ_r and σ measured was in better agreement with the actual antenna admittance. Therefore, the electrical properties of the antenna environment were measured instead of estimated.

To position the antenna underground, a drill was used with a diameter equal to that of the antenna insulation, in order to minimise any soil disturbance. In all the measurements, the antenna element with its dielectric shield was in the ground while the ground screen was on the interface between ground and air. The antenna which was designed to resonate in air at 150 MHz resonated, in moist soil, at 96 MHz as shown in figure 3.7. The agreement between measurement and simulation was very good. The soil type was determined to be keuper marl mixed with a small quantity of sand and humus. Its moisture constant, expressed as the mass of the water contained in the sample related to the sample mass, in percentage, was measured to be 6.5%. Resonance occurs at $h=0.25\lambda_{\text{soil}}$. Figure 3.9 shows the resonance frequency of an antenna with length $h=0.556$ m, simulated with the ambient medium data of keuper marl and river sand with various different moisture content. A

higher moisture content of the soil resulted in a higher dielectric constant of the ambient medium, but also a higher conductivity and therefore a higher loss. Increasing the moisture content of the sample from 5% to 10.8% made the antenna resonant frequency decrease from 96 MHz to 93 MHz respectively. This was because the dielectric constant increases making the wavelength shorter for a given frequency.

3.2.6. Antenna Effective Height

As shown in figure 3.13 the antenna effective length h_e was dependent the ambient medium of the antenna. For antenna with a length of 0.441 m, as was used in the experiments, $|h_e| = 0.041$ m in relatively dry keuper marl clay, while $|h_e| = 0.015$ m in moist clay at its resonant frequency, when $h/\lambda = 0.25$. At this frequency, the antenna was a more effective radiator in dry soil greater than a factor of two. This was due to the loss in the ambient medium that reduces the amplitude of the current propagating into the antenna conductor. When comparing the results in figure 3.10, a shorter antenna has a relative greater effective length in a high loss medium. Measurements showed that the predicted Q of the antenna increases with a higher soil moisture content, resulting in more energy stored in the antenna, decreasing its efficiency. It was calculated that the dielectric sheath should have a dielectric constant close to 1.0 to achieve the optimum antenna efficiency.

3.2.7. Radiated Field

The standard method for describing the antenna radiation pattern in air was not suitable in a conducting medium [9] because the pattern was highly dependent upon the choice of the origin of the co-ordinate system. This was due to high dissipation of energy in the immediate vicinity of the antenna. For an antenna in air, part of the energy in the near field was stored. In a conductive medium a major part of this energy was dissipated. In experimental determination of the radiation pattern of antennas in air it is customary to rotate the transmitter antenna while using a fixed receiver. The minor change in distance of the transmitter to the receiver antenna when it rotates becomes significant in a conductive medium. Figure 3.11 shows $|E_r|$ as a function of distance from the centre of the antenna wire. The calculated field on the conductor was zero, increasing to 16 dB for dry soil, and -8 dB for wet soil, at the insulation. The overall field strength for dry soil was 25

dB below that of wet soil. In figures 3.12 and 3.13 the $|E_z|$ was predicted for dry and moist soil. For dry soil a minimum was observed at 37° from the positive ρ -axis. The overall radiation pattern was more omnidirectional in the higher conductive medium of wet soil.

3.3. Conclusion

A method was developed to predict the admittance of an insulated monopole antenna in soil, using measured data of the ambient medium. The model was based on transmission line like equations and can be applied to monopole and dipole wire antennas but was tested for insulated monopole antennas in soil and water. The electrical properties of soil and water samples were measured on-site using a coaxial probe. There was good agreement between the predictions and the measurements of the antenna impedance. The dielectric constant and conductivity of soils can vary per soil type, soil moisture content and frequency used. An increase in the moisture content of the sample from 5% to 10.8% made the antenna resonant frequency increase. This was because the dielectric constant increases making the wavelength shorter for a given frequency. The insulated monopole antenna had a higher effective length in a low loss dielectric. In comparison with dry soil as ambient medium, the dipole antenna in wet soil had a shorter effective length and its radiation pattern was more omnidirectional. It was calculated that the dielectric sheath should have a dielectric constant close to 1.0 to achieve the optimum antenna efficiency

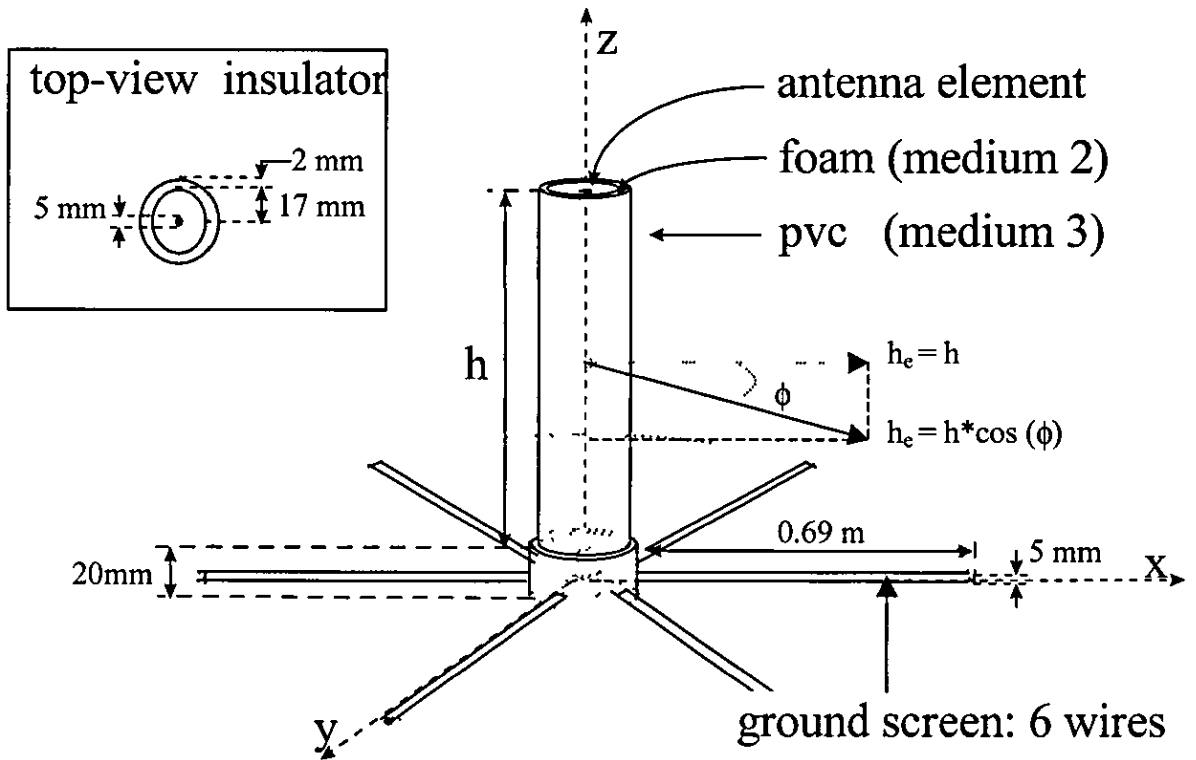


Figure 3.1 Monopole antenna used in the experiment

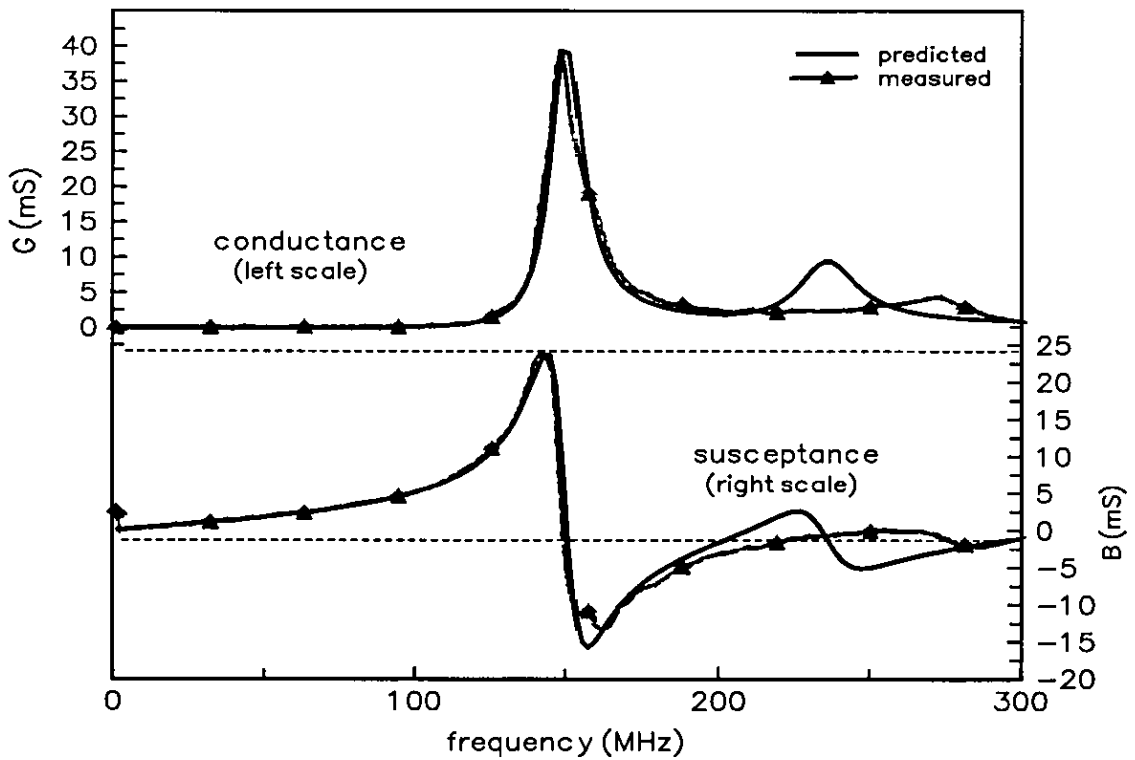


Figure 3.2 Admittance of an insulated monopole antenna, $h=44.10$ cm, $a=2.5$ mm, $b=15$ mm and $c=17$ mm. Ambient medium is air. Calculation done with Minnec Professional

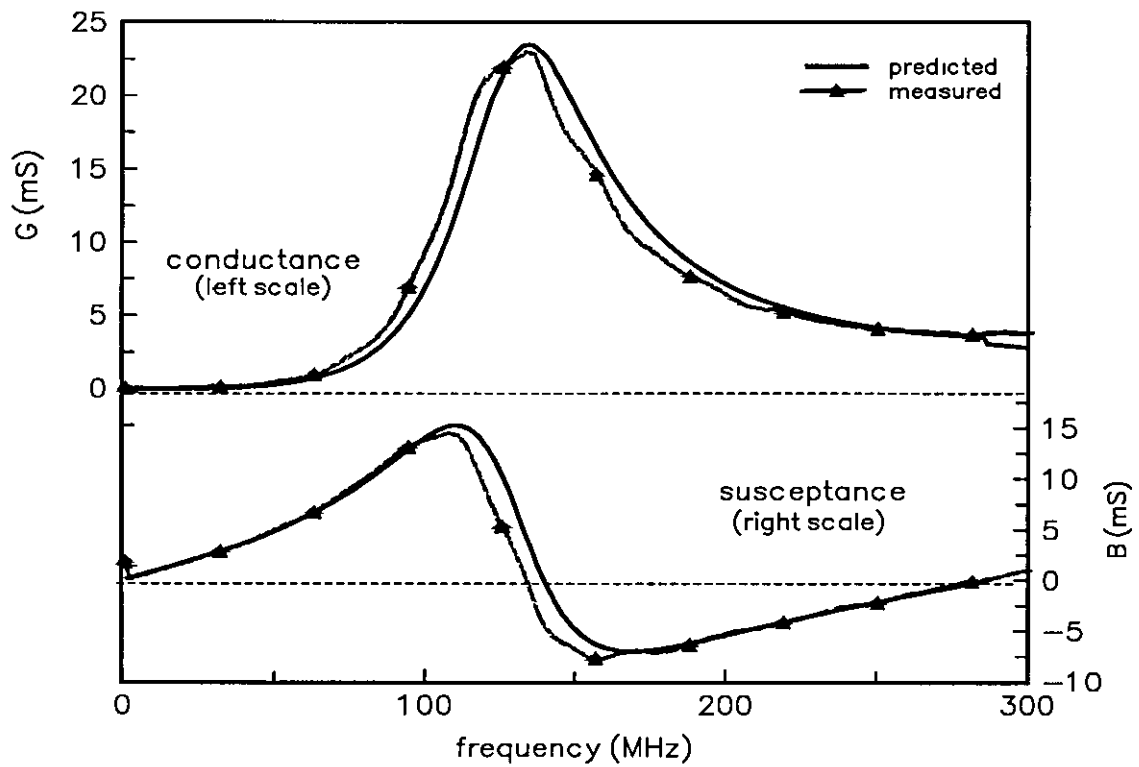


Figure 3.3 The admittance of an insulated monopole when 0.50 m deep in water. Antenna dimensions: $h=44.10$ cm, $a=2.5$ mm, $b=15$ mm, $c=17$ mm. Ambient medium is water, $\epsilon_r=79$, $\sigma=0.1$ S/m (1 MHz) increasing to 0.4 S/m (300 MHz).

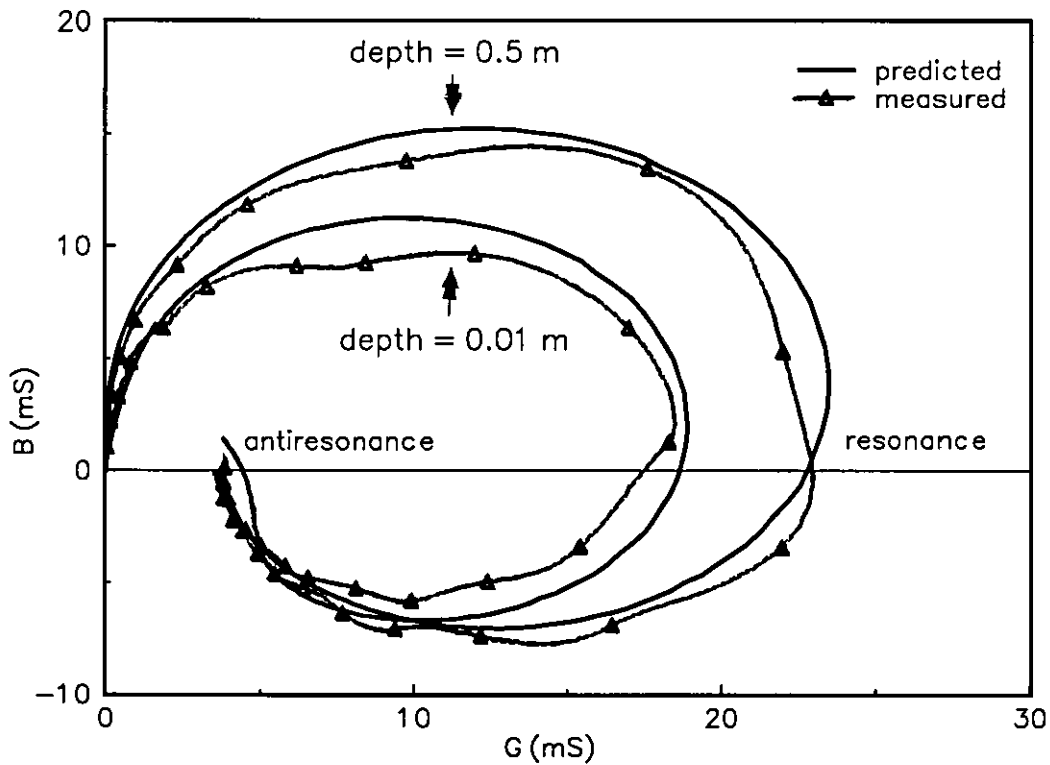


Figure 3.4 The admittance of an insulated monopole when 0.10 m (inner circle) and 0.50 m deep in water. Antenna dimensions: $h=44.10$ cm, $a=2.5$ mm, $b=15$ mm, $c=17$ mm. Ambient medium is water, $\epsilon_r=79$, $\sigma=0.1$ S/m (1 MHz) increasing to 0.4 S/m (300 MHz).

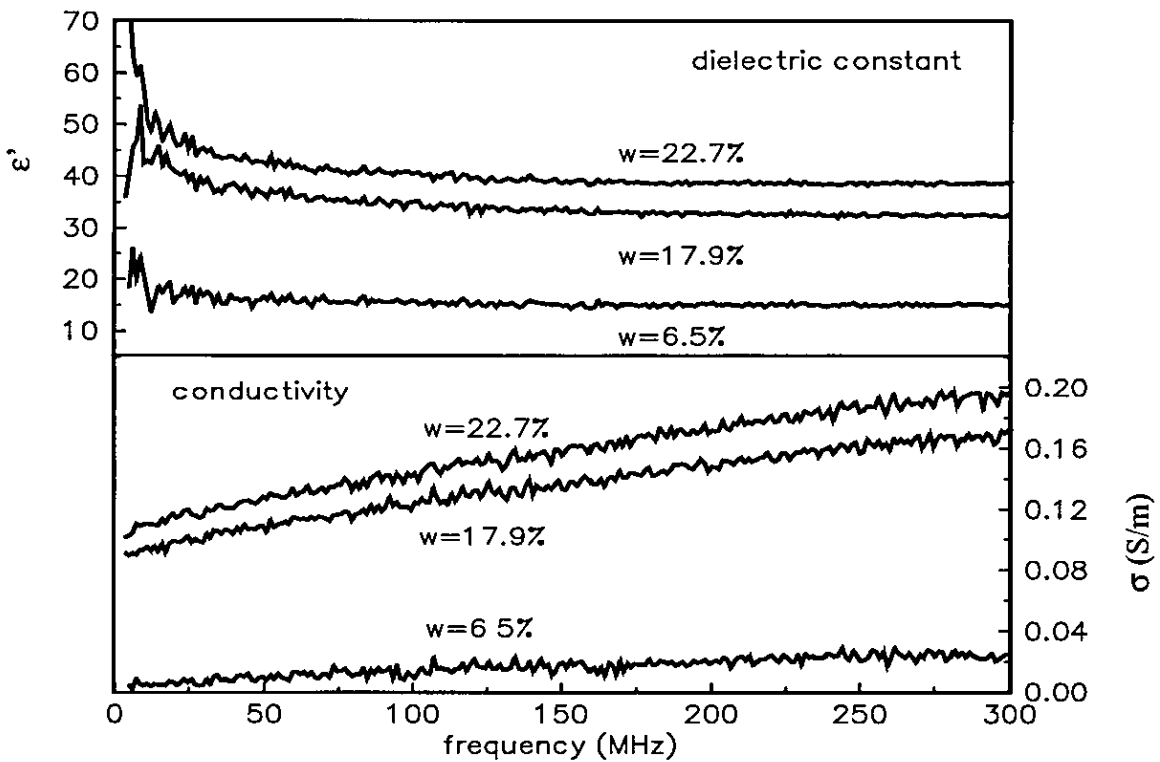


Figure 3.5 Dielectric constant and conductivity of Keuper marl for samples with different moisture content. The moisture content w is the percentage of the mass of the water in the sample relative to the total mass of the dry sample.

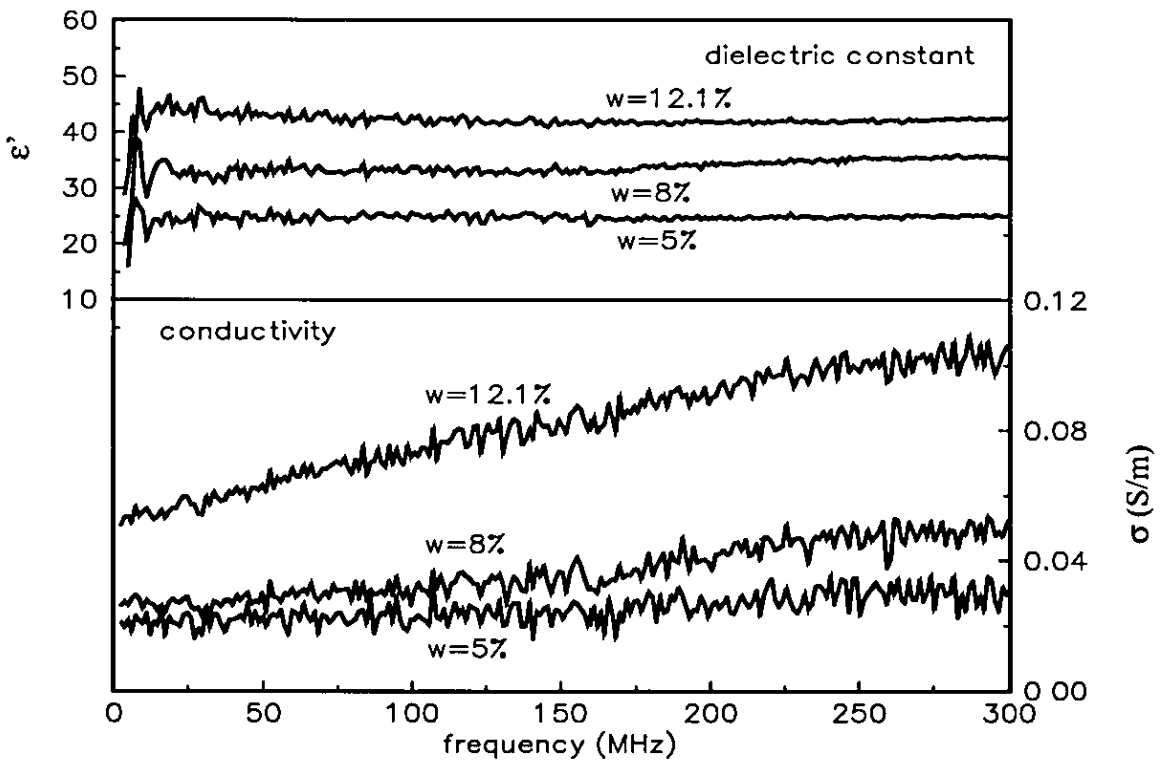


Figure 3.6 Dielectric constant and conductivity of Leighton Buzzard sand for samples with different moisture content.

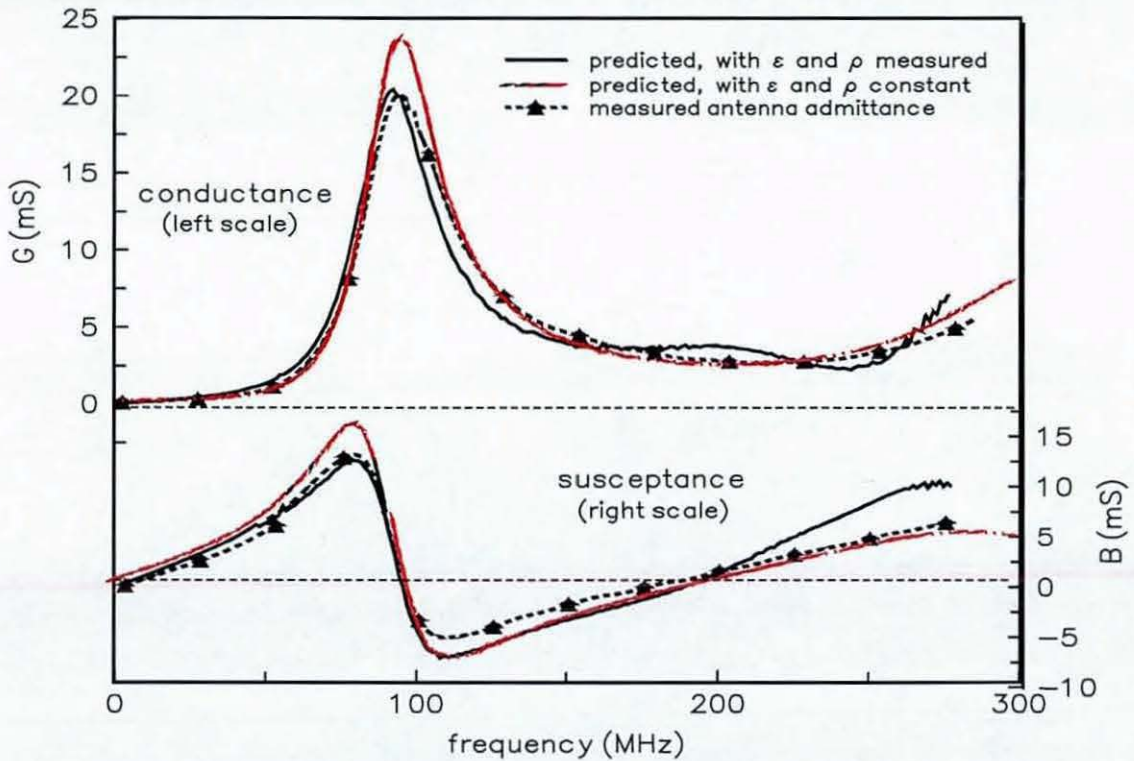


Figure 3.7. Comparison of the antenna admittance predicted with an ambient medium having a constant electrical properties Monopole antenna: $h=0.556$ m, $a=2.5$ mm, $b=15$ mm, $c=17$ Ambient medium is soil type keuper marl with a moisture content of 6.5%, $\epsilon_r=18$ and $\sigma=0.1$ S/m (1MHz) changing to $\epsilon_r=14$ and $\sigma=0.4$ S/m (300 MHz).

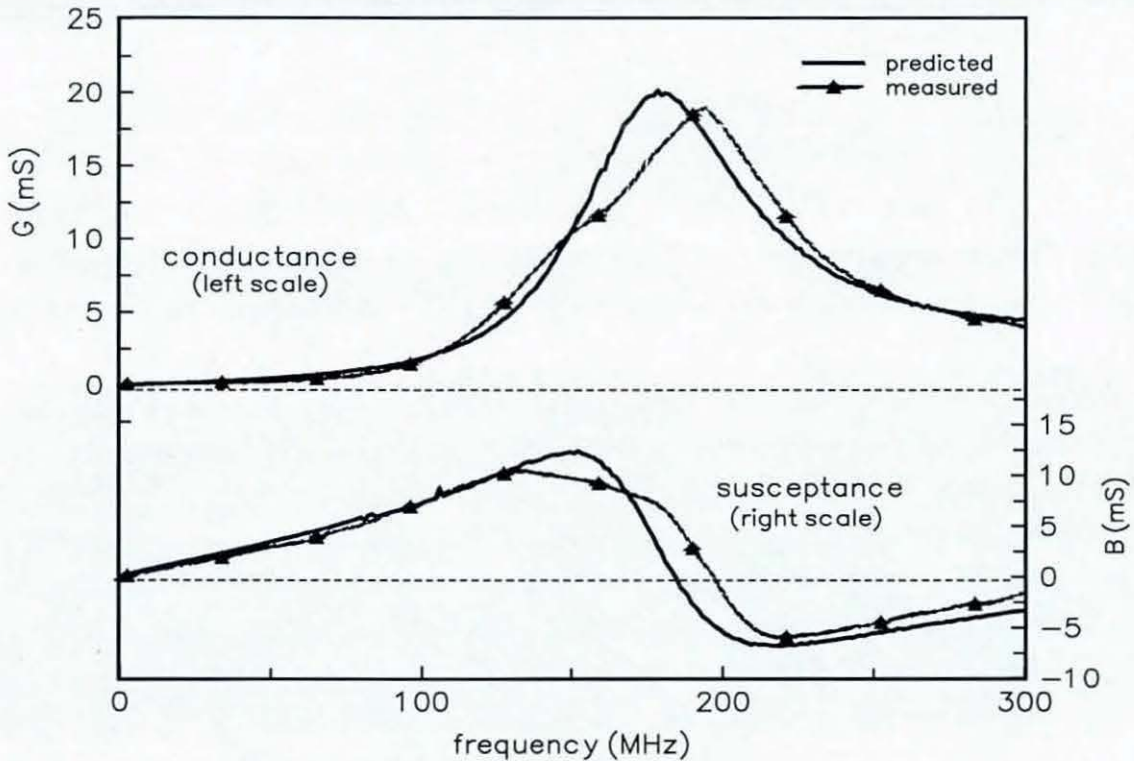


Figure 3.8. Admittance of an insulated monopole antenna: $h=0.305$ m, $a=2.5$ mm, $b=15$ mm, $c=17$ Ambient medium is soil type keuper marl with a moisture content of 6.5%, $\epsilon_r=18$ and $\sigma=0.1$ S/m (1MHz) changing to $\epsilon_r=14$ and $\sigma=0.4$ S/m (300 MHz).

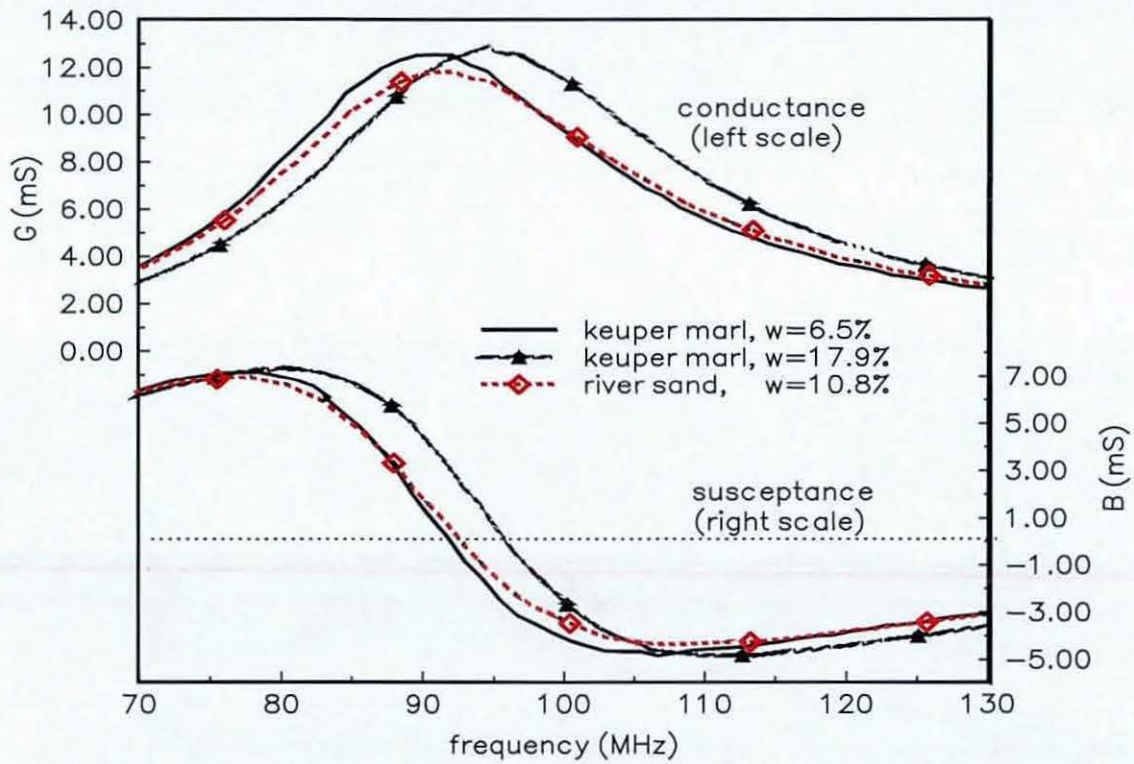


Figure 3.9. Simulated admittance for monopole with length $h=0.556$ m in three different soils.

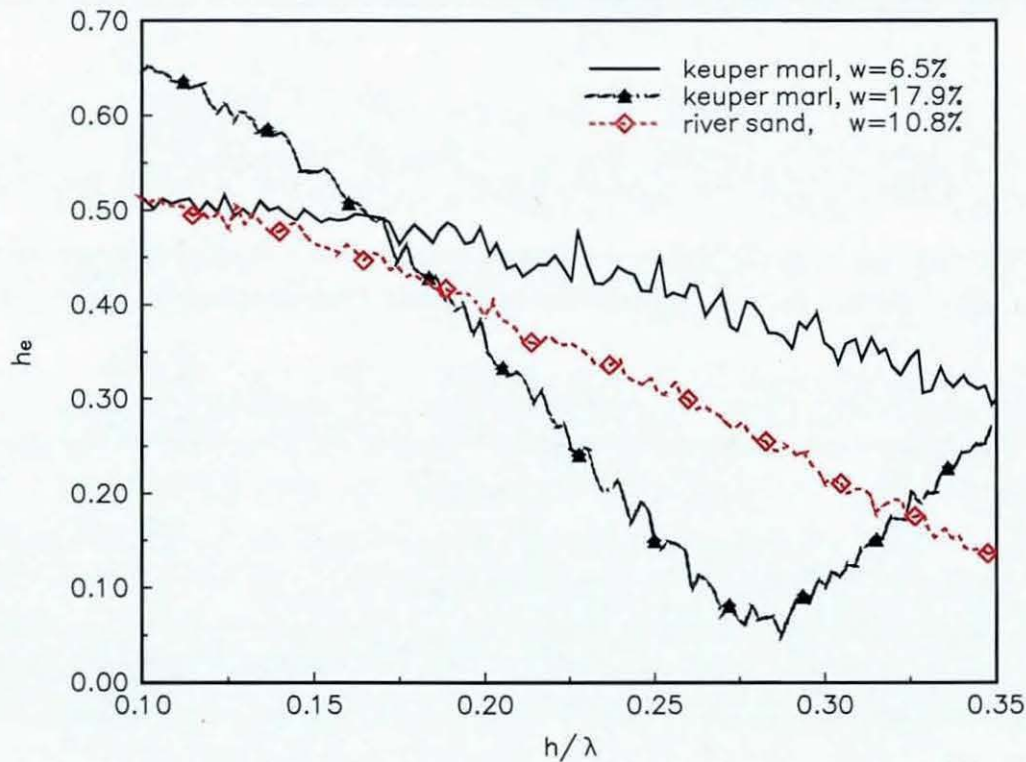


Figure 3.10. Effective length of a monopole antenna with length $h=0.441$ m in different soils. At resonance, when $h/\lambda=0.25$, the effect of the soil electrical properties on the antenna effective length is significant.

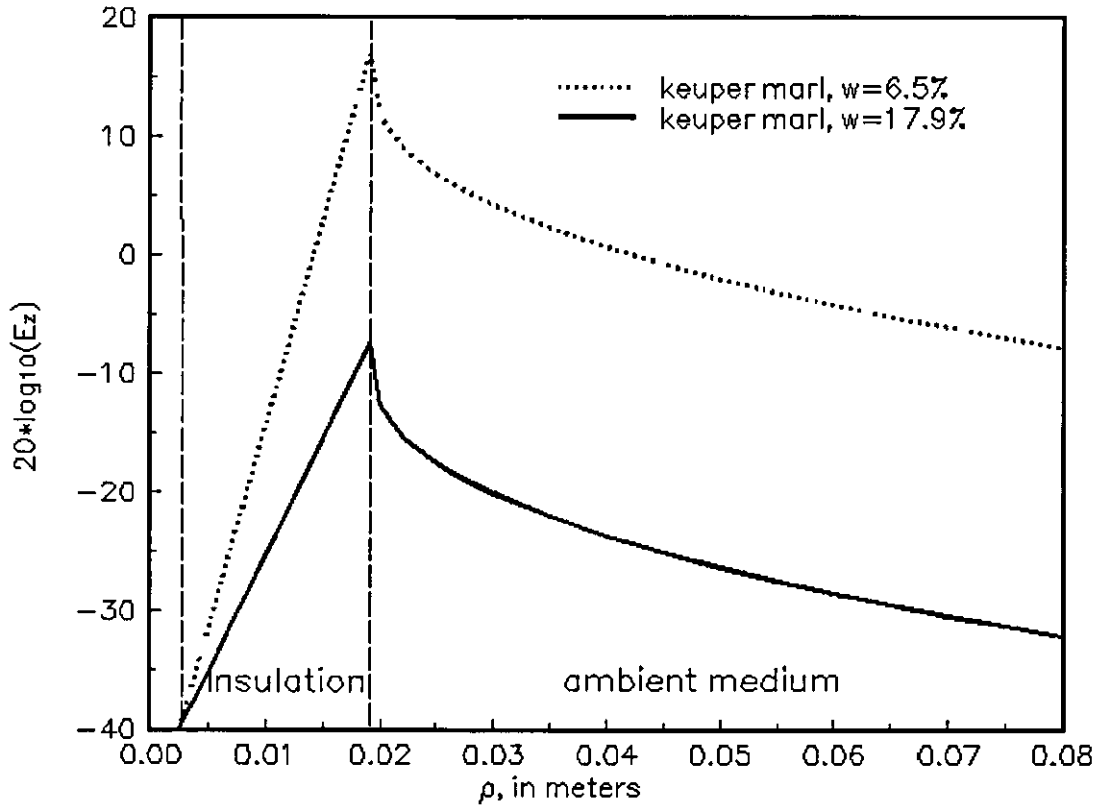


Figure 3.11 Predicted field of a dipole antenna with length $h=0.441$ m in different soils

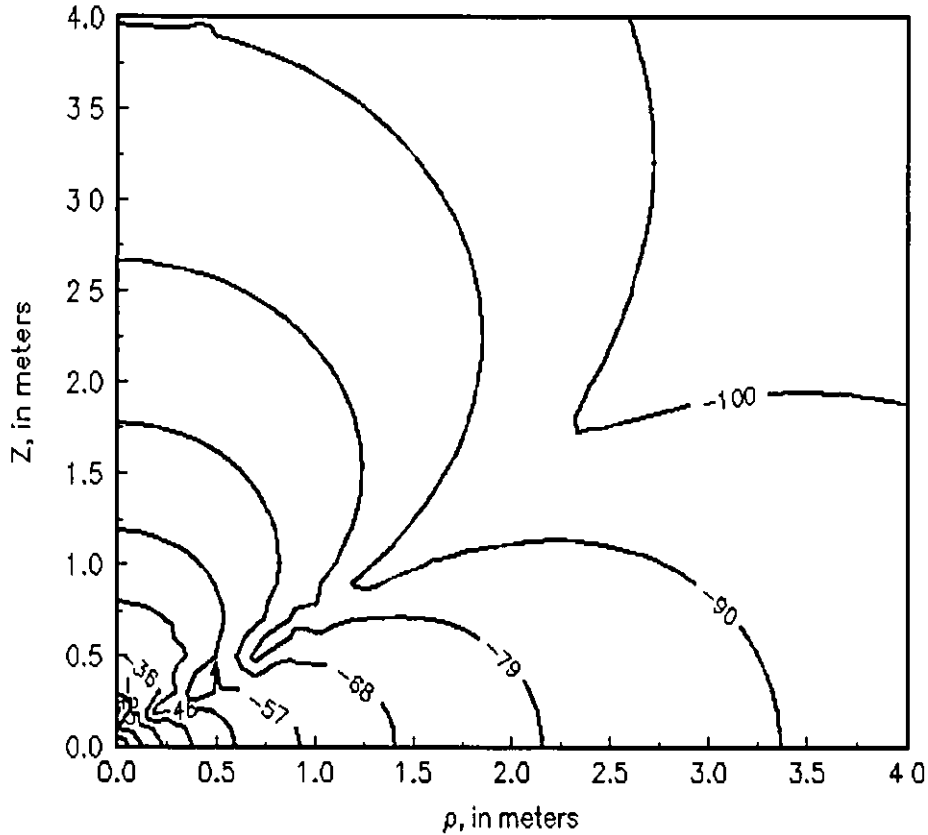


Figure 3.12 Predicted field of a dipole antenna with length $h=0.441$ m. Ambient medium is keuper marl, $w=6.5\%$, $\epsilon_r=14.59$, $\sigma=0.0084$. Input voltage at antenna terminal: 50 Volts

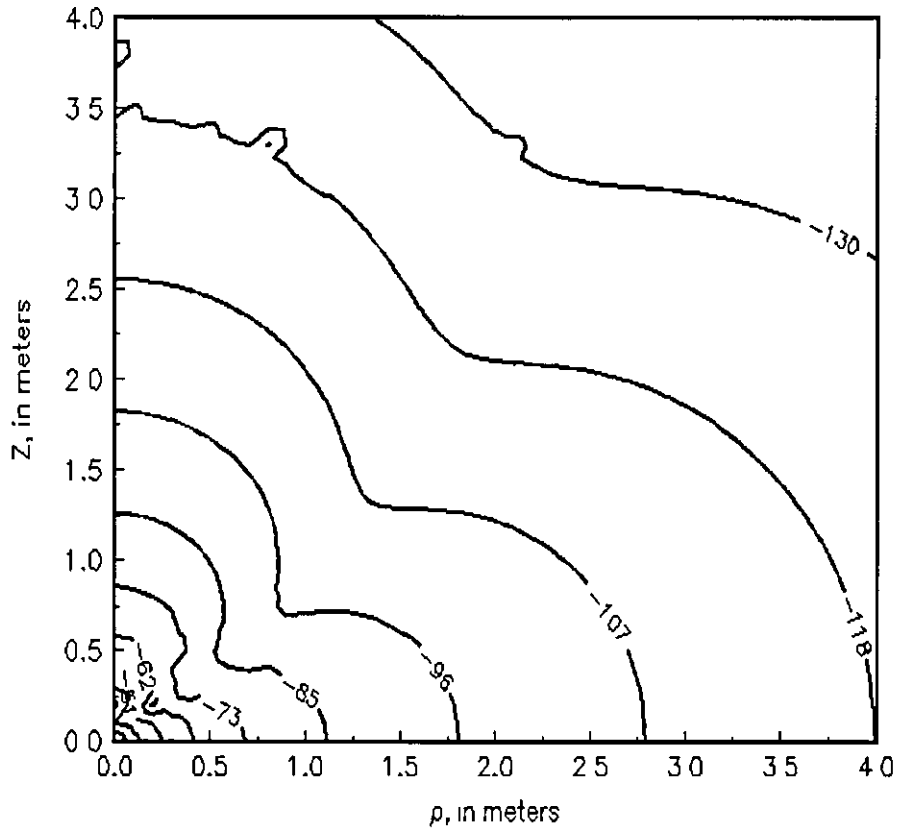


Figure 3.13 Predicted field of a dipole antenna with length $h=0.441$ m. Ambient medium is keuper marl, $w=6.5\%$, $\epsilon_r=32.99$, $\sigma=0.1305$. Input voltage at antenna terminal 50 Volts

References

- [1] Galejs, J, '*Antennas in Inhomogeneous Media*,' Pergamon, 1969.
- [2] Chatterjee, R, '*Dielectric and Dielectric-Loaded Wire Antennas*,' Research Study Press, James, J.R. (Ed.), John Wiley & Sons, New York, 1985.
- [3] Lee, M K , Smith, G.S., 'Measured Properties of Bare and Insulated Antennas in Sand,' *IEEE Trans. Antennas & Propagation*, AP-23, p664, 1975.
- [4] King, R.W P., 'Insulated Linear Antennas' Theory and Experiment, '*Journal of Applied Physics*, Vol 45, No. 4, April 1974, pp 1688-1697.
- [5] Tillema, N.J.P., Vardaxoglou, J C , Parish, D.J., 'Dielectric Constant Measurement of Soil samples Using a Coaxial Probe,' 24th *Automated RF & Microwave Measurement Society (ARMMS) Conference*, Windermere, 18th and 19th April 1996.
- [6] King, R.W P., Smith, G.S., '*Antennas in Matter*,' Chapter 1, The MIT Press, Cambridge, MA, 1984.
- [7] Casey, J.P., "*Dielectrically Loaded Wire Antennas*", PhD thesis, University of Connecticut, 1987.
- [8] Bahl, I.J., Stuchly, S.S., "Effect of Finite Size of Ground Plane on the Impedance of a Monopole Immersed in a Lossy Medium," *Elect Lett.*, Vol 15, No 22, 1979, pp728-729
- [9] Moore, R K , "Effects of a Surrounding Conducting Medium on Antenna Analysis," *IEEE Transactions on Antennas & Propagation*, May 1963, pp 216-225.

4.Underground Propagation

4.1. Introduction

In comparison with electromagnetic wave propagation in air, underground propagation is limited by the high attenuation due to the conductivity of soils and rocks. Environmental factors like soil electrical properties and soil structure are seldom known, making the prediction of underground propagation difficult. In this study the range of depth of the transmitter was in between 0.01 and 3 m while the receiver was at 0.05 m depth and hence the air-ground boundary affected the mode of propagation.

The research aimed to have a simulation model that predicted the path loss for an electromagnetic wave propagating underground. Using the simulation model and the results from extensive field trials, the feasibility of underground navigation using electromagnetic waves was investigated. The antenna characteristics and the soil structure and electrical properties discussed in previous chapters were used here as an input into the model.

This problem of underground propagation can be approached in two different ways. One approach would be by using numerical algorithms to calculate closed form integral equations of the problem. An example of this is the Numerical Electromagnetic Code (NEC) version 3, developed at the Lawrence Livermore Laboratory [1]. NEC combines an electrical field integral equation for wires and a magnetic field integral equation for surfaces to model wire antennas in their environment. The equations are solved numerically using the Method of Moments (MoM) method. The other approach would be to derive approximate simple equations that represent the different polarisation of the wave propagating underground [2]. In understanding and optimising underground propagation, this second method allows the analysis of the wave components

independently and therefore gives more information. The path loss and phase velocity measured in the field trials were compared with the predicted results. The investigation into underground navigation using electromagnetic waves discussed in this chapter was based on the results of experiments of underground and underwater electromagnetic wave propagation

4.2. Background

The study of the propagation of electromagnetic waves in an imperfect dielectric is of relevance to geophysical exploration, subsurface communication, terrestrial mobile communication and medical imaging. Some early publications [1,2] focus on communication through the earth's crust. The ground is assumed to consist of a flat layer of dry rock of approximately constant thickness over the transmission path, surrounded on both sides by wet layers of higher conductivity and a thickness greater than the skin depth. The basement layer of granite rocks in the earth's crust has a low conductivity. If the transmitting and receiving antennas can be placed within the basement granite, the propagation attenuation is expected to be very low. Early publications on submarine communications described experiments in which electromagnetic waves transmitted from submarines submerged 6 m deep could be detected in air at a distance of 1 km [3]. Electromagnetic waves are highly attenuated in seawater, due to its high conductivity, except at low frequencies for which practical distances are in the near field. The sea can be assumed to be a homogeneous dielectric and the propagation can be modelled as occurring in a dielectric halfspace with a dielectric constant and conductivity.

Measurements in a lake [4] at 144 MHz conclude that the path loss over 100 m is 50 dB. The transmitter and receiver dipole antennas are positioned in the lake water, just below the air-water boundary. The relative permittivity and conductivity of the lake water were measured and found to be 81 and 0.06 S/m, respectively. This conductivity is very low compared to that measured for soil samples in this study and the loss experienced in underground propagation are therefore expected to be much higher. The lake water can be assumed to be a homogeneous dielectric and, therefore, there were no reflections other than at the boundary with the air.

Other research has suggested the use of electromagnetic waves for holographic imaging of underground objects [5,6]. The propagation velocity of electromagnetic waves in soil is an essential parameter for reconstructing object images. The subject depth and the

propagation velocity in soil can be estimated, in principle, from any two transmitter-receiver tracks. The depth of the object is estimated from the time between transmission and reception of the radio burst, taking into account the distance between the transmitter and receiver. Using many of different distances between transmitter and receiver results in a high accuracy of the estimated velocity. The frequencies used are in the range 500 – 1000 MHz. The ground acts like a lowpass filter. Dipole antennas are used, laying on the ground surface or sometimes buried up to a depth of 50 cm. A similar system was developed to find underground water in the desert [7]. Both the transmitting and receiving antennas were on the ground surface. In order to ensure the minimum amount of refraction and to avoid total reflection from various underground strata, the incident wave should be as near to normal as possible. This means that the receiving and transmitting antennas are positioned close to each other. Using the variable distance between transmitter and receiver, water can be detected at depths in the range of 100 to 2000 m. The frequencies used are in the between 300 Hz and 4 kHz. Similar techniques are used to find geological faults [8]. From the reflection from the air-ground boundary, the ground intrinsic impedance is calculated. The soil stratified structure can be predicted from the impedance. The power of the reflected wave measured was lower than calculated with ray-optics theory that was used to find the impedance. Propagation studies through dense forest in which both the receiver and transmitter antenna are in the vegetation concluded that for a constant antenna height the received field varies inversely as the distance square [9]. The presence of the vegetation causes a constant loss. The wave travels from the transmitter antenna to the air-vegetation boundary and travels laterally along the boundary. The frequencies of the measurements are in the range 1-100 MHz. These results are relevant to terrestrial mobile communication, for example for Terrestrial Trunked Radio (TETRA) in the 420 MHz frequency band.

In seismology the lateral wave is usually called the head wave. Analogous to underground electromagnetic wave propagation, in acoustics there is a transversal wave, which is the direct wave, and the longitudinal wave, which is lateral wave. In the case of pulsed radiation the lateral wave reaches the point of observation first. Effective methods of seismic exploration are based on its recording and analysis [10]. The different velocities of the direct and lateral waves makes it possible to determine the epicentre of an earthquake.

4.3. Theory

The study of the propagation of electromagnetic waves along the boundaries of finite regions that may have irregularities, obstacles and discontinuities is made difficult by the uncertainty of the soil structure and properties. In one possible situation the soil was dry sand and its electrical behaviour could be approximated by a lossless homogeneous dielectric halfspace. Another situation was when the soil consisted of stratified layers of soil types with various dielectric constants and conductivities. Here, the wave propagates between the ground – boundary and any boundary between the strata of soil. To be able to solve Maxwell's equations for the boundary conditions in an inhomogeneous medium, it would be necessary to model the material on a microscopic level. From the dielectric constant and conductivity survey as reported in chapter 3, it became clear that the soil structure was far too complicated to model on a microscopic level. Hence the soil was assumed to a homogeneous isotropic dielectric halfspace. On the day of the field measurements, soil samples were taken and the dielectric constant was measured on site.

4.3.1. Modes of Propagation

The properties and structure of what was underground allows for various modes of propagation. A single dielectric interface supports a lateral wave while structures with multiple boundaries support other field varieties, known as leaky waves. The energy shifting properties of leaky waves are much stronger than these of lateral waves. Within the half space region the wave must satisfy the Helmholtz equation:

$$(\nabla^2 + k^2)\varphi = 0, \quad (4.1)$$

where φ is any of the field components and k is the propagation constant in region 0 (air). Given that the wave propagates in the x direction, the solutions appear in the form. (Stratton)

$$\varphi = e^{i(k_x x - k_z z - \omega t)}, \quad (4.2)$$

where k_x and k_z satisfy the dispersion equation:

$$k_z = \sqrt{k^2 - k_x^2}, \quad (4.3)$$

These boundary conditions satisfy for complex values k_p of k_x , which can be written as:

$$k_p = \beta + i\alpha. \quad (4.4)$$

The phase factor of the wave is $k \sin(\theta)$, where the wave is incident or reflected at an angle θ . There are a number of possible solutions that satisfy the boundary conditions [11]. When the wavenumber k_x is in between $-k$ and k , then the wavenumber is real and ϕ is a homogeneous wave. In the case that $|k_x|$ is larger than k , k_z must be imaginary therefore ϕ is an inhomogeneous wave. For discrete values of k_x the continuity equation at the boundary is satisfied and ϕ is a surface wave. A surface wave propagates along an interface between two different media without radiation. This radiation is energy converted from the surface wave field to some other form. The wave propagates along an idealised surface, which is a perfectly smooth and longitudinal straight interface [12]. The surface is assumed to be smooth when any obstacle is smaller than $1/16 \lambda$.

When $k_x = k_p$, ϕ is a complex guided wave. In case of a single dielectric interface, this guided wave is a lateral wave, while structures with multiple boundaries this will be a leaky wave. When the medium is lossless, k is real and to satisfy equation (4.3), k_z has to be complex also, resulting in an evanescent incident wave. Because of this decay, a homogeneous (plane) wave cannot by itself excite a lateral wave. When vertically polarised, an inhomogeneous wave suffers an exponential delay in the z direction and therefore possesses a field structure with an evanescent distribution over the wavefront. Therefore, a line source or point source can nevertheless excite a lateral wave in a lossless medium.

The entire wave splits in two groups of waves in propagating along the boundary. In the first group there are the usual incident wave, the corresponding reflected wave, and the refracted wave, which are all exponentially decaying waves, as is shown in figure 4.1. In the second group is the wave refracted and propagating along the boundary, and the lateral wave. Each group propagates with its own velocity and satisfies the boundary conditions separately [10]. A way of analysing the propagation of surface waves and lateral waves is by defining the surface impedance of the guiding structure in terms of field components. The wave attenuation depends not only on the physical properties of the guiding structure, but also on the nature of the field. For a given structure there are two possible values for this impedance, one depending on the transversal electric field and longitudinal magnetic field and the other (for perpendicular surface waves) on the longitudinal electric field and the transversal magnetic field. Once the surface impedance has been defined, the decay factor of the surface wave can be related to it. This relation also depends on the surface

geometry. The field must penetrate a finite distance into the guiding structure, because a finite volume is required for the storage of energy [12]. In general, an increase in the reactance will reduce the effective spread of the surface wave field outside the surface, and at the same time reduce its phase velocity along the interface. Any increase in the resistance tends to tilt the wavefront (represented by an equi-phase plane outside the surface) forward, so that a larger proportion of the power is directed into the surface. This results in increasing the value of the phase velocity in the direction of the interface. The higher the reactance of the supporting surface the more closely is the dense part of the field confined to the surface region and the smaller is the radiation arising from any slight curvature in the direction of propagation.

4.3.2. Approximate Equations for the Lateral Wave

The first investigator to present a theory of ground-wave propagation over flat earth was Sommerfeld in 1899 [13]. The wave he described is excited by a vertical dipole antenna above earth. Zenneck, one of Sommerfeld's students, gave the appropriate solution of Maxwell's equations for the inhomogeneous plane wave over a flat surface with finite losses, and this is a surface wave. In 1936, Norton published simplified equations for the lateral wave component of Sommerfeld's complicated solution [14]. Baños [15] derived approximate equations for subsurface dipoles in seawater. In this model the wavenumber in air, region 0, is $k_0 = \omega(\mu_0 \epsilon_3)^{1/2}$ and the sea water, region 4, has a wavenumber $k_4 = \omega[\mu_4(\epsilon_4 + i\sigma_4/\omega)]^{1/2}$ in which $\epsilon = (\epsilon_r' - i\epsilon_r'')\epsilon_0$ is the dielectric constant, $\mu = \mu_0$ is the magnetic permeability and $\sigma = \omega\epsilon_r''\epsilon_0$ is the conductivity of the medium. The seawater is assumed to be non-magnetic. The radial distance between the transmitter and receiver dipoles is ρ , while the transmitter and receiver are at depths d and z respectively. The point of observation is specified in cylindrical co-ordinates (ρ, ϕ, z) with region 4 defined by $z > 0$ and region 0 (air) by $z < 0$. The positive x-axis lies along the axis of the dipole and its origin coincides with the origin of the cylindrical co-ordinates as is shown in figure 4.2. The source is a dipole normalised to have an unit electric moment ($I \Delta l = 1$ Am). For the near field the field components for distances in between: $k_0 \rho < 1 < |k_4 \rho|$

$$E_{4\rho} = \frac{i\omega\mu_0}{2\pi k_4^2} \frac{\cos\phi}{\rho^3} e^{i(k_0\rho + k_4(d+z))} \quad (4.5)$$

$$E_{4\phi} = -\frac{i\omega\mu_0}{\pi k_4^2} \frac{\sin\phi}{\rho^3} e^{i(k_0\rho + k_4(d+z))} \quad (4.6)$$

$$E_{4z} = -\frac{\omega\mu_0 k_0^2}{2\pi k_4^3} \frac{\cos\phi}{\rho^2} e^{i(k_0\rho + k_4(d+z))} \quad (4.7)$$

The field components for the intermediate field, for distances ranging from:

$$\left| \left(k_0/k_4^2 \right) k_0 \rho \right| < 1 < k_0 \rho$$

$$E_{4\rho} = -\frac{i\omega\mu_0 k_0^2}{2\pi k_4^2} \frac{\cos\phi}{\rho} \left[1 + i \frac{k_0}{k_4} \sqrt{i\pi k_0 \left(\frac{\rho}{2} \right)} \right] e^{i(k_0\rho + k_4(d+z))} \quad (4.8)$$

$$E_{4\phi} = -\frac{\omega\mu_0 k_0}{2\pi k_4^2} \frac{\sin\phi}{\rho^2} \left[1 + i \frac{k_0}{2k_4} \sqrt{i\pi k_0 \left(\frac{\rho}{2} \right)} \right] e^{i(k_0\rho + k_4(d+z))} \quad (4.9)$$

$$E_{4z} = \frac{i\omega\mu_0 k_0^3}{2\pi k_4^3} \frac{\cos\phi}{\rho} \left[1 + i \frac{k_0}{k_4} \sqrt{i\pi k_0 \left(\frac{\rho}{2} \right)} \right] e^{i(k_0\rho + k_4(d+z))} \quad (4.10)$$

In comparing these equations for $E_{4\rho}$ the wave attenuation is proportional to $1/\rho^2$ in the near field and approximately $1/\rho$ in the intermediate field. The attenuation is expected to reduce when the wave travels from the near to the intermediate field. Also in the near field E_{4z} shows the lowest attenuation. The attenuation as a function of depth of the transmitter and receiver is exponential and has a major contribution to the overall attenuation, as k_4 is higher for lossy material. The model as proposed by R.W.P. King has shown to be accurate for propagation in sea and lake water [2]

The lateral-wave field of electric type has the following components in the earth or sea:

$$E_{4\rho}(\rho, \phi, z) = -\frac{\omega\mu_0}{2\pi k_4^2} \cos(\phi) \left\{ k_0 g(\rho, k_4, k_0) e^{ik_0\rho} e^{ik_4(z+d)} \right. \quad (4.11)$$

$$\begin{aligned} & - \left(\frac{k_4}{r_1^2} + \frac{i}{r_1^3} \right) e^{ik_4 r_1} + \left(\frac{z+d}{\rho} \right) \left(\frac{ik_4}{\rho^2} - \frac{3}{2\rho^3} \right) e^{k_4 r_2} \\ & \left. - \frac{1}{2} \left[\left(\frac{z-d}{r_1} \right)^2 \left(\frac{ik_4^2}{r_1} - \frac{3k_4}{r_1^2} - \frac{3i}{r_1^2} \right) e^{ik_4 r_1} + \left(\frac{z+d}{r_2} \right)^2 \left(\frac{ik_4^2}{r_2} - \frac{3k_4}{r_2^2} - \frac{3i}{r_2^2} \right) e^{ik_4 r_2} \right] \right\} \end{aligned}$$

$$\begin{aligned}
E_{4\phi}(\rho, \phi, z) = & -\frac{\omega\mu_0}{2\pi k_4^2} \sin(\phi) \left\{ k_0 h(\rho, k_4, k_0) e^{ik_0 \rho} e^{ik_4(z+d)} \right. \\
& + \frac{1}{2} \left[\left(\frac{ik_4^2}{r_2} - \frac{3k_4}{r_2^2} - \frac{3i}{r_2^3} \right) e^{ik_4 r_2} - \left(\frac{ik_4^2}{r_1} - \frac{k_4}{r_1^2} - \frac{i}{r_1^3} \right) e^{ik_4 r_1} \right] \\
& \left. + i \left(\frac{z+d}{r_2} \right) \left(\frac{ik_4^2}{\rho} - \frac{3k_4}{2\rho^2} - \frac{5i}{8\rho^3} \right) e^{ik_4 r_2} - \left(\frac{z+d}{r_2} \right) \left(\frac{ik_4^2}{r_2} - \frac{3k_4}{r_2^2} - \frac{3i}{r_2^2} \right) e^{ik_4 r_1} \right\}
\end{aligned} \quad (4.12)$$

$$\begin{aligned}
E_{4z}(\rho, \phi, z) = & -\frac{\omega\mu_0}{2\pi k_4^2} \cos(\phi) \left\{ \frac{k_0}{k_4} f(\rho, k_4, k_0) e^{ik_0 \rho} e^{ik_4(z+d)} \right. \\
& - \frac{1}{2} \left[\left(\frac{\rho}{r_1} \right) \left(\frac{z-d}{r_1} \right) \left(\frac{ik_4^2}{r_1} - \frac{3k_4}{r_1^2} - \frac{3i}{r_1^3} \right) e^{ik_4 r_1} \right. \\
& \left. \left. + \left(\frac{\rho}{r_2} \right) \left(\frac{z+d}{r_2} \right) \left(\frac{ik_4^2}{r_2} - \frac{3k_4}{r_2^2} - \frac{3i}{r_2^3} \right) e^{ik_4 r_2} \right] \right\}
\end{aligned} \quad (4.13)$$

In these equations $f(\rho, k_1, k_2)$, $g(\rho, k_1, k_2)$ and $h(\rho, k_1, k_2)$ are:

$$f(\rho, k_1, k_2) = \frac{ik_2}{\rho} - \frac{1}{\rho^2} - \frac{k_2^3}{k_4} \left(\frac{\pi}{k_2 \rho} \right)^{1/2} e^{-ip} F(p) \quad (4.14)$$

$$g(\rho, k_1, k_2) = \frac{ik_2}{\rho} - \frac{1}{\rho^2} - \frac{i}{k_2 \rho^3} - \frac{k_2^3}{k_4} \left(\frac{\pi}{k_2 \rho} \right)^{1/2} e^{-ip} F(p) \quad (4.15)$$

$$h(\rho, k_1, k_2) = \frac{2}{\rho^2} + \frac{2i}{k_2 \rho^3} + \frac{ik_2^2}{k_1 \rho} \left(\frac{\pi}{k_2 \rho} \right)^{1/2} e^{-ip} F(p) \quad (4.16)$$

With the Fresnel Integral equation:

$$F(P) = \frac{1}{2}(1+i) - C_2(P) - iS_2(P) \quad (4.17)$$

where

$$C_2(P) + iS_2(P) = \int_0^P \frac{e^{it^2}}{\sqrt{2\pi i}} dt \quad (4.18)$$

The equation $C_2(P) + iS_2(P)$ can be written in the form of a series expansion of the complex error function [16]. The parameters P, R and Z are:

$$P = \frac{(R-Z)^2}{R} \quad R = \frac{k_2^3 \rho}{2k_1^2} \quad Z = \frac{k_2^2 z}{2k_4} \leq 0 \quad (4.19)$$

In (4.11), (4.12) and (4.13) the radial distances r_1 and r_2 are given by:

$$r_0 = \sqrt{\rho^2 + z^2} \quad r_d = \sqrt{\rho^2 + d^2} \quad (4.20)$$

The direct field is given by all terms with $e^{ik_4 r_1}$, in which r_1 is the direct path and k_4 is the complex wavenumber of the electromagnetic wave in the dielectric. The reflected field is the sum of all terms with $e^{ik_4 r_2}$. The lateral wave field is given by all term with $e^{ik_0 \rho} e^{ik_4(z+d)}$. From this equation, it becomes clear that the magnitude of the received signal is exponentially attenuated with the depth of both the transmitting and receiving antennas. When z and d are constant, the lateral wave attenuates exponentially with distance ρ and with a wavenumber k_0 .

In region 4, when $z \geq 0$ and $|k_4| \gg |k_2|$. Equations (4.11) to (4.13) were tested for lake water and seawater, whereby water, by its nature, can assumed to be homogeneous. In these measurements, the properties of the dielectric are constant in time. Electromagnetic wave propagation underground is made difficult by the uncertainty of the composition of the soil and its electrical properties. Additionally, weather causes the dielectric constant and conductivity to change, making electromagnetic wave propagation underground change with time and location. As discussed in chapter 3, an increase in soil moisture content increases the dielectric constant and conductivity and, therefore, also the wavenumber and the mode of propagation of the electromagnetic wave underground. This means that the path of the strongest signal received also depends on environmental conditions like the weather. Also, the path of the strongest signal varies, as it is a function of distance between the transmitter and receiver. As part of this research, extensive field trials were undertaken to measure the amplitude and phase of the received signal. Equations (4.11) to (4.13) were used to simulate the field trials to evaluate their validity for various conditions. The first measurements are on underwater propagation, as the medium is homogenous and the environmental conditions for the experiment are easily controlled. The electrical properties of the medium are measured on site at the day of the measurements and used in the simulations. When the theoretical results are in good agreement with the measurements, the propagation modes are analysed. Then the environmental parameters were changed to study possible variations in phase and

amplitude of the received wave. The aim of the study was to predict the displacement of an underground transmitter, using one or more receiver antennas on the ground surface. Related publications were on underground radar, which focus on applications where the transmitting and receiving antennas are a few m above the target. A situation where the transmitter is 3 m deep underground and with a radius up to 60 m away from the receiver antenna is a different problem. Soil aggregates, by their nature give a variation of attenuation and wavelength change of electromagnetic waves travelling through them. Abrupt changes in dielectric constant or underground pipes or objects may result in wave reflection. Reflections from underground pipes will greatly depend on the location and orientation of the pipe relative to the wave polarisation. Also the conductivity of their material makes a difference to the reflection. The data from the field trials are examined for evidence of reflections on objects. In the prediction of underground wave propagation, the soil was assumed to be a semi-infinite homogeneous medium. The data from the survey was used to find realistic values for the ϵ_r and σ used as input parameters in the model. The survey data was also used to explain the propagation measurements. An important question in the study was the strength of the lateral wave and surface wave, if present at all. It was expected that the irregular surface of the field where the trials were taking place might obstruct such a mode of propagation.

To analyse the modes of propagation that exist near the boundary between medium 0 (air) and medium 4 (ground), first the reflection coefficient of a homogeneous plane wave excited by a source (1) in air and (2) underground were calculated. The plane wave reflection coefficient of magnetic type, in which the electric field is perpendicular to the plane of incidence, is

$$f_{mr} = |f_{mr}| e^{-j\phi_{mr}} = \frac{\cos(\theta) - y_m(\theta)}{\cos(\theta) + y_m(\theta)}, \quad (4.21)$$

where y_m is the normalised magnetic surface admittance given by.

$$y(\theta) = \sqrt{n^2 - \sin^2(\theta)}, \quad n^2 = \left(\frac{k_4}{k_0} \right)^2 = \epsilon_4 - \frac{j\sigma_4}{\omega\epsilon_0} \quad (4.22)$$

In equation (4.22) n is the refraction index for both types of reflection coefficient. The plane wave reflection coefficient of electric type, in which the electric field is parallel to the plane of incidence, is

$$f_{er} = |f_{er}| e^{-j\phi_{er}} = \frac{\cos(\theta) - z_e(\theta)}{\cos(\theta) + z_e(\theta)}, \quad (4.23)$$

where z_{se} is the normalised electric surface impedance given by:

$$z_{se}(\theta) = \frac{\sqrt{n^2 - \sin^2(\theta)}}{n^2}, \quad (4.24)$$

Figure 4.3 shows the magnitude of f_{er} and f_{mr} for a homogeneous plane wave in air, reflected on the ground. Medium 4 is soil and was assumed to be a homogenous isotropic medium. The soil characteristics vary from relatively dry sand and clay aggregate soil with a gravimetric moisture content of $w = 6.3\%$ to wet soil with $w = 22.7\%$. The conductivity varied between $\sigma = 0.02$ S/m and 0.17 S/m. Figure 4.4 shows the magnitude of f_{er} and f_{mr} as a function of conductivity. The magnitude of f_{er} was at a deep minimum when the angle of incidence is near $\pi/2$. When medium 4 (ground) had the highest conductivity and dielectric constant, the reflection coefficient was the lowest. This suggested the highest absorption of energy caused by currents at the surface. From geometric optics, the Brewster angle is the critical angle of incidence ϕ_c when there is no reflection or transmission and the wave is refracted and propagates along the surface. When the medium below the surface is lossless the angle of incidence ϕ_c is real. For a lossy dielectric like the soils in figure 4.3, the plane homogeneous wave can no longer experience zero reflection and the angle of incidence is known as the pseudo-Brewster angle for which f_{er} is a minimum. In these circumstances, the wave cannot be regarded as a characteristic mode of the surface [12]. Only an inhomogeneous wave is capable of satisfying the requirements of a pure mode supported by a lossy surface. The Zenneck surface wave is an inhomogeneous plane wave in air incident on a flat surface at the Brewster angle. Graphs of f_{er} and f_{mr} for a homogeneous plane wave in medium 4 (underground) reflected against the boundary with medium 0 (air) are shown in figure 4.5. The magnitude for f_{er} shows the deepest minimum for the soil with the low conductivity. This minimum moves closer to zero when the conductivity increases. The differences in f_{er} and f_{mr} for a given angle of incidence is less significant than in figure 4.3. Overall, the reflection coefficients are high indicating that little energy is transmitted into medium 0 (air) or refracted along the surface when the angle of incidence is at the Brewster angle. The conditions under which the lateral surface wave exists are an inhomogeneous wave incident on the boundary with an angle of incidence that is near the Brewster angle. A lateral wave is a bundle of rays or a beam of bounded extent incident at the boundary at an angle ϕ , close to ϕ_c . A lateral wave is absent if the incident field is a homogeneous plane wave, so that the finite width of the incident field is essential in producing a lateral

wave The lateral wave manifests itself by (a) producing a lateral shift of the bounded reflected wave and (b) exciting a weak field that accompanies the reflected field. Neither of these two effects is accounted for by geometric optics [17].

Experiments have confirmed the validity of equations (4.11) to (4.13) by R.W.P. King when medium 4 is lake water. A comparison between these and the approximate equations for the near field and intermediate field derived by Baños are shown in figure 4.6. Between 0.3 m and 3 m distance the agreement between both approximations is good. At close range and far distances the differences are large. Equations (4.11) and (4.13) have been shown to be in very good agreement with numerical solutions of the Sommerfeld integral equations [2]. Hence they will be used in the rest of this chapter.

4.4. Equipment for Field Trials

4.4.1. Frequencies used

At the start of the field trials the modes of propagation excited by a transmitter underground were difficult to predict. The rough terrain surface and the uncertainty of what is underground made the excitation of surface waves unlikely. The use of HF or lower frequencies would make the size of effective antennas impractical for field trials. From the measurements of soil dielectric constant and conductivity that were used to predict the plane wave attenuation it was clear that transmission on frequencies above 500 MHz results in a very high attenuation. Partly from the predictions and partly from the practical concerns, it was decided to use frequencies in the range of 100 to 300 MHz.

4.4.2. Antennas Used

Unlike a conventional antenna in air, with parameters that are independent of the electromagnetic environment, reflections from the conducting surrounding media impinging upon an antenna underground can degrade such parameters as gain, bandwidth, sidelobe level. Also the absorption and storage of energy in medium 4 changes the antenna pattern. As was concluded in chapter 3, the positioning of a dielectric loaded dipole in a conductive medium resulted in a limited gain increase but also in desensitisation. In order to create a large electrical moment, it was possible to increase the

current to compensate for a small electrical length, but only up to the current carrying capacity of the conductor and the available power. It was evidently desirable to have as larger effective length as possible and to use minimum power. Therefore, dielectric loaded antennas were used with a length matched for the frequency and environmental parameters. As in the field trials, the circumstances in which the antennas were used varied greatly, dielectric loaded monopoles or dielectric loaded dipole antennas without a balun were used. The characteristics of the antennas were predicted after the field trials and fed into the simulation. Samples of the soil at the site were taken on the day of the trials and their characteristics measured on-site and in the laboratory.

4.5. Underwater Propagation Experiments

Experiments of underwater propagation were conducted in the basin in the Underwater Acoustics Laboratory at Loughborough University. The aim of the experiments was to measure electromagnetic wave propagation in a homogeneous half-space with a smooth plane boundary, as is assumed on the simulation model. Interference from reflections was very small, as the attenuation of the electromagnetic wave in water is significant. The measurements were done in the centre of the basin, away from the walls. The dielectric constant and conductivity of water were measured to be $\epsilon_r = 76.4$ and $\sigma = 0.0145$ S/m respectively. Two bare dipole antennas were used with a physical length of 0.75 m. The power fed into the transmitter antenna was 24 dBm. The measurement set-up is described in Appendix C. Both the transmitter and receiver antennas were submerged in the water to a depth of 0.02 m. The distance between them was varied between 0.10 and 2.00 m. Figure 4.7 shows the measured amplitude of the received signal, compared with the predicted signal, while figure 4.8 shows the phase. The agreement was very good except for distances smaller than 0.30 m, where the predicted power level was higher. The attenuation between 0.10 and 0.30 m was exponential and hence very sensitive to small errors in measurement of the distance between the antennas or the antenna horizontal alignment. The $1/r^3$ attenuation was characteristic of the direct wave. The phase of the received signal is shown in figure 4.8. Between 0.10 and 3.50 m the phase was nearly linear indicating a pure direct wave. The wavelength seen was the wavelength in water, which was 0.69 m, as calculated from the electrical properties of water. Between 3.5 and 8 m the lateral wave takes over from the direct wave, until after 8 m the lateral wave

becomes dominant. The amplitude of the reflected wave was very small. As the antennas were very close to the water surface, there is no reflected field.

4.6. Underground Propagation Experiments

The measurements of underwater propagation have confirmed the validity of the theory in a situation where the medium in which the source was located was homogeneous and could be assumed to be a half-space. The study of the propagation of electromagnetic waves underground along the boundaries of finite regions that may have irregularities, obstacles and discontinuities was expected to result in greater differences between the prediction and the actual experiment. In this study the discontinuities were not included in the propagation simulation model, but any unexpected irregularities in the measurement were examined qualitatively. Studies of the dielectric constant and conductivity of soils in Chapter 2 have shown that the path loss of a plane electromagnetic wave underground was on average 15 dB/m for moist soils. Plane wave transmission over distances larger than 10 m in moist soil was therefore not feasible. This clearly suggested that the analyses of the underground propagation measurements should be focussed on lateral wave propagation near the air-ground boundary. In the extensive field experiments conducted as part of this study both the transmitter and receiver antennas were within 2 m from the air – ground boundary. The measurements were done in a field on the campus of Loughborough University. For a distance of 30 m a pipe was laid underground, using a micro tunnelling machine. The maximum depth of the pipe was 1.5 m. The depth and location of the underground pipe was estimated from a location system, based on the magnetic field excited from a coil in the drill. By finding the strongest signal, the location of the drill was found. Then the depth of the drill was estimated, using the strength of the magnetic field. This location system requires the receiver to be above the drill, which may not be possible in many applications. Examples are the drilling under a river or railway line. The plastic pipe has an inner diameter of 48.5 mm and a thickness of 6 mm. A diagram of the site and pictures are included in Appendix B. The pipe functions as a micro tunnel through which the transmitter was moved. The aim of the project was to estimate the underground displacement of the transmitter by measuring the amplitude and phase at the receiver antenna(s). There was a frequency spectrum because the oscillation died out in a finite time. The damped oscillations of the soils and water particles produced a narrow band of frequencies. In all the measurements, a dielectric loaded dipole antenna

underground was used as the transmitter antenna. In the experiments where the receiver antenna was underground, a dielectric loaded dipole antenna was used. For one experiment a monopole in medium 0 (air) was used as a receiver antenna.

In order to achieve a higher accuracy in locating the underground transmitter the phase of the received signal was measured, in addition to the amplitude. These measurements proved more difficult as the phase measurements were more sensitive to errors as slight movements were detected. As in the previous measurement, the transmitter was moved through the pipe on campus at Loughborough University, and measurements were taken at steps of 0.10 m. The receiver antenna was positioned at various locations underground and, for one measurement, at 0.5 m height above ground. The measurement of both amplitude and phase started in December 1995 and lasted until July 1996. As this period included three of the annual seasons, the weather conditions during the measurements varied between a temperature of -5 degrees Celsius and snow, to $+26$ degrees C. and sunshine. These variations were reflected in the moisture of the soil. As the soil electrical properties were measured at the start of each field trial, the changes in environmental parameters were included in the simulations. Equations (4.11) to (4.13) were used to predict underground wave propagation. The equations were derived for dipole antennas with a uniform current distribution.

4.6.1. Field Trial 1, Receiver Antenna Underground

The location of an underground transmitter by means of measuring the received amplitude only has shown to give results that compared well with the simulations. At the start and end of the measurements, when the transmitter was near position 0 and 30 m displacement, there was a difference between the average power measured and predicted. The radial field component $E_{4\rho}(\rho, \phi, z)$ was measured due to a horizontal dipole at various locations in the pipe underground. Figure 4.9 shows the magnitude of the received signal when the receiver antenna was located in position A3 (see appendix C). In this position the receiver antenna was 2.5 m away from the starting position of the transmitter and aligned perpendicular to the transmitter antenna. The starting position of the transmitter was 2 m behind the transceiver. Figure 4.9 shows a maximum at 2 m displacement when the distance between the transmitter and receiver is a minimum. The measurements were done at $f = 146.5$ MHz. The receiver antenna was a dielectric loaded dipole antenna at

0.02 m depth underground while the transmitter was moved through the pipe in steps of 0.10 m. The dielectric constant and conductivity of the soil were measured to be $\epsilon = 15$ and $\sigma = 0.012$ S/m. The antenna efficiency h_e was predicted from the antenna physical dimension, its depth and the soil electrical properties. From this, $h_e = -0.0074 + 0.1315j$. From the wavenumber of the soil k_4 , the wavelength underground was $\lambda_4 = 0.52$ m. The wavelength in air was $\lambda_0 = 2.0$ m. There was a good agreement between the measured and predicted amplitude. In the short distance when the displacement was in between the start and 6 m, the prediction shows the interference of the direct and the lateral waves. The interference pattern measured was different from the prediction, but the amplitude variation was in the same order of magnitude. The differences were attributed to the inhomogeneous soil and inaccuracies in the measurement of distances. At displacement distances greater than 6 m, the prediction showed no ripple. Figure 4.11 shows the prediction of the direct wave $E_{4p, \text{direct}}$, the reflected wave $E_{4p, \text{reflected}}$ and the lateral wave $E_{4p, \text{lateral}}$ of the total field E_{4p} for identical conditions as the measurements in figure 4.9, but for a dipole normalised to have an unit electric moment ($I \Delta l = 1$ Am). Analyses of figure 4.11 shows that the lateral wave component $E_{4p, \text{lateral}}$ was stronger at every point in the measurement. When the transmitter and receiver were separated at a short distance, $E_{4p, \text{lateral}}$ is still approximately 11 dB above $E_{4p, \text{direct}}$ while the magnitude of $E_{4p, \text{reflected}}$ is insignificant. The minimum of $E_{4p, \text{reflected}}$ at approximately 2 m displacement was because at this point the transmitter and receiver antennas alignment was perpendicular. Between 6 and 10 m displacement, the lateral wave component was 20 dB stronger than the direct wave and approximately 40 dB stronger than the reflected wave. The lateral wave was significantly stronger than the direct wave and the interference pattern seen at closer distances disappear after 6 m displacement. Overall the ripple of the amplitude at distances greater than 6 m corresponded to two wavelengths: $\lambda/2 = 0.26$ m and $\lambda/2 = 1.00$ m. For example, between 16 and 18 m displacement the wavelength of the ripple was approximately 0.26 m, suggesting a standing wave underground. This pattern was seen on various locations evenly distributed over the graph. From this observation it is likely that the standing waves were caused by discontinuities underground or on the ground surface at various locations, in the form of rocks or metal objects. Between 10 and 14 m displacement the ripple has higher amplitude and its wavelength of approximately of 2.0 m was of that in air. The propagation path of the lateral wave starts at the transmitter,

travels to the ground – air boundary, then followed the ground surface and travels back into the ground to the receiver antenna. When it propagated along the surface in air, the wavelength $\lambda_{\text{lateral}} \sim \lambda_0 = 2.0$ m. Reflections of the lateral wave on the surface were caused by irregularities on the surface or objects, like the car with equipment used in the field trials, that reflected the wave.

Between 4 and 10 m displacement the phase was nearly linear indicating an almost pure travelling wave, as shown in figure 4.10. The measured wavelength λ was approximately 1.5 m. Between 3.2 m and 4.3 m displacement, $\lambda = 1.1$ m, between 4.3 and 5.7 m, $\lambda = 1.4$ m, between 5.7 and 7.2 m $\lambda = 1.5$ m and between 7.2 m and 9.3 m $\lambda = 1.9$ m. This increase in λ was due to the fact that while the transmitter moves away from the receiver, it also descends deeper into the ground, making the distance the wave travels underground longer. As $k_4 > k_0$ the wavelength increased as a result. The measured phase gives information on the increase in distance between transmitter and receiver, but also on the change in depth of the transmitter. If measurements were done at two or more frequencies, which would mean two phase measurements with the transmitter in the same position, it would be possible to distinguish the change of depth of the transmitter from the displacement in the x-plane.

The pure travelling wave stopped at 10 m displacement. This was the point at which the magnitude showed a standing wave pattern with a wavelength that approximates λ_0 . This suggests that the phase measurements were sensitive to the obstructions in the propagation path in air. After 10 m displacement, the measured period of the phase change follows the prediction, but the range of phase variation was less than predicted. Here the received signal consisted of two interfering vectors, in which one vector rotated as a result of the displacement of the transmitter and the other vector was fairly static. From observations during the measurements this was seen on the vector display of the HP8410 Vector Analyser. Taking into account any possible errors in the measurement of the transmitter displacement, the phase measurements showed a fairly good agreement with the predictions.

Figure 4.12 shows the total fields of $E_r(\rho, \phi, z)$, $E_\phi(\rho, \phi, z)$ and, for comparison again, $E_\rho(\rho, \phi, z)$ for a horizontal dipole normalised to have an unit electric moment ($|\Delta l| = 1$ Am). The normalisation shifted the graph of $E_\rho(\rho, \phi, z)$ approximately 20 dB down. At short distances, the relative magnitude of $E_r(\rho, \phi, z)$ and $E_\phi(\rho, \phi, z)$ is larger than $E_\rho(\rho, \phi, z)$.

The power level of $E_\phi(\rho, \phi, z)$ falls off very rapidly when the distance between transmitter and receiver increased. The magnitude of $E_z(\rho, \phi, z)$ is approximately 10 dB stronger than $E_\rho(\rho, \phi, z)$ up to 25 m displacement. As the wave is circular polarised, $E_z(\rho, \phi, z)$ shows a ripple that increases with distance. This ripple is not seen on the predictions of $E_\rho(\rho, \phi, z)$, as the ρ -vector was aligned with the Pointing vector. At longer distances $E_\rho(\rho, \phi, z)$ is stronger than $E_z(\rho, \phi, z)$. Because in the field trials the available power in the transmitter was limited, $E_\rho(\rho, \phi, z)$ was measured to achieve underground transmission over at least 30 m.

4.6.2. Field Trial 2, Receiver Antenna Underground

This field trial was done at the same site as trial 1. Also the antennas and equipment used were the same. The receiver antennas was located 2.5 m from the starting point at the beginning of the pipe, at position A2 in appendix C. Compared to field trial 1, the antenna is 5 m. closer to the pipe. The antenna was aligned parallel to the pipe and therefore $\phi = 0$ at the start of the measurement. The dielectric constant and conductivity of the medium 4 (soil) were measured to be $\epsilon_r = 15$ and $\sigma = 0.012$ S/m. The power fed into the transmitter antenna was measured to be 43.6 dBm (23 W). The radial field component $E_{4\rho}(\rho, \phi, z)$ was measured due to a horizontal dipole at various locations in the pipe underground. Figure 4.13 shows the magnitude of $E_{4\rho}(\rho, \phi, z)$. The graph shows that at the start $E_{4\rho}(\rho, \phi, z)$ was approximately 14 dB stronger than at field trial 1, because the receiver antenna was 5 m closer to the transmitter. Because of the shorter distance, the contribution of $E_{4\rho, \text{direct}}(\rho, \phi, z)$ to the total field was larger, which manifested itself in an interference pattern of $E_{4\rho, \text{direct}}(\rho, \phi, z)$ and $E_{4\rho, \text{lateral}}(\rho, \phi, z)$ up to 6 m displacement. The prediction showed that the interference pattern stops after 6 m displacement. There was a good agreement between the measured average power and the prediction. When the distance between transmitter and receiver increased, the measurement showed a ripple. The nature of the ripple suggested a standing wave pattern with approximate wavelengths of $\lambda_4 = 0.52$ m and $\lambda_0 = 2.0$ m. This was caused by reflections in air, for example between 12 m and 14 m displacement, when $\lambda_{\text{ripple}} = \lambda_0$, or reflection from discontinuities underground, for example between 20 and 21 m displacement, when $\lambda_{\text{ripple}} = \lambda_4$. Between 26m and 28m the ripple was caused by reflections both in air and underground. Both the measurements in field trials 1 and 2 showed a strong reflection in air at approximately 11 m displacement.

Figure 4.14 shows the phase of $E_{4\rho}(\rho, \phi, z)$. At intervals the agreement between measurement and prediction was good, but overall the assumption of the medium to be a homogeneous half space was not correct. The reflections that were also visible in the measurement of the magnitude, gave a significant change in phase of $E_{4\rho}(\rho, \phi, z)$. Between 11 m and 23 m displacement, the standing wave pattern, largely caused by reflections of the lateral wave component $E_{4\rho, \text{lateral}}(\rho, \phi, z)$ in air, dominated the measured phase. Its component dominated the phase. Between 16 m and 18 m displacement, the display of the HP8410 Vector Analyser showed a static vector \vec{R} at approximately $-3/2 \pi$ rad, while on top of this vector, a phase vector \vec{P} rotated around (0,R) when the transmitter was moved, describing a circle with (0,R) as its origin.

4.6.3. Field Trial 3, Receiver Antenna Underground

This field trial was done with the same equipment as field trials 1 and 2. The frequency used was 145 MHz. The soil dielectric constant and conductivity were measured to be $\epsilon_r = 20$ and $\sigma = 0.17$ S/m. The receiver antenna was aligned parallel to the pipe, 18 m from the start, 2.5 m from the pipe, as is drawn in Appendix C, position B2. The conductivity of the soil is higher than in previous field trials and the predicted magnitude of $E_{4\rho}(\rho, \phi, z)$ in figure 4.15, showed no sign of interference between $E_{4\rho, \text{direct}}(\rho, \phi, z)$ and $E_{4\rho, \text{lateral}}(\rho, \phi, z)$. The direct wave $E_{4\rho, \text{direct}}(\rho, \phi, z)$ is highly attenuated in wet soil. Figure 4.15 shows that there was a good agreement between the measurement and the prediction. The wavelength of the ripple on the magnitude of $E_{4\rho}(\rho, \phi, z)$ is near λ_4 and most reflections were caused by irregularities underground. At 18 m displacement, $E_{4\rho}(\rho, \phi, z)$ showed a local maximum as the transmitter was near the receiver. For this field trial, there was little agreement between the measured and predicted phase, as is shown in figure 4.16. Between 12 m and 17 m displacement the phase was constant -1.6π rad, until at 17 m it changed abruptly to $+1.6 \pi$ rad. Sensitivity of the phase to interference both underground and on the ground surface were also apparent in the previous field trials.

4.6.4. Field Trial 4, Receiver Antenna Underground

Field trial 4 was done with 1.5 W signal generator and a 7 W amplifier. The power fed into the transmitter antenna was measured to be 38.5 dBm (7 W). The measurements were done at a frequency of 146 MHz. The receiver antenna was positioned 2.5 m from the

pipe at 4 m from the start at a depth of 0.02 m. It was aligned parallel to the pipe. The dielectric constant and conductivity of the medium 4 (soil) were measured to be $\epsilon_r = 20$ and $\sigma = 0.012$ S/m. The transmitter was moved in the pipe in 1 m steps and at every step the amplitude and phase of the received signal were recorded. Figure 4.17 shows a good agreement between the predicted and measured magnitude of $E_{4p}(\rho, \phi, z)$. At 4 m displacement, the direct wave, $E_{4p, \text{direct}}(\rho, \phi, z)$, was 25 dB lower than the lateral wave, $E_{4p, \text{lateral}}(\rho, \phi, z)$. Nevertheless, it caused an interference pattern that diminished after 8 m displacement. The minimum seen at 12 m displacement was similar in as was seen in figures 4.9 and 4.13. This suggested an irregularity underground near the ground surface at this position. The measured phase of $E_{4p}(\rho, \phi, z)$ in figure 4.18, shows that after 12 m displacement the phase variation is within $\frac{1}{4} \pi$ rad, similar to that in figures 4.10 and 4.14.

4.6.5. Field Trial 5, Phase Measurement

This field trial was focussed on the phase measurement. The equipment used was the same as in all previous trials. The dielectric loaded dipole receiver antenna was located 1 m away from the pipe, and 7 m from the start position, at 0.04 m depth. The relative dielectric constant and conductivity of the soil were measured to be $\epsilon_r = 18$ and $\sigma_4 = 0.055$ S/m. The power fed into the transmitter antenna was measured to be 43.6 dBm (23 W). The measured and predicted phase of $E_{4p}(\rho, \phi, z)$ is shown in figure 4.19. Between 6 m and 14 m displacement the direct wave $E_{4p, \text{direct}}(\rho, \phi, z)$ dominates the phase of $E_{4p}(\rho, \phi, z)$. In this range the transmitter was within approximately 8 m distance from the receiver. The relatively low conductivity of the soil allows $E_{4p, \text{direct}}(\rho, \phi, z)$ to dominate over $E_{4p, \text{lateral}}(\rho, \phi, z)$. When the relative dielectric constant and conductivity of medium 4 (soil) was taken the same as in field trials 2 and 3, $\epsilon_r = 18$ and $\sigma_4 = 0.17$ S/m, the simulation predicted that the phase of $E_{4p}(\rho, \phi, z)$ was solely the phase of $E_{4p, \text{lateral}}(\rho, \phi, z)$. This measurement stopped after 17 m displacement, because the signal was lost. After $E_{4p, \text{direct}}(\rho, \phi, z)$ diminishes at 15 m displacement, $E_{4p, \text{lateral}}(\rho, \phi, z)$ did not take over as the strongest signal. This was probably caused by an obstruction on the surface or underground. At 5 m displacement, the magnitude of $E_{4p, \text{lateral}}(\rho, \phi, z)$ shows a local minimum, reducing the received power strength from -33 dBm to -56 dBm. Then $E_{4p, \text{direct}}(\rho, \phi, z)$ increased to -34 dBm, as the transmitter was moved closer to the receiver.

antenna. The obstruction of the lateral wave was probably caused by the car with measurement equipment.

4.6.6. Scattering

Scattering of lateral electromagnetic waves was studied in a tank with salt water (medium 4) [19]. The objects were: an air square well made of foam, a water square well which was a Styrofoam enclosed casing filled with salt water and metal cylinder. The lateral wave due to a submerged horizontal dipole was studied. Metal cylinders were positioned perpendicular and transversal to the direction of propagation, submerged and partially submerged in the salt water. Scattering by completely submerged metal cylinders was too weak to provide an observable scattering pattern. Partial submerged metal cylinders resulted in a significant reflection in front of the obstacles. The same experiments were done with wells of Styrofoam enclosed casings with air. Partial submerged wells caused similar results as the partially submerged metal cylinders. When deeper submerged, no standing wave pattern was observed, while the propagating amplitude increased above the expected level. Down field from all the obstacles the curve goes through a minimum but after half a wavelength (in air) returns to a power level analogous to that predicted theoretically for an unbounded, unperturbed propagating lateral wave. The localisation of effects to the vicinity of the scattered is of fundamental importance to propagation studies of lateral waves. The qualitative features of the incident wave were preserved downfield from the obstacles. In the field trials in this study, it was observed that the magnitude of $E_{4\rho}(\rho, \varphi, z)$ was preserved after a reflection underground, but the phase was distorted. An example is the measured phase of $E_{4\rho}(\rho, \varphi, z)$ in figure 4.14, which shows that after 12 m displacement the phase variation is within $\frac{1}{4} \pi$ rad, similar to that in figure 4.10. However, the magnitude of $E_{4\rho}(\rho, \varphi, z)$ follows the prediction after 12 m displacement in figures 4.9, 4.13 and 4.17. Scattering from completely submerged cylinders was too weak to provide an observable scattering pattern [19]. Scattering from a partially submerged metal object resulted in a reflected and transmitted interference wave pattern. In the field trials reflections of the lateral wave from metal objects on the surface were clearly seen in figures 4.10 and figure 4.14, when $\lambda_{\text{ripple}} = \lambda_0$. The effects of obstacles and discontinuities in medium 4 (soil) are very small, relative to the reflection seen from objects in medium 0 (air).

4.6.7. Field Trial 6, Receiver Antenna in Air

A measurement was done where the receiver antenna in medium 0 (air) at 0.5 m above the ground in which the receiver antenna was a bare monopole antenna tilted downwards, in the z - ϕ plane at an angle of 45 deg with the positive y -axis. Dielectric loading of the receiver antenna was not necessary as the antenna was in air. The antenna was trimmed to resonate at $f = 145$ MHz, the frequency at which the measurements were done. The total field measured was $E_{0,total}(\rho, \phi, z) = \sqrt{E_{0,z}^2(\rho, \phi, z) + E_{0,\phi}^2(\rho, \phi, z)}$. The receiver antenna was located at a distance of 3 m from the pipe and 17 m from the start of the pipe. The amplitude of $E_{0,total}(\rho, \phi, z)$ was measured when the transmitter was in the pipe underground at 14 locations. The measured soil relative dielectric constant was $\epsilon_r = 30$ and the conductivity $\sigma = 0.09$ S/m. The power fed into the antenna was 33.1 dBm. Figure 4.20 shows the measured and predicted $E_{0,total}(\rho, \phi, z)$ [18]. When the transmitter displacement is 17 m and therefore below the receiver antenna, the amplitude of $E_{0,total}(\rho, \phi, z)$ shows a local maximum. Although at this point the absolute distance is shortest, the propagation loss is relatively high, due to the depth of the transmitter. This illustrates that the highest attenuation was in the propagation between the transmitter and the boundary with air. The rapid increase in received power between 23 m and 24 m displacement indicated a fast surfacing of the transmitter. There was a good agreement between measurement and prediction, except at 8 m displacement. Any reflections against the irregularities on the surface, or against the car with equipment is expected to be the cause of this. The wavelength of any reflections cannot be determined because of the limited number of measurement points. Figure 4.21 shows the predicted phase of $E_{0,total}(\rho, \phi, z)$. The graph is partly symmetrical with a vertical line at 17 m displacement as the axis. This represents the decrease and, after 17 m, increase in propagation distance. The transmitter started to submerge faster after 4 m displacement. Hence, the irregularity in the phase seen in the figure. This measurement showed a strong correlation between the amplitude of the received signal and the depth of the transmitter. The phase was a measure of the length of the propagation path. The discontinuities at 5 m and 20 m displacement were caused by the functions used to estimate the depth. This was done using 3 different exponential functions, where function 1 ranged from 0 to 5 m, function 2

from 5 to 20 m and function 3 from 20 to 30 m. The depth function is shown in figure C2 in appendix C.

4.6.8. Field Trial 7, Two Receiver Antennas

In the use of electromagnetic waves for the underground location of a transmitter, the accuracy was improved by using two receiver antennas were used simultaneously. The receiver antennas were positioned 4 m away from the pipe, at the starting position. The amplitude of $E_{4p}(\rho, \phi, z)$ was measured with the axis of the dipole antennas parallel to the direction of the transmitter antenna. The receiver antennas were dialectically loaded dipoles, located at a depth of 0.02 m. The power fed into the transmitter antenna was 31.7 dBm. The soil electrical properties were measured to be $\epsilon_r = 15$ and $\sigma = 0.017$ S/m. The frequency was 145 MHz. The magnitude of $E_{4p}(\rho, \phi, z)$ at both receiver antennas, shown in figure 4.22, was very similar. The difference between the prediction and measurement indicate that the soil is not as homogenous as was assumed. Some of the variations in $E_{4p}(\rho, \phi, z)$ were not predicted, but nevertheless were consistent in both measurements. For example $E_{4p}(\rho, \phi, z)$ is higher than predicted between displacement distances 20 m and 22 m for both measurements. The limited number of measurement points does not give much information on the wavelength of a possible standing wave. The ripple had an amplitude of approximately 5 dB. The difference in powers received at both antennas is shown in figure 4.23. Antenna d2 received no signal when the transmitter was at 12 m displacement. As the transmitter moves in the pipe between antennas d1 and d2, any differences in received amplitude of $E_{4p}(\rho, \phi, z)$ was expected to be an error caused by irregularities in medium 4 (the soil) or on the surface. The maximum error was -9.10 dB, at 22 m displacement. From the predicted signal, this error relates to approximately 7 m displacement of the transmitter. The average difference between the power levels received at antennas d1 and d2, which is the median error, is -0.84 dB which confirms that the transmitter was in the middle. As was seen in field trials 1 and 2, reflections in medium 4 (underground) and medium 0 (air) cause standing wave pattern with wavelengths corresponding to λ_4 and λ_0 . Hence the average error was less than 1 dB. This corresponds to approximately 2 m horizontal displacement or approximately 0.5 m change in depth. The alternating nature of positive and negative errors in figure 4.9 indicates that the error was caused by the ripple. Its maximum and minimum on antenna d1 were 2 m delayed on

antenna d2. Taking the average of two measurement point reduces the error in locating the transmitter and will result in an accuracy closer to medium error.

4.7. Optimum Frequency

To transmit an electromagnetic wave underground using low power, it was essential to use the optimum frequency, if there was one. Chapter 2 has shown that the conductivity of soil increases with frequency and hence the attenuation at high frequencies is high. The lateral wave mode of propagation made finding an optimum frequency more complex. The mode and the path of propagation of the strongest signal depends on the constitutive parameters, ϵ_r and σ , of the soil. Figure 4.24 shows the magnitude of $E_{4p, \text{direct}}(\rho, \phi, z)$, $E_{4p, \text{lateral}}(\rho, \phi, z)$ and $E_{4p, \text{reflected}}(\rho, \phi, z)$ due to a horizontal dipole at a depth of 1.0 m as a function of frequency. The position of the observer was 0.05 m underground and at a radius of 1.0 m. The soil type was keuper marl with a moisture content of 6.5 %. At the frequency of 145 MHz, the relative dielectric constant and conductivity of the soil were $\epsilon_r=14.6$ and $\sigma=0.0084$ as is shown in figure 2.6 in Chapter 2. Figure 4.24 shows that at 10 MHz, when $\epsilon_r \approx 22$ and $\sigma \approx 0.01$ S/m, the magnitude of $E_{4p, \text{direct}}(\rho, \phi, z)$, $E_{4p, \text{lateral}}(\rho, \phi, z)$ and $E_{4p, \text{reflected}}(\rho, \phi, z)$ was relatively high, increasing to a maximum at 200 MHz. At 300 MHz the magnitude falls off sharply, this decrease being more rapidly for $E_{4p, \text{direct}}(\rho, \phi, z)$ and $E_{4p, \text{reflected}}(\rho, \phi, z)$. The figure shows a local minimum at 5 GHz. This minimum for $E_{4p, \text{lateral}}(\rho, \phi, z)$ was at least 60 dB stronger than for $E_{4p, \text{direct}}(\rho, \phi, z)$ and $E_{4p, \text{reflected}}(\rho, \phi, z)$. Hence, at the higher frequencies, the lateral wave, $E_{4p, \text{lateral}}(\rho, \phi, z)$, was significantly stronger. Note that at 100 MHz the direct wave was the strongest because it travels the shortest path and the conductivity of the soil was relatively low. When the soil has a higher moisture content, the path loss of $E_{4p, \text{direct}}(\rho, \phi, z)$ was higher than that of $E_{4p, \text{lateral}}(\rho, \phi, z)$ and the advantage of a shorter propagation path was eliminated as is shown in figure 4.25. The moisture content of medium 4 was 11.3%. The conductivity of the soil $\sigma \approx 0.08$ S/m at 10 MHz increasing to $\sigma \approx 0.01$ S/m at 10 GHz. The magnitudes of both $E_{4p, \text{direct}}(\rho, \phi, z)$ and $E_{4p, \text{reflected}}(\rho, \phi, z)$ are insignificant. This shows that the lateral wave, $E_{4p, \text{lateral}}(\rho, \phi, z)$, is the only mode of propagation in wet soils in given conditions. The knee-curve in figure 4.25 shows a maximum at 200 MHz. Figures 4.24 and 4.25 show a clear optimum range of frequencies of 100 MHz to 300 MHz. The soil acts like a lowpass filter with a cut-off frequency of 300 MHz for the current simulations. As the magnitude of the

direct wave has shown to be very sensitive for soil conditions, the results illustrate the importance of the depth of the transmitter and receiver antennas, because for the lateral wave $E_{4\rho, \text{ lateral}}(\rho, \phi, z)$, the initial path from the transmitter in medium 4 (soil) to the boundary with medium 0 (air) has an attenuation similar to the direct wave $E_{4\rho, \text{ direct}}(\rho, \phi, z)$. Figures 4.26 and 4.27 show the same simulations for different depths and radial distances. The position of the observer is 0.05 m underground with radial distances of 0.1 m, 0.5 m, 1.0 m, 10 m, and 50 m. The graphs for $d = 1.0$ m, when the transmitter is 1.0 m deep underground, show a local maximum at approximately 200 MHz. The wavelength decreases with frequency and therefore the radial distance from the transmitter antenna to the border between the near- and the far-field decreases with frequency. Figure 4.26 shows three distinctive regions. At frequencies below 200 MHz the point of observation is in the reactive near-field of the antenna. Between 200 MHz and 2 GHz, it was in the intermediate field the rapid decrease of $E_{4\rho, (\rho, \phi, z)}$ was due to exponential attenuation. The far-field started at approximately 2 GHz. The interference patterns of $E_{4\rho, \text{ lateral}}(\rho, \phi, z) + E_{4\rho, \text{ direct}}(\rho, \phi, z)$, for $d=0.1$ m resemble those for $d=1.0$ m. At the higher frequencies soil behaves more like a good conductor and the attenuation was very high when the transmitter is 1.0 m deep. When $d=0.1$ m, the received power was approximately independent of frequency. This clearly suggested that the major attenuation was when the lateral wave propagates in medium 4 between transmitter and the boundary with medium 0 (air). From figures 4.24 to 4.27 it was apparent that the best frequency to use is in the range of 100 MHz to 300 MHz.

4.8. Underground Navigation

The field trials have shown a clear potential for measuring the displacement of an electromagnetic wave transmitter underground. It was shown that an electromagnetic wave was received from a transmitter that was up to 1.5 m deep underground and at a distance of up to 30 m away from the receiver. For the majority of environmental conditions, the strongest signal received was the lateral wave, except for very short distances where the direct wave was dominant. In not all field trials propagation of $E_{4\rho}(\rho, \phi, z)$ was achieved over a distance of 30 m. This was due to irregularities underground and on the ground surface. Using more than one receiver antenna would

increase the possibility of a signal reception significantly. Also the theory suggested that $E_{4z}(\rho, \phi, z)$ was stronger than $E_{4\rho}(\rho, \phi, z)$ at distances less than 20 m, as is shown in figure 4.12. The use of a vertical antenna, for example a vertical electric monopole antenna, will further increase the probability of receiving a signal. Any algorithm that calculates the transmitter displacement should be based on the prediction of the propagation of the lateral electromagnetic wave. The difference between the predicted and measured signal strength was the expected error in predicting the displacement of an underground transmitter. The field trials show a good agreement between the prediction and measurement. Accurate knowledge of the dielectric constant ϵ_{4r} and conductivity σ_4 have been shown crucial in predicting the modes of propagation. Their estimation at the field trials was therefore important for the accuracy in calculating the displacement of the transmitter. Therefore any commercial system should include a coaxial probe for determining the constitutive parameters of the soil on-site. Alternatively, the dielectric constant and conductivity could be calculated by transmitting at more than one frequency at the start of the trial when both the transmitter and receiver are at a fixed position.

In paragraph 4.4.2.3, where two receiver antennas were used to locate the transmitter antenna, the median error was -0.84 dB, which in the worst case corresponded to approximately 2 m horizontal displacement or 0.5 m change of depth of the transmitter. The worst case is when the power of received signal changes very slowly with displacement of the transmitter, and hence the function displacement – received power is a nearly flat line. This is the case between 22 m and 26 m displacement in figure 4.22. Figure 4.28 shows the predicted magnitude of $E_{4\rho}(\rho, \phi, z)$ in the XZ-plane, due to a horizontal dipole normalised to have an unit electric moment ($I \Delta l = 1$ Am), at $(0, 0, 0.1)$ in Orthogonal co-ordinates. The dielectric constant and conductivity of the soil are $\epsilon_{4r}=15$ and $\sigma_4=0.012$ S/m. The magnitude is shown from 3 m deep to 3 m above the ground. At the transmitter dipole, a depth of 0.1 m, the magnitude was at a maximum. When the graph was followed from $z = 3$ m underground to $z = -3$ m in air at $x = 0$, the decrease of $E_{4\rho}(\rho, \phi, z)$ with distance was significant. The interference of the direct wave and lateral wave was seen underground near the transmitter, but not in air as the direct wave is reflected against the boundary and propagates back underground. As the lateral wave propagates along the surface in air, there was a sharp increase in power at the boundary between medium 4 (soil) and medium 0 (air). The phase of $E_{4\rho}(\rho, \phi, z)$ in figure 4.29 is for

the same prediction as figure 4.28 and shows that the wavelength in air was approximately λ_0 , while underground the wavelength was much smaller. In a system where the phase is used for estimating the displacement of an underground transmitter, the sampling rate should be higher when the receiver antenna is underground. Figure 4.30 shows $E_{4\rho}(\rho, \phi, z)$ in the z -plane (horizontal) when $z = -1$ m (1 m above ground). The transmitter antenna was a horizontal dipole at (0 0,1). At observation point (0 0,-1) the magnitude of $E_{4\rho}(\rho, \phi, z)$ was at a minimum. The lateral wave travels to the boundary at the Brewster angle and hence the cone shaped minimum around the location of the transmitter antenna. As the transmitter was 1 m deep it was expected that the magnitude of the refracted wave in air would be very low. The top rim of the cone was created by the lateral wave incident on the boundary at the Brewster angle. Figure 4.31 shows the phase of $E_{4\rho}(\rho, \phi, z)$ for the simulation in figure 4.30. Next the result from this simulation were viewed at $z = 1.0$ m, underground. The magnitude and phase of $E_{4\rho}(\rho, \phi, z)$ were shown in figure 4.32 and 4.33 respectively. In the area where the cone was seen in figure 4.30, the magnitude shows an interference of the lateral and direct waves underground. Away from the transmitter, the magnitude is more flat, compared with $E_{4\rho}(\rho, \phi, z)$ in air (figure 4.30). The field trials have shown that reflections were an important cause of error. An example is figure 4.9, where the ripple caused by reflections is a major cause of error in the measured magnitude of $E_{4\rho}(\rho, \phi, z)$. As the wavelengths of the standing wave were known, intelligent signal processing could eliminate this error. An improvement in accuracy of locating the transmitter would be achieved by averaging the measurement points over a minimum distance equal to λ_0 , while taking measurements at intervals where the transmitter has moved over a distance that is a fraction of λ_0 . When disregarding the ripple caused by reflections, the results of field trial 2 show a maximum difference between prediction and measurement of 6 dB, shown in figure 4.13. This corresponds to approximately 3 m horizontal displacement at this location. As the lateral wave propagated most of its path in air along the boundary between medium 4 (soil) and medium 0 (air), reflection in underground were expected to be limited. Previous studies [19] have shown a metal object on the ground causes reflections of the lateral wave, but the qualitative features of the incident wave were preserved away from the obstacle. In the field trials in this study, it was observed that the magnitude of $E_{4\rho}(\rho, \phi, z)$ was preserved after a reflection underground, but the phase was distorted. The use of more than one

receiver antenna will limit the errors in estimating the displacement of an underground transmitter caused by reflections. Tracing the movement of the transmitter using the phase of $E_{4p}(\rho, \phi, z)$ proved to be more difficult. The phase was more sensitive to reflections caused by irregularities underground and on the ground surface. However, good phase information was obtained during intervals in the measurements. Hence phase information when available, can be used to enhance the accuracy of estimating the movement of the transmitter.

In civil engineering, remote steered micro-tunnelling machines are used for laying pipes or cables underground. This makes it possible to lay pipes or cables under a road, canal or railway, without the necessarily of digging a trench. The social cost of digging trenches in cities is significant. Hence, there is a growing interest in trenchless technology. A problem with this system is the uncertainty of where it is underground. Obstacles underground can divert the tunnelling machine and sometimes this is unnoticed by the driver. An application of the system described in this thesis is to mount a transmitter on the drill.

It is recommended that a commercial system should consist of four antennas placed in holes in the ground, in two pairs on either side of the transport route. The depth to which the antennas should be placed should initially be the same as the depth of the proposed drilling operation, although with experience of the technique this is likely to prove unnecessary. Three receivers should be positioned accordingly and a transmitter should initially be placed in the fourth hole to ensure that signal reception at that depth is possible. If no signal is received, then an obstruction or other adverse condition is present. Adjustment of the depth, either by raising or lowering the proposed line of operation could be examined by raising or lowering the transmitter/receivers until signals are received. Transmission across the other diagonal should be assured by swapping over the receiver and transmitter on one side of the transport route. Analysis of the signals (received at known separations directly across the line of the mole's path) will assist with subsequent analysis of the drillhead location. In addition samples of soil taken from the four receiver location holes will allow soil classification, measurement of water content, and determination of dielectric constant. (This can be done either directly using the equipment developed herein or indirectly from the soil classification and water content measurements in conjunction with the dielectric constant measurement database compiled as a result of this project.) These data together will permit an accurate model to be generated for subsequent location analysis.

With all four receivers in position, the steerable drill should be positioned at the start of the proposed crossing, its location measured and the signals at the antennas recorded. Height control should be effected using an accurate tiltmeter. (An investigation of the possibilities of using the same technique to monitor the change in depth proved that measurements would be relatively imprecise due to the orientation of the antennas and although a possible development for the future was not practical from the data recorded in this study.) The progress of the drillhead should be tracked by halting the operation after every 1 m advanced (or less as required) and allowing a short signal from the transmitter to be recorded without vibration caused by the mole. The progressive advance of the drill would be tracked by the signals received and adjustments to the steering made accordingly.

If the signal transmission prior to commencing driving was unacceptably poor, then the technique should be deemed to be unsuitable at that location. An investigation of the reason why would be recommended in such a case to ensure that no obstacles exist. If signal transmission were lost during a drive, then reversion to overhead location would be necessary. However, neither of these scenarios appears likely from the research data. The relatively long wavelength chosen means that only large underground pipes or services would be likely to cause a major discontinuity in the dielectric constant, a large steel pipe being the worst case. High voltage cables or other services would not unduly affect signal transmission. It is consequently only major discrepancies in water content of the soil that would result in problems, and such changes are unlikely at one location under a transport route (excepting possibly a buried river channel). In any case this would be revealed by the testing prior to drilling on the site. Also the dominant mode of propagation is the lateral wave, which travels most of its path along the ground surface, minimising the possibility of reflections underground.

The accuracy of the system in a soil of unknown properties using pairs of antennas spaced 60m apart and using three received signals to locate a transmitter of unknown initial position is expected to be significantly better than 4 m (i.e. ≈ 2 m). Increasing the signals from three to four will make a further improvement. Knowing the location of the transmitter prior to drilling will improve subsequent location considerably, as will prior testing across the site since this will serve to calibrate the analytical techniques. Use of phase information, when available, has been shown to produce an accuracy of within 200

mm (i.e. ≈ 100 mm), and this was demonstrated in the field trials on campus at Loughborough University.

Experiments on the effect of obstacles in and above seawater were taken in a model lithosphere. Metal cylinders were positioned perpendicular and transversal to the direction of propagation, submerged and partially submerged in the salt water. Scattering by completely submerged metal cylinders was too weak to provide an observable scattering pattern. Partial submerged metal cylinders resulted in a significant reflection in front of the obstacles. The same experiments were done with wells of Styrofoam enclosed casings with air. Partial submerged wells caused similar results as the partially submerged metal cylinders. When deeper submerged, no standing wave pattern was observed, while the propagating amplitude increased above the expected level. Downfield from all the obstacles the curve goes through a minimum but after half a wavelength (in air) returns to a power level analogous to that predicted theoretically for an unbounded, unperturbed propagating lateral wave. The localisation of effects to the vicinity of the scatterer is of fundamental importance to propagation studies of lateral waves.

Instead of using a constant wave (CW), it was considered to transmit short pulses. The spectrum of the δ -function is dominated by high frequencies. The pulse of the dipole in a homogeneous single medium follows the far field behaviour of the steady state and this is the direct field with high attenuation.

4.9. Conclusion

The field trials have shown that propagation of an electromagnetic wave from a transmitter underground to a receiver underground is possible over a distance of 30 m and to a depth of 1.5 m. Also, when the receiver was placed at 0.5 m above the ground, an electromagnetic wave was received from the same transmitter. When underground, dielectric loaded dipole antennas were used. In one field trial, a horizontal monopole antenna was used. The antenna impedance was measured, which was used in simulation together with antenna dimensions and position to calculate the antenna efficiency in the given environment. The dielectric constant ϵ_r and conductivity σ were measured at the field trials. A simulation model was used to predict the electromagnetic wave propagation

from the source underground, using the measured ϵ_r and σ . The simulation outcome compared well with the measured results. The difference between the measured and predicted results was mainly because of a ripple. The average measured received power is close to the one predicted. The ripple showed two different standing wave patterns. The wavelength of the ripple was either that of the wave in air or underground. This was caused by reflection due to irregularities underground or on the ground surface. Although reflection against objects on the ground surface causes a deep minimum at close distance, once past the object, the incident wave regains its characteristics. The simulation model included the analyses of the modes of propagation. It predicted that the lateral wave was the strongest mode of propagation in the majority of the field trials. Only at short distances was the direct wave dominant. The field trials confirmed these findings, as examples of direct waves and lateral waves were seen in the measurements. The lateral wave starts at the source underground, travels to the boundary, follows the air-ground boundary and then propagates back into the ground to the receiver antenna. As the wave travels a significant part of its path in air, it is less susceptible to irregularities underground. Measurement of the phase has shown it to be sensitive to errors caused by reflections. This is the reason why information of the phase was not always available during the field trials. The field trials have shown the possibility of using electromagnetic wave to track a moving transmitter underground. A possible application is the tracking a micro-tunnelling machines, used for laying pipes or cables under through roads. The micro-tunnelling drill using in Civil Engineering can be steered by the driver, but its position underground is not known. Mounting a transmitter on the drill-head would allow its movements to be calculated from the magnitude and phase of the electromagnetic wave at the receiver antennas. Any system that estimated the underground displacement of the transmitter should have 2 or more receiver antennas. Field trials have shown an accuracy of such a system of approximately 2 m.

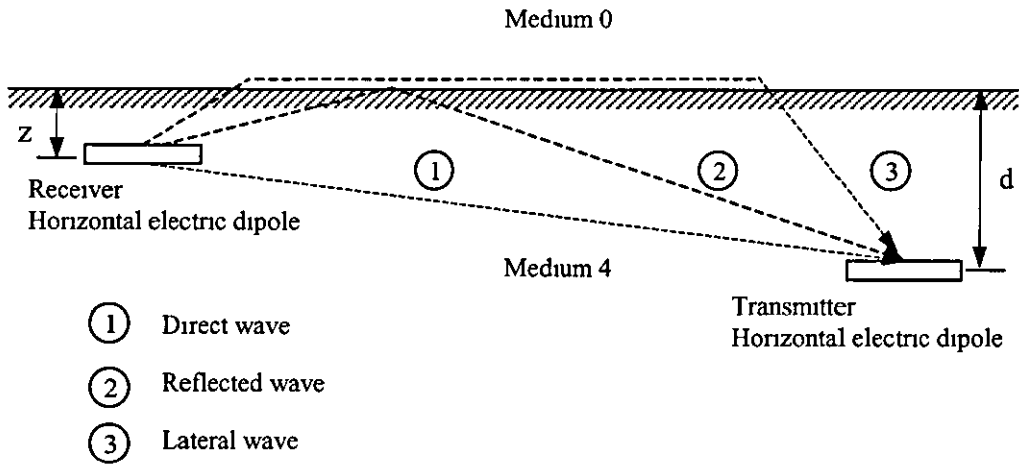


Figure 4.1 Propagation path of the direct, reflected and lateral electromagnetic wave

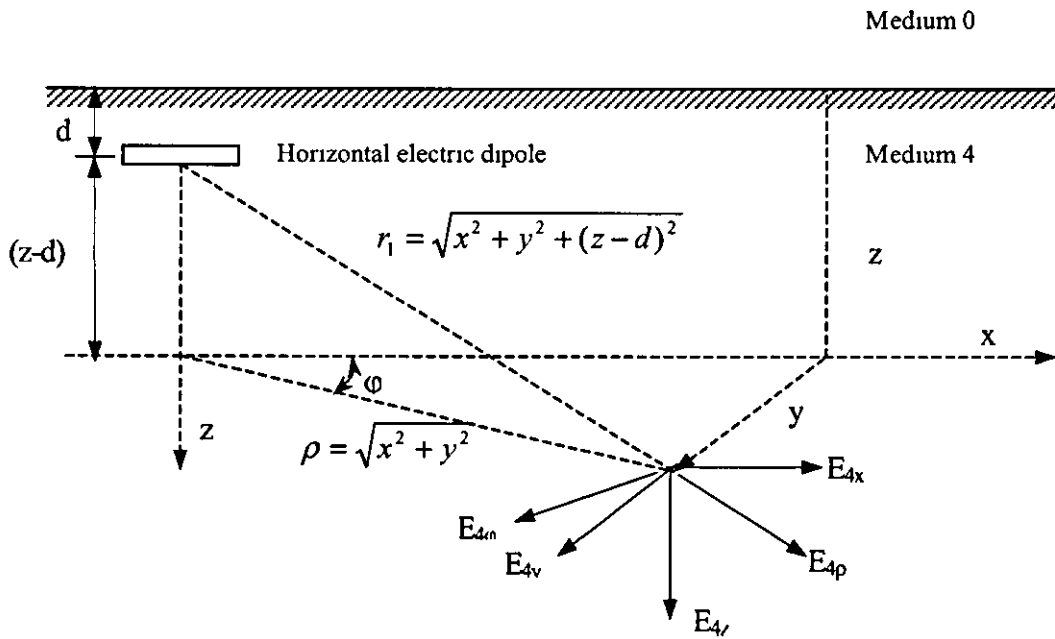


Figure 4.2 Co-ordinate systems used in calculating the electromagnetic wave propagation Underground

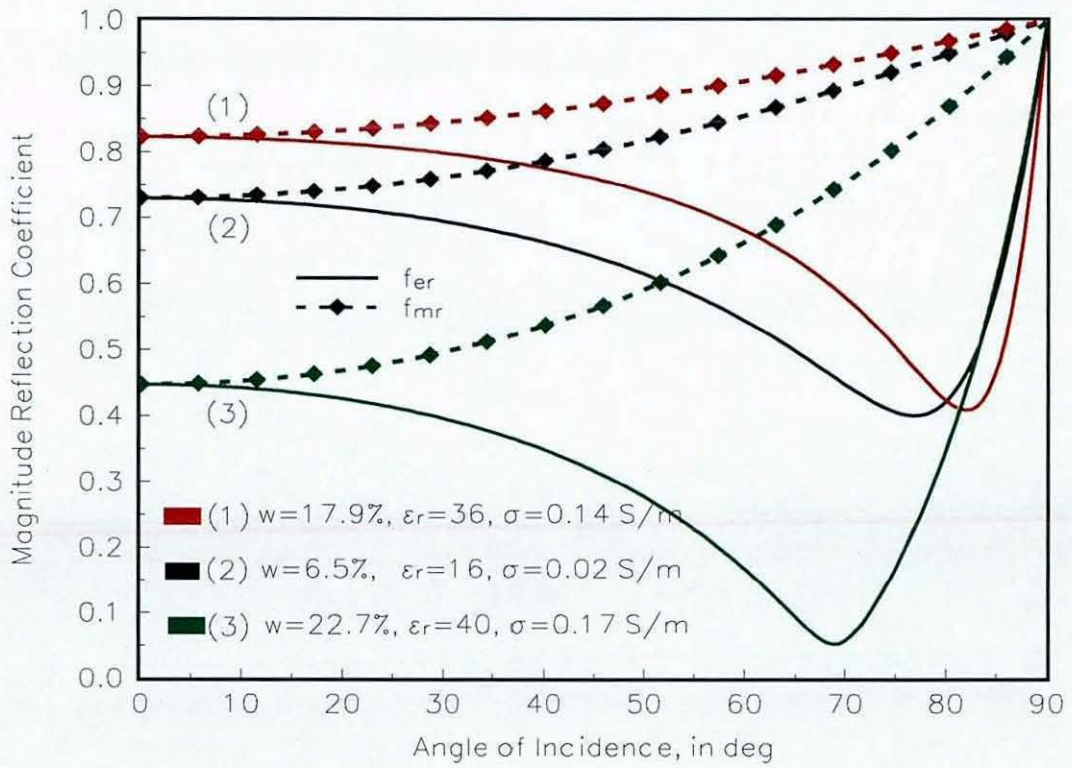


Figure 4.3 Plane wave reflection against ground. The overall trend is that when σ increases a minimum for f_{er} (and a maximum for f_{mr}) occurs near an angle of incidence of 90 deg [2].

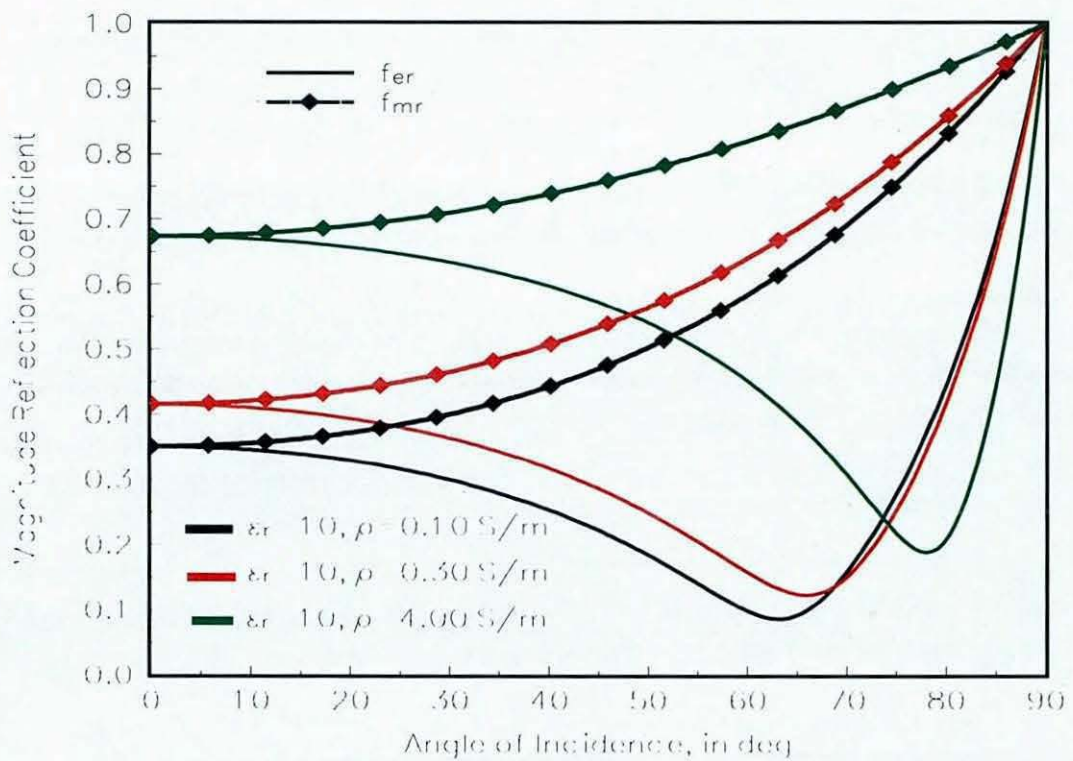


Figure 4.4 Plane wave reflection against ground. The overall trend is that when σ increases a minimum for f_{er} (and a maximum for f_{mr}) occurs near an angle of incidence of 90 deg [2].

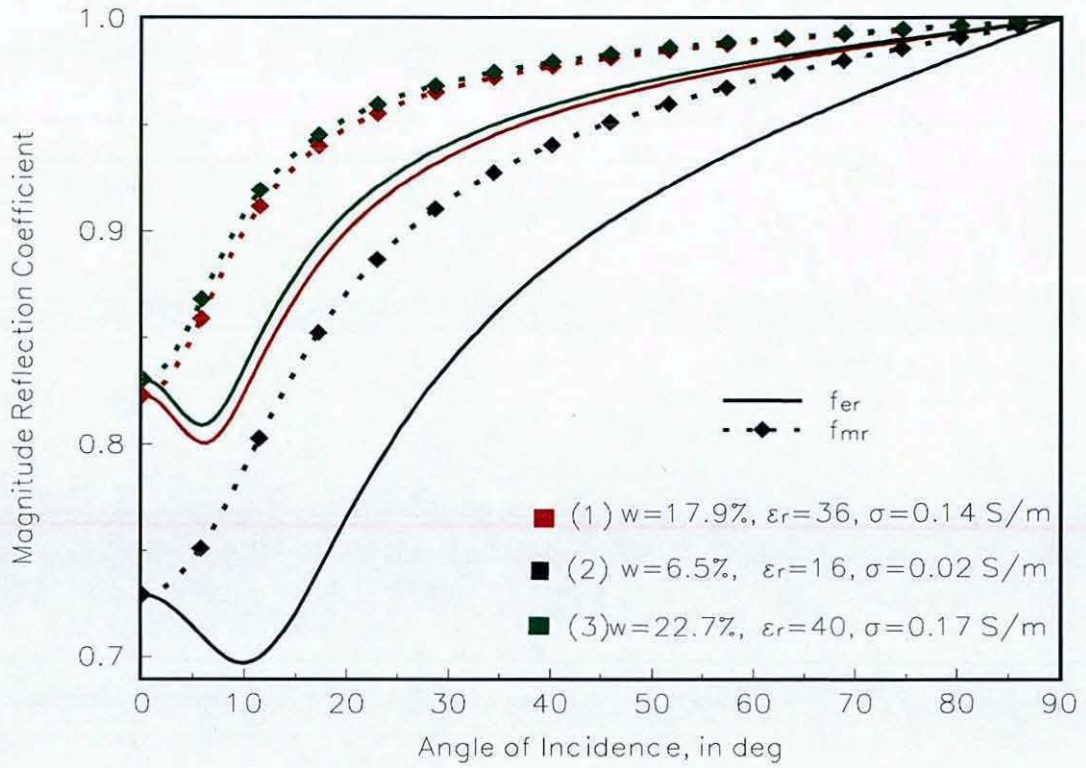


Figure 4.5 Plane wave reflection from underground to ground-air boundary

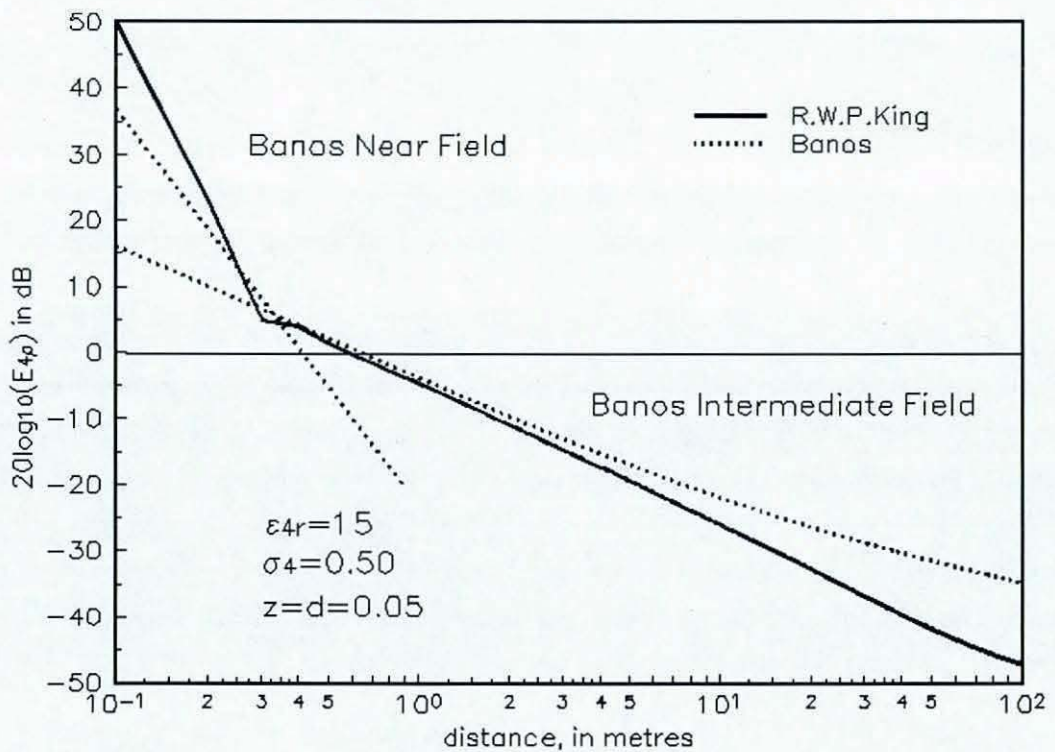
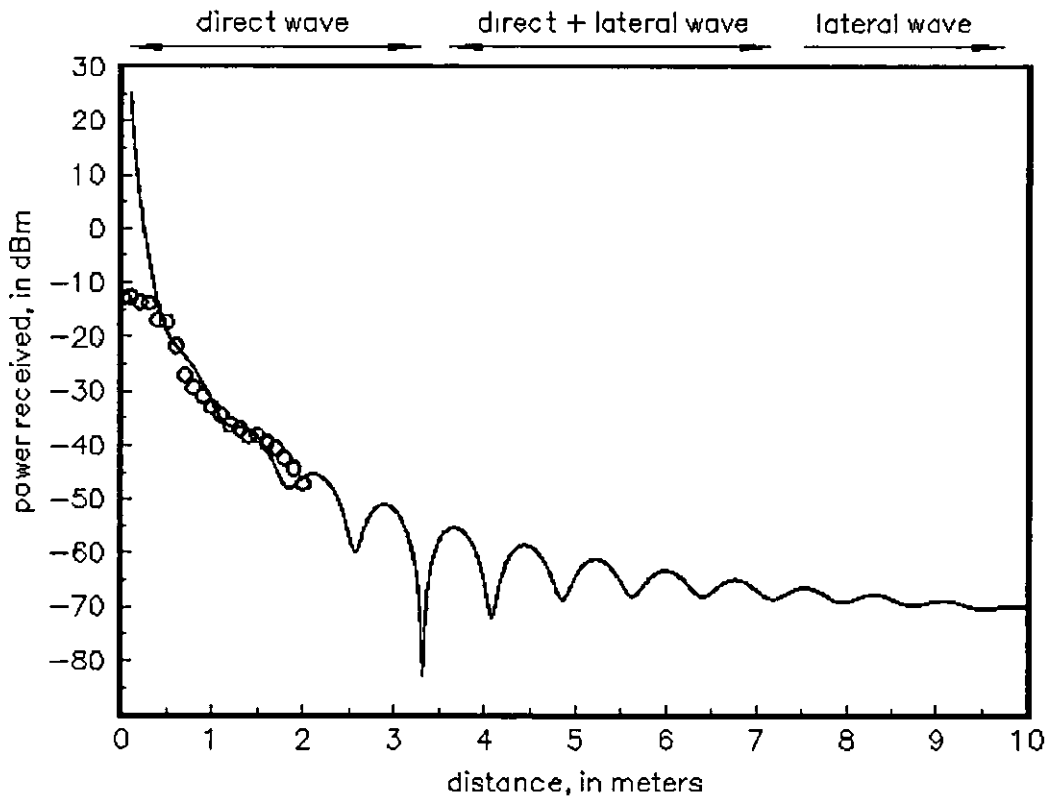
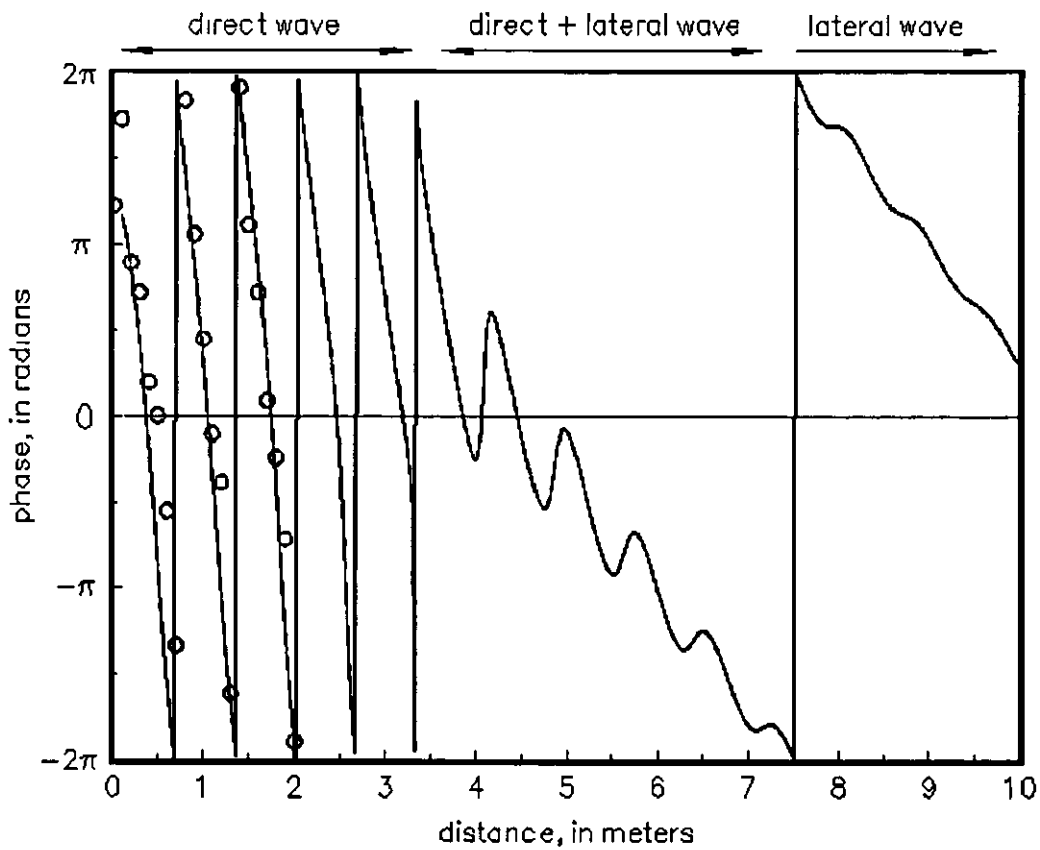


Figure 4.6 Prediction results for the near-field and far-field of due to a horizontal dipole buried at a depth of 0.05 m. The observer is at 0.05 m depth underground. The frequency is 145 MHz.


 Figure 4.7 Magnitude of $E_4(\rho, \phi, z)$, received by a dipole underwater

 Figure 4.8 Magnitude of $E_4(\rho, \phi, z)$, received by a dipole underwater

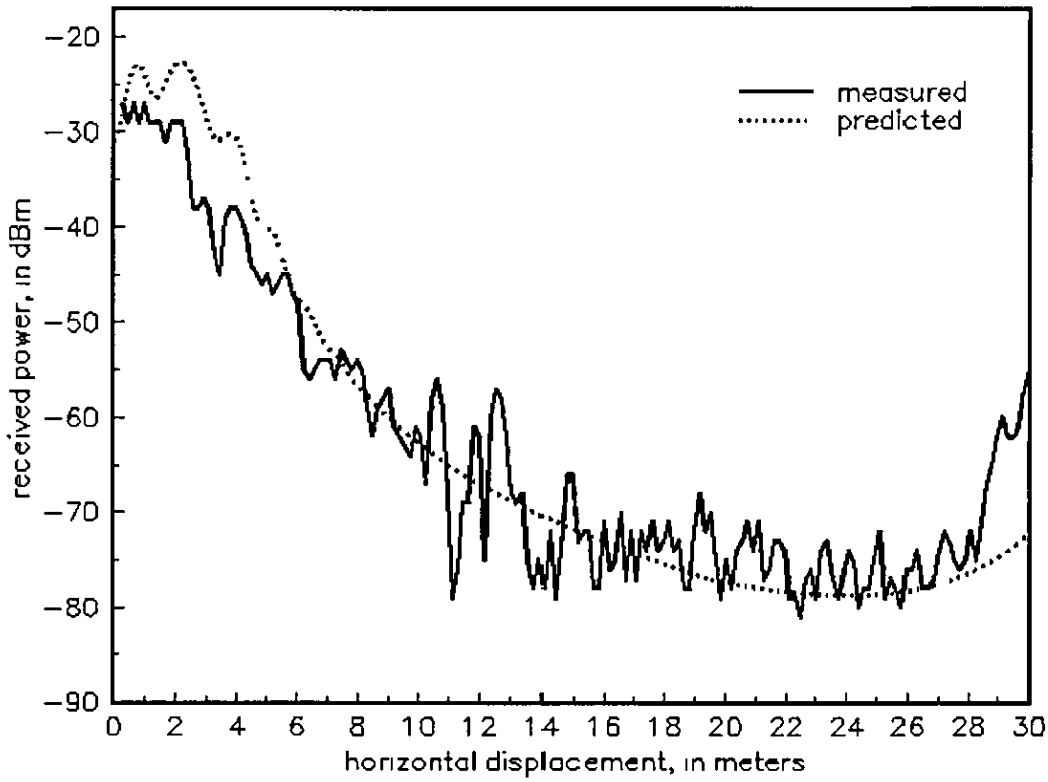


Figure 4.9 Magnitude $E_{4p}(\rho, \phi, z)$ of in dBm as function of the horizontal displacement of the transmitter Receiver antenna is at location A3

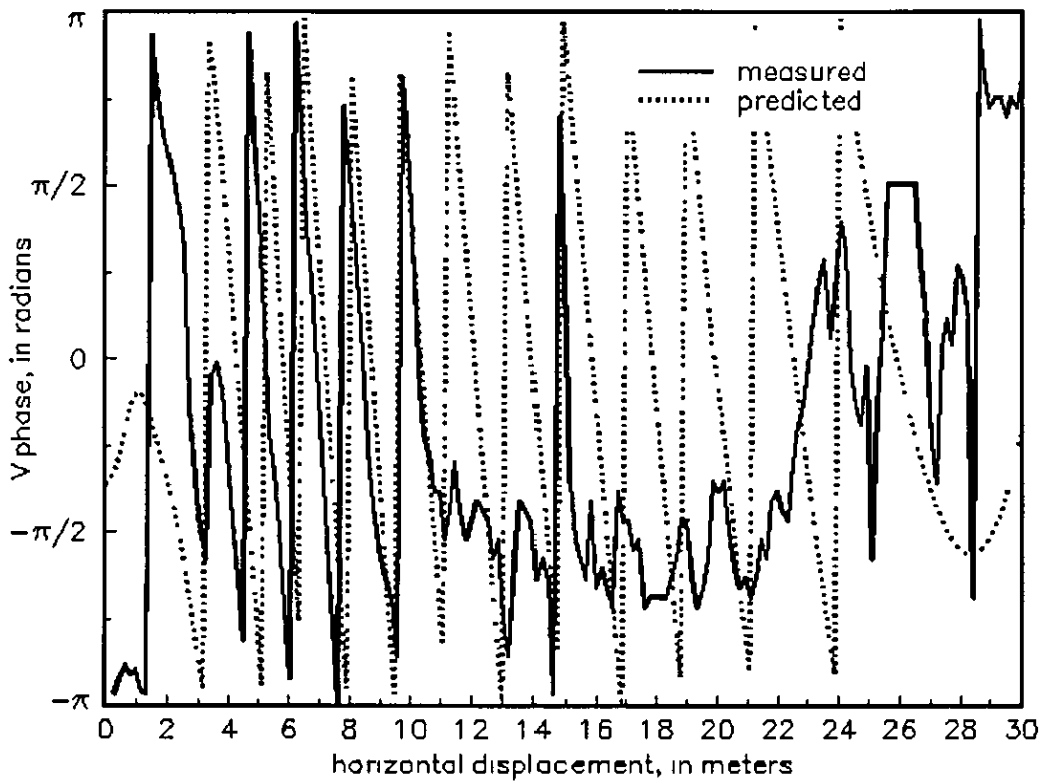


Figure 4.10 Receiver and transmitter located underground Normalised phase of $E_{4p}(\rho, \phi, z)$ measured with the induced voltage on the receiver antenna as function of the horizontal displacement of the transmitter Receiver is at location A3.

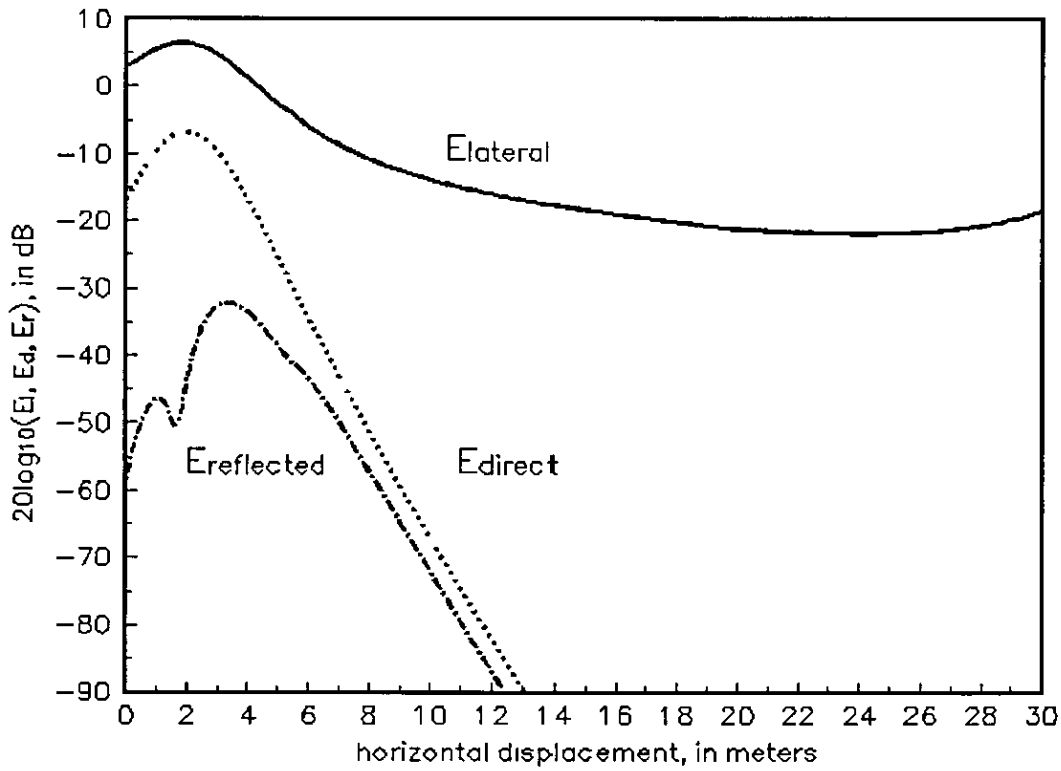


Figure 4.11 Predicted magnitude of $E_{4p \text{ direct}}(\rho, \phi, z)$, $E_{4p \text{ reflected}}(\rho, \phi, z)$ and $E_{4p \text{ lateral}}(\rho, \phi, z)$ for simulation in figure 4 9, for a dipole with normalised electric moment of $|A| = 1 \text{ Am}$

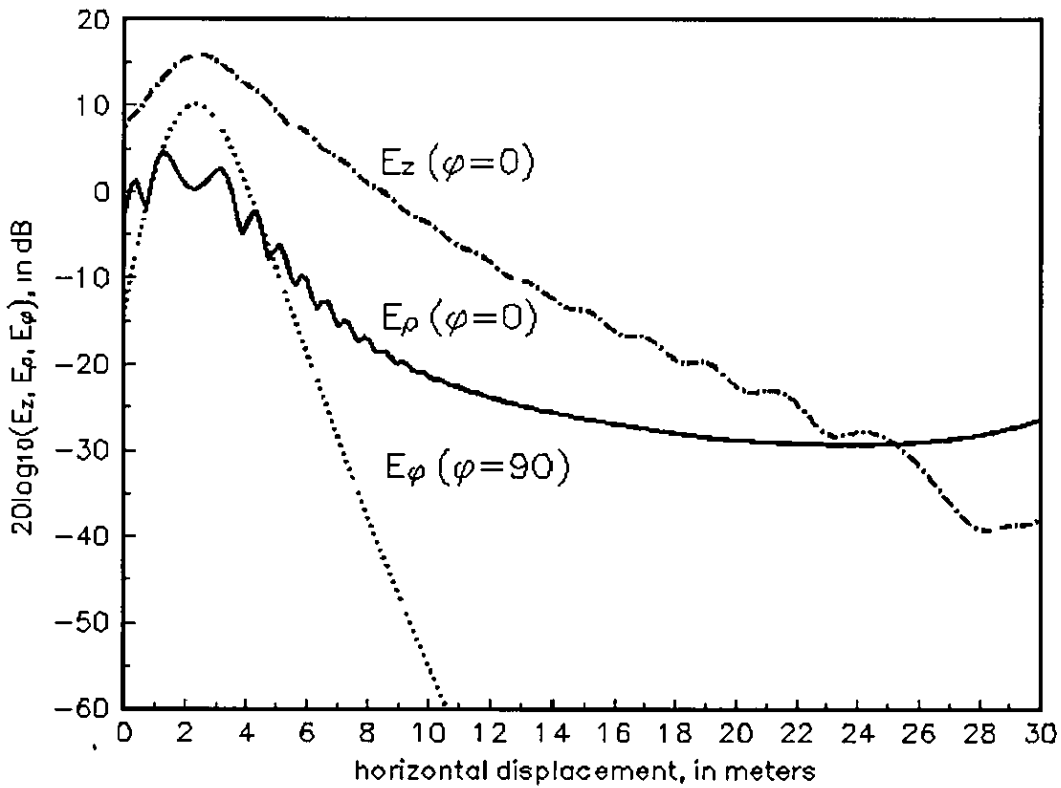


Figure 4.12 Predicted magnitude of $E_{4p}(\rho, \phi, z)$, $E_{4\phi}(\rho, \phi, z)$ and $E_{4z}(\rho, \phi, z)$ for simulation in figure 4 9, for a dipole with normalised electric moment of $|A| = 1 \text{ Am}$

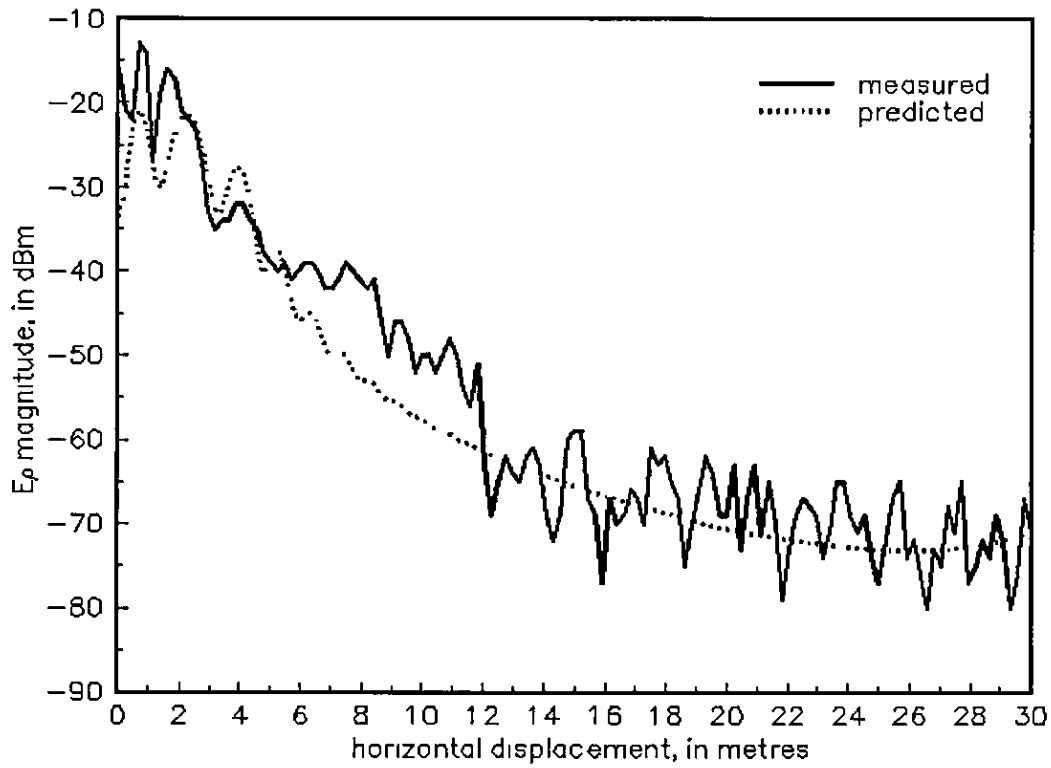


Figure 4.13 Magnitude $E_{\rho}(\rho, \phi, z)$ of in dBm as function of the horizontal displacement of the transmitter Receiver antenna is at location A2

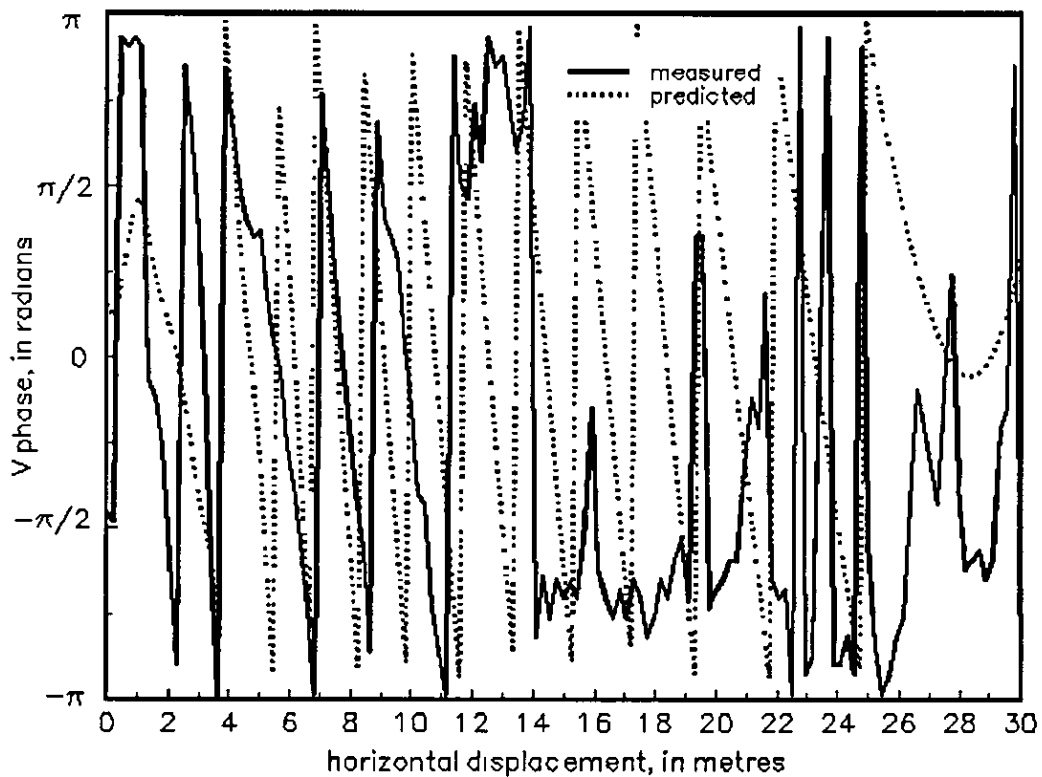


Figure 4.14 Phase of $E_{\rho}(\rho, \phi, z)$ of in dBm as function of the horizontal displacement of the Transmitter Receiver antenna is at location A2

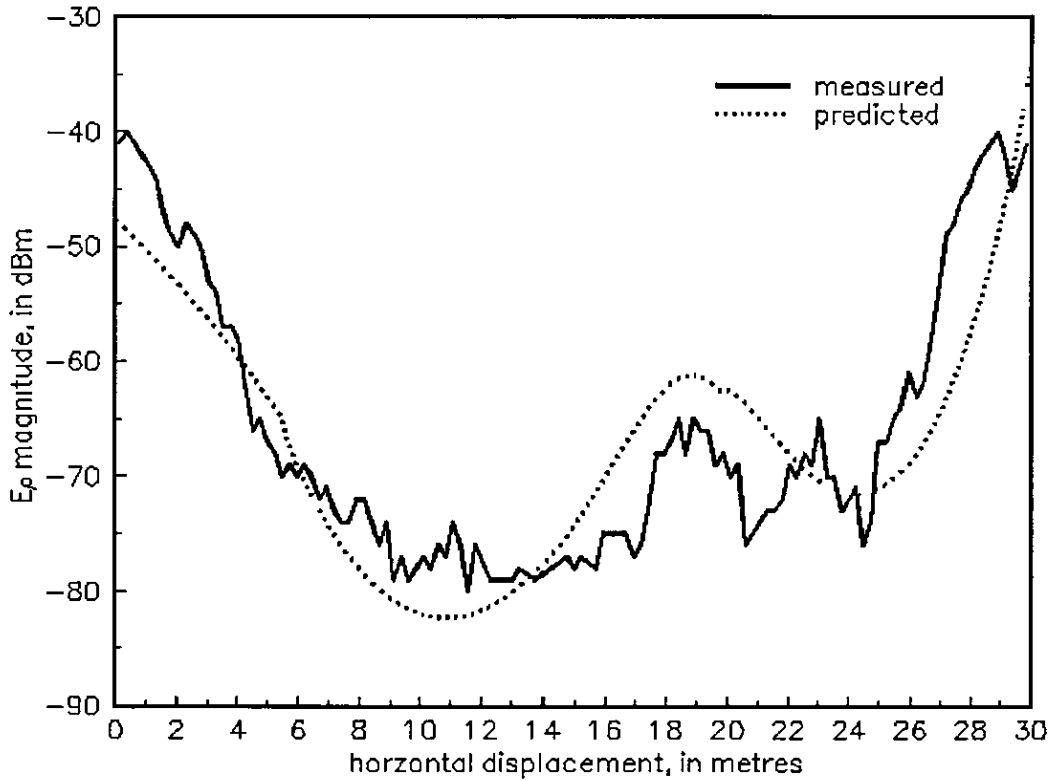


Figure 4.15 Magnitude $E_{\rho}(\rho, \phi, z)$ of in dBm as function of the horizontal displacement of the transmitter Receiver antenna is at location B2

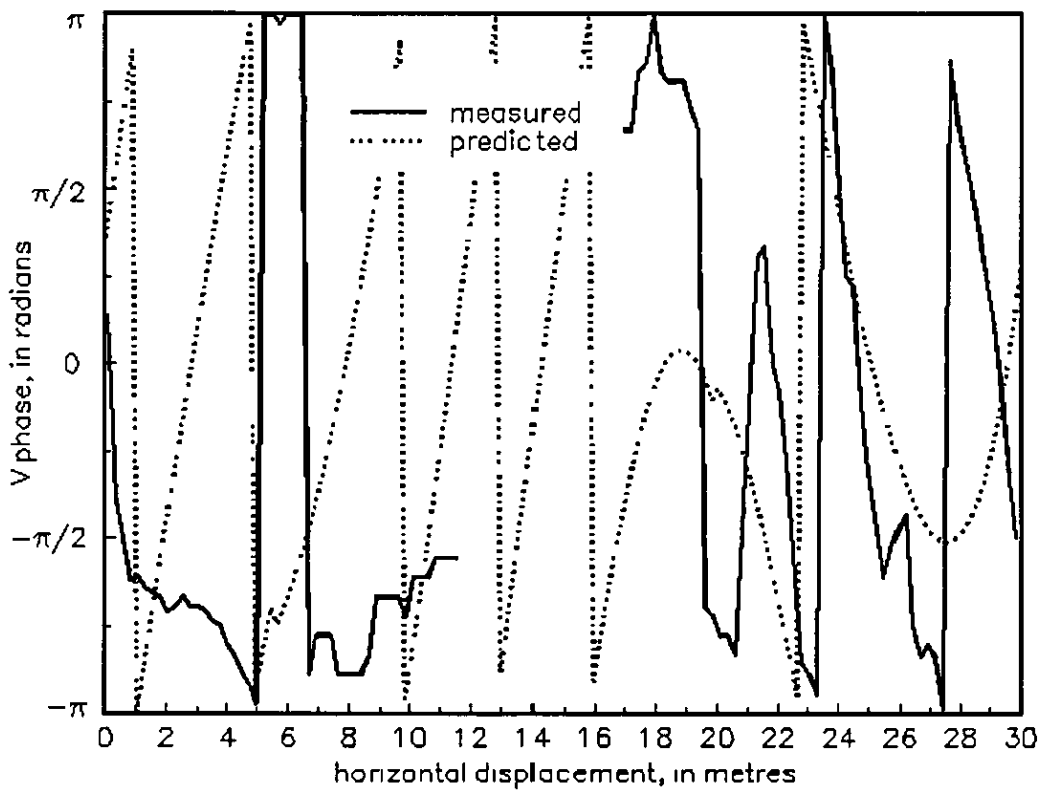


Figure 4.16 Phase of $E_{\rho}(\rho, \phi, z)$ of in dBm as function of the horizontal displacement of the Transmitter Receiver antenna is at location B2

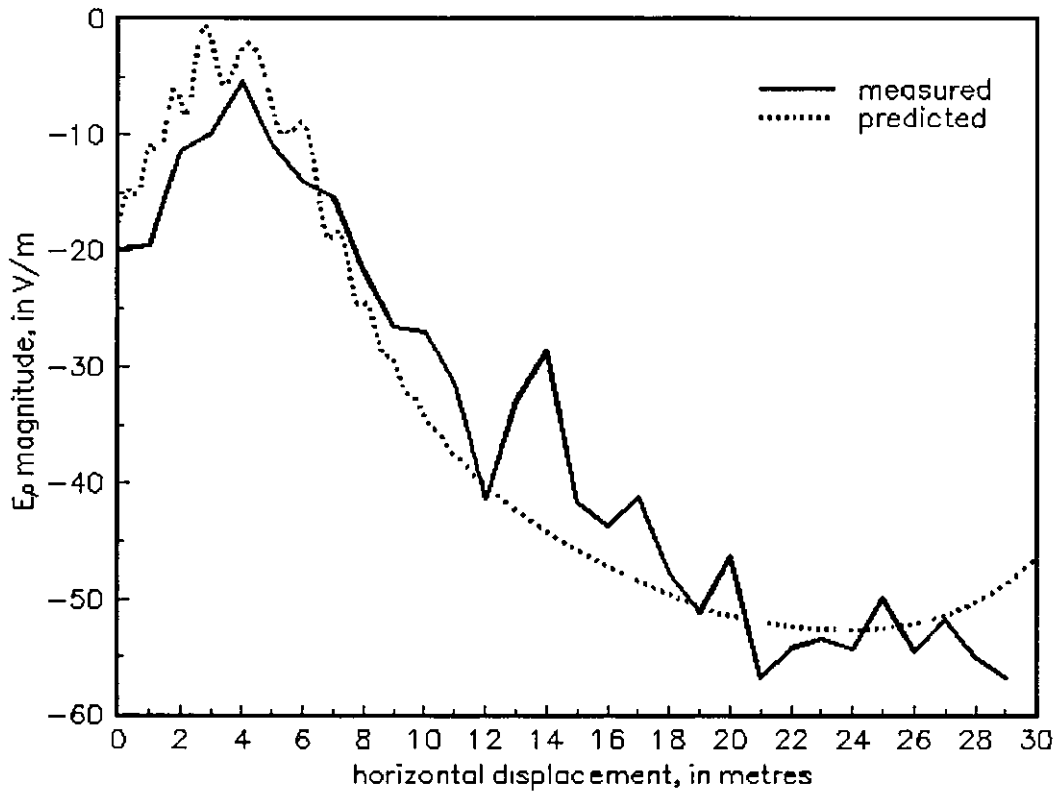


Figure 4.17 Magnitude $E_{\rho}(\rho, \phi, z)$ of in dBm as function of the horizontal displacement of the transmitter Receiver antenna is at location B2

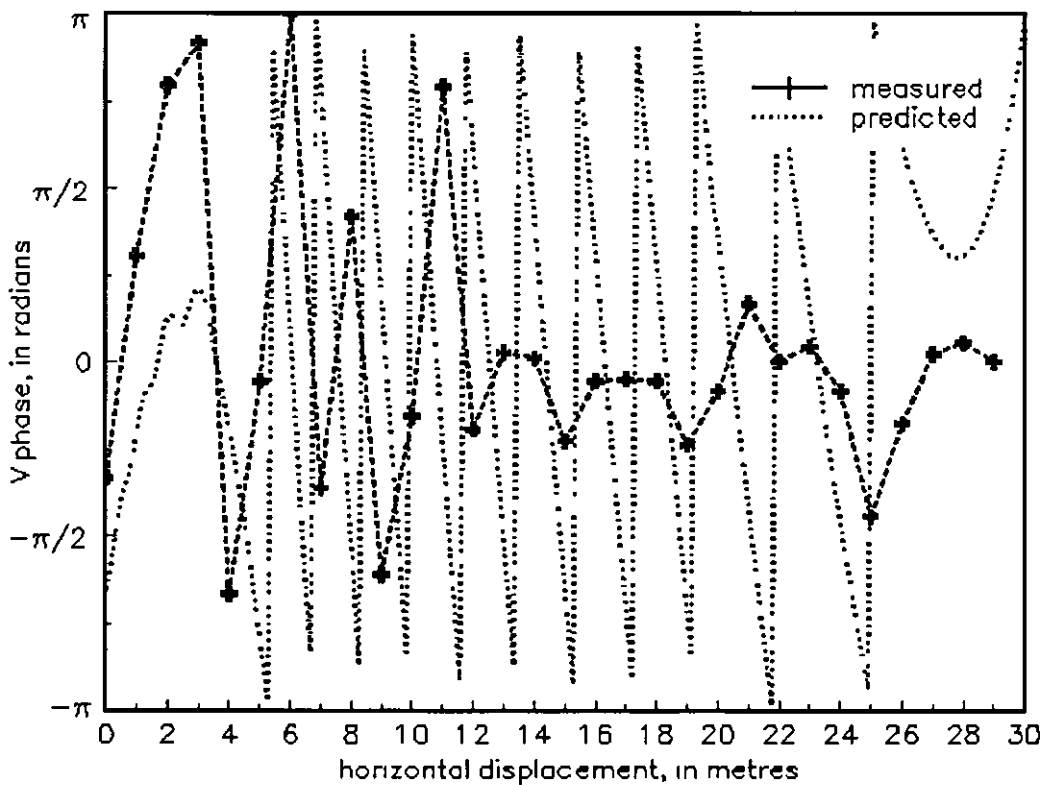


Figure 4.18 Phase of $E_{\rho}(\rho, \phi, z)$ of in dBm as function of the horizontal displacement of the Transmitter Receiver antenna is at location J

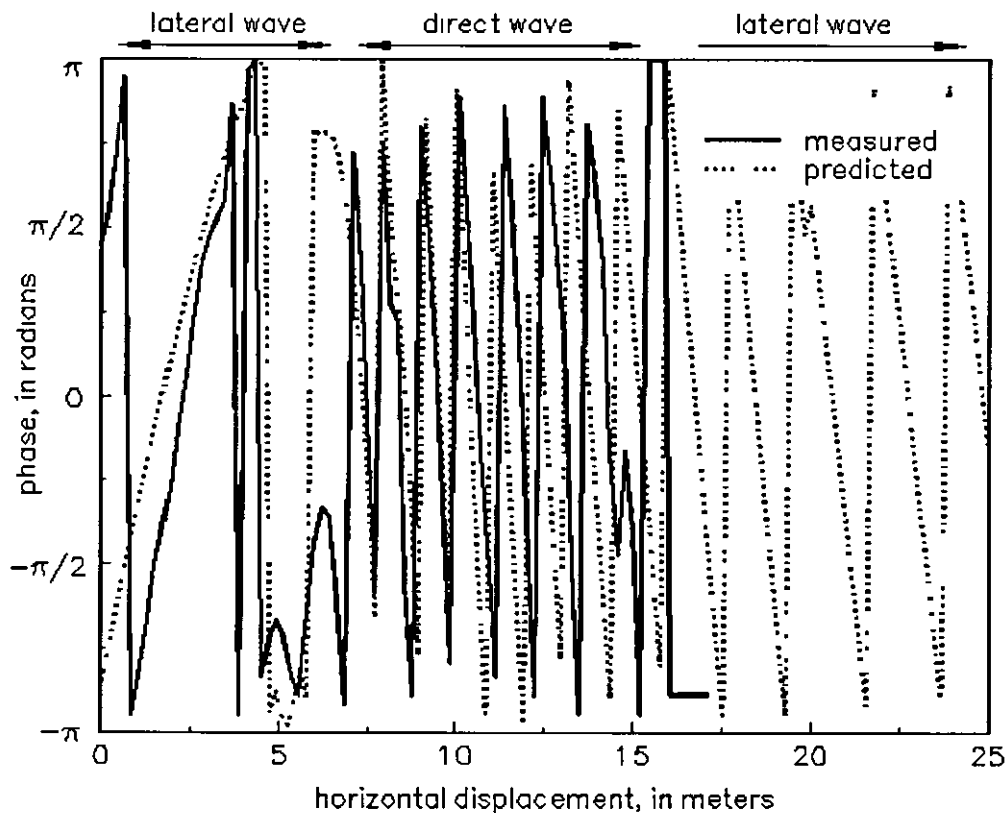


Figure 4.19 Phase of $E_{4\rho}(\rho, \phi, z)$ of in dBm as function of the horizontal displacement of the Transmitter Receiver antenna is at location X

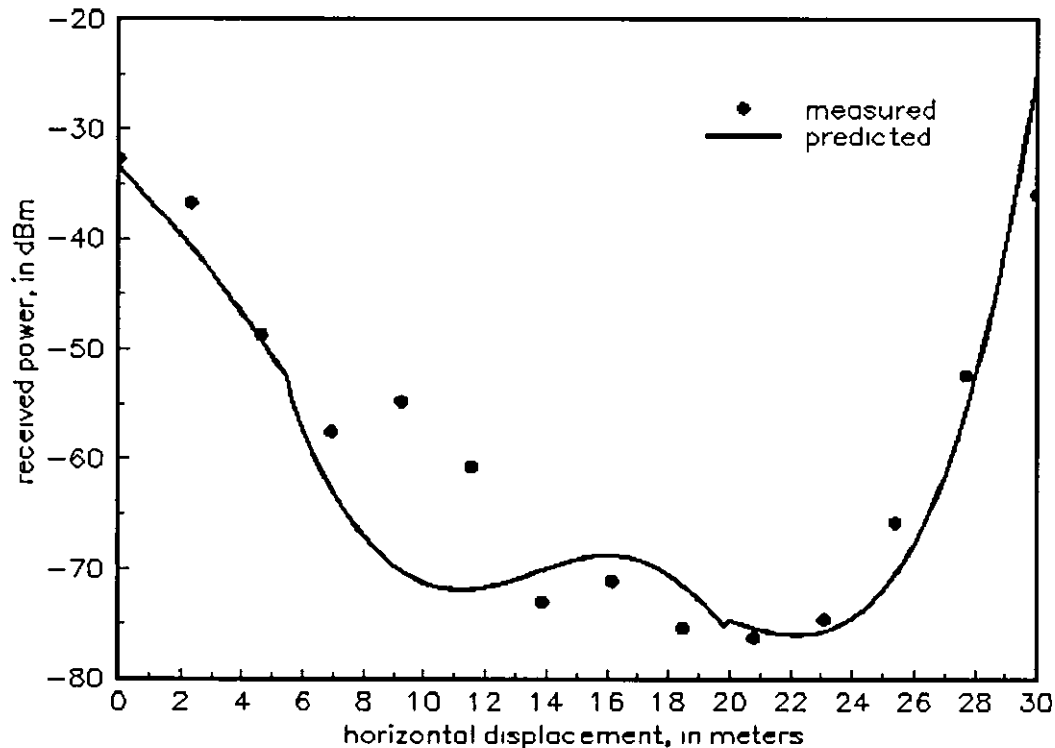


Figure 4.20 Magnitude $E_{0 \text{ total}}(\rho, \phi, z)$ of in dBm as function of the horizontal displacement of the transmitter Receiver antenna is at location B2 Receiver antenna is a monopole antenna at $h=0.5$ m pointing towards the ground with an angle of 45°

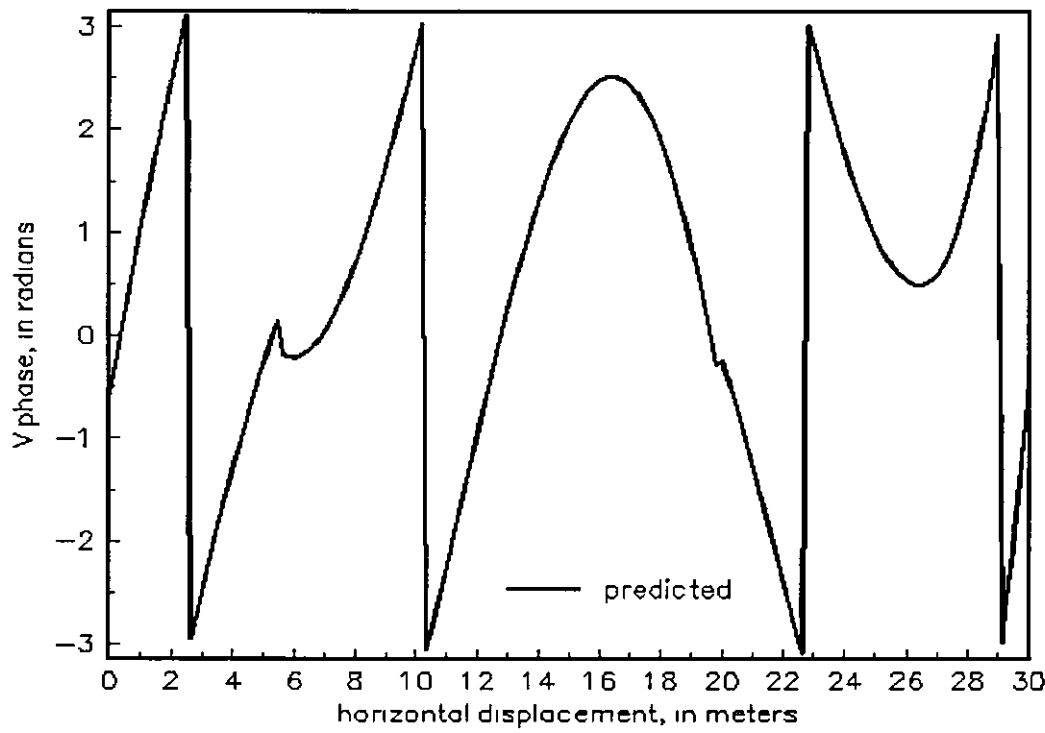


Figure 4.21 Phase of $E_{0 \text{ total}}(\rho, \phi, z)$ of in dBm as function of the horizontal displacement of the transmitter Receiver antenna is at location B2 Receiver antenna is a monopole antenna at $h=0.5\text{ m}$ pointing towards the ground with an angle of 45°

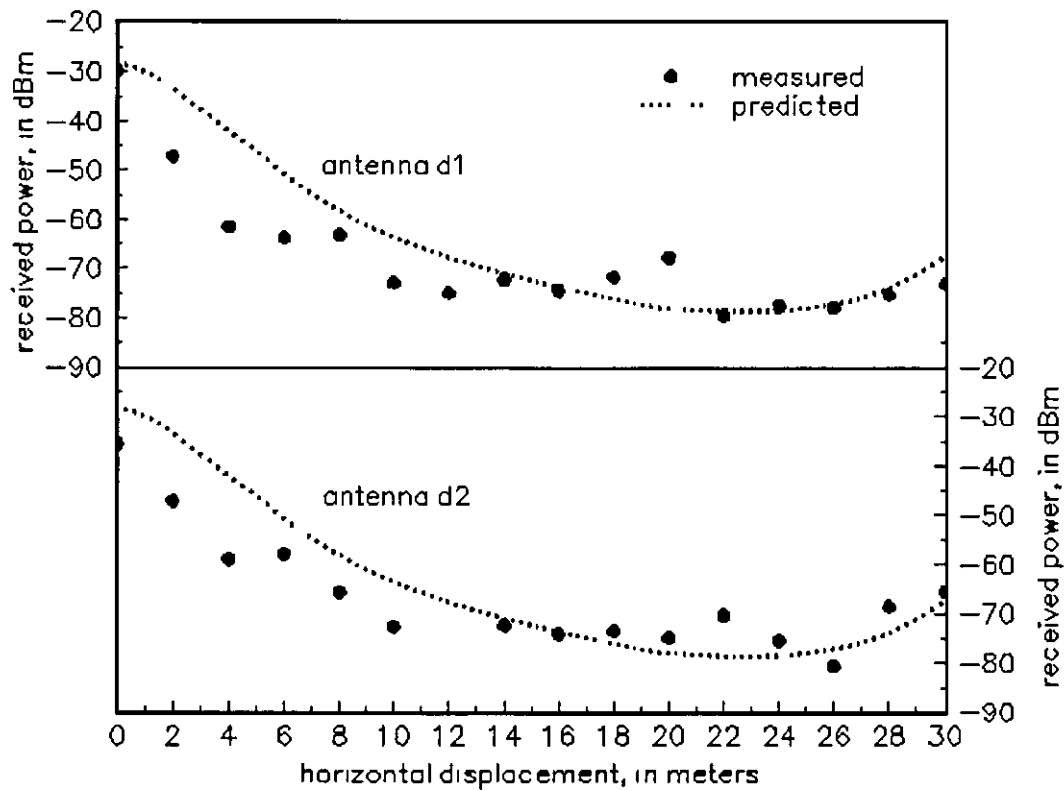


Figure 4.22 Magnitude $E_{4\rho}(\rho, \phi, z)$ of in dBm as function of the horizontal displacement of the transmitter Two receiver antenna is at locations D1 and D2

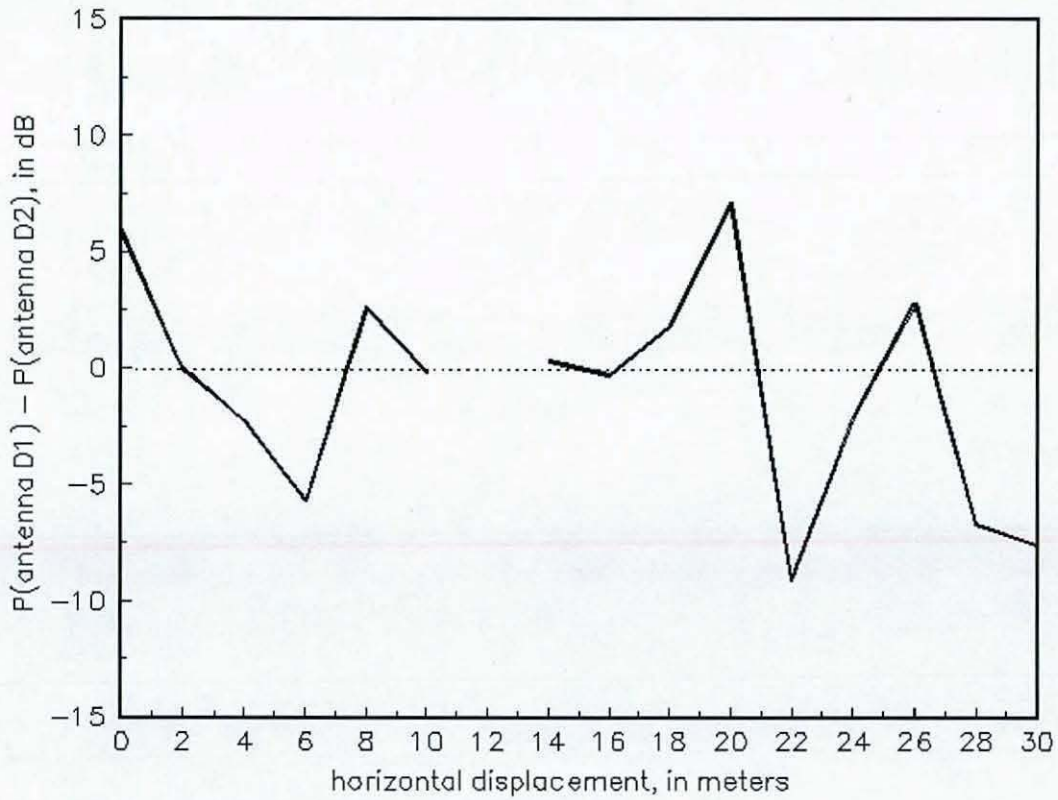


Figure 4.23 Difference of D1 and D2 in figure4.20

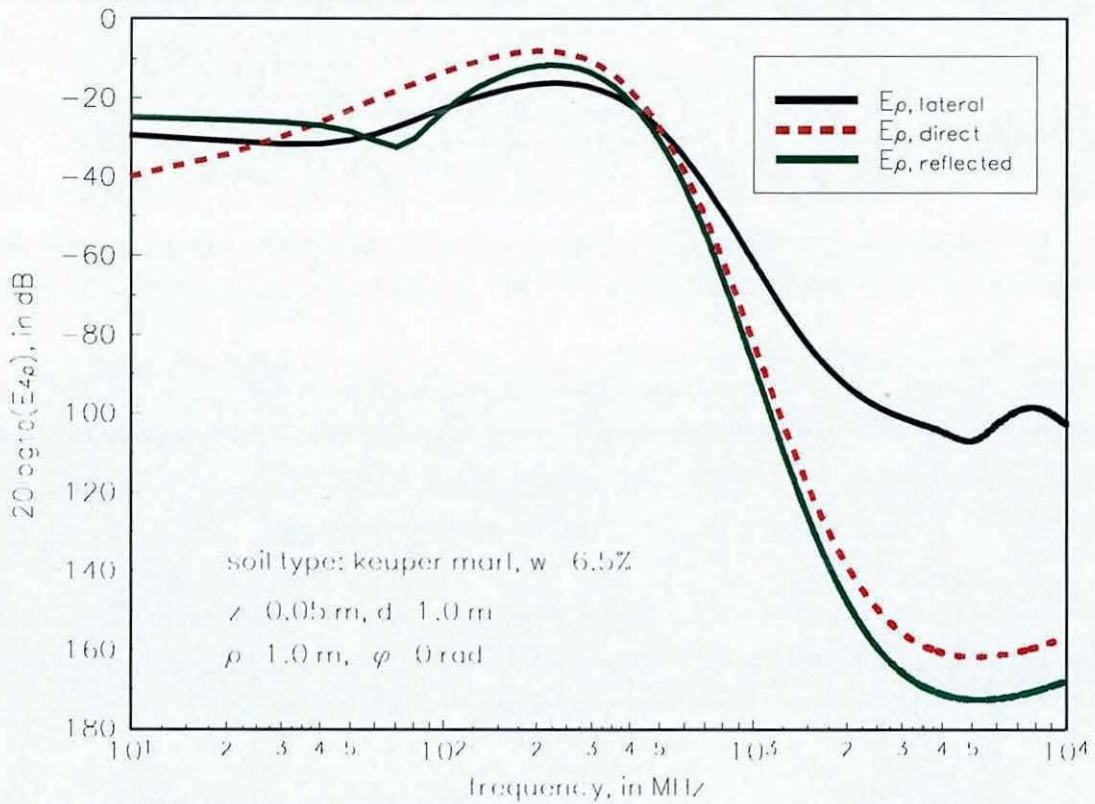


Figure 4.24 Predicted field due to a horizontal dipole underground at 1.0 m distance, as a function of frequency. Medium 4 is a relative dry keuper marl clay.

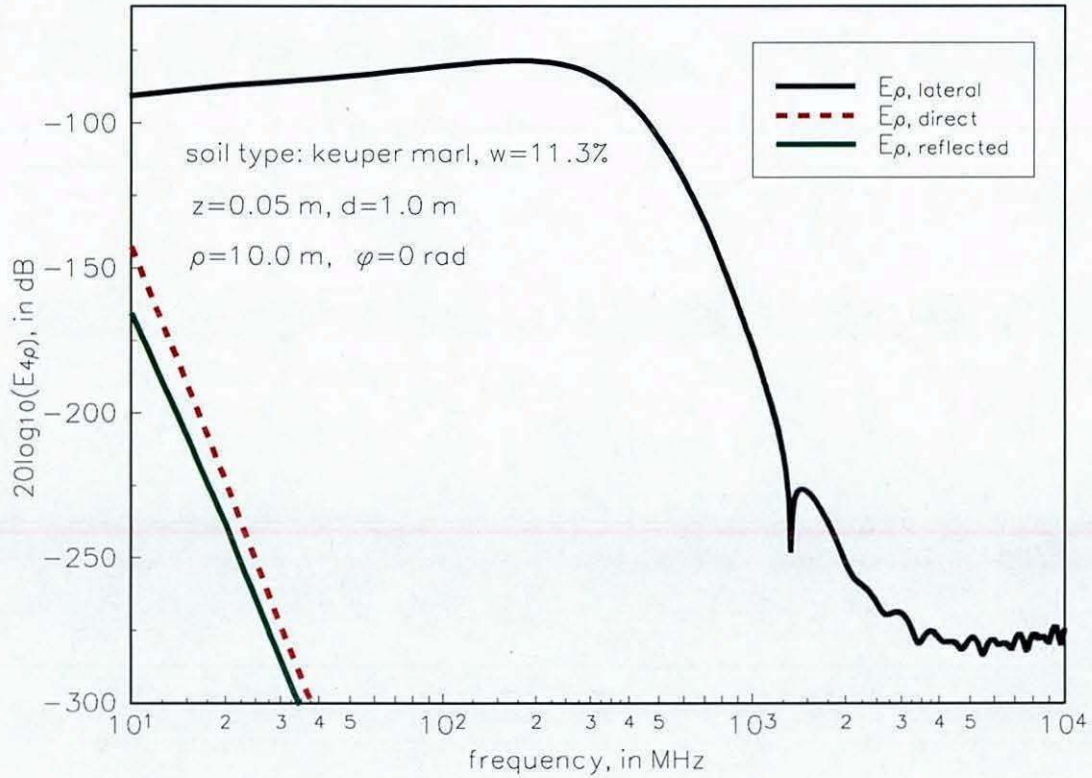


Figure 4.25 Predicted field due to a horizontal dipole underground at 1.0 m distance, as a function of frequency. Medium 4 is a relative wet keuper marl clay

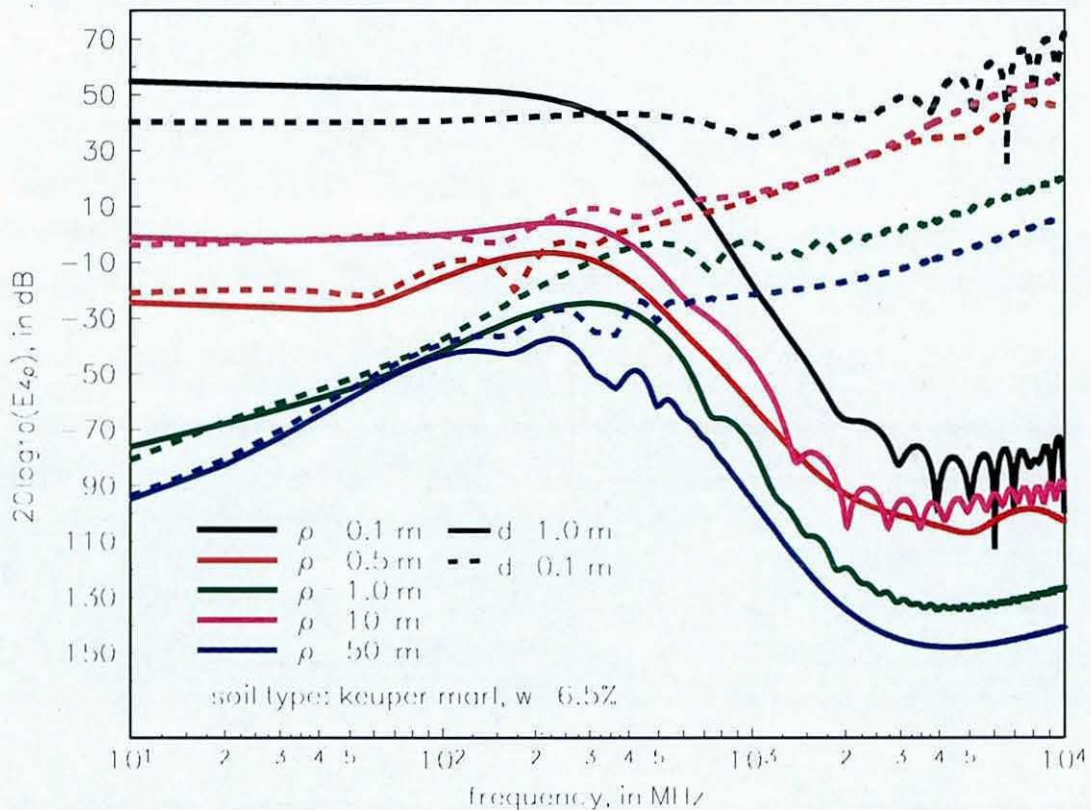


Figure 4.26 Predicted field due to a horizontal dipole underground at various distances, as a function of frequency. Medium 4 is a relative dry keuper marl clay.

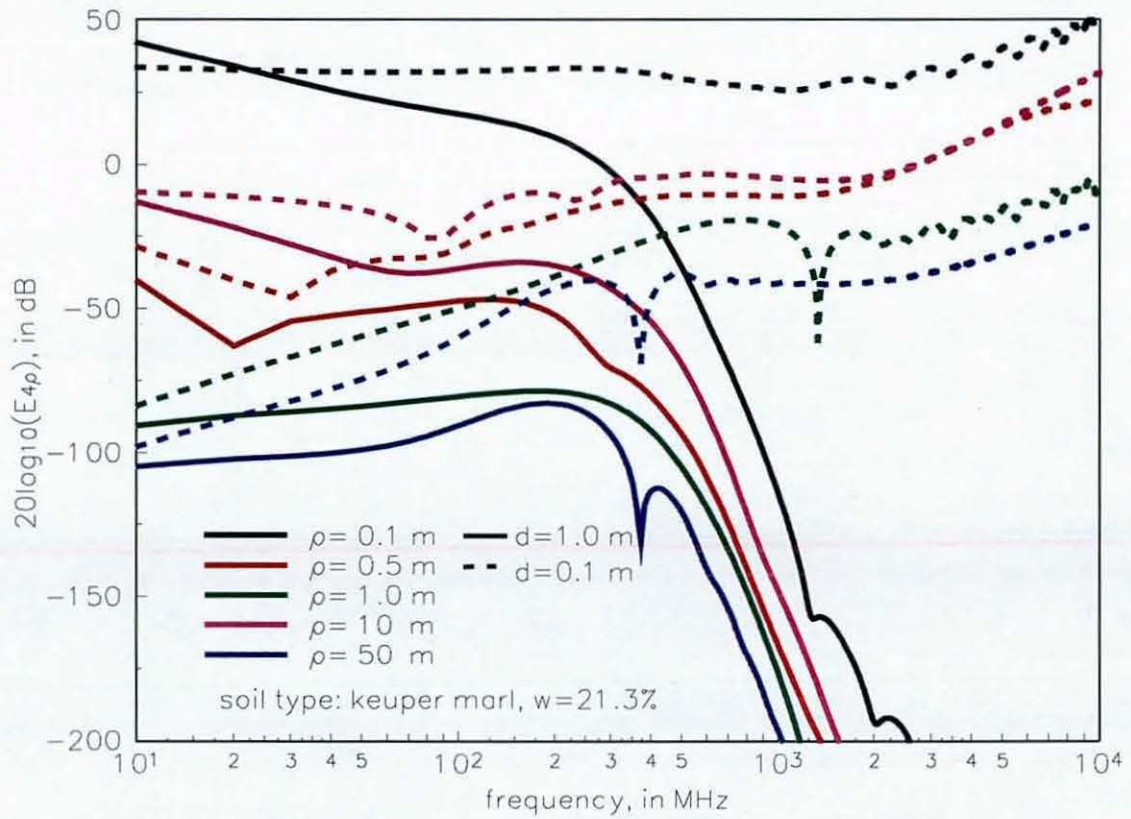


Figure 4.27 Predicted field due to a horizontal dipole underground at various distances, as a function of frequency. Medium 4 is a relative dry keuper marl clay.

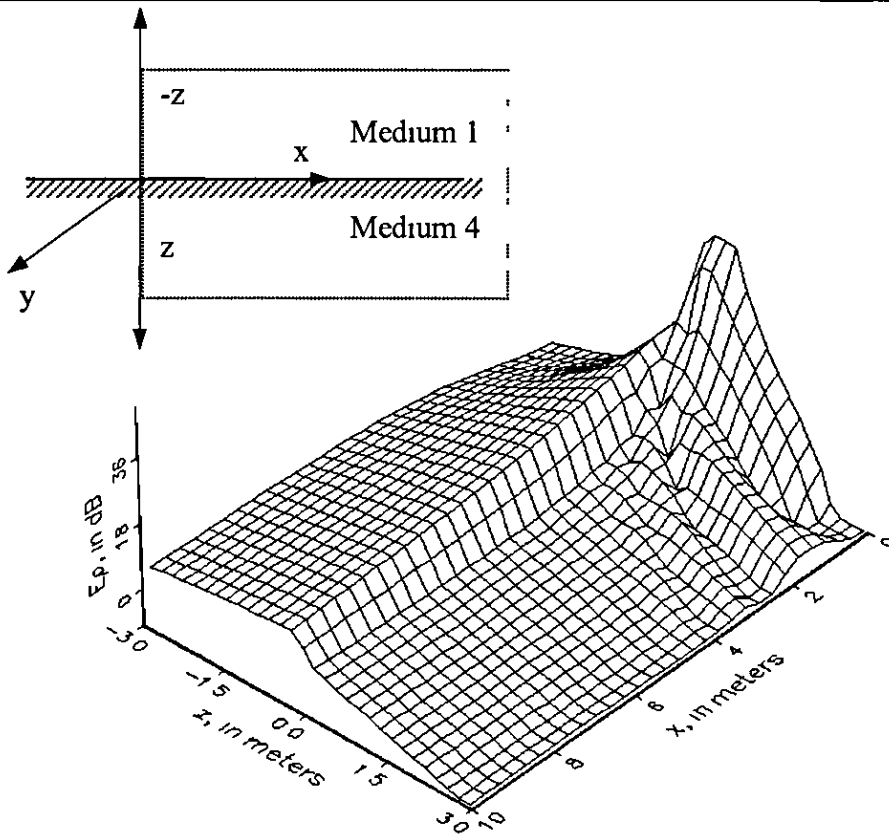


Figure 4.28 Predicted magnitude of $E_p(\rho, \phi, z)$ in the XZ-plane The transmitter is located at $(0,0,0.1)$ The boundary between medium 4 and 1 is at $z=0$ For $z<0$ the observer (receiver antenna) is underground

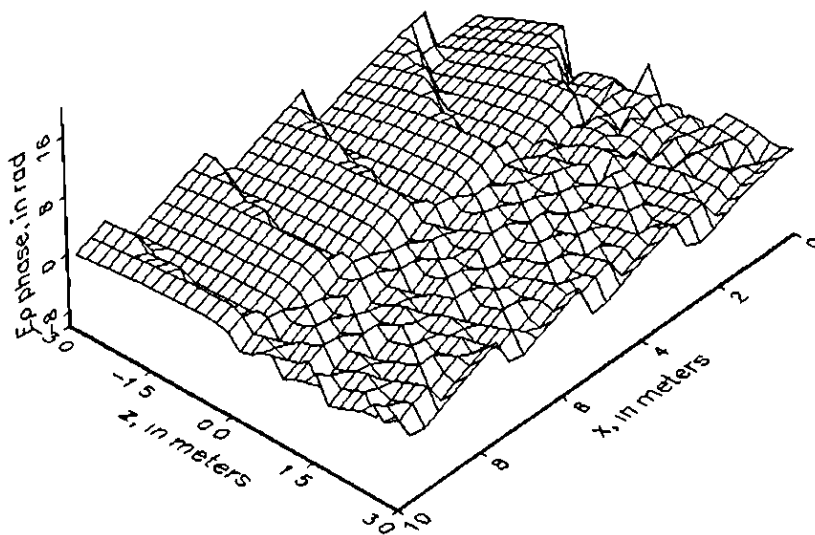


Figure 4.29 Predicted magnitude of $E_p(\rho, \phi, z)$ in the XY-plane The transmitter is located at $(0,0,0.1)$ The boundary between medium 4 and 1 is at $z=0$ For $z<0$ the observer (receiver antenna) is underground

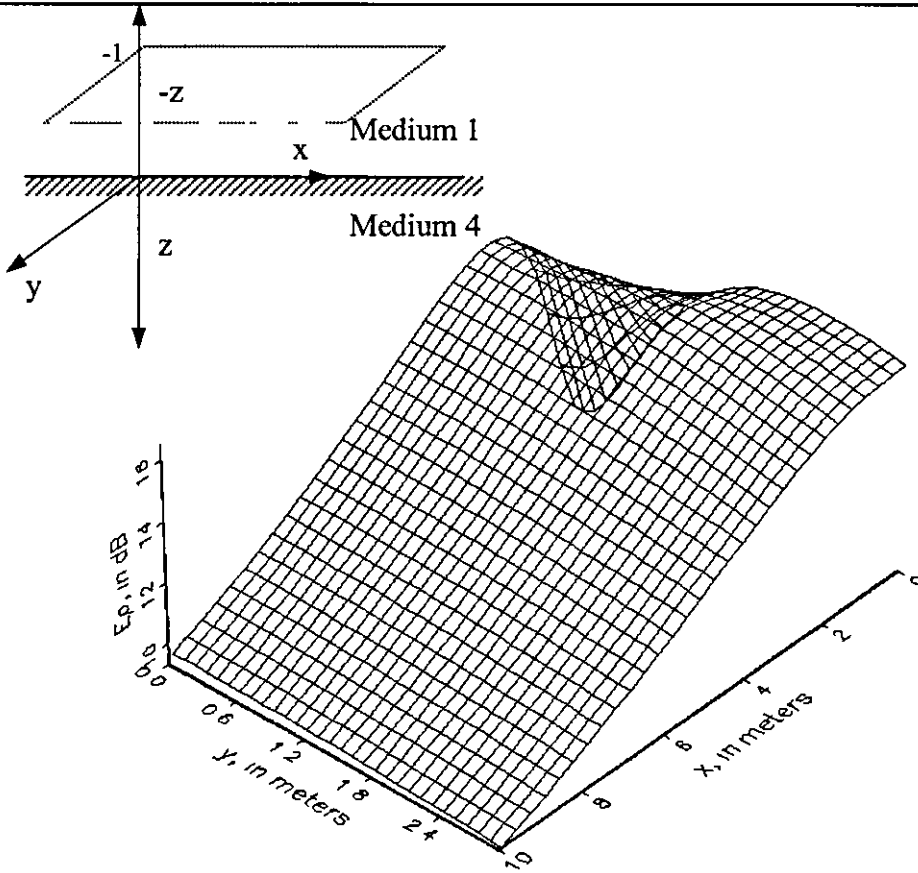


Figure 4.30 Predicted magnitude of $E_{4p}(\rho, \phi, z)$ in the XY-plane. The transmitter is located at $(0,0,0,1)$. The boundary between medium 4 and 1 is at $z=0$. The observer (receiver antenna) is 1.0 m above ground.

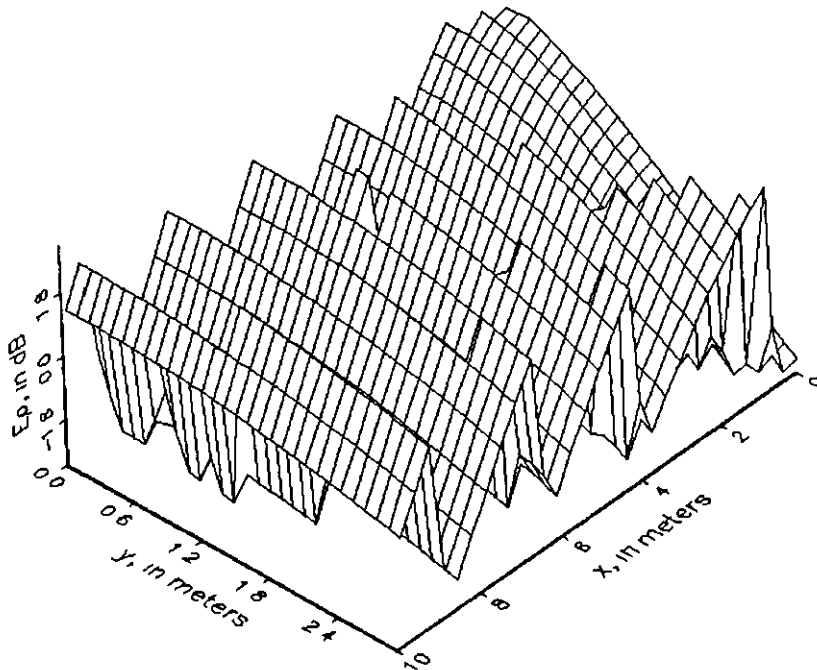


Figure 4.31 Predicted phase of $E_{4p}(\rho, \phi, z)$ in the XY-plane. The transmitter is located at $(0,0,0,1)$. The boundary between medium 4 and 1 is at $z=0$. The observer (receiver antenna) is 1.0 m above ground.

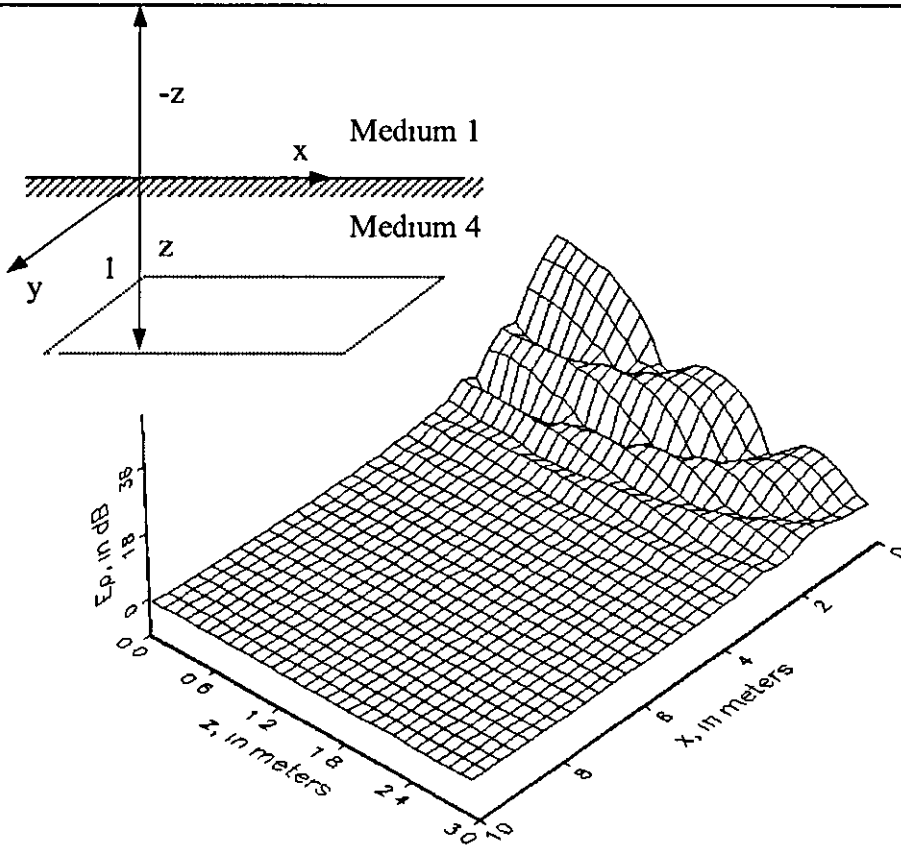


Figure 4.32 Predicted magnitude of $E_{4p}(\rho, \phi, z)$ in the XY-plane. The transmitter is located at $(0,0,0,1)$. The boundary between medium 4 and 1 is at $z=0$. The observer (receiver antenna) is 1.0 m deep underground.

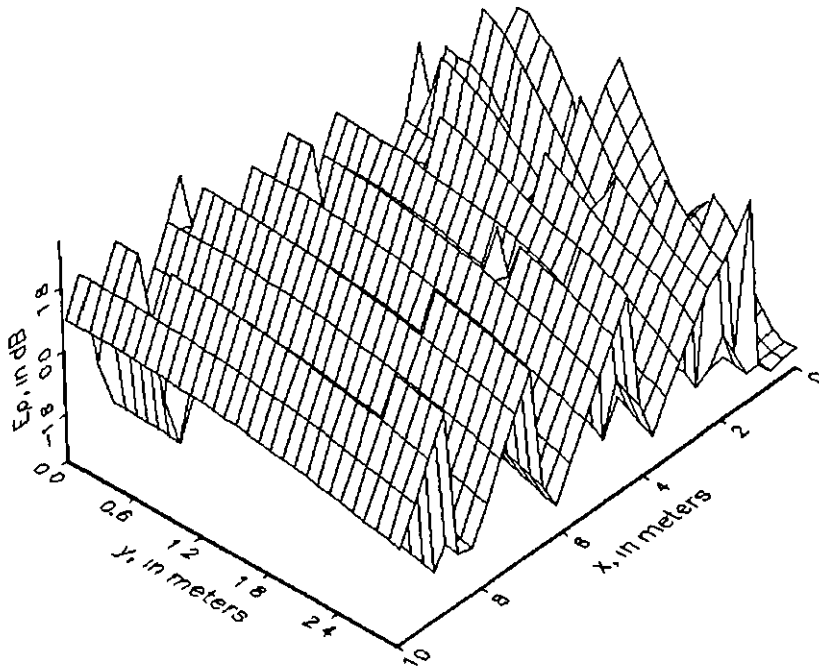


Figure 4.33 Predicted magnitude of $E_{4p}(\rho, \phi, z)$ in the XY-plane. The transmitter is located at $(0,0,0,1)$. The boundary between medium 4 and 1 is at $z=0$. The observer (receiver antenna) is 1.0 m deep underground.

References

- [1] Burke, G.J. 'Recent Advances to NEC' *Application and Validation*, UCRL-100651, Lawrence Livermore Laboratory, March 3, 1989.
- [2] King, R.W.K. 'Lateral Electromagnetic Waves,' Springer-Verlag, New York, 1992
- [1] Viggh, M E. 'Modes in Lossy Stratified Media with Application to Underground Propagation of Radio Waves,' *IEEE Tans Antennas & Propagation*, AP-11, Vol 3, pp318-323, 1963.
- [2] Burrows, C.R. 'Radio Communication Within the Earth's Crust', *IEEE Trans Antennas & Propagation*, Vol AP-11, No. 3, pp 311 – 317, May 1963.
- [3] Willoughby, J.A., Lowell, P.D., 'Development of Loop Aerial for Submarine Radio Communications,' *Physics Review*, Vol 14, pp. 193-194, August 1919
- [4] Shen, L C. King, R.W P. et al. "Measured field of a Directional Antenna Submerged in a Lake," *IEEE Trans. Antennas and Propagation*, November 1976, pp.891-894.
- [5] Osumi, N. and Ueno, K. 'Microwave Holographic Imaging of Underground Objects,' *IEEE Trans. Antennas and Propagation* , Vol AP-33, No 2, Feb. 1985
- [6] Daniels, D.J., 'Surface Penetrating Radar for Industrial and Security Applications,' *Microwave Journal*, Vol. 37, No. 12, Dec '95, pp. 68 –82.
- [7] El-Said, M.A.H., 'Geophysical Prospecting of Underground Water in the Desert by Means of Electromagnetic Interference Fringes,' *Proc IRE*, Vol 44, No 1, Jan 1956, pp 24-30
- [8] Jeffrey, R, et.al. 'Subsurface Probing by High Frequency Measurements of Wave Tilt of Electromagnetic Surface Waves,' *IEEE Trans on Geoscience Electronics*, Vol. GE-14, No. 4, Oct. 1976.
- [9] Tamir, T., "On Radio Wave Propagation in Forest Environments," *IEEE Transactions on Antennas & Propagation*, AP-15, No. 6, Nov 1967, pp. 806- 817
- [10] Brekhovskikh, L.M , 'Waves in Layered Media,' part of the series: Applied Mathematics and Physics, Second Edition, 1980, Academic Press, New York, London

- [11] Tamir, T., Bertoni, H.L. 'Lateral Displacement of Optical Beams at Multilayered and Periodic Structures', *Journal of the Optical Society of America*, Vol.61, No. 10, Oct 1971.
- [12] Barlow, 'Radio Surface Waves', Oxford, Clarendon Press, 1962.
- [13] Sommerfeld, A., 'Electromagnetic Waves Near Wires,' *Wied. Annalen*, 67, pp. 233-290, 1899.
- [14] Norton, K A , 'The Propagation of Radio Waves over the Surface of the earth and in the upper atmosphere,' *Proc IRE.*, Vol. 24, pp. 1684-1387, Oct. 1936.
- [15] Baños, A, Jr., 'Dipole Radiation in the Presence of a Conducting Half-Space,' Oxford, England, Pergamon Press, 1966.
- [16] Abramowitz, M., Stegun, L.A., (eds.), "Handbook of Mathematical Functions", New York, Dover Publications, 1972, p 299, equation 7.1.29.
- [17] Boardman, A D. (ed), "Electromagnetic Surface Modes", New York, John Wiley & Sons, 1982.
- [18] Equations (5.5.48) and (5.5.49) of reference [2].
- [19] King, R.W.P., "On the Reflection of Lateral Electromagnetic Waves from Perpendicular Boundaries," *Journal of Applied Physics*, Vol. 55, No. 11, June 1984.

5. Conclusions and Further Work

The work described in this thesis is concerned with the feasibility of a system that is able to transmit an electromagnetic wave from a source underground, receive it at a distance of up to 30 m, and calculate the displacement of the transmitter from the phase and magnitude of the received signal. This study has concluded that in principle such a system is feasible, but more work is necessary to achieve a higher confidence level of its performance.

5.1. Summary

A coaxial probe for the measurement of the dielectric constant of soil samples was used on-site during the field trials, enabling the estimation of environmental parameters for the prediction of the antenna characteristics and underground electromagnetic wave propagation. The coaxial probe used in the experiments was suitable for measuring the dielectric constant of high loss and low loss soil samples in the frequency range of 1 MHz to 2 GHz. Soil moisture content was shown to be an important factor of its dielectric behaviour as is its grain size. Wet samples exhibit a higher dielectric conductivity, being dispersed for both sands and clays. Clays showed a higher dielectric conductivity. A site survey has been conducted at the location where the underground propagation measurements were undertaken. The dielectric constant and conductivity was measured at 12 different locations and to a depth of 2 m. The distribution of the relative dielectric constant was narrower at the higher frequencies. This suggests that the wave impedance for an electromagnetic wave travelling through the medium changes less at 300 MHz, as compared to the changes at lower frequencies. Hence less reflection and refraction was expected at this frequency, but a higher overall attenuation due to the increased conductivity of the soil. The dielectric constant and conductivity of soils were temperature dependent.

A method has been developed to predict the admittance of insulated monopole antennas in soil, using measured data of the ambient medium. The model was based on transmission line like equations and can be applied to monopole and dipole wire antennas but was tested for insulated monopole antennas in soil and water. There was good agreement between the predictions and the measurements of the antenna impedance. An increase in the moisture constant of the soil from 5% to 10.8% resulted in an increase of the antenna resonant frequency. This was because the dielectric constant increased making the wavelength shorter for a given frequency. The insulated monopole antenna had a longer effective length in a low loss dielectric. In comparison with dry soil as ambient medium, the dipole antenna in wet soil had a shorter effective length and its radiation pattern was more omnidirectional. It was calculated that the dielectric sheath should have a dielectric constant close to 1.0 to achieve the optimum antenna efficiency.

The field trials have shown that propagation of an electromagnetic wave from a transmitter underground to a receiver underground was possible over a distance of 30 m and to a depth of 1.5 m. Also when the receiver was placed at 0.5 m above the ground, an electromagnetic wave was received from the same transmitter. A simulation model was used to predict the electromagnetic wave propagation from the source underground, using the measured ϵ_r and σ . The difference between the measured and predicted results were mainly because of a ripple which showed two different standing wave patterns. The wavelength of the ripple was either that of the wave in air or underground. This was caused by reflection due to irregularities underground or on the ground surface. Although reflection against objects on the ground surface causes a deep minimum at close distance, once passed the object, the incident wave regains its characteristics. The simulation predicted that the lateral wave was the strongest mode of propagation in the majority of the field trials. Only at short distances was the direct wave dominant. The field trials confirmed these findings. The lateral wave starts at the source underground, travels to the boundary, follows the air-ground boundary and then propagates back into the ground to the receiver antenna. As the wave travels a significant part of its path in air, it is less susceptible to irregularities underground. Measurement of the phase has shown it to be sensitive to errors caused by reflections. The field trials have shown the possibility of using electromagnetic waves to track a moving transmitter underground. A possible application is the tracking of a micro-tunnelling machine, used for laying pipes or cables.

Mounting a transmitter on the drill-head would allow its movements to be calculated from the magnitude and phase of the electromagnetic wave at the receiver antennas. Any system that estimated the underground displacement of the transmitter should have 2 or more receiver antennas. Field trials have shown an accuracy of such a system of approximately 2 m.

5.2. Sponsor Problems

The research project described in this thesis started in 1993 as a link project between the Department of Trade and Industry (DTI) and PTE Ltd, which is contractor which takes on 'trenchless' pipelaying orders. The input of PTE Ltd would be the sponsorship of equipment and the help in providing access to digging trials. The plan was to develop a prototype, which could be tested in these trials.

However, after 14 months of work, PTE Ltd. went into receivership. The new company that took over PTE's business was not able to continue the financial sponsoring of the project. Nevertheless, it was able to provide assistance in laying a 30 m and a 20 m pipe under the campus at Loughborough University. The project was continued with a very limited budget.)

5.3. Recommendations for Further Work

The research discussed in this thesis has given an understanding of the problems encountered when an electromagnetic signal is transmitted underground.

The simulations predict that, as is shown in figure 4.10, the magnitude of $E_r(\rho, \phi, z)$ is the strongest signal at distances up to approximately 20 m from the transmitter. The probability of receiving $E_r(\rho, \phi, z)$ is therefore higher than receiving $E_\rho(\rho, \phi, z)$. It would be an enhancement of the system if $E_r(\rho, \phi, z)$ could be measured also in the field trials.

The measurements have shown standing waves that suggest reflection underground and on the ground surface. A further investigation of reflections of both $E_r(\rho, \phi, z)$ and

$E_p(\rho, \phi, z)$ by objects on the ground would give a better understanding why in some instances in the field trials a signal was not received.

The surprising result of the lateral wave being the strongest mode of propagation, despite the very rough terrain surface, with vegetation and a tree, creates the opportunity to design and test antennas specifically for the reception of lateral waves. An example is the Beverage antenna, which is a wire antenna with a matched load, positioned in a horizontal position above the ground. The Beverage antenna has shown to be efficient in transmitting an electromagnetic wave into the ground. Also, its location above surface makes it sensitive to lateral waves.

There is an increased interest in intelligent highways in the U.S A. The intelligence comes from sensors in the road surface that can help navigate a car. Dielectric loaded antennas could be used in road surfaces to detect traffic or could be used for communication. Communication with cars using lateral electromagnetic waves could be very efficient.

Currently mobile phone coverage is not provided in the London Underground. Use of conventional Microcell is difficult because the short delay times of the bounced wave. As for indoor measurement, the correlation between the arrival times is very high. One solution could be to use antennas embedded in the wall. The lateral wave created by it will propagate along the wall and attenuate very rapidly further away from it, reducing reflections.

A. Survey Results

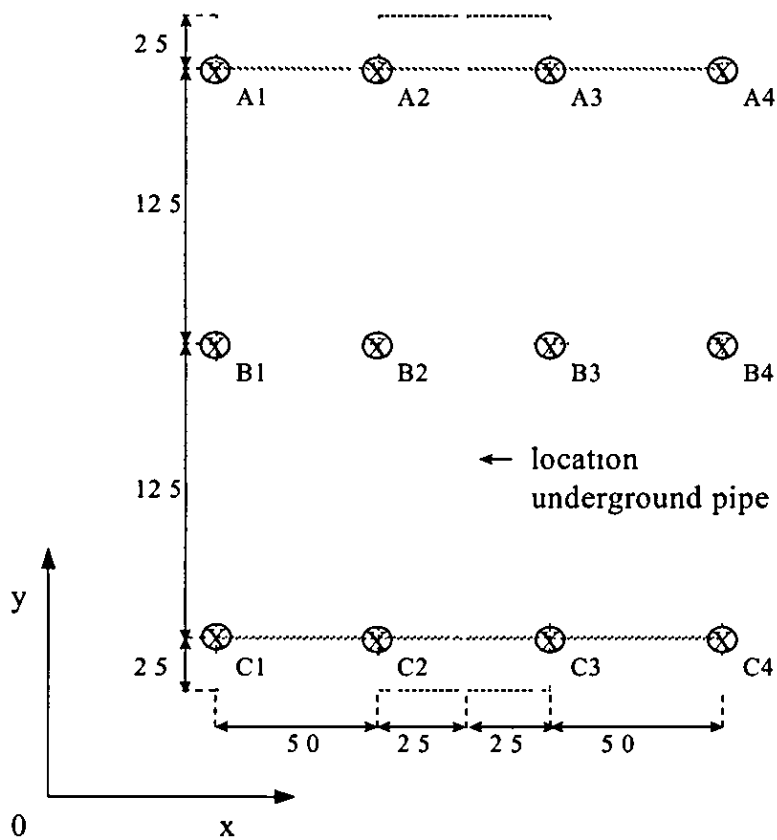


Figure A1 Top view of the site of the field trials. The numbers A1 to C4 indicate the locations where the samples were taken.

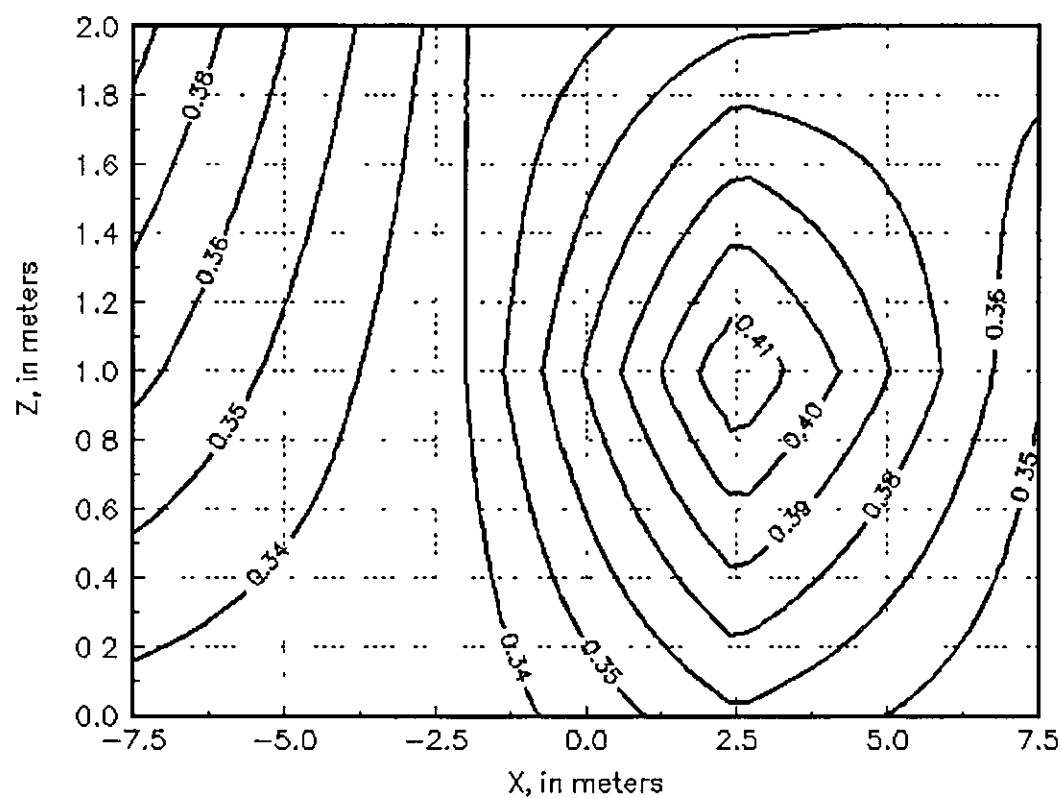


Figure A2 Cross-section AXZ, freq=1 0 MHz Conductivity, in S/m

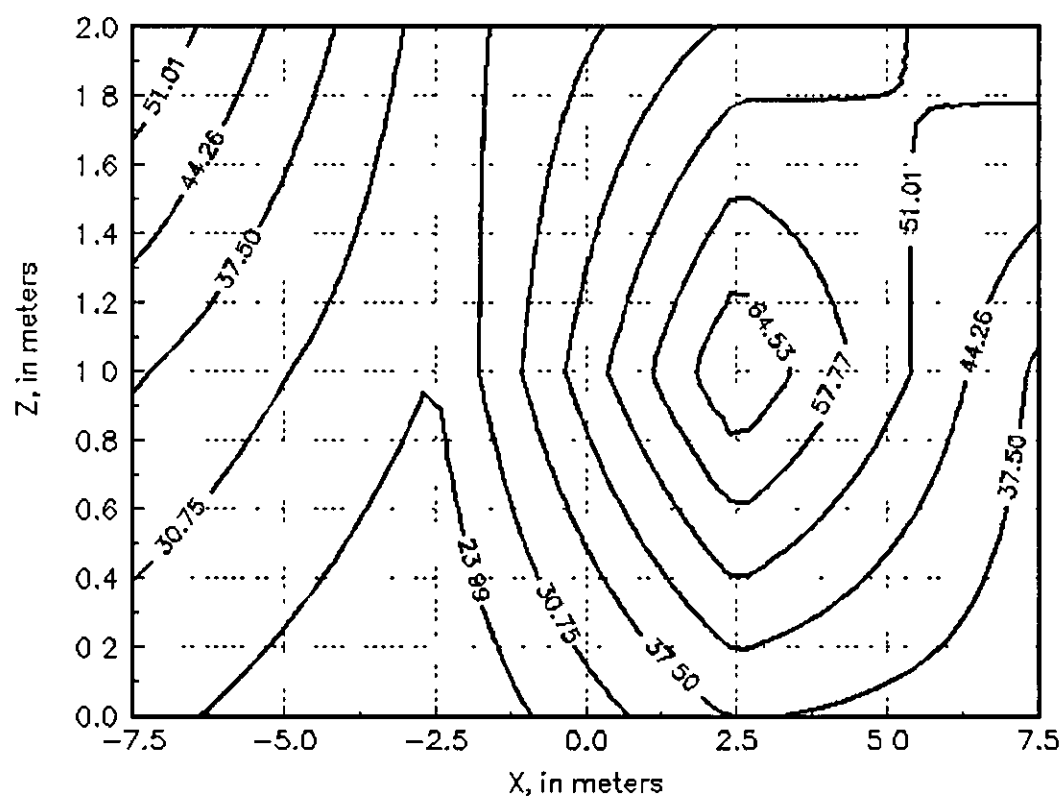


Figure A3 Cross section AXZ, freq=1 0 MHz Relative dielectric constant

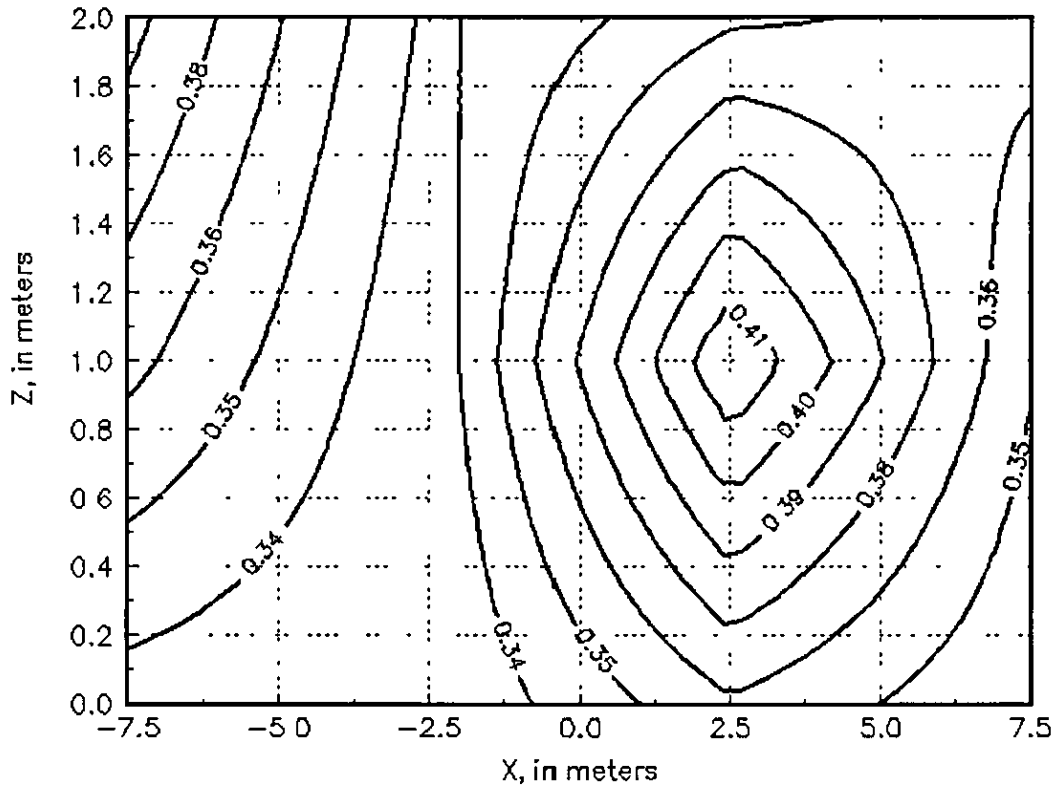


Figure A4 Cross-section AXZ, freq=146 MHz Conductivity, in S/m

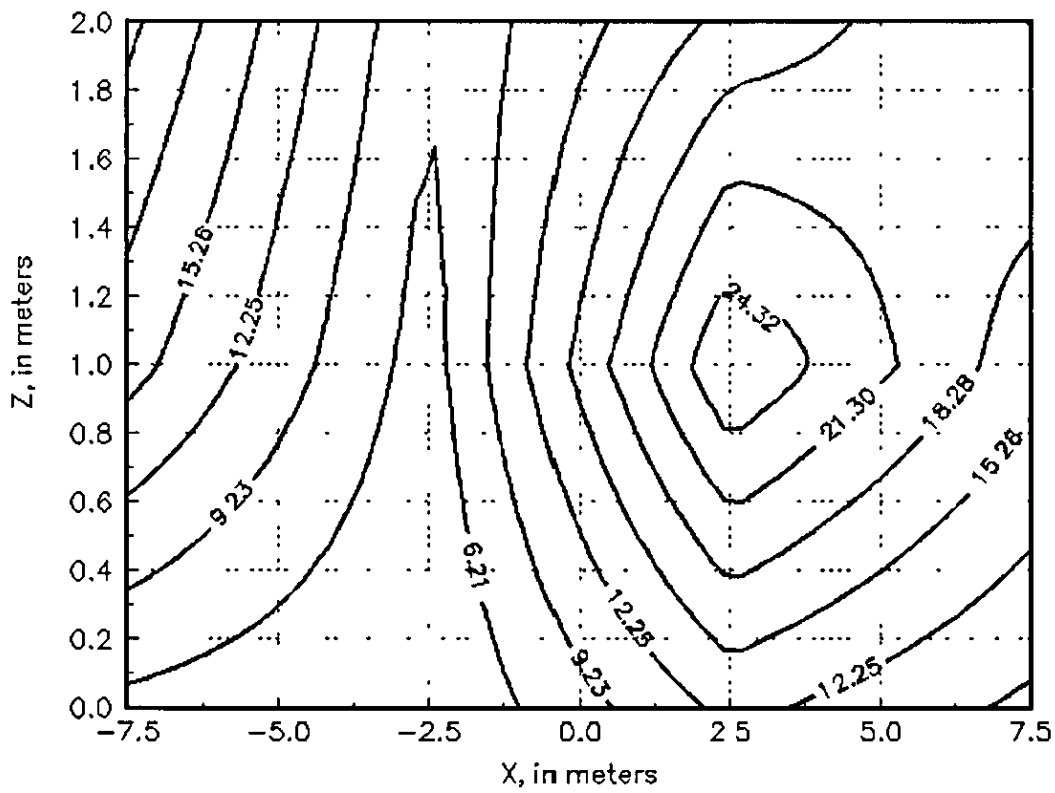


Figure A5 Cross section AXZ, freq=146 MHz Relative dielectric constant

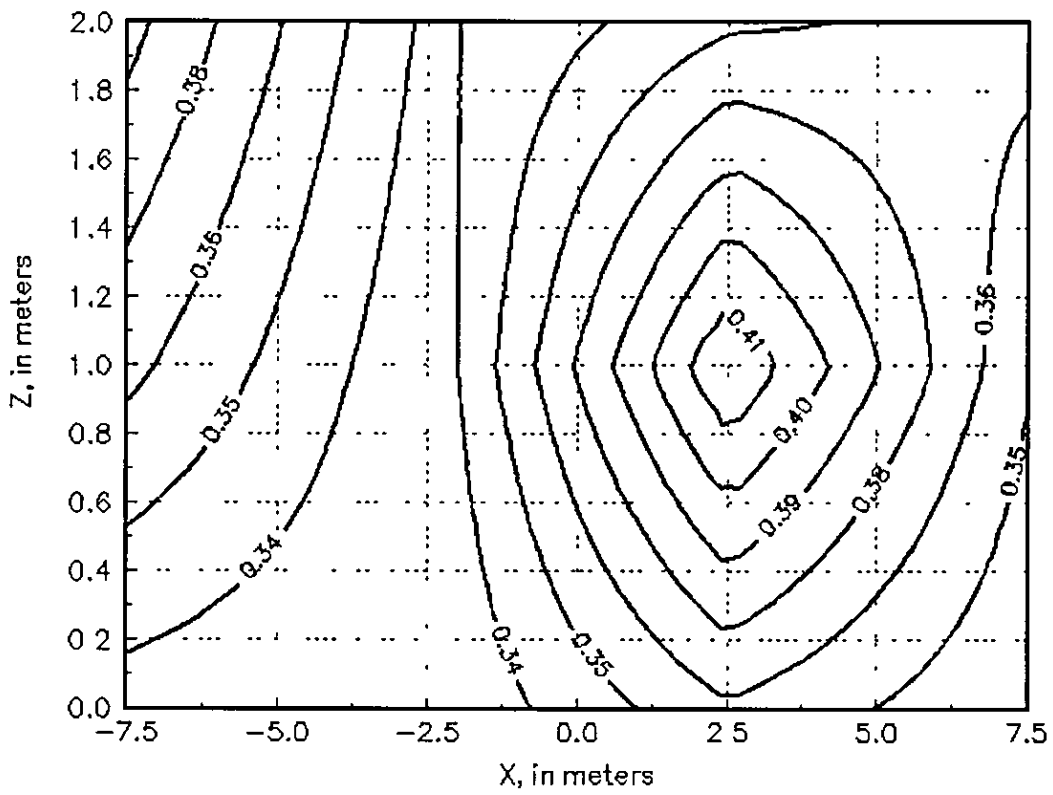


Figure A6 Cross-section AXZ, freq=300 MHz Conductivity, in S/m

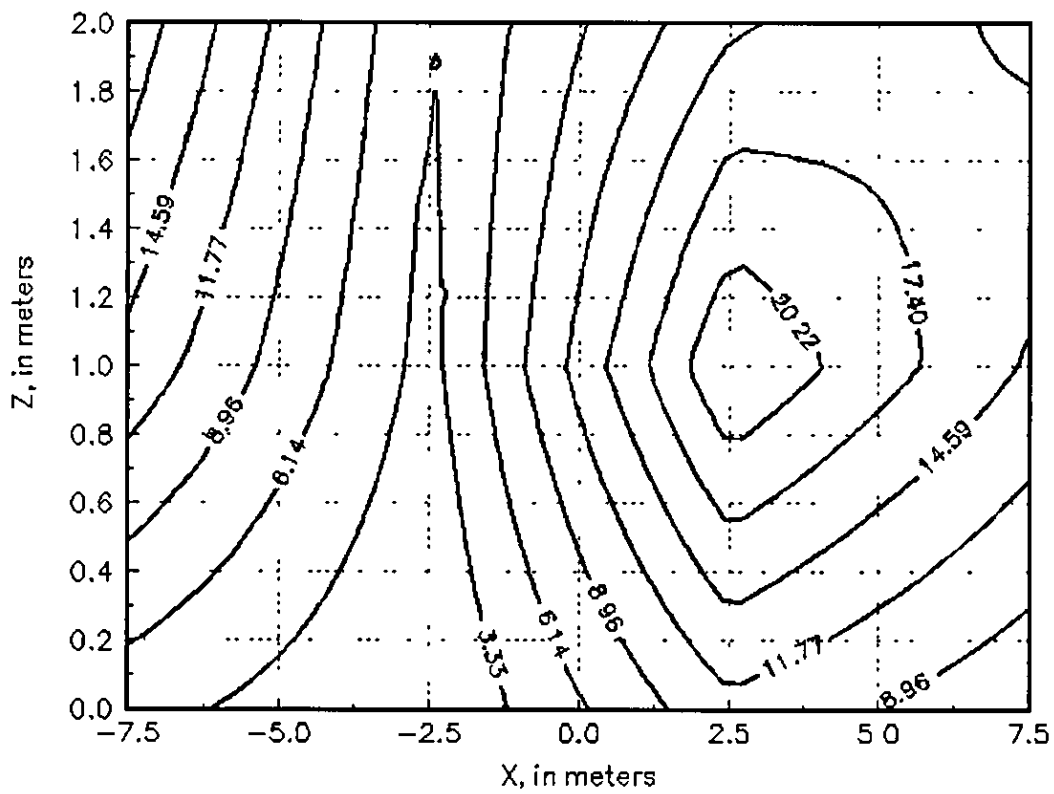


Figure A7 Cross-section AXZ, freq=300 MHz Relative dielectric constant

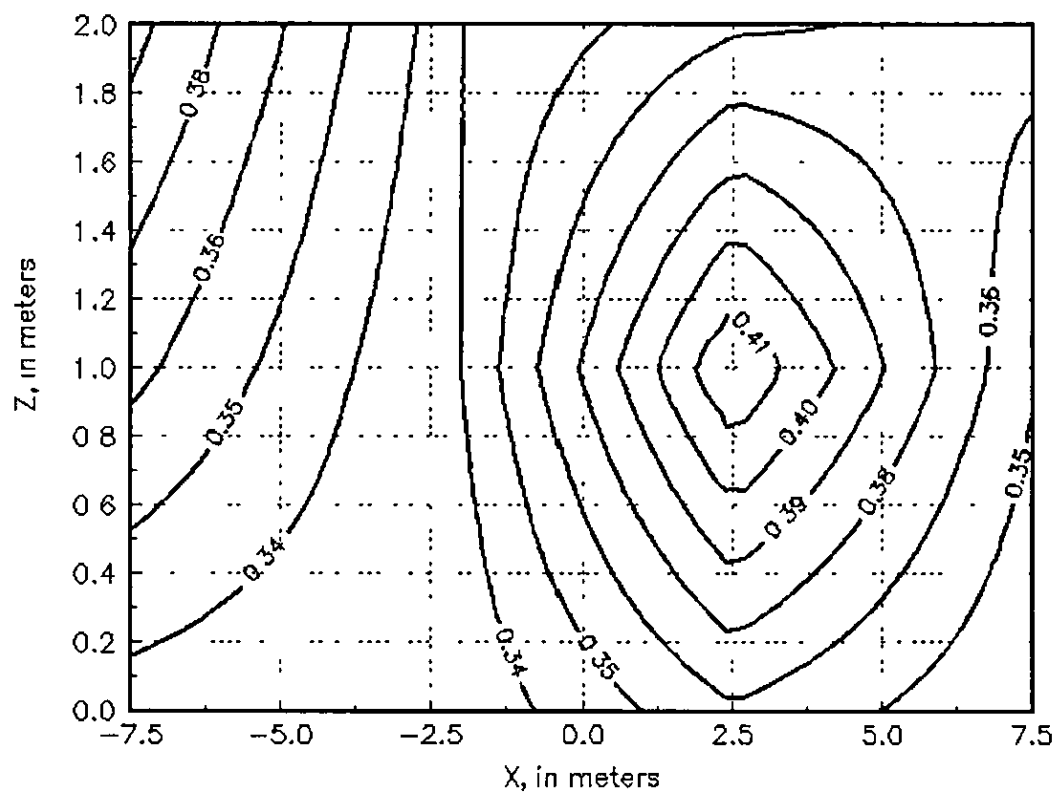


Figure A8 Cross-section BXZ, freq=1.0 MHz Conductivity, in S/m

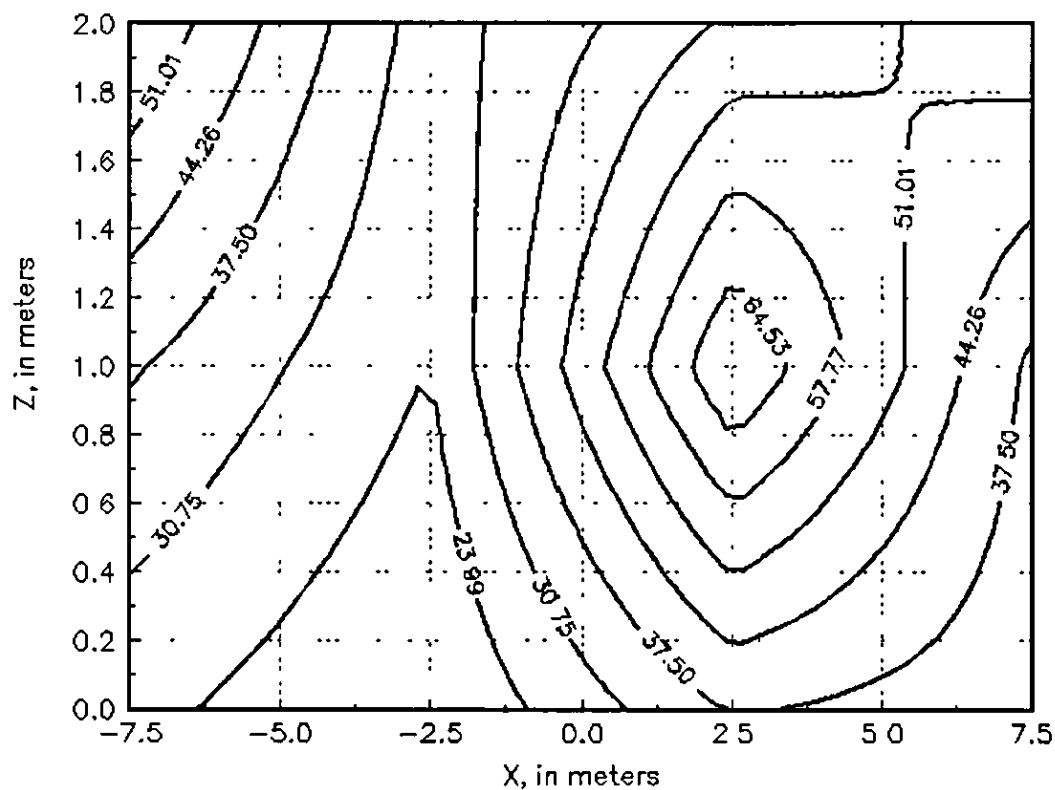


Figure A9 Cross-section BXZ, freq=1.0 MHz Relative dielectric constant

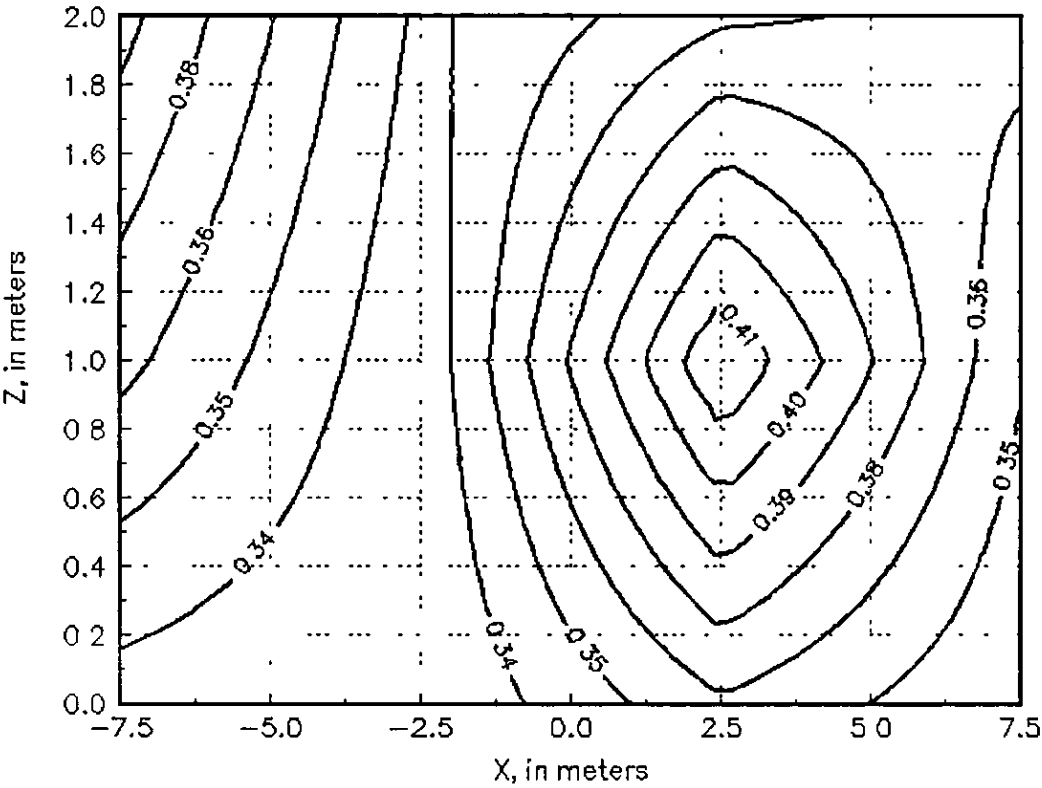


Figure A10 Cross-section BXZ, freq=146 MHz Conductivity in S/m

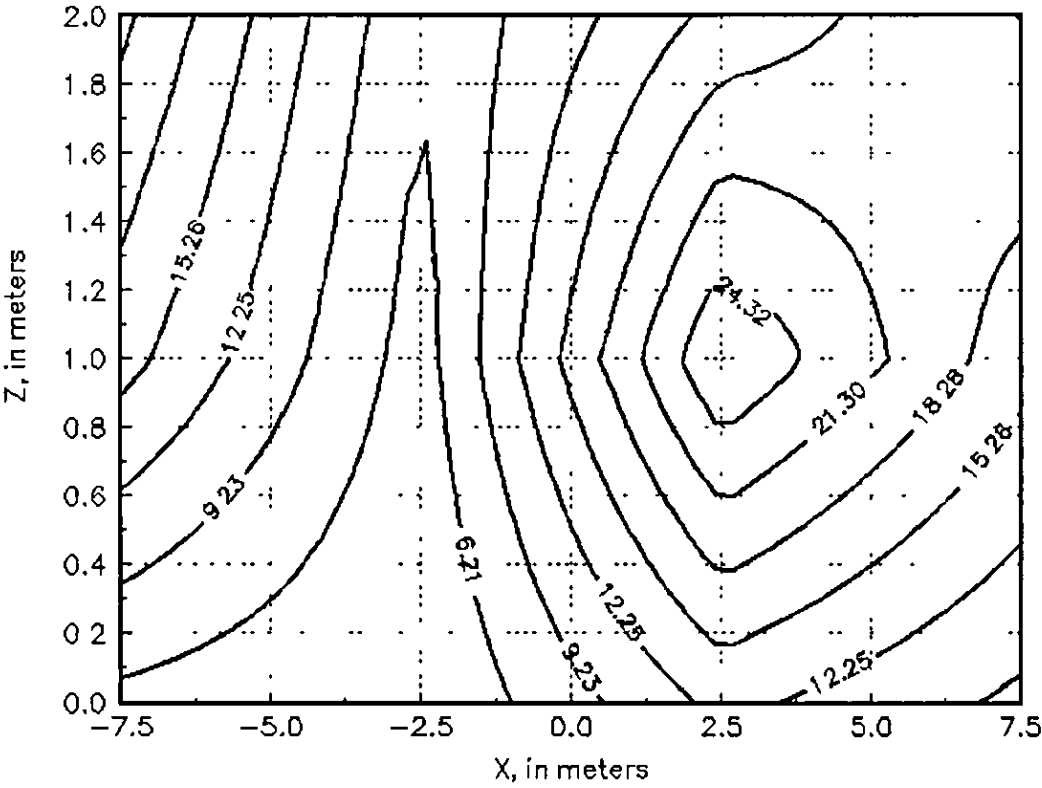


Figure A11 Cross-section BXZ, freq=146 MHz Relative dielectric constant

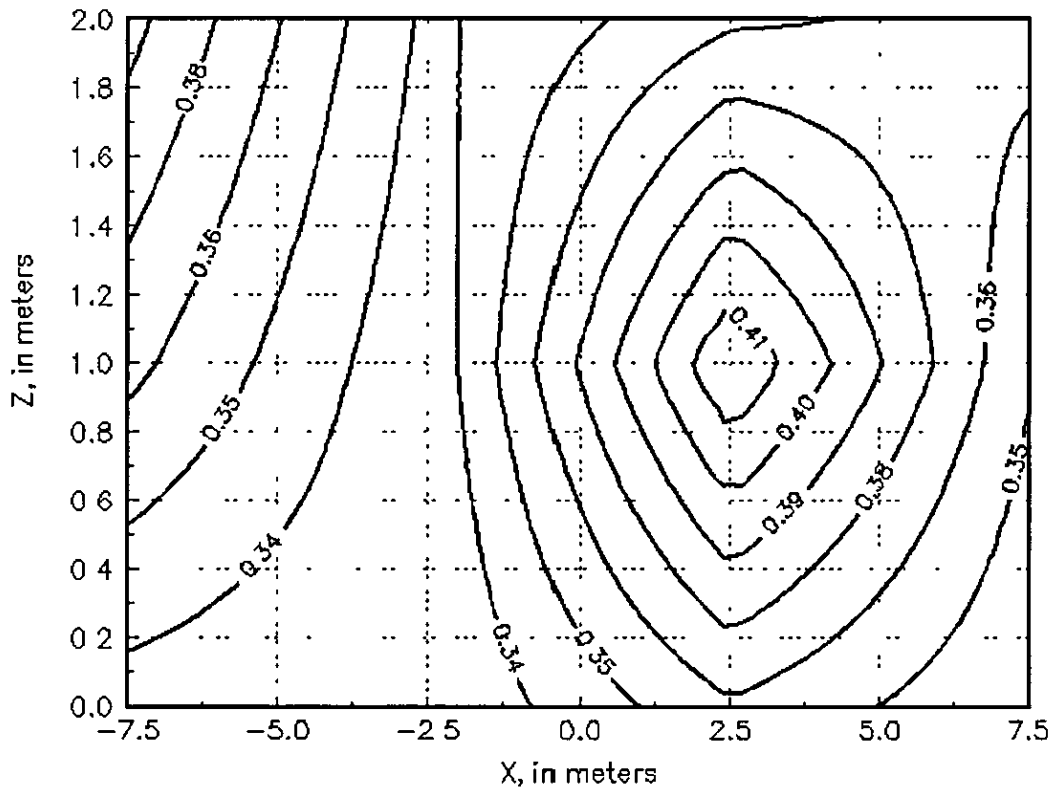


Figure A12 Cross-section BXZ, freq=300 MHz Conductivity in S/m

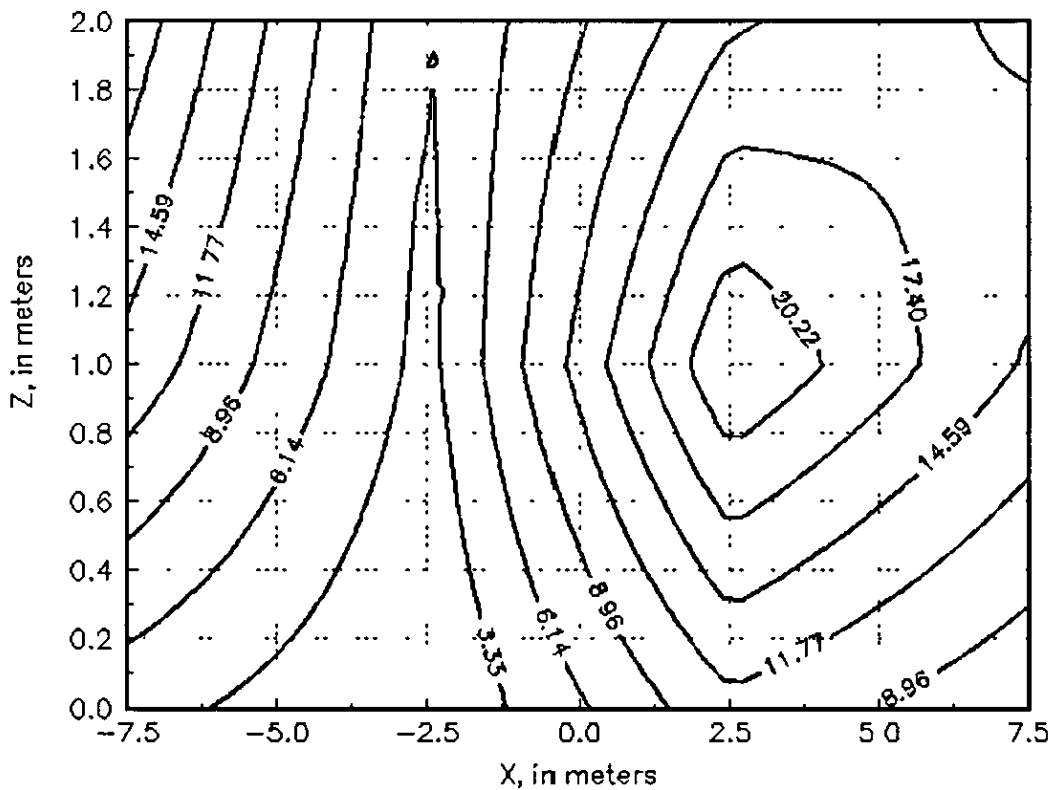


Figure A13 Cross-section BXZ, freq=300 MHz Relative dielectric constant

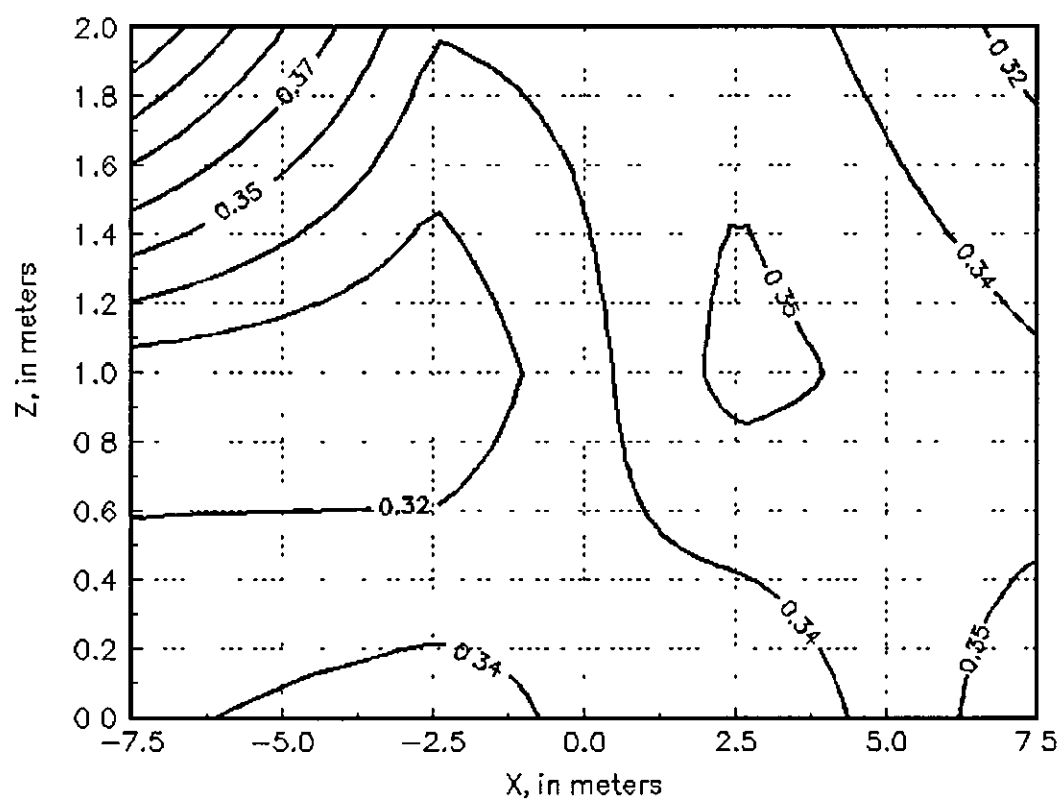


Figure A14 Cross-section CXZ, freq=1.0 MHz Conductivity in S/m

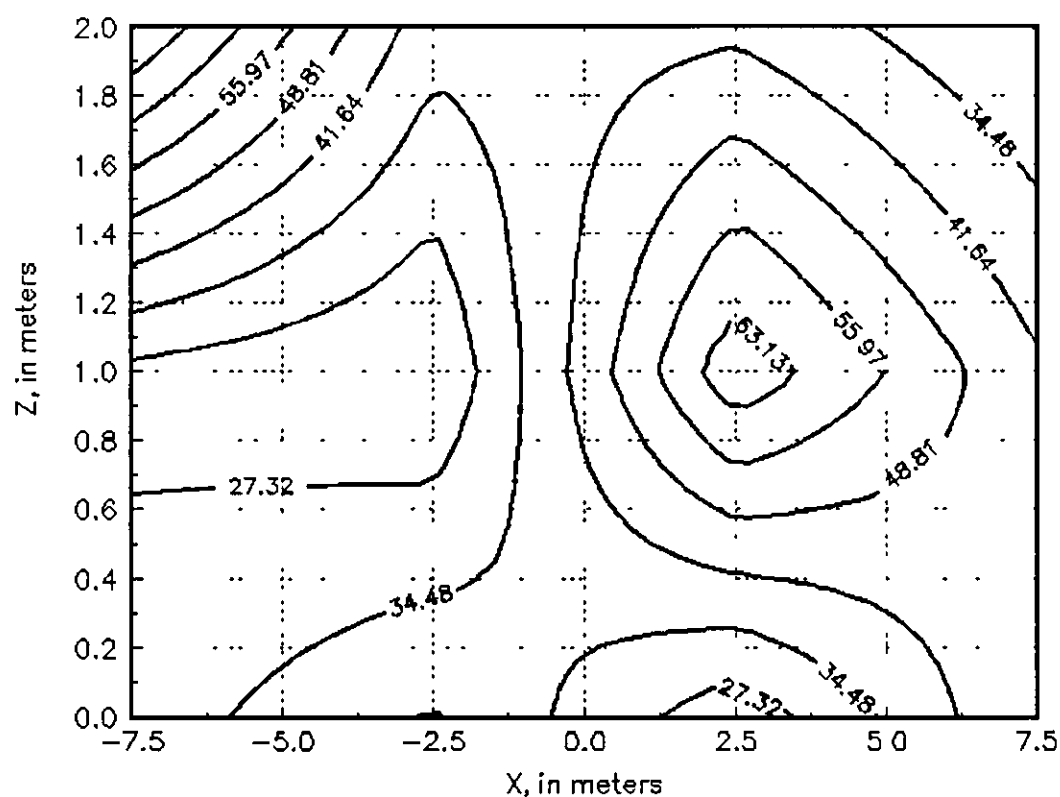


Figure A15 Cross-section CXZ, freq=1.0 MHz Relative dielectric constant

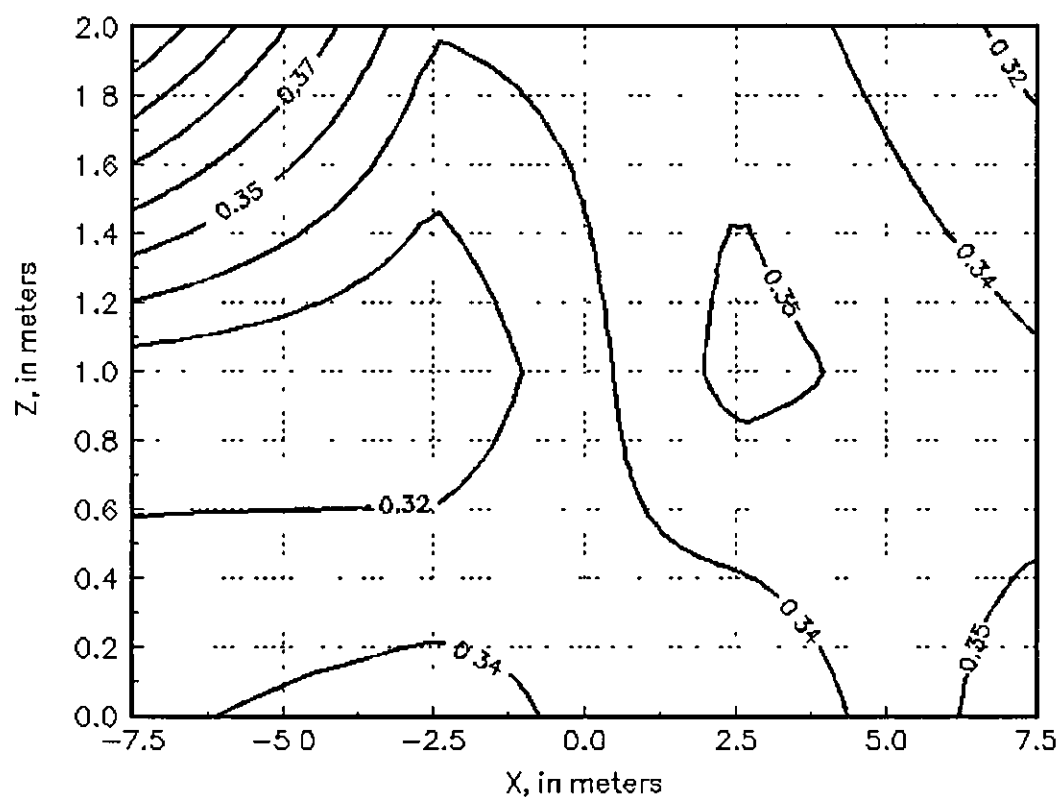


Figure A16 Cross-section CXZ, freq=146 MHz Conductivity, in S/m

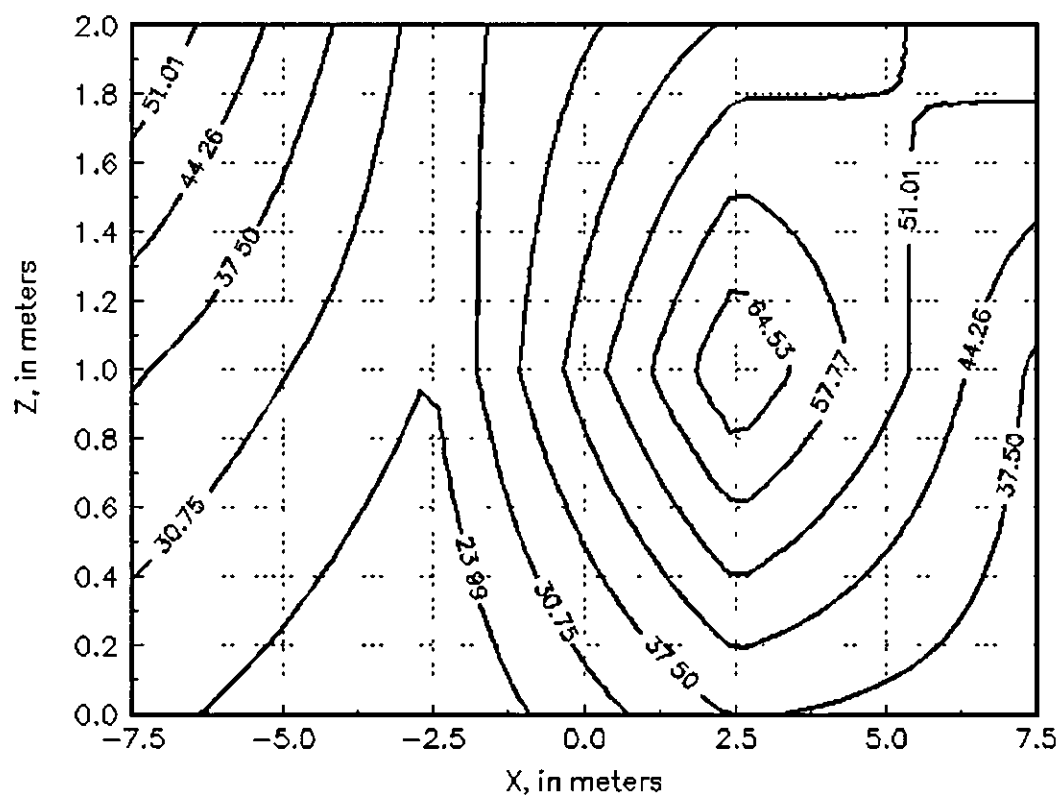


Figure A17 Cross-section CXZ, freq=146 MHz Relative dielectric constant

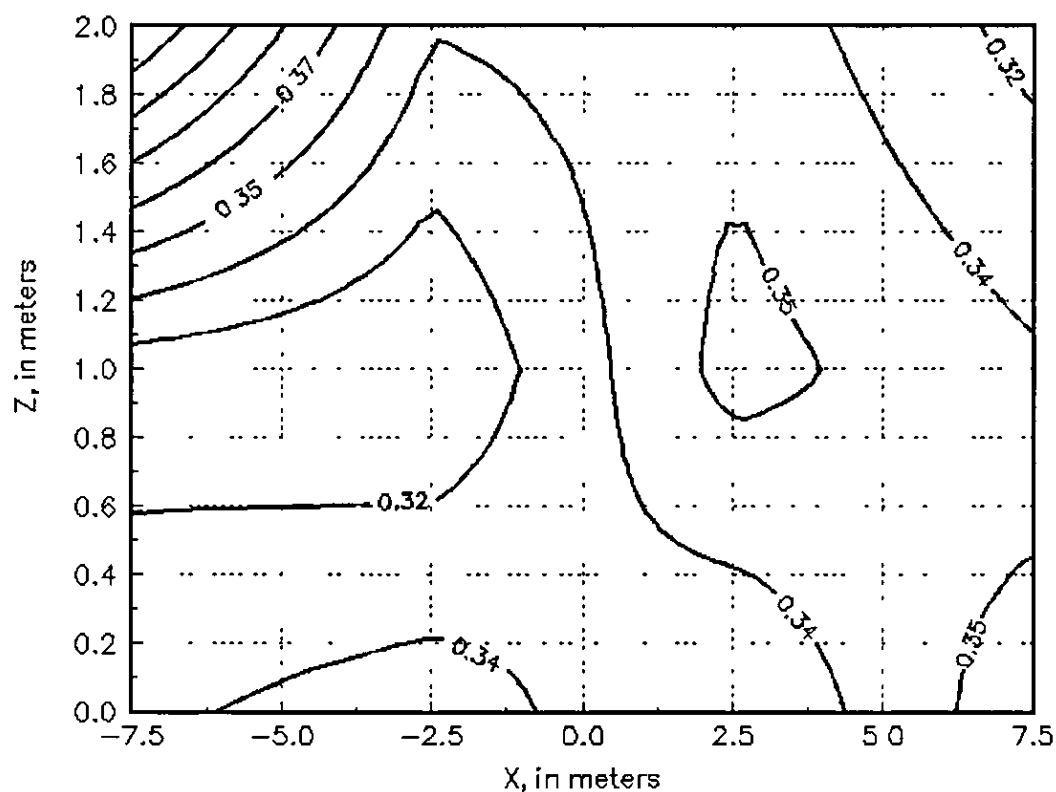


Figure A18 Cross-section CXZ, freq=300 MHz Conductivity, in S/m

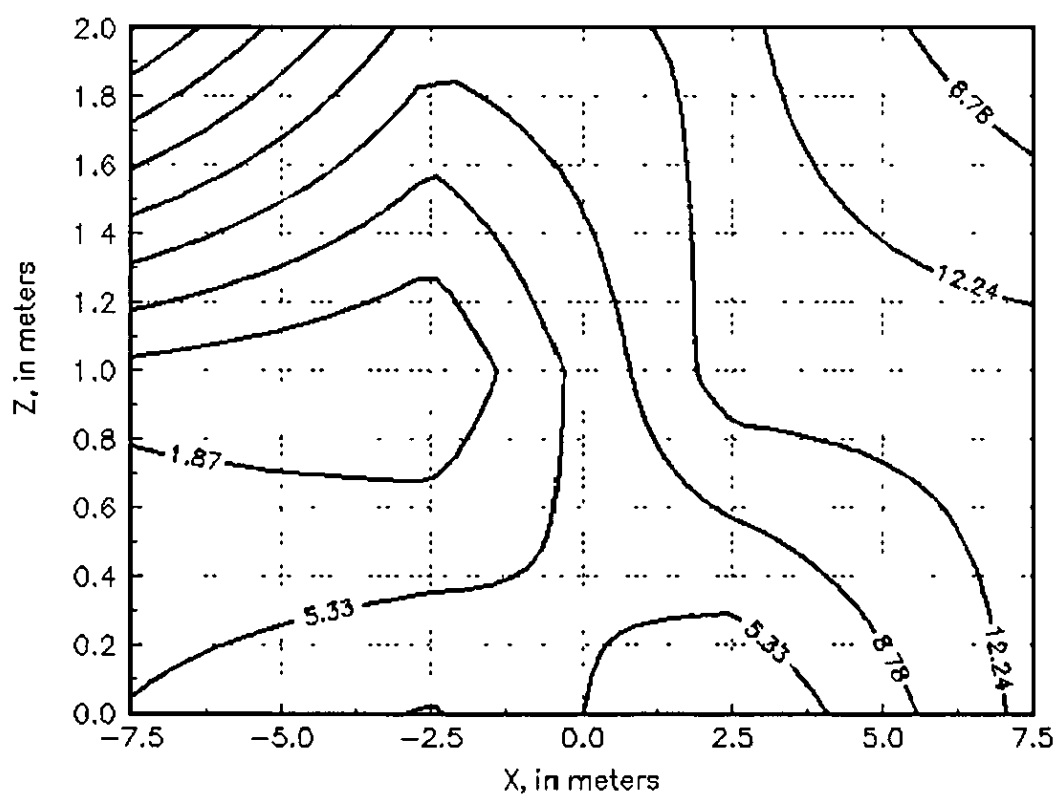


Figure A19 Cross-section CXZ, freq=300 MHz. Relative dielectric constant.

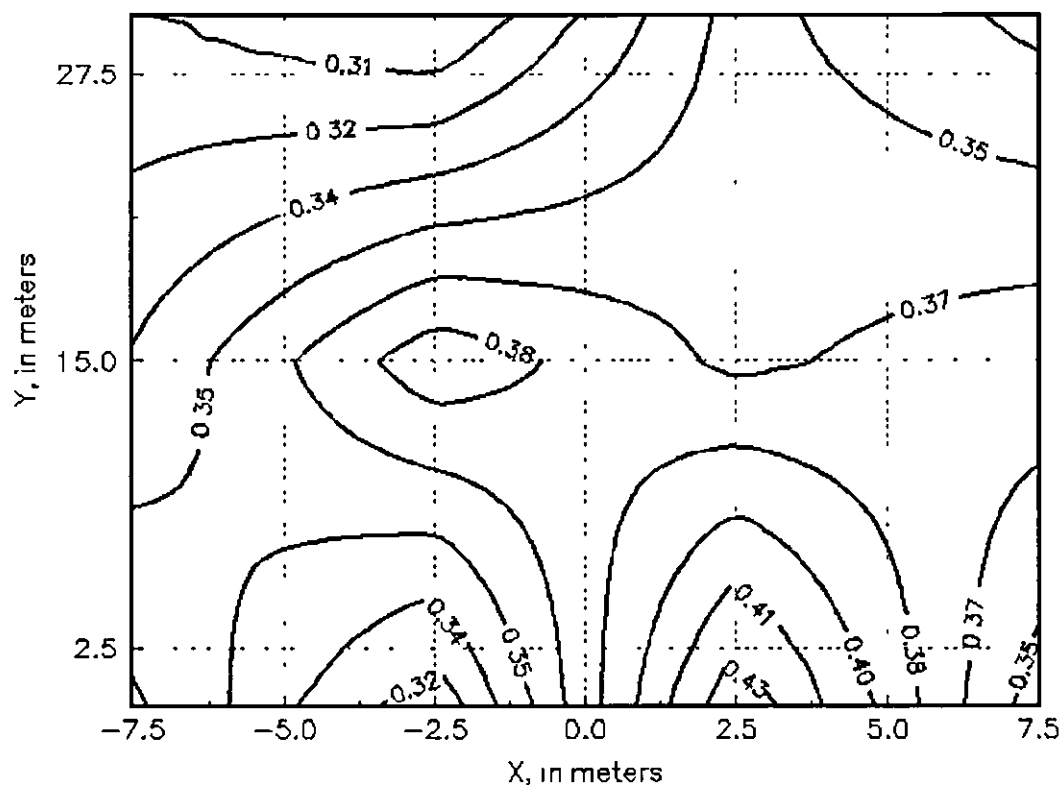


Figure A20 Cross section in the XY plane at 0.25 m depth, frequency is 146 MHz Conductivity in S/m

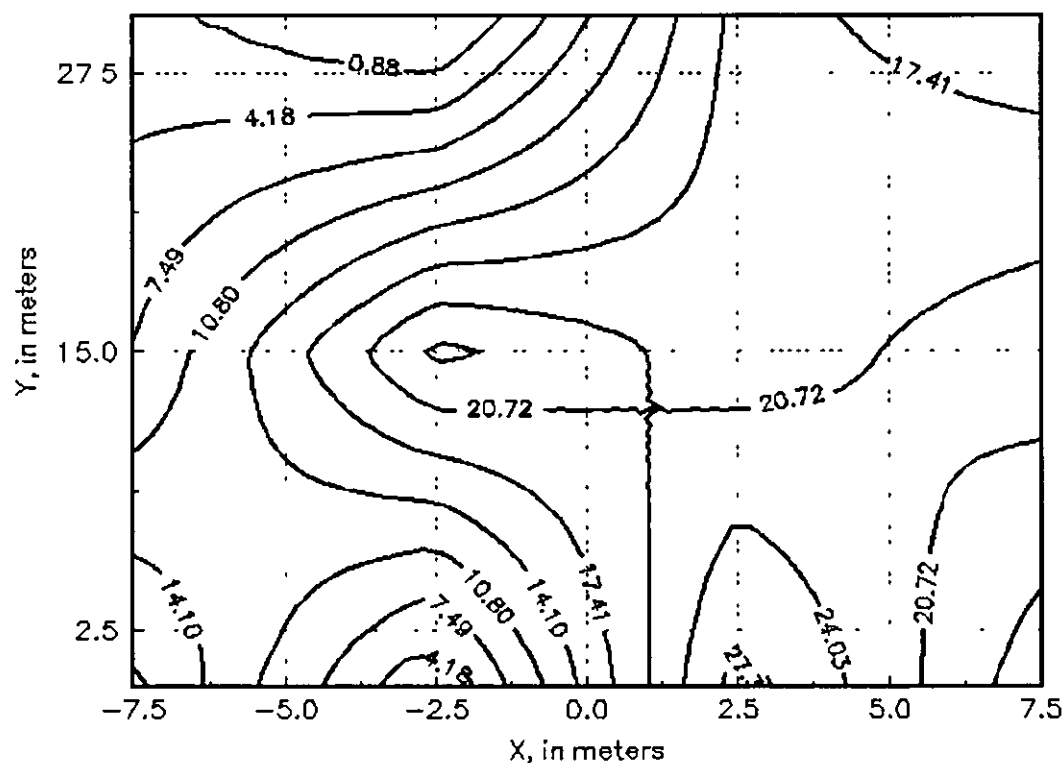


Figure A21 Cross section in the XY plane at 0.25 m depth, frequency is 146 MHz. Relative dielectric constant

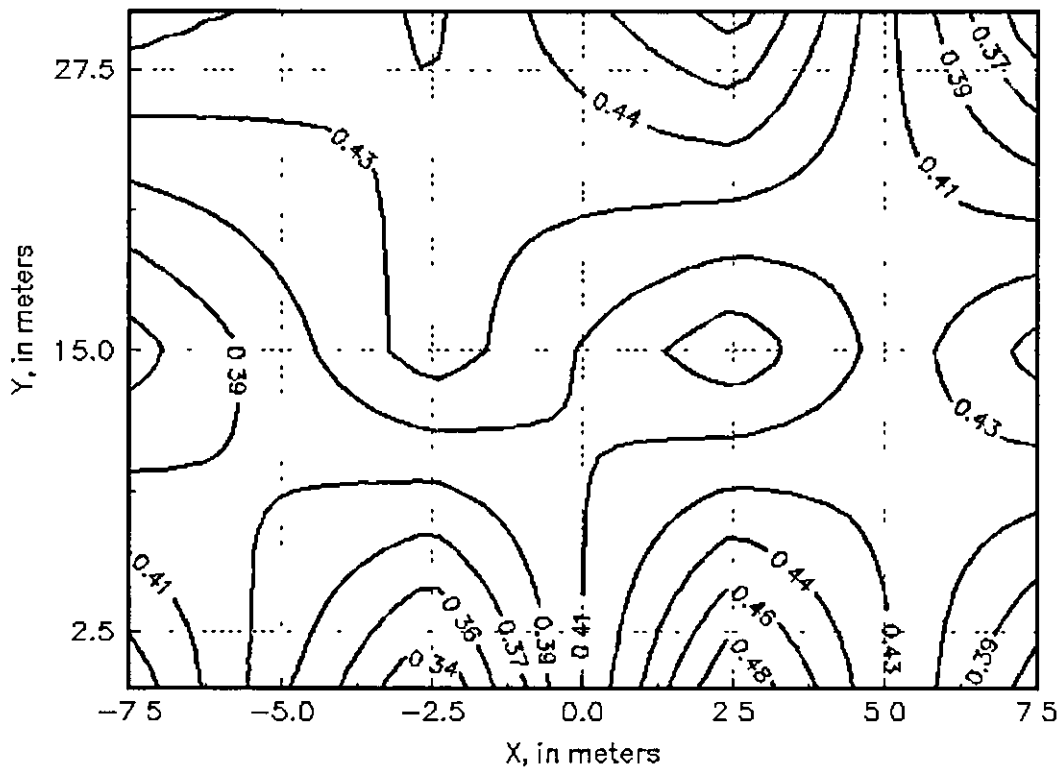


Figure A22 Cross section in the XY plane at 10 m depth, frequency is 146 MHz Conductivity in S/m

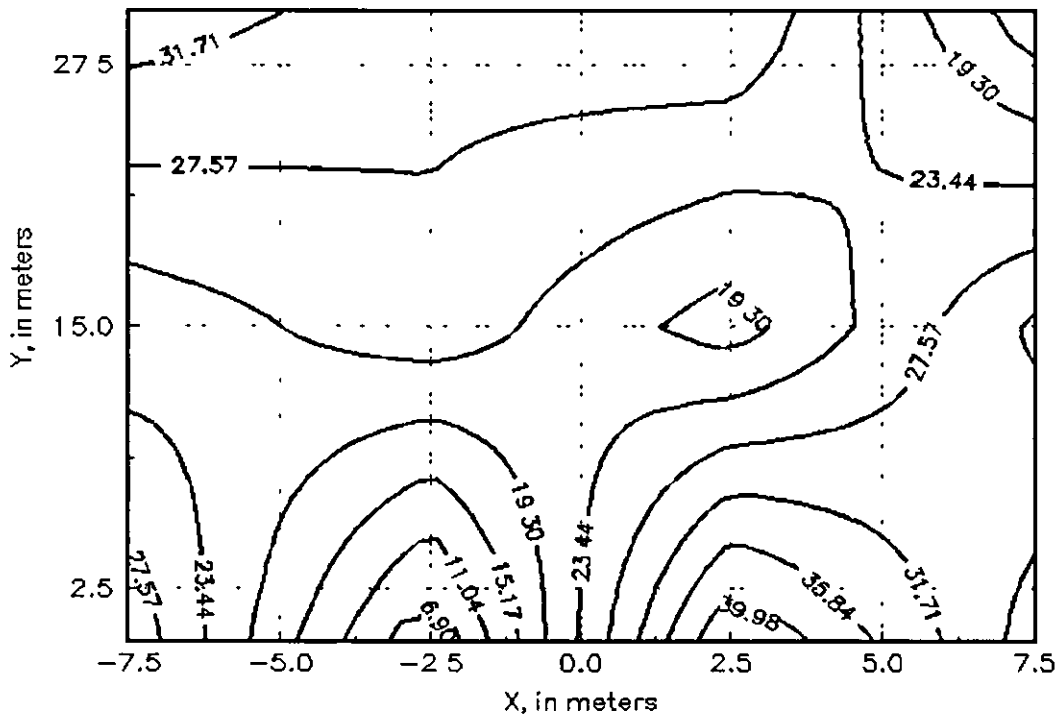


Figure A23 Cross-section in the XY plane at a depth of 10 m The frequency is 146 MHz The graph shows the relative dielectric constant

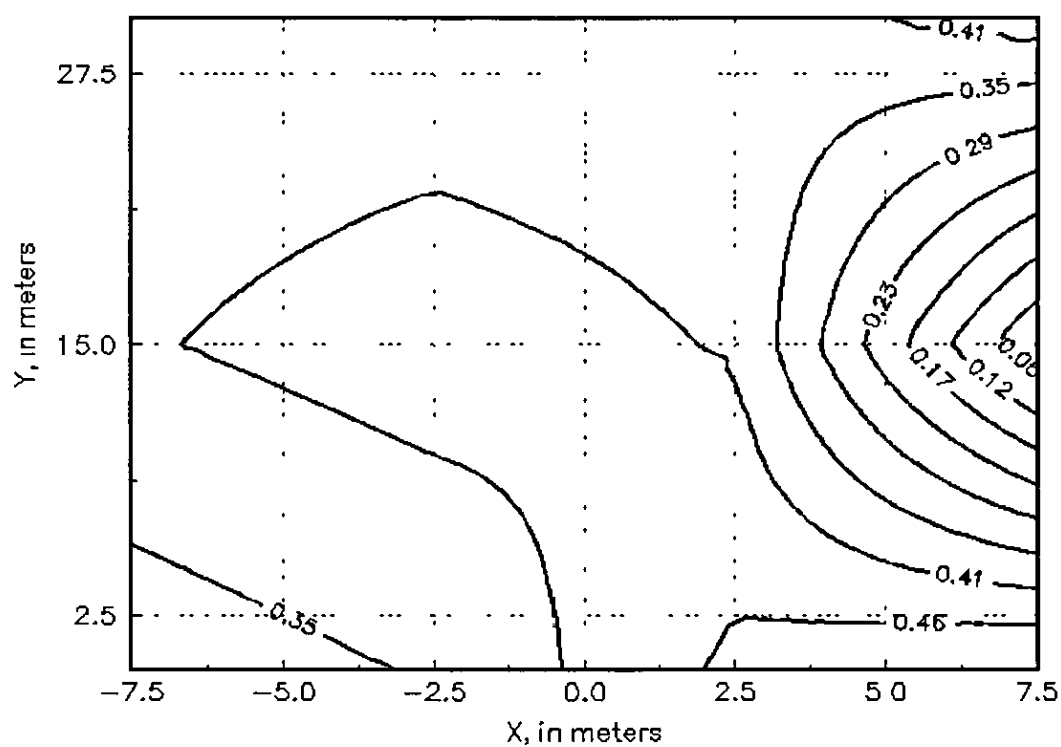


Figure A24 Cross-section in the XY plane at a depth of 1.75 m The frequency is 146 MHz The graph shows the Conductivity in S/m

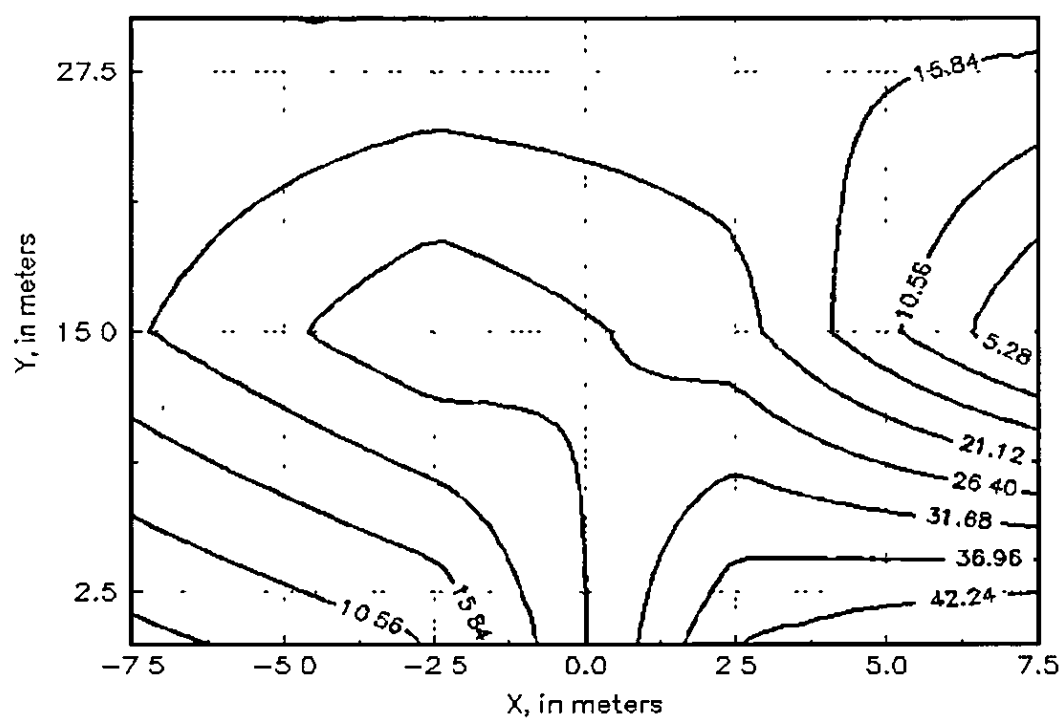


Figure A25 Cross-section in the XY plane at a depth of 1.75 m The frequency is 146 MHz The graph shows the relative dielectric constant

B. Co-ordinate systems

An Orthogonal co-ordinate system is used to express the positions of the transmitter and receiver antennas, while a cylindrical co-ordinate system is superimposed over it to calculate the lengths of the propagation paths and of the polarisation of the antennas and electromagnetic waves. The z -axis of the orthogonal co-ordinate system coincides with the axis of the cylinder in the cylindrical co-ordinate system.

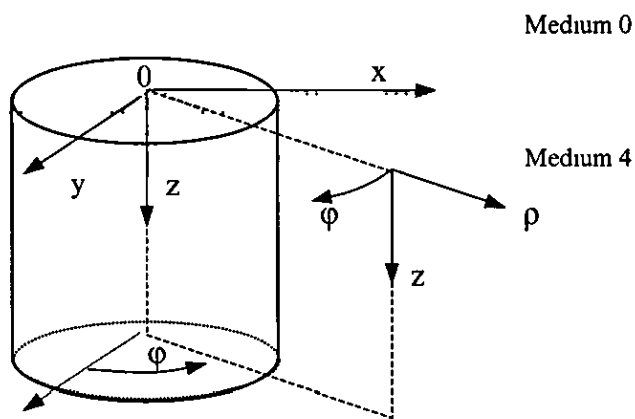


Figure C1.1 Cylindrical co-ordinate system on top of the orthogonal co-ordinate system. Note that the positive z -axis is pointing downwards into medium 4.

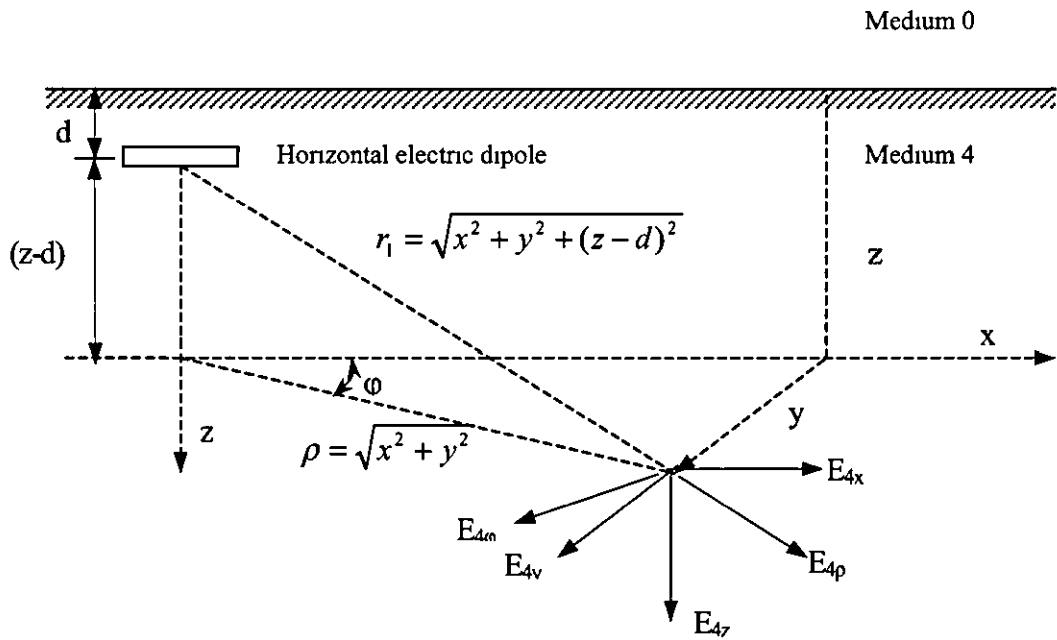


Figure C2 Cylindrical co-ordinate system on top of the orthogonal co-ordinate system. Note that the positive z-axis is pointing downwards into medium 4

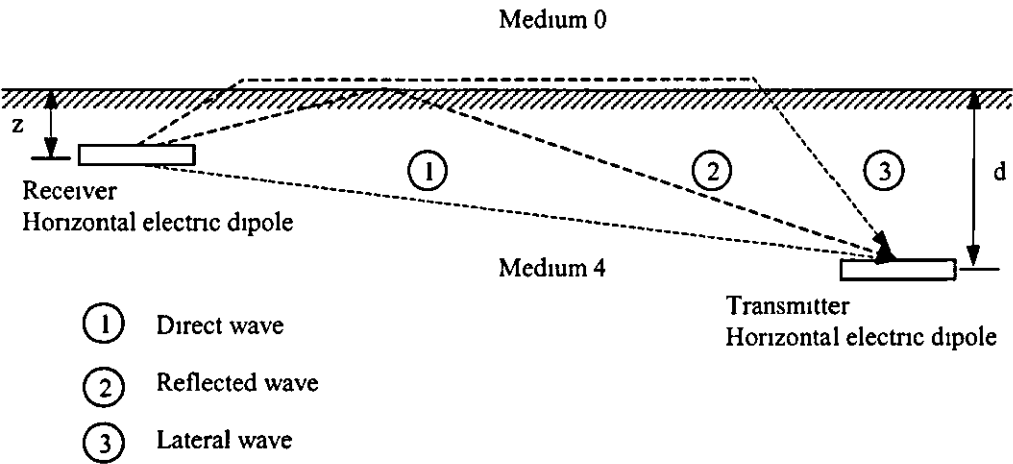


Figure C3 Modes of propagation of the electromagnetic wave underground

C. Field Trials

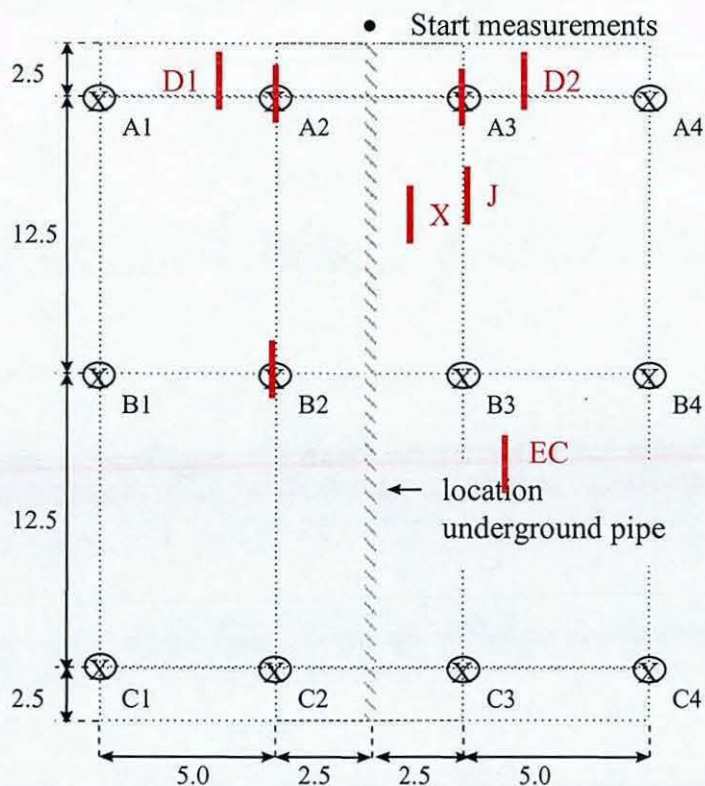


Figure C1 Top view of the trials site

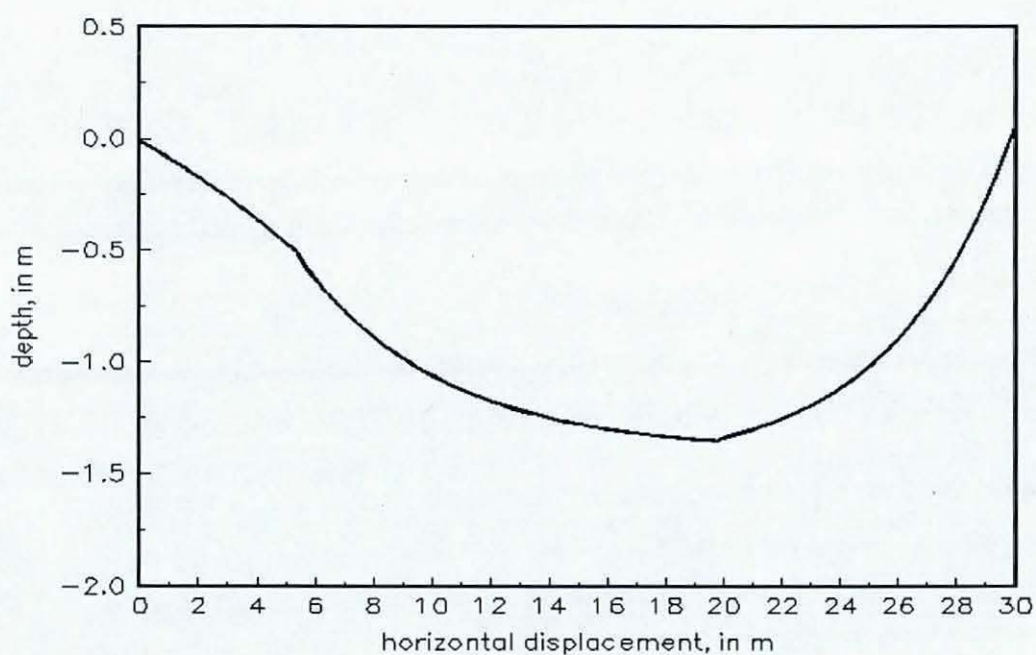


Figure C2 Depth of the transmitter as a function of the horizontal location.

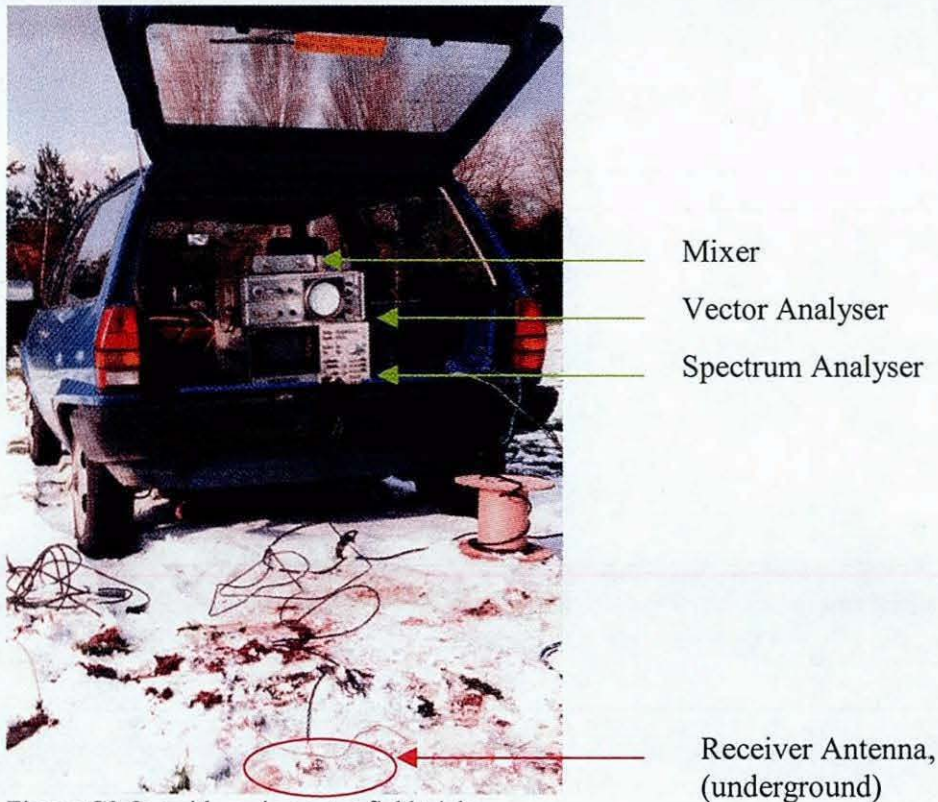


Figure C3 Car with equipment at field trials

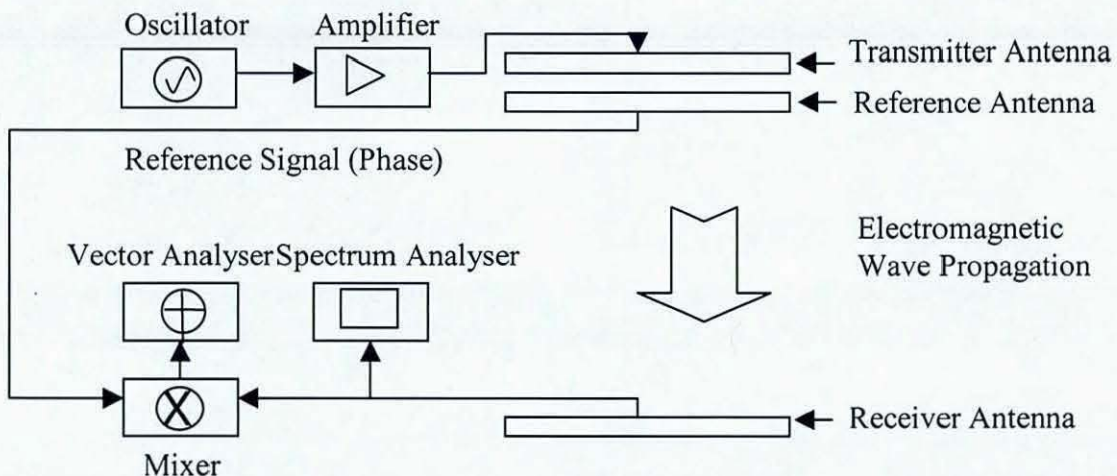


Figure C4 Schematic diagram of the test equipment

The field where the underground measurements were undertaken was at the back of the campus of Loughborough University. The picture in figure C3 was taken in December 1995. In the summer, the grass in the field grows to a height of approximately 1m. The ground surface was irregular. Field trials 1,2 and 3 were taken in the summer of 1996. Problems in conducting the field trials included access to mains power supply and interference between instruments. A 60 m long cable was used to get to the mains supply from the nearest building. Inductors (acting as chokes) were included in the long DC power supply wires to the transmitter underground to reduce interference. The Printed Circuit Board (PCB) of the RF oscillator had to be resized to allow it to fit into the 9 cm diameter pipe.

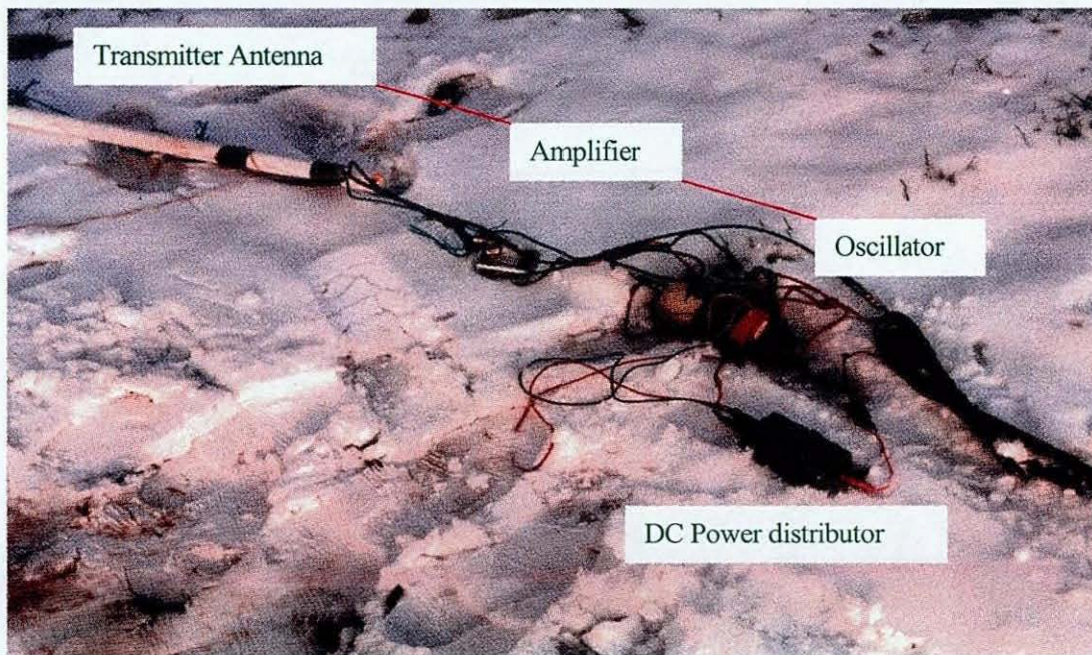


Figure C5 Transmitter Antenna (first version), Amplifier and Oscillator.

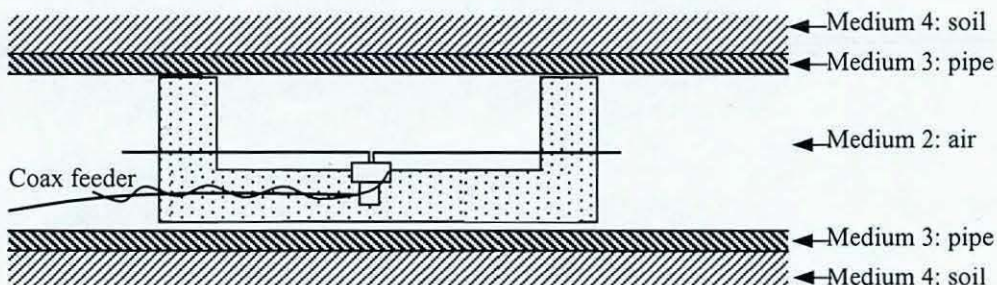


Figure C6 Improved version of the transmitter antenna. The dipole antenna is hold in place by a polystyrene structure. The relative dielectric constant of the polystyrene was measured to be 1.1. The loose wire from the feeder is to balance the current input.

The picture in figure C5 shows the transmitter antenna used in the initial measurements. The problem with this antenna was that it acted like an eccentrically dielectric loaded dipole, which had a high gain pointing downwards in the positive z -direction. The antenna shown in figure C6 was used in the trials reported in this thesis. It was positioned in the middle of the pipe, making it nearly omnidirectional in the azimuth plane. It was modelled as a dielectric loaded wire antenna with the air surrounding it and the pipe medium acting as its dielectric sheath. Using this model, its impedance and effective length were calculated.

D. Underwater Measurements

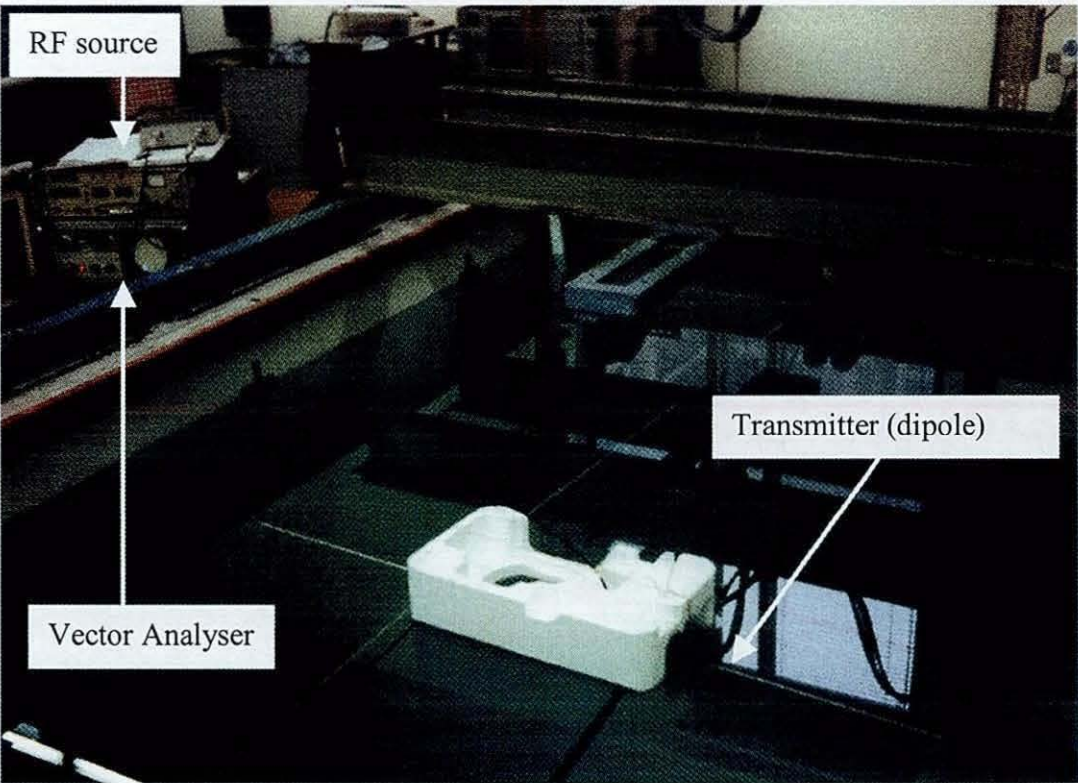


Figure D1 Underwater measurement in the basin at Loughborough University

Underwater measurements were undertaken in the basin at Loughborough University. The power used was low, to minimise reflection against the basin boundaries.

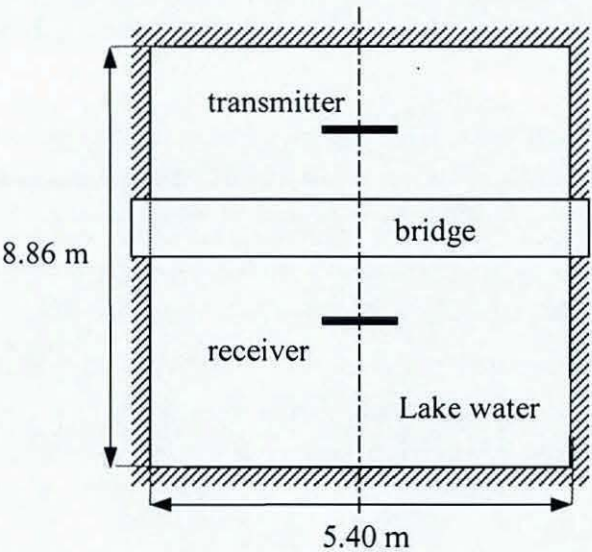


Figure D2 Drawing with dimensions of the 1.8 m deep basin at Loughborough University.

E. Underground Antenna Measurements

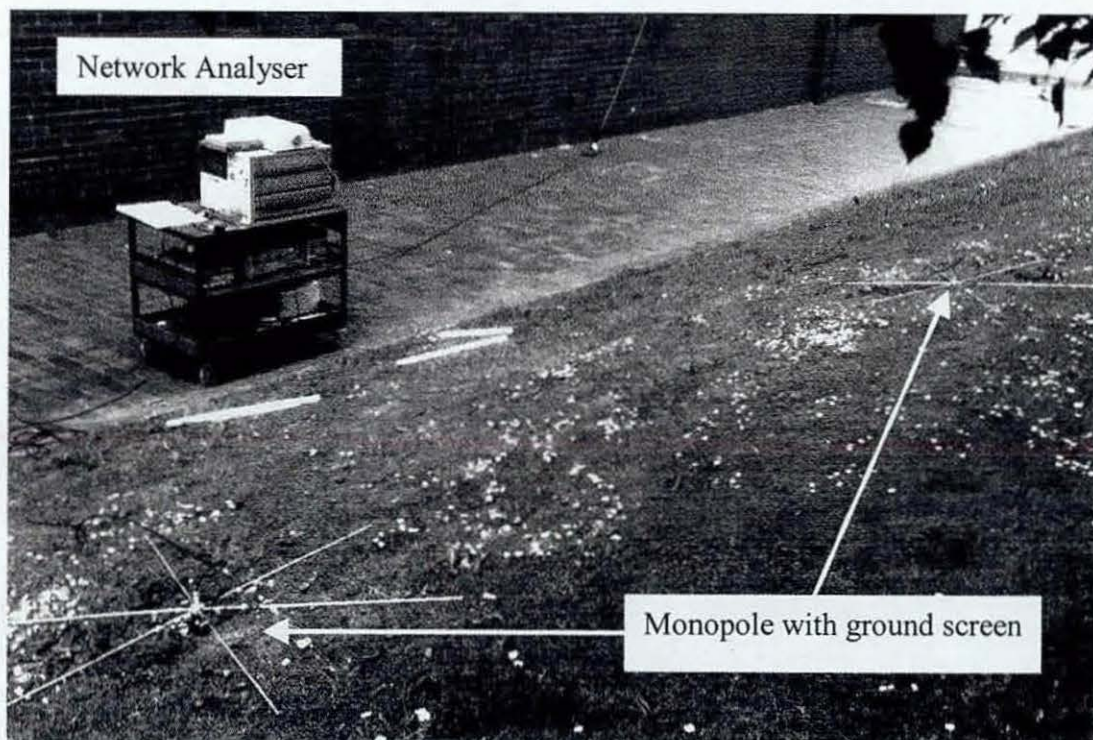


Figure E.1 Measurement of input impedance of dielectric loaded monopole antenna

F. Complex Dielectric Constant Measurements

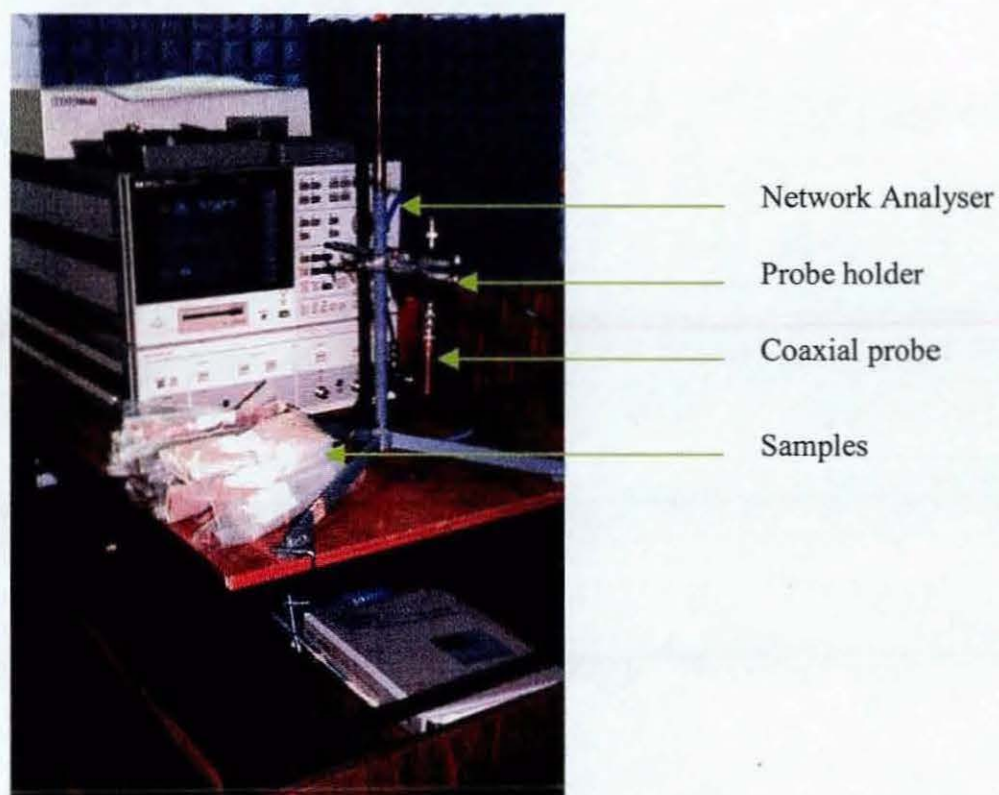


Figure C5.1 Experiment for complex dielectric constant measurement

